2011

Tissue Engineering an Acellular Bioresorbable Vascular Graft to Promote Regeneration

Patricia Wolfe
Virginia Commonwealth University

TISSUE ENGINEERING AN ACELLULAR BIORESORBABLE VASCULAR GRAFT TO PROMOTE REGENERATION

A dissertation submitted in partial fulfillment of the requirements for the degree of Doctor of Philosophy in Biomedical Engineering at Virginia Commonwealth University.

by

PATRICIA SARAH WOLFE
B.S., Virginia Polytechnic Institute and State University, 2007

Director: GARY L. BOWLIN, PH.D.
PROFESSOR, BIOMEDICAL ENGINEERING

Virginia Commonwealth University
Richmond, VA
December 2011

Acknowledgement

There are many people I would like to thank that helped guide me through this process. To my committee members, Dr. Bowlin, Dr. Greisler, Dr. Simpson, Dr. Yang, and Dr. Heise – thank you for being on my committee, and for offering your knowledge and honest opinions. Whether it was searching for an answer to a question, needing to use laboratory equipment, or having great conversations at conference receptions; I have enjoyed working with you, and I thank you all for your patience and guidance. To Dr. Bowlin especially, thank you for all of the unbelievable opportunities that you enabled me to have in being a part of your lab over the past four years. The experiences and opportunities I was given are ones I will never forget, and ones that I never thought were possible for a graduate student! Also, for always believing in me and pushing me to be my best, whether that be in terms of research, in future success, or just in life in general; I've learned so much from you that I will surely take with me in the future. Dr. Greisler, it has been a joy getting to know you and talking with you at many of the conferences – from Chicago to Boston, Paris to Thailand, I look forward to sharing many more great times, in great places, with you in the future.

To all of my lab mates, past and present – thank you for a great four years! We have had a lot of great times together, from conferences to birthday celebrations, moving labs (playing with dry ice), happy hours, cook outs, graduation parties, etc. Thank you for making me laugh, listening to me vent, and for just being great people to have as colleagues. It's been a lot of fun, and I will truly miss all of you! Special shout out to Scott – thanks for being my partner in crime, for dealing with me on a daily basis (or

should you be thanking me for dealing with you?!), and for infecting your own computer, and jump drives, to help me through my virus crisis.

To all my friends, in Richmond and elsewhere, thank you for being there for me in so many different ways throughout the past four years. I am so glad to have such great people in my life that I know I can lean on when I need to and that believe in me. I have made many great memories throughout the past four years that I will never forget.

And finally, most importantly, to my family – I could not have done it without your unconditional love, support, and interest. This all wouldn't have been possible without you! Thank you for always being there for me and for always reminding me that I can do anything I put my mind to. No matter where I go in life I know you will always be by my side as my number one fans!

Table of Contents

List of Tables

Page

List of Figures

Page

List of Abbreviations

aFGF	Acidic firoblast growth factor
bFGF	Basic fibroblast growth factor
ADSC	Adipose-derived stem cell
Ang	Angiopoietin
aPRP	Activated platelet-rich plasma
BMCs	Bone marrow cells
BSA	Bovine serum albumin
CHD	Coronary heart disease
CVD	Cardiovascular disease
DAPI	4',6-diamidino-2-phenylindole
DL-3-MeDX	DL-3-methyl-1,4-dioxan-2-one
DSC	Differential scanning calorimetry
DX	1,4-Dioxan-2-one
ECM	Extracellular matrix
EC	Endothelial cells
EDC	1-ethyl-3-(3-dimethylaminopropyl)carbodiimide
EGF	Endothelial growth factor
ELISA	Enzyme-linked immunosorbent assay
EPC	Endothelial progenitor cells
eNOS	Endothelial nitric oxide synthase
EU	Endotoxin Units
e-PTFE	Expanded-poly(tetrafluoroehtylene)
FB	Fibroblasts
FBG	Fibrinogen
FGF	Fibroblast growth factor
FTF	Freeze-thaw-freeze
gel/NMCS	Gelatin/*N*-Maleicacyl-chitosan
H&E	Hematoxylin and Eosin
hbEGF	Heparin-binding endothelial growth factor
HFIP	1,1,1,3,3,3 hexafluoro-2-propanol
HGF	Hepatocyte growth factor
HUVEC	Human umbilical vein endothelial cells
ICW	In-Cell Western
IFN-γ	Interferon-gamma
IL-1-23	Interleukin-1-23
LXA_4	Lipoxin A_4
MSFM	Macrophage serum-free media
myoFB	Myofibroblasts
NaCl	Sodium chloride
NHS	N-hydroxysuccinimide
PCL	Polycaprolactone
PDGF-BB	Platelet derived growth factor
PDO	Polydioxanone

PEG	Poly(ethylene glycol)
PEN	Poly(ethylene naphthalate)
PEO	Polyethylene oxide
PET	Poly(ethylene terephthalate)
PEUU	Poly(ester urethane)
PEEUU	Poly(ether ester urethane) urea
PGA	Poly(glycolic acid)
PGI_2	Protacylin I_2
PLA	Polylactic acid
PLGA	Polylactide-co-glycolide
PLLA	Poly(L-lactic acid)
PMAA	Poly(methacrylic acid)
PPO	Poly(propylene oxide)
PPP	Platelet-poor plasma
PRGF	Preparation rich in growth factors
PRP	Platelet-rich plasma
PVA	Poly(vinyl alcohol)
RANTES	Regulated upon activation, normal T-cell expressed and secreted
RGDS	Arg-Gly-Asp-Ser
SDF-1	Stromal cell derived factor-1
SEM	Scanning electron micrographs
SF	Silk fibroin
SIS	Subintenstinal submucosa
SMC	Smooth muscle cells
T_C	Crystallization temperature
TCPS	Tissue culture polystyrene
T_G	Glass transition temperature
T_M	Melting temperature
TF	Tissue factor
TGF-β	Transforming growth factor-beta
THF	Tetrahydrofuran
TIPS	Thermally induced phase separation
TNF-α	Tumor necrosis factor-α
TxA_2	Thromboxane A_2
VEGF	Vascular endothelial growth factor
vWF	vonWillebrand Factor

Abstract

TISSUE ENGINEERING AN ACELLULAR BIORESORBABLE VASCULAR GRAFT TO PROMOTE REGENERATION

By Patricia Sarah Wolfe, B.S.

A dissertation submitted in partial fulfillment of the requirements for the degree of Doctor of Philosophy in Biomedical Engineering at Virginia Commonwealth University.

Virginia Commonwealth University, 2011

Director: Gary L. Bowlin, Ph.D.
Professor, Department of Biomedical Engineering

Tissue engineering is an interdisciplinary field that aims to restore, maintain, or improve diseased or damaged tissues. Electrospinning has become one of the most popular means to fabricate a scaffold for various tissue engineering applications as the process is extremely versatile and inexpensive. The ability for electrospinning to consistently create nanofibrous structures capable of mimicking the native extracellular matrix (ECM) is the basis behind why this technique is so successful in tissue engineering. Cardiovascular disease has been the leading cause of death in the United States for over 100 years, and because of this, the need for coronary artery replacements

is in serious demand. More specifically, small diameter vessels (<6 mm I.D.) are most needed, due to the fact that they are most often affected and the current clinical replacements provide less than optimal long-term patency and regenerative ability. Tissue engineering of vascular grafts has been investigated for over 50 years, however, synthetic replacements made of Dacron® and expanded-poly(tetrafluoroethylene) (e-PTFE) still remain the clinical standard. This study examines a variety of different ways to alter different characteristics of electrospun constructs, to create scaffolds that would be favorable for use as a blood vessel replacement; the end goal being the creation of an acellular bioresorbable vascular graft that would provide sufficient mechanical support to withstand physiological forces, as well as ample biocompatibility to allow host cells to infiltrate and regenerate the graft as the structure degrades. As a way of tailoring the mechanical and thermal properties of a scaffold to be more conducive to that of a native artery, a novel co-polymer was created from the random copolymerization of two monomers; 1,4-Dioxan-2-one (DX) and DL-3-methyl-1,4-dioxan-2-one (DL-3-MeDX) were mixed at different ratios and electrospun, forming nanofibrous scaffolds that exhibited different mechanical and thermal properties. Next, scaffolds were electrospun from natural and synthetic polymers, and the potential for these materials to elicit the formation of an acute thrombotic occlusion was investigated by quantifying tissue factor expression from monocytes using a novel technique. Tissue factor expression by monocytes on the electrospun natural and synthetic polymer scaffolds was compared to that of e-PTFE to determine their potential for use as vascular graft materials. Platelet-rich plasma (PRP), a naturally occurring blood component which is comprised of supraphysiologic concentrations of autologous growth factors, was activated and

lyophilized to form a preparation rich in growth factors (PRGF). PRGF was electrospun for the first time, to create a scaffold that would mimic the role of the native ECM in the wound healing cascade. Characterization of these scaffolds proved their bioactivity was enhanced, with cell infiltration occurring throughout the structures in as little as 3 days. Lastly, PRP/PRGF and/or heparin were incorporated into electrospun PCL scaffolds as a means of enhancing the regenerative potential and reducing the thrombogenic potential of the scaffolds, while supplying the constructs with mechanical stability. The release of several pro-regenerative growth factors and chemokines from the PRP incorporated scaffolds was analyzed and the effect of PRP and heparin on scaffold degradation characteristics was determined. Additionally, cell proliferation, migration, sprout formation, and chemokine release were evaluated, and results from these experiments proved the addition of PRP could enhance the regenerative potential of the electrospun scaffolds. The results from this study reveal the variety of ways in which a number of characteristics of an electrospun scaffold can be altered to create a more ideal bioresorbable vascular graft that has the potential to be regenerated within the body, while providing enough mechanical support for this to occur over time.

Chapter 1: TISSUE ENGINEERING BACKGROUND

Preface: The following chapter is an excerpt from a book chapter which appeared in Tissue Engineering: From Lab to Clinic, edited by N. Pallua and C. Suschek and published by Springer Science and Business Media, Pg. 41-67, 2011. The work included is a broad overview on tissue engineering as a whole, and provides insight into the aim of the discipline, as well as clinical applications that have emerged from the field thus far.

Natural and Synthetic Scaffolds

Patricia S. Wolfe, Scott A. Sell, Gary L. Bowlin

Department of Biomedical Engineering
Virginia Commonwealth University
Richmond, VA 23284

Introduction

Tissue engineering is an interdisciplinary field aimed at the application of the principles and methods of engineering and the life sciences toward the fundamental understanding of structure-function relationships in normal and pathological mammalian tissues and the development of biological substitutes to restore, maintain, or improve tissue functions [1-6]. Typically this involves collaborative efforts between materials scientists, cell and molecular biologists, immunologists, surgeons, and engineers to create replacement tissues that will be accepted by the body and promote native extracellular matrix (ECM) production. This requires the use of materials that do not activate catabolic

pathways in the body, ultimately leading to fibrous encapsulation or destruction of the material [4, 6-8].

Natural and synthetic ECM analogues have played a vital role in the field of tissue engineering since the early 1980s [5, 9, 10]. Improvements in the fabrication process as well as scaffold structure continue to occur in hopes of finding an ideal scaffold for each specific tissue engineering application. The overall function of the biodegradable scaffold is to create a 3D microenvironment that will provide the necessary support for transplanted or host cells to induce normal physiologic regeneration and function. Ideally, the scaffold should mimic the native ECM it is going to replace. In order for this to happen, several design considerations should be taken into account including fabrication, structure, biocompatibility, and biodegradability [10]. Many different materials have been used to create scaffolds for different tissue engineering applications, each one offering different features and characteristics.

Although tissue engineering scaffolds have come a long way since they were first introduced, there are currently very few products on the market to show for their success. As for the products that are available, even though they have made a remarkable impact in the medical industry and have improved the quality of life for many, there are still several limitations and drawbacks, which will be discussed in a later section.

Aim of the Discipline

Tissue Engineering ECM

The use of isolated cells or cell substitutes is the most direct tissue engineering approach, typically using autologous or allogenic cells as therapeutic agents. This allows for the replacement of cells in areas of damaged tissue, ultimately using the cell's ability for replication to promote tissue repair and resumed function [3, 4]. These cells can be differentiated and tissue specific (i.e. injecting chondrocytes into cartilage [11]) or can be undifferentiated, generic stem cells that could be injected into areas of damaged tissue and allowed to differentiate as needed [8, 12]. The upside of such an approach is the avoidance of surgery, as well as the ability to manipulate cells as needed *in vitro* prior to their implantation into the body. However, the major drawback of this approach is the time required to culture a usable number of cells. Without the presence of a large universal cell bank, cells must be taken from a donor and cultured to a usable number prior to implantation in their eventual recipient [3, 8].

Another approach to tissue engineering is the use of either pre-cellularized or acellular ECM analogues. The use of matrix analogues may be the most challenging, albeit potentially the most beneficial, approach to tissue engineering. The ultimate goal of this approach to tissue engineering is to enhance the body's ability to heal and repair itself by introducing a scaffold that the body recognizes and incorporates directly into the reparative process of the tissue. These systems are meant to mimic the native ECM and can serve as a structural framework for both cells and signaling molecules using the body as a bioreactor, exerting normal physiologic biomechanical and biochemical signals upon the scaffold. The idea being that the ECM analogue will induce cells to more accurately

reproduce their normal physiological behavior, thereby improving tissue regeneration and repair [5, 13, 14]. A number of tissue-inducing signaling molecules have been incorporated into ECM analogue scaffolds to aid this process. These signaling molecules can include a wide number of cytokines and chemokines to promote cell growth, instruct differentiation, and promote cellular migration [4]. Since they are open to immunological attack, much research has been done on the material composition of these matrix analogue systems in order to produce matrices that elicit little to no immune response and most closely mimic both the structure and function of native ECM.

Native ECM

Mammalian tissue is composed of two major components: cells (both parenchymal and mesenchymal) and ECM. A large majority of tissue volume is composed of the ECM component, which also provides much of a tissue's geometric shape. From a structural standpoint, the ECM is a complex arrangement of proteins and polysaccharides such as collagen, hyaluronic acid, proteoglycans, glycosaminoglycans, and elastin (Table 1.1). These ECM components are constantly being synthesized, secreted, oriented, modified, and degraded by the cellular components that they support. Historically, the function of native ECM was only believed to be as a structural framework for tissues. However, it is now understood that the ECM, through interaction with receptors on the surfaces of cells, directly takes part in promoting cell adhesion, migration, growth, differentiation, and apoptosis. The ECM also plays a role in cytokine activity and intracellular signaling. Growth factors and signaling molecules can be stored

within ECM to preserve against their degradation, or they can attach to the surface of the ECM to present themselves more efficiently to cell receptors [4, 7, 15].

Table 1.1. Some major ECM components, their function, and location. Adapted from [4].

Component	Function	Location
Collagen	Tissue architecture, tensile strength, cell-matrix interaction, matrix-matrix interaction	Widely distributed
Elastin	Tissue architecture, elasticity	Tissues requiring elasticity (lung, blood vessel, skin)
Proteoglycans	Cell-matrix interaction, matrix-matrix interaction, cell proliferation, cell migration	Widely distributed
Hyaluronan	Cell-matrix interaction, matrix-matrix interaction, cell proliferation, cell migration	Widely distributed
Laminin	Basement membrane component, cell migration	Basement membranes
Fibronectin	Tissue architecture, cell-matrix interaction, matrix-matrix interaction, cell proliferation, cell migration	Widely distributed
Fibrinogen	Cell proliferation, cell migration, hemostasis	Blood, wound healing

Interactions between cells and the ECM are complex and dynamic, and play critical roles during development, wound healing, and environmental maintenance (Figure 1.1). During development, cell-ECM interaction is responsible for pattern formation, morphogenesis, and phenotype acquisition and maintenance. During the wound healing process, clot formation, inflammation, formation of granulation tissue, and remodeling are all mediated by cell-ECM interaction. Initial attraction and adhesion of cells to the ECM is induced by multiple, low affinity charge and hydrophobic interactions. During the spreading phase of adhesion, heterodimeric transmembrane proteins known as integrins, as well as other receptors, on the cell surface bind to specific small peptide fragment sequences on the ECM molecules. This allows for cells to bind to the ECM, through focal adhesions, and promote direct communication between the two.

Integrin binding is both specific and reversible and allows cells to differentiate, secrete and absorb matrix, and transmit signals [7]. Signals are sent from the ECM across the cell membrane to soluble molecules in the cytoplasm and through direct connections with the cytoskeleton and into the cell nucleus, evoking a cellular response, termed "outside-in" signalling. This direct contact allows for stronger, more specific signaling than through the release of diffusible signaling molecules. Cell-ECM interactions can also be of an "inside-out" nature, when changes within the cell feed back to alter the activity of surface receptors, ultimately creating changes in the integrin and non-integrin receptors in focal adhesions [7]. In what is known as dynamic reciprocity, the cellular response to the ECM signaling can often alter the state of the ECM. For example cells may release matrix metalloproteases to break down an overly dense ECM to allow for their migration or proliferation [4, 15].

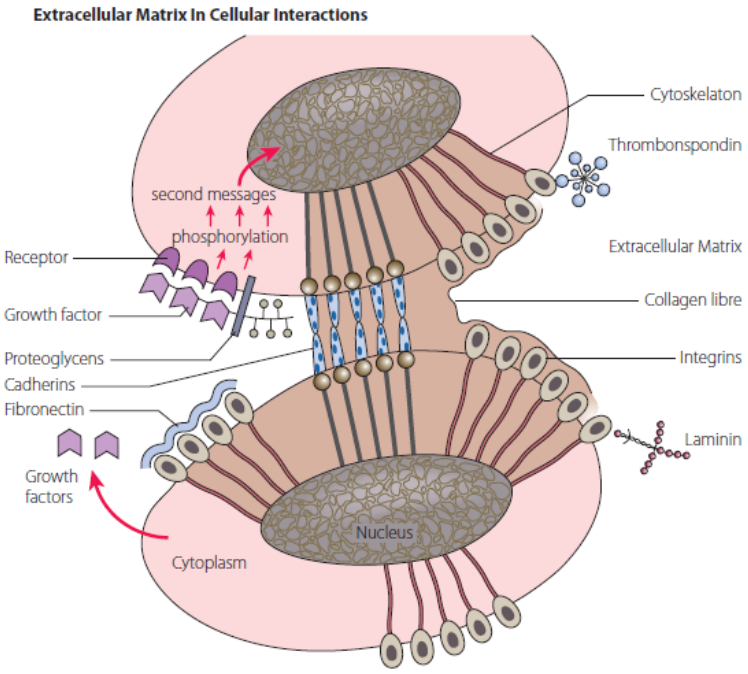

Figure 1.1. ECM-cell interaction depicting integrin receptors. Reprinted from [4].

ECM Analogue Scaffolds

As complex a structure as the native ECM has been revealed to be, it should be no surprise that the creation of a successful engineered ECM analogue has proven to be extremely challenging. Ideally, one would like to mimic both the fibrillar form and the complex function of the native ECM [16-18]. To attain a successful ECM analogue scaffold, there are several design and material criteria that must be met. First and foremost, the scaffolding material should be subjected to the same standards as any other biomaterial implanted in the body, namely, the scaffold should not initiate any adverse tissue or immune reactions. For many applications, scaffolding materials should be biodegradable or bioabsorbable at a rate that will allow for their gradual incorporation into the surrounding tissue without any fibrous encapsulation or residual evidence of their presence [6, 9, 16, 17]. ECM analogue scaffolds have been fabricated from an extensive array of materials through a number of different fabrication techniques. A wide number of different polymers, both synthetic and natural in origin, have been used as ECM analogues. The most common matrix materials in use today are polymers such as poly(glycolic acid) (PGA), poly(lactic acid) (PLA), and their copolymer, polylactide-co-glycolide (PLGA). However there has also been extensive work done with polycaprolactone (PCL) and polydioxanone (PDO), as well as some polyanhydrides, polyorthoesters, polycarbonates, and polyfumarates [6, 17]. As for ECM analogues engineered from natural materials, collagens [19], elastin [20], fibrinogen [21], and silk [22] have been used. ECM substitutes of this variety have the potential for a greater upside than their synthetic counterparts due to the fact that they are constructed from native ECM materials and may be expected to retain some of their biologic behavior [6,

23]. Inorganic materials such as hydroxyapatite, tricalciumphosphate, ceramics, and glass have also been used [6, 12].

The architecture of the scaffold is every bit as important as the material from which it is fabricated. As previously stated, an ECM analogue should mimic the form of the native ECM. To be ideal, this ECM analogue would need to mimic the topographical features and geometry on the macro-scale, micro-scale, and even nano-scale levels, as each influences cell response to the scaffold [24]. Native ECM is composed of nanoscale fibers that can provide structural integrity to tissues. Recent advances in fabrication techniques (self-assembly, phase separation, and electrospinning) have made the creation of consistently nanofibrous scaffolds possible. The use of nanofibrous scaffolds creates structures with a very high surface area to volume ratio to support cell growth and infiltration [9, 25, 26]. In addition, the morphological similarities between the nanofibrous structures and the native ECM are believed to improve cellular response and overall biocompatibility [25].

Success as a tissue-engineering scaffold in many applications is ultimately dependant upon the ability for cells to infiltrate the ECM analogue, migrate throughout its thickness, proliferate, and restore normal physiologic function [27, 28]. The scaffold's porous structure, a combination of microporous (pore diameters < 2 μm), mesoporous (pores with diameter 2 μm – 50 μm), or macroporous (pore diameters > 50 μm) void spaces, plays a major role in cellular penetration [23, 29]. As yet there has been no concrete claim to an ideal pore diameter, but it has been documented that pores with a small diameter, yet larger than the diameter of a cell, are favorable [9]. Not only do the pores of an ECM analogue scaffold need to be of a sufficient size for tissue growth to

occur, but they also need to be open and interconnected. Interconnectivity refers to the extent of which pores are connected with their neighboring pores, and has a large effect on nutrient and waste diffusion, cell migration, and overall scaffold permeability [6, 30, 31]. The terms porosity and permeability are often incorrectly used interchangeably in the realm of tissue engineering and in the consideration of ECM analogue scaffolds. By definition, porosity is the amount of void space contained within a structure, while permeability is a measure of the ease of which a fluid can move through the structure. Matrix permeability ultimately depends on the combination of scaffold porosity, pore size and distribution, pore interconnectivity, and pore orientation and scaffold porosity to determine the hydraulic permeability of an ECM analogue scaffold [30, 31].

Although not commonly reported for tissue engineered scaffolds, permeability and porosity are extremely important to the success of an ECM analogue. Healthy, living tissue *in vivo* relies on the microvasculature to distribute blood and exchange metabolites through a combination of diffusion over short distances and flow-limited exchange. There are currently no tissue engineered products that contain their own pre-vascularised capillary bed to provide nutrients to the structure, chaining their initial effectiveness to the limits of passive diffusion [32]. The limitations of diffusion-based nutrient transport restrict the maximum thickness of avascular tissue engineered constructs to less than 2 mm [33]. Scaffolds with increased porosity and permeability help to promote the diffusion of nutrients to cellular constituents, while promoting the diffusion of metabolic waste away from the cells. An increase in nutrient penetration distance will promote cell migration away from the scaffold periphery, and the presence of interconnected macropores will augment their ability to migrate [30, 31]. The degradation behavior of

synthetic polymer-based scaffolds is also controlled in part by the permeability of the ECM analogue. Low porosity and permeability scaffolds made of poly(α-hydroxy acids) have exhibited increased rates of degradation due to an increase in autocatalytic activity. Essentially, as the polymers breakdown via hydrolysis, the acidic byproducts become trapped within the scaffold and lower the local pH. This reduced pH then accelerates the degradation of the polymer from the inside out resulting in a rapid loss of mechanical stability [30, 34].

Clinical application

The use of ECM as a commercially available product has grown dramatically in recent years, with the majority of products consisting of decelullarized xenogenic ECM materials. SIS based products such as Restore™, CuffPatch™, Surgisis®, Oasis®, and Durasis® are packaged as sheets and used for tissue reinforcement and wound repair. TEI Biosciences produces a number of products for specialized applications derived of fetal bovine skin. These include TissueMend® for rotator cuff repair, Durepair® for repair of cranial or spinal dura, Xenoform™ for gastrointestinal and urologic repair, SurgiMend™ for soft tissue membranes, and PriMatrix™ for general wound management. Horse and bovine pericardium-based products have been created and used for a number of different repair and reinforcement applications by Pegassus Biologicals (OrthADAPT™, and DurADAPT™) and Synovis Surgical (Veritas®, Dura-Guard®, Vascu-Guard®, and Peri-Guard®), respectively.

Allogenic decellularized ECM-based products have also made it to market for a number of different applications. Alloderm is a human skin product that has been used in

the abdominal wall, breast, and grafting applications. Graft Jacket® is a skin-based product used for foot ulcers, while Axis™ Dermis has been used for pelvic organ prolapse. Another allogenic product on the market is Suspend™, composed of decellularized human fascia lata and used as a urethral sling.

Current with the writing of this chapter, there are four cellular based ECM products on the market. Smith & Nephew produces both Dermagraft™ and Transcyte™. Dermagraft™ is a full thickness diabetic ulcer graft composed of fibroblasts on a bioabsorbable ECM scaffold, while Transcyte™ is a graft for mid to intermediate partial thickness burns made from the ECM produced by human fibroblasts. Organogenesis, Inc. markets Apligraf®, composed of human fibroblasts on a matrix of collagen and secreted ECM, used to treat venous and diabetic foot ulcers. Finally, a product made from bovine collagen seeded with human fibroblasts, OrCel™ is manufactured by Ortec International to treat burn wounds [35].

To date, there are no engineered ECM analogue products in clinical use. While there has been a large amount of funding and research committed to the development of such a product, engineered ECM products are currently limited strictly to the laboratory setting.

Conclusions

Tissue Engineering has made a profound impact on the quality of life for many, and with the field growing at a rapid rate, that number will continue to increase as more exciting and path breaking discoveries are made. Polymeric scaffolds, both synthetic and natural, used as ECM analogues have the potential to replace, and further regenerate new

tissue by providing a suitable environment for cells to be able to communicate through signals and function properly through attachment, differentiation, migration and proliferation. ECM analogues created by different techniques design the structural characteristics needed to mimic the native ECM, which will open the doors to many new clinical options for applications including bone, cartilage, cardiovascular, nerve, skin, ligament, tendon, breast, and liver. Although there are limitations that still stand in the way of having an ideal scaffold, the challenge of designing a successful ECM analogue is slowly being conquered as professionals in the field continue to make significant improvements on a daily basis.

Chapter 2: TISSUE ENGINEERING BLOOD VESSEL REPLACEMENTS

Preface: The following chapter is a combination of sections from two different manuscripts: "Bioengineered vascular grafts: improving vascular tissue engineering through scaffold design" published in Journal of Drug Delivery Science and Technology, 21(3), pg. 211-227, 2011 and "Electrospinning of collagen/biopolymers for regenerative medicine and cardiovascular tissue engineering" published in Advanced Drug Delivery Reviews, 61, pg. 1007-1019, 2009.

Bioengineered vascular grafts: improving vascular tissue engineering through scaffold design

Michael J. McClure, Patricia S. Wolfe, Isaac A. Rodriguez, and Gary L. Bowlin

Department of Biomedical Engineering, Virginia Commonwealth University, Richmond, Virginia 23284

Electrospinning of collagen/biopolymers for regenerative medicine and cardiovascular tissue engineering

Scott A. Sell, Koyal Garg, Patricia S. Wolfe, and Gary L. Bowlin

Department of Biomedical Engineering, Virginia Commonwealth University, Richmond, Virginia 23284

Abstract

Arteriosclerosis has accounted for three quarters of the deaths related to cardiovascular disease (CVD). Arteriosclerosis is a vascular disease that is characterized

by a thickening of the arterial wall and subsequent decrease in the arterial lumen, eventually causing loss of circulation distal to the site of disease. Small diameter arteries (< 6 mm) are affected the most by CVD due to their already decreased blood flow. The increasing populations of people who are obese, diabetic, or aging supplement a strong need for the production of a commercially available small diameter vascular graft. Tissue engineering has become a promising approach for generating a biocompatible vessel with the potential to regenerate new tissue. Multiple factors have to be accounted for when designing a vascular graft that has the ability to self-repair and self-remodel such as the choice of polymer, choice of cell type, and choice of growth conditions. To date, historical landmarks such as the initial research of Weinberg and Bell have led researchers closer and closer to a functional end product [36].

Introduction

Cardiovascular disease, specifically coronary heart disease (CHD) resulting from arteriosclerosis, remains the leading cause of death in the United States and has been so virtually every year since 1900 [37]. Once blood flow in the coronary artery is compromised, vascular bypass is an option to restore blood flow to tissues distal to the restriction or blockage [38]. In 2005 there were 469,000 bypass procedures performed due to CHD [37], which typically involve the replacement of a coronary artery with a patients own saphenous vein or internal mammary artery. Biological grafts are a formidable option since they already retain the natural architecture that arteries require. When these grafts are used as replacements, they begin to adapt to their new environment, altering their structure to match the mechanical requirements of the tissue.

While these autologous replacements have an acceptable patency rate, they are not always a viable option as the patient may also suffer from peripheral vascular disease, affecting upwards of 8 million Americans and up to 20% of those 65 years of age or older [37]. Further complicating the use of autologous vessels is the fact that they are limited in number and a previous bypass operation may have already required the vessel's use [39]. Currently available commercial alternatives to the autologous vessel gold standard are limited to synthetic vessels made of e-PTFE and woven or knitted Dacron®. These materials have been used with moderate success as medium and large diameter prosthetics, but their efficacy is severely limited when used as small diameter vessels. Larger diameter vessels experience higher flows and less resistance than small diameter vessels, such as the popliteal or coronary arteries, where low blood flow and high shear makes the synthetic graft more prone to thrombus formation and intimal hyperplasia [38-49]. Dacron® and e-PTFE grafts are non-degradable and lack the ability to promote native tissue regeneration, making them a permanent fixture in the body. As a permanent fixture, the graft is constantly threatened with attack from the patient's own foreign body response as well as bacterial graft infection [46, 48, 50]. To this extent, a vascular replacement that matches the body's mechanical and cellular requirements is highly necessary in the field of vascular tissue engineering, requiring "ideal" characteristics. A tissue engineered vascular graft needs to meet several criteria to be considered ideal:

1. Easy for surgeons to handle with excellent suture retention and resistance to kinking while remaining flexible.

2. Grafts need to be biocompatible and retain non-toxic, non-thrombogenic, and infection resistant characteristics, all of which are associated with a confluent, quiescent, nonactivated endothelium.

3. They must induce an appropriate healing response that does not result in inflammation, hyperplasia, or fibrous capsule formation.

4. It is necessary for the grafts to be leak resistant yet have sufficient porosity to allow for the ingrowth of autologous tissue, leading to tissue that is indistinguishable from the native vessel.

5. Mechanical strength is a paramount concern where grafts must retain a compliance, the ability to withstand long-term hemodynamic stress without failure, similar to that of native artery to prevent intimal hyperplasia while;

6. Resisting creep and permanent deformation leading to aneurysm formation.

7. Grafts should express physiological properties such as vasoconstriction and relaxation.

8. Finally, they should be easy to manufacture, produce, sterilize, and store, as well as be economical and available off-the-shelf in a variety of sizes [46, 51].

Vascular tissue, more specifically arterial tissue, is subdivided into two separate categories: elastic (> 6 mm inner diameter (ID)) and muscular (< 6 mm ID). The architecture of both elastic and muscular arteries is composed of three separate layers: intima, media, and adventitia, which vary in thickness and composition as a function of anatomic location (Figure 2.1). The intima is the innermost layer of all blood vessels and is composed of a single layer of endothelial cells (EC) lining the vascular wall, a thin basal lamina, and a subendothelial layer containing collagenous bundles, elastic fibrils, smooth muscle cells (SMC), and some fibroblasts (FB). The media, the thickest of the

three layers, is made up of SMC, a various number of laminae depending on location, bundles of collagenous fibrils, and a network of elastin fibrils. The adventitia is the outermost layer of the vessel wall and like the media, its thickness varies as a function of anatomic location, consisting of dense fibroelastic connective tissue containing FB [52, 53]. Incorporated with these three layers, is the vasa vasorum, a network of blood vessels which innervate both the media and adventitial layers to supply oxygen and nutrients to the cells in those regions.

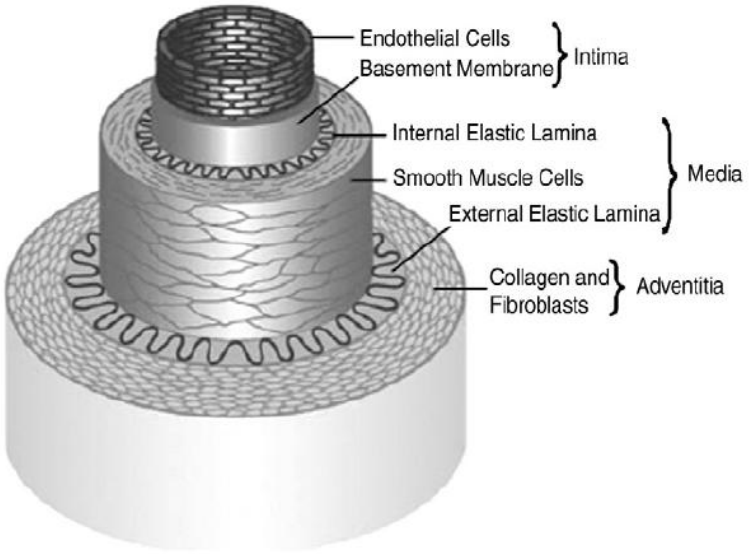

Figure 2.1. Drawing of arterial wall depicting the native tissue's three primary layers: intima, media, adventitia. Reprinted with permission from [44].

As arteries move away from the heart and towards the periphery, their diameter decreases. This decrease in diameter coincides with changes in the architectural makeup. Structurally, the intima is similar in both elastic and muscular arteries and therefore does not affect the overall properties when comparing the two. Instead, both the medial and adventitial layers change in thickness and composition as arteries move away from the heart and toward the periphery. Those arteries with larger diameters, such as the aorta or

carotid, contain a medial layer with SMC and numerous elastic laminae. Muscular arteries, such as the femoral, retain the three layered structure yet their medial layer contains a higher density of SMC and a lower number of elastic laminae. As for the adventitia, elastic arteries contain a relatively thin outer layer that constitutes only 10% of the vascular wall whereas in muscular arteries the adventitia often occupies 50% of the vascular wall. Functionally, for the media, this design change is due to a smaller circumferential stress in the wall of the muscular artery, decreasing the overall demand for elastic recoil and energy dissipation [54], while increases in nerve innervations account for the increased adventitial thickness [52].

Blood vessels are continuously subjected to stress and strain in the circumferential and longitudinal directions. Each layer in the wall plays a significant mechanical role to its proper functionality. *In vivo* studies and clinical observations have shown that decreased values of tensile and shear stress in surgically injured vessels are correlated with activation of cell proliferation and ECM production, leading to vessel occlusion [55]. A decrease in tensile properties is not just a change in the circumferential direction, but a multi-directional change. As a consequence, compliance, hoop stress, and overall hysteretic properties can be affected. These changes can affect cell and fiber orientation.

In addition to circumferential and longitudinal stress, one of the most important stresses exerted on the inner lumen of arterial tissue is shear stress. Arteriosclerosis tends to develop in regions of the circulation where flow is either low or turbulent, such as regions where arteries bifurcate [56-58]. EC respond to increased blood flow by causing the relaxation of the surrounding smooth muscle through nitric oxide. Conversely, decreased flow induces vessel narrowing that is also mediated by signals from the

endothelium, and in severe cases low flow leads to vessel regression and apoptosis of EC [59].

Besides the ultimate importance of shear stress, circumferential stress due to cyclic loading also mediates proper functionality of the arterial wall, preventing arteriosclerosis. Vascular EC sense and respond to cyclic strain both morphologically and phenotypically. However, if hypertension occurs in a blood vessel, EC, in addition to SMC, are highly affected. Accumulating evidence demonstrates that high cyclic strain affects EC, whereby in one study Reape *et al.* found that monocyte chemotactic protein-1 is synthesized when EC are subjected to high mechanical deformation [60], while other studies have found that mechanical strain in hypertensive models influences atherosclerotic plaque development through increased expression of adhesion molecules [61-63]. SMC are mostly affected by increases or decreases in blood pressure. Normal blood pressure and flow allows both SMC and EC to cross-talk and maintain the integrity of the vascular wall over time. If blood pressure rises over a long period of time, signal transduction pathways begin to break down the ECM and remodel the arterial wall, resulting in vascular hypertrophy [64]. If the pathophysiology involved in vascular disease was better understood, then this knowledge may produce vascular graft designs that approach what would be considered ideal.

Historical Vascular Replacements

Vascular grafts have been in the process of development since the late 19th century when Eck attempted the first delineation of a basic technique for vascular suture, performing a lateral anastomosis of the portal vein to the inferior vena cava [65].

However, it was not until the early 20th century when Alexis Carrel explored the basic patterns of healing of arteries and veins, the reactions to different types of sutures, and the possibility of organ transplantation, winning him the Nobel Prize for Physiology or Medicine in 1912 [66].

There were many ventures into bridging the gap of a particular blood vessel. In World War I, German surgeons treated aneurysms by bridging the defect with pieces of the patient's vein [66]. A femoro-popliteal bypass with a reversed saphenous vein graft was first performed by Kunlin in 1948. During the same period, fresh arterial allografts were beginning to be used in human vascular reconstructive surgery. In 1952, Blakemore and Voorhees developed one of the first synthetic vascular prostheses, Vinyon-N cloth, which was used to bridge arterial defects in dogs [67]. Although early clinical results were promising, Vinyon-N did not display sufficient long-term stability, nor did it provide an appropriate scaffold for tissue in-growth. These historical experimentations paved the way towards tissue engineered vascular grafts, and set into motion the quest for the ideal vascular replacement.

Endothelial Cell Seeding

This quest began by modifying materials that were already approved for vascular replacement surgeries, e-PTFE and Dacron. In 1978, Herring *et al.* introduced a single-stage technique whereby venous ECs were seeded onto Dacron grafts with enhanced patency in canine models [68]. Since this point, numerous methodologies have been used to gain a confluent monolayer of ECs: gravitational, hydrostatic, and electrostatic. The most basic and extensively studied of these is gravitational EC seeding. Coating the graft

surface prior to this method of seeding has been performed in many cases. For instance, Zilla and associates have looked into multiple ways in which to increase EC attachment onto e-PTFE grafts through lining the graft with fibronectin [69] and fibrin glue [70]. However, outcomes from these studies demonstrated insufficient cell density, poor adhesion under flow conditions, and failure to achieve confluence. Another major disadvantage of this technique is any surface that is not covered by ECs becomes highly thrombogenic. Poor adhesion of cells under flow conditions was due to a number of factors, one of which being cell seeding duration was too short (<2 hours) [71]. This was leading to a significant loss of cells upon implantation. Therefore, studies such as Shindo *et al.* and Prendiville *et al.* were performed to increase maturation time [72, 73]. Biological glues and adhesive proteins such as fibronectin, collagen, laminin, fibrin, FB matrix, and plasma have been extensively studied as further means to adhere ECs to the inner lumen surface of a vascular graft [74-80]. The necessity for an incubation period to allow for significant adhesion and maturation of ECs is related to the basic nature of the electrostatic interactions between the polymeric graft materials and the cells. Clinically successful vascular prosthetics such as e-PTFE are highly negatively charged, which can repel cells. Several *in vitro* studies have been performed utilizing the electrostatic seeding technique. Bowlin *et al.* found that when umbilical vein ECs were seeded onto e-PTFE through electrostatics, complete nodal area coverage of morphologically mature ECs was obtained within 16 minutes [81]. Using this same technique under flow conditions with a wall shear stress of 15 dynes/cm^2 for up to 120 minutes revealed no significant loss of ECs [82]. However, problems associated with permanent synthetic graft material still pose major hurdles. Therefore, bioresorbable vascular grafts became of interest since they

deviate from the permanent scaffolding and resorb *in situ* while autologous tissue remodels the graft.

Scaffold-Based Approaches to Improve Vascular Grafts

Bioresorbable grafts are advantageous due to the fact that a resorbable vascular prosthetic with adequate mechanical properties can be implanted and degraded gradually over a period of time, leaving behind no permanent synthetic materials to initiate a chronic foreign-body reaction [48]. Through the years, there have been many different approaches. Wesolowski *et al.* first introduced the concept of a bioresorbable vascular prosthetic in the early 1960s. These first bioresorbable incarnations were composed of a variety of Dacron® yarns, collagen coatings, and collagen fibers. The permanent Dacron® provided mechanical stability, while the collagen added bioactivity to the structure and promoted the ingrowth of native tissue as it was degraded and remodeled [83, 84]. The 1970s and '80s saw the advent of a number of different aliphatic polyesters (PLA, PGA, PDO, etc.). These polymers breakdown through hydrolysis in the body, and can have their rate of degradation tailored by altering their structures [48, 85-89]. While this preliminary work failed to result in a successful commercially available graft, it laid the foundation for current research in bioresorbable prosthetics and demonstrated the possibilities of *in situ* tissue engineering. Despite the ability of bioresorbable grafts to have products added to or subtracted from the created matrix to aid the body in regeneration, other approaches find that the body alone is not sufficient enough to sustain a fully regenerative capacity, and that much of that work should be done *in vitro*. This type of tissue engineering approach can be accomplished with the combination of cells

and specific scaffold materials. Regardless of approach, the way in which a scaffold material is designed is equally as important as the source of the cells that are utilized in the experimental procedures.

The ideal cell source should be non-immunogenic, functional and easy to achieve and expand in culture. Cells are arguably the most important element in any tissue engineering model. For an arterial replacement, a functional graft cannot be achieved without an endothelium-like interface to the circulating blood and vasoactive SMC within the wall [90]. Autologous ECs and SMCs isolated from patients themselves are usually the first choice. However, this procedure is quite limited in the number of cells that are able to come from a single biopsy punch of an autologous vascular tissue. Therefore, stem and progenitor cells become a more viable option as they have a higher capacity to expand in culture. Endothelial progenitor cells (EPC) typically circulate throughout the bloodstream and can be isolated using techniques such as those done by Asahara *et al.* [91, 92], where magnetic beads coated with antibodies such as CD34, AC133, or markers common to both early and more differentiated progenitors were used to capture EPC. Autologous bone marrow sources have also shown promise through studies that have been done by Shin'oka *et al.* [93], seeding the cells onto a poly(D,L-lactide-*co*-ε-caprolactone) (PLCL) copolymer and then implanting in humans. Campbell *et al.* have shown that the cells located in the peritoneal cavity display promise, where silicone tubing was implanted into the peritoneal and pleural cavities of dogs for 2-3 weeks, and cells from those cavities migrated onto the tubing, subsequently forming a biological graft material [94, 95]. Nieponice *et al.* has shown how muscle-derived stem cells are also a plausible autologous source for vascular tissue engineering, combining these cells

with poly(ester urethane) (PEUU) scaffolds through a vacuum seeding procedure and implanting them as an aortic interposition bypass graft [96]. Non-autologous cell sources also include those of embryonic stem cells, which have the capability to differentiate into several different cell types including those of the vasculature.

Electrospinning

The resurgent interest in electrospinning in recent years has helped to rejuvenate the research of bioresorbable vascular grafts. One of the main attractions of electrospinning is the fact that it is a simple process, requiring little specialized equipment. A standard electrospinning setup consists of a high voltage power supply, syringe pump, grounded target, and a spinneret (typically a syringe fitted with a blunt tip needle, Figure 2.2). The process itself can be easily performed in a laboratory setting or scaled up for large-scale production with little modification. In brief, a polymer solution is drawn into the spinneret and charged with a large electric potential in the range of several kilovolts. A grounded target is placed a set distance from the charged polymer solution to create a static electric field. When the electric potential reaches a critical level, the electrostatic repulsions of the polymer solution overcomes the surface tension at the tip of the spinneret, and a fine jet of entangled polymer chains is drawn out. This jet whips through the air towards the grounded target, creating a dry fiber through the evaporation of the polymer's solvent. The electrospinning process has the capacity to produce fibers that range from 50 nm to 10 µm in diameter, collected on the grounded target, dependant upon the processing conditions of the polymer solution/solvent used [16, 97-100]. Apart from the simplicity of its setup, the versatility of the electrospinning

process has also made it ideal for tissue engineering. The process is compatible with a wide array of polymers, both natural and synthetic in origin, as well as the combination of any number of different polymers. Polymer solutions can be combined in a single reservoir, spun side by side from separate spinnerets, or layered sequentially to provide a large number of options for altering scaffold properties. In addition, electrospun scaffolds can be created in nearly any shape required, and can consist of fibers in an assortment of orientations [100]. Electrospinning provides researchers with the ability to create, not only flat sheets, but also the seamless tubes required for vascular applications. These tubes can be created in any diameter to fit the specifications of any vascular conduit.

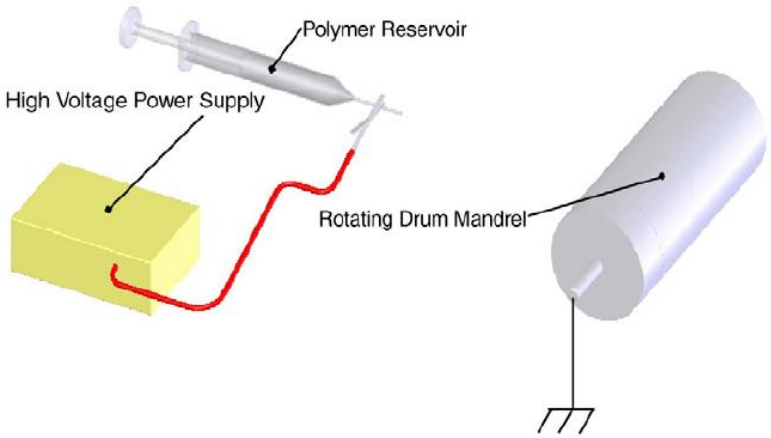

Figure 2.2. Schematic representation of a simple electrospinning setup utilizing a grounded rotating drum as a collection mandrel.

The combination of specific cell types and biomaterials to create a structure which mimics both mechanically and architecturally the native tissue is at the heart of the tissue engineering field. Vascular tissue engineering has looked at a myriad of scaffold-based approaches involving the use of pure polymer, polymer blends, and manufacturing co-polymers to achieve its ideal goal.

Poly(glycolic acid), Poly(lactic acid), and Copolymer Blends

PGA is a biodegradable aliphatic polyester with a glass transition temperature between 35-40°C, melting point between 225-230°C, and a crystalline fraction of 44-55% Table 2.1). Within the field of vascular surgery, PGA was first used as a biomaterial for sutures in the 1970s [101, 102]. In 1983, Lauritzen was the first to conduct preliminary studies on PGA tubes as vessel grafts. This experiment suggested PGA tubes as a promising construct for instant and absorbable microvascular grafts [103]. Since then, various approaches to improving PGA grafts have been developed and extensively studied. Niklason *et al.* fabricated tubular PGA scaffolds with a chemically modified surface (NaOH) and seeded grafts with bovine SMCs exposed to pulsatile flow conditions for 8 weeks. After 8 weeks of culture, the gross appearance of the scaffolds was similar to native arteries with histology showing migration of SMCs forming a smooth luminal surface for EC seeding. After 4 weeks implantation in pigs, scaffolds showed 100% patency [104]. In order to minimize residual polymer fragments after culture, Prabhakar *et al.* treated PGA mesh tubes by exposing them to heat, 1.0M NaOH, and γ-irradiation to hasten degradation. Porcine carotid SMCs were cultured on treated PGA scaffolds under pulsatile conditions. After 8 weeks of culture, treatment with NaOH increased polymer degradation rate under hydrated conditions and NaOH and γ-modified scaffolds showed native vessel morphology, a more even distribution of SMCs, and fewer polymer residual fragments. It was also noted that the collagen content of some scaffolds were approximately similar to that of native vessels, however, the mechanical integrity of the engineered scaffolds was less than native [105]. Boland *et al.* were the first to publish results on electrospun PGA as a tissue engineering scaffold comprised of submicron fiber

diameters. In this study, HCl pretreated PGA scaffolds were incorporated into the surrounding tissue and showed increased cell proliferation rates when implanted in rats [106]. The above studies have demonstrated that independent of scaffold fabrication technique, PGA grafts with a chemically modified surface can serve as potential vascular grafts. More recently, Iwasaki *et al.* bioengineered a three-layered tubular scaffold where PGA, PCL, and PGA layered sheets were seeded with three types of vascular cells under pulsatile conditions to mimic artery structure, integrity, and blood flow. Results from this study demonstrated that the engineered vessels produced sufficient amounts of collagen and elastin and exhibited similar appearance, elasticity, and ultimate strength as native arteries [107].

Table 2.1. PGA, PLA, and Copolymer Blends.

Biodegradable Polymer	Manufacturing Method	Improvement	Cell Seeded	Culture Condition	Ref
PGA					
Nikalson *et al.*	Chemically modified w/ NaOH	Cell attachment and proliferation	SMCs	Pulsatile and Pig Implant	[104]
Prabhakar *et al.*	Mesh tube w/ NaOH, γ-irradiation	Cell attachment and proliferation	SMCs	Pulsatile	[105]
Boland *et al.*	Chemically modified electrospun PGA w/ HCL	Cell proliferation	—	Rat Implant	[106]
Iwasaki *et al.*	PGA, PCL, PGA layered sheets	Cell attachment, proliferation, collagen, and elastin content	EC, SMC, FB	Pulsatile	[107]
PLA/PLLA					
Stitzel *et al.*	Electrospun PLA w/ wound collagen	Cell attachment and orientation	SMC	Static	[108]
Wang *et al.*	Electrospun PLA and silk-gelatin	Mechanical strength	—	—	[109]
Zhu *et al.*	Surface modified w/ gelatin/N-Maleic acyl-chitosan	Cell attachment, proliferation, and high expression of CD31 and vWF	hUVEC	Static	[110]
PGA-PLA					
Hibino *et al.*	PGA and PCL/PLLA woven fabric	No evidence of rupture, infection, calcification, or aneurysm	—	Human Implant	[111]
Mooney *et al.*	PGA mesh coated w/ PLGA	Mechanical properties and cell proliferation	SMC and EC	Static and Rat Implant	[112]
Wen *et al.*	70:30 PLGA sponge	Cell attachment and proliferation	SMC and EC	Static	[113]
Izhar *et al.*	PELA coated filament-wound Lycra	Enhanced healing and mechanical properties	—	Dog Implant	[114]
Roh *et al.*	PGA mesh coated w/ P(CL/LLA)	Pre-seeding led to no calcification, a neo-intima, and neo-tissue formation	BMC	Static and Lamb Implant	[115]

PLA is a biodegradable, aliphatic polyester with a glass transition temperature between 60-65°C, melting temperature between 173-178°C, and crystallinity of approximately 37%. PLA can exist in several distinct isoforms, most commonly as poly-L-lactic acid (PLLA). In the 1980s the first studies were conducted exploring the possibilities of PLA as a vascular graft coating [116] and PLLA as a microporous, compliant, biodegradable vascular graft [117-120]. In 2001 Stitzel *et al.* developed a tubular scaffold comprised of a helical wind of collagen fibers encompassed by a layer of electrospun PLA fibers. After 10 days incubation, SMC formed a 100% confluent

monolayer on the tubular scaffold oriented along the principle stress lines [108]. Within the past few years electrospun PLA and PLLA have been extensively studied and are considered an ideal biomaterial candidate for tissue engineering blood vessels. Wang *et al.* electrospun a tubular graft composed of PLA (outside layer) and silk fibroin-gelatin (inner layer) with a porosity of 82 $\pm$ 2%, breaking strength (2.2 MPa), pliability (60.6%), suture retention strength (4.6 N), and a burst pressure strength of 1596 mmHg [121]. Whereas many PGA studies use surface modifications to achieve desired results, PLA can be more readily used "as is" to produce vascular engineered scaffolds. However, there are certain advantages to chemically modifying PLA surfaces. To improve EC biocompatibility, Zhu *et al.* grafted a gelatin/*N*-Maleic acyl-chitosan (gel/NMCS) complex on the surface of PLA films. This study concluded that gel/NMCS modified PLA enhanced human umbilical vein EC proliferation and expressed a higher structured CD31 and vonWillebrand Factor (vWF), ultimately suggesting photo-initiated grafting of gel/NMCS complexes as an effective method for modifying the surfaces of vascular grafts [110].

PGA and PLA have also been combined to create novel biodegradable vascular tissue engineering scaffolds. Most recently in 2010, Hibino *et al.* developed a tubular woven fabric vascular scaffold composed of PGA and polycaprolactone (PCL)/PLLA which was implanted in 25 human patients as a extracardiac cavopulmonary conduit. After a mean follow up of 5.8 years, scaffolds showed no evidence of rupture, infection, ectopic calcification, aneurysm formation, or scaffold related mortality. One patient had partial thrombosis and four patients had scaffold stenosis but all were successfully treated [122]. PGA and PLA have been combined with each other as well as other polymers to

form new copolymers: PLGA, poly(ethylene glycol/lactic acid) (PELA), and PLLA-PCL to name a few. Overall, the versatility of PGA and PLA fuels the use of these polymers as practical materials for fabricating vascular grafts. Although, both these synthetic polymers have demonstrated promising results there are several drawbacks to using such materials. Both PLA and PGA are stiff and significantly different from native artery, which could lead to hyperplasia at the site of anastomosis. Additionally, PGA's quick degradation characteristics make it desirable for designing a functional artery and dangerous as an implant which could lead to aneurysm or rupture.

Polycaprolactone and Copolymer Blends

PCL is a semicrystalline, non-toxic, tissue compatible biomaterial with a degradation rate of around 12 months (Table 2.2). Mechanically, PCL displays highly desirable characteristics for vascular grafts, mostly high strength and excellent compliance. Surface properties of biomaterials, such as surface roughness, affect cell behavior and may induce thrombotic clots in some cases. Researchers have found that rough and smooth surfaces will encourage different types of cell adhesion [123]. Some groups have attempted to modify the hydrophobic surface of PCL to provide more hydrophilic groups. Zhu *et al.* first looked to modify PCL's surface chemistry with poly(methacrylic acid) (PMAA) [124]. This was accomplished by immersing a PCL membrane in a quartz tube with 30% hydrogen peroxide, and subsequently exposing the tube to UV light. The photo-oxidized membrane was then placed in a copolymerization tube containing 4% PMAA and irradiated with UV, leading to a higher EC attachment when compared to non-modified grafts.

Table 2.2. PCL and Copolymer Blends.

Biodegradable Polymer	Manufacturing Method	Improvement	Cell Seeded	Culture Condition	Ref
PCL					
Zhu *et al.*	Surface modified PCL film w/ PMMA	Cell attachment	EC	Static	[124]
Serrano *et al.*	Surface modified PCL film w/ NaOH	Increased hydrophilicity and cell attachment	EC and SMC	Static	[125]
Ma *et al.*	Surface modified electrospun PCL w/ carboxyl groups	Increased hydrophilicity and cell attachment	EC	Static	[126]
Duling *et al.*	Electrospun PCL	Mechanical properties	—	—	[127]
Pektok *et al.*	Electrospun PCL	*In situ* degradation	—	Rat Implant	[128]
Drilling *et al.*	Different concentrations of electrospun PCL	Optimized burst pressure	—	—	[129]
Lee *et al.*	Thermal treatment of electrospun PCL	Suture retention, burst pressure	—	—	[130]
Vaz *et al.*	Electrospun PCL and PLA	Cell attachment and mechanical properties	FB and myoFB	Static	[131]
Hanson *et al.*	Dip casted PCL and PLA	Mechanical properties	—	Canine	[132]
Watanabe *et al.*	50:50 P(CL/LA) poured into PGA mesh	Mechanical properties and cell attachment	Mixed population from femoral vein	Canine	[133]

Serrano *et al.* used a NaOH treatment of the PCL grafts to provide better adherence of vascular ECs and SMCs through increased hydrophilicity [125]. In this study, PCL films were prepared by hot pressing and then submerged in a solution of 2 N NaOH for two hours. Scanning electron micrographs (SEM) of cell morphology showed both cell types growing properly on NaOH treated films, but untreated films did not seem appropriate substrates to support cell growth by causing cytoplasmic retraction. Serrano *et al.* then followed this preliminary study up 3 years later, evaluating EPC adherence proliferation to NaOH treated films, and the effect of PCL on nitric oxide content [134]. EC-derived cells from EPCs were first characterized using classical markers CD31, von Willebrand factor, and endothelial nitric oxide synthase (eNOS) using flow cytometry, where CD31 is a clear marker of EC maturation. After 4 days, it was found that PCL-NaOH films contained large numbers of cells on their surface; however, PCL films had significantly lower numbers, further demonstrating the benefits of NaOH treatment.

Furthermore, Ma *et al.* improved the surface chemistry of PCL through modification of electrospun fibers with air plasma treatment, introducing carboxyl groups on PCL nanofiber surfaces. These carboxyl groups were then used to bind gelatin to the surface, increasing hydrophilicity and increasing EC proliferation when compared to no treatment [126]. Surface modification of PCL films to increase hydrophilicity, definitively improved scaffold materials for enhanced cellular attachment. However, an implanted vascular graft will not respond well to a tubular film, leading to encapsulation with no cellular infiltration of the scaffold material. For this reason, porous scaffolds have been manufactured through the process of electrospinning.

Mechanically, PCL is a highly desirable material for vascular tissue engineering in addition to other soft tissue applications. Several studies have set out to characterize the mechanical behavior of PCL. Duling *et al.* punched out "dogbone" shapes from electrospun nanofibers to test for stress relaxation, loading response, tensile failure testing, and cyclic stress relaxation, comparing these results using Fung's quasilinear viscoelastic theory [127]. Others have looked at the degradation characteristics both in a rat descending aorta for 24 weeks (Pektok *et al.*) [128], and *in vitro* in Ringer solution stirred gently for 6 months (Bolgen *et al.*) [135]. Pektok *et al.* found that after 24 weeks molecular weight decreased by 20%, while Bolgen found that molecular weight decreased by only 5%, indicating that *in situ* degradation occurs faster. In these cases if degradation occurs too fast or too slow, then the vascular graft will either become too weak and develop an aneurysm or not dissolve out quickly enough causing other downstream affects. Therefore, optimization of graft mechanical and cellular parameters is necessary. Nottelet *et al.* demonstrated an optimal design for electrospun PCL grafts in

a rat model by electrospinning several combinations of solvent/polymer concentrations [136]. Drilling *et al.* optimized burst pressure results of electrospun PCL grafts through analyzing several different solvent/polymer concentrations, resulting in 5 mm diameter grafts that could withstand in excess of 2000 mmHg [129]. Lee *et al.* demonstrated increased mechanical properties through thermal treatment of electrospun PCL grafts, which resulted in increased suture retention and burst pressure, without much change in compliance [130]. While there are many studies surrounding the sole use of PCL as the vascular graft material, other studies have combined PCL and other synthetics by copolymerizing the two structures together or separately manufacturing them.

Vaz *et al.* selected two different polymers to be electrospun together, PCL and PLA, in a multilayered approach, characterizing their properties through uniaxial tensile testing, 3T3 mouse FB, and human venous myofibroblasts (myoFB) [137]. While this study produced good results, the addition of a stiff material such as PLA could significantly reduce compliance and increase the downstream affects of compliance mismatch. Williamson *et al.* created a more compliant, bi-layered structure from a PCL-polyurethane (PU) composite graft by using gravity spun PCL fibers out of acetone and spinning PU fibers directly onto the PCL fibers [138]. In 1988, Hanson *et al.* looked into the mechanical properties of selected copolymers, PLA and PCL [132]. These vascular grafts were dip casted using three different kinds of copolymers to produce single layer and bi-layered grafts. These grafts were then tested for compliance, tensile strength, and kink resistance. Mechanical results looked promising except for compliance, which was significantly lower than a canine femoral artery, where this once again demonstrates the stiffness of PLA. Watanabe *et al.* synthesized a P(CL/LA) copolymer in a 50:50

combination to be poured into a PGA nonwoven fabric and subsequently freeze dried. Mechanical testing, cell seeding, and implantation of the vascular scaffold into the inferior vena cava of a canine were performed with promising results as an "ideal" venous scaffold with antithrombogenic activity [133]. However, a venous graft is not subjected to the same circumferential and shear stresses that occur in the arterial network. Several other PLCL copolymers have been used for vascular tissue engineering applications demonstrating the possible use of bone marrow cells (BMCs) seeded onto scaffolds and implanted into a non-human model [139, 140], and evaluating electrospun PLCL scaffolds with SEM, porosimetry, tensile testing, and cell culture analysis using human umbilical EC [141].

Polydioxanone

PDO is a colorless, crystalline, bioabsorable polymer that was developed specificially for wound closure sutures. PDO exhibits a crystalline fraction of 55% and a glass transition temperature between -10^{o}C and 0^{o}C (Table 2.3). Greisler *et al.* were the first to have published several results on PDO absorbable vascular prosthetics using a mesh tube with 250 μm fiber diameter and 400 μm pore size. Evaluations of these first took place in a rabbit aorta [89] at 2 weeks up to 12 months, displaying myoFB migration occurring in parallel to the macrophage-mediated degradation of the PDO structure. This study was followed with the aorta-iliac canine model using 70% PDO and 30% polypropylene. Results from the study of up to a 1 year implantation demonstrated 86% patency rates compared to Dacron® and ePTFE which had a rate of 68% and 54%, respectively. An additional study examined prostacylin (PGI_2) and thromboxane A_2

(TxA_2) production from the endothelium. The rationale for this was based on the importance of these components with the endothelium non-thrombogenic properties. This is attributed to a balance between PGI_2 and TxA_2 (or the PGI_2/TxA_2 ratio), where it is more desirable to have a higher PGI_2 levels than TxA_2 in native vessels. The results of Greisler's study demonstrated that the explanted PDO graft had the highest ratio of PGI_2/TxA_2 versus PGA and almost equal to native aorta control [142].

Since Dr. Greisler's extensive research using animal models, PDO has only been used in a handful of studies. Teebken *et al.* performed a comparison study between EC seeded decellularized carotid arteries and woven 4 mm diameter PDO prostheses, concluding that decellularized vascular tissue had higher patency rates than that of PDO prostheses [143]. A few years later, Boland *et al.* produced a study on electrospinning PDO into non-woven nanofibers examining the effects of polymer concentration on fiber diameter, pore area, and mechanical properties [144]. This led to several studies out of the same lab to test PDO in combination with biopolymers such as elastin [20, 145-147], collagen [146, 148], and silk [149] to determine both cellular and mechanical behavior. Sell *et al.* developed PDO-elastin vascular conduits using a range of polymer-elastin blends and characterized them utilizing compliance, suture retention, uniaxial tensile testing, and cellular seeding with human dermal FB. Since compliance mismatch between the graft and native artery is one of the major causes of graft failure, the authors of this manuscript have tested several combinations of PDO and elastin in order to determine its mechanical behavior *in vitro* [20]. A difference in this study, compared to other publications of vascular graft compliance, was that compliance was determined under dynamic conditions mimicking physiological parameters, therefore providing a lucid

interpretation as to how the graft should perform in the body. In this study, it was determined that certain PDO/elastin blends closely matched those of native artery.

Mechanical properties, specifically compliance, are of utmost importance in order to prevent a mismatch and ultimately intimal hyperplasia at the site of anastomosis; however, chemical properties of the vascular materials once implanted inside the body must also be evaluated so as to determine the material's response to monocytes and macrophages *in vivo*. Garg *et al.* aimed to evaluate the angiogenic potential of PDO-elastin vascular grafts to promote *in situ* arterial tissue regeneration by measuring the amount of vascular endothelial growth factor (VEGF), acidic fibroblast growth factor (aFGF), basic fibroblast growth factor (bFGF), and transforming growth factor beta-1 (TGF-β1) released upon interaction between the macrophages and the polymer-elastin blend [150]. Results demonstrated that macrophages remained on the surface of high elastin content PDO-elastin blends, but penetrated both low elastin content blends and pure PDO grafts. As a consequence, at day 28 VEGF was high for all grafts, aFGF was found to remain largely independent of graft material, and TGF- β1 was gradually decreased from day 7 to day 21. Through these studies, PDO has proven itself to retain low thrombogenicity and excellent mechanical properties by itself and when blended with other biopolymers. However, more information still needs to be examined in regards to cellularization of the scaffold materials and degradation characterization.

Polyester Urethane Urea

For engineering soft tissues such as the vascular system, elastic scaffolds are highly desirable since they are amenable to mechanical conditioning regimens that might

be desirable to tissue development [151]. Martz *et al.* developed one of the first small diameter vascular graft from Mitrathane, a polyether urethane urea (Table 2.3) [152]. However, after a subsequent study in a canine carotid artery, all grafts were occluded after 4 to 6 months [153]. Since then, polyurethanes have been redeveloped by Wagner and associates through synthesis of two kinds of biodegradable polyurethaneureas, namely PEUU and poly(ether ester urethane)urea (PEEUU) from PCL, polycaprolactone-b-polyethylene glycol-b-polycaprolactone, 1,4-diisocyanatobutane and putrescine. Grafts were fabricated by thermally induced phase separation and subsequent solvent extraction. Hydrolytic degradation of the grafts demonstrated a clear loss in scaffold weight after 56 days. Grafts were also conducive to SMC attachment and growth after 7 days in culture [151]. This sparked the use of PEUU by both the Wagner and Vorp labs using several different scenarios: electrospinning to form a whole tube [154], electrospinning on top of a porcine internal jugular vein as a reinforcement for venous graft replacements [155], thermally induced phase separation (TIPS) to create a tubular scaffold for cell seeding with muscle derived stem cells [156], a TIPS tubular scaffold with an additional electrospun PEUU layer on top [157], and a blended electrospun scaffold using PEUU and poly(2-methacryloyloxyethyl phosphorylcholine-co-methacryloyloxyethyl butylurethane) [158]. These studies have had excellent results in terms of mechanical properties associated with their application and cellular seeding and proliferation *in vitro* and *in situ*. However, one of the possible disadvantages of using PEUU, especially in human implantation models, is its cytotoxicity due to the urethane component as the scaffold material degrades.

Table 2.3. PDO and PEUU.

Biodegradable Polymer	Manufacturing Method	Improvement	Cell Seeded	Culture Condition	Ref
PDO					
Greisler *et al.*	70:30 PDO:Polypropylene Mesh Tube	Lower thrombogenic properties compared to PGA	—	Rabbit Aorta	[142]
Boland *et al.*	Electrospun PDO	Mechanical properties	—	—	[144]
Sell *et al.*	Electrospun PDO and elastin	Mechanical properties and compliance	FB	Static	[20]
Garg *et al.*	Electrospun PDO and elastin	Cell penetration of low elastin content	Macrophage	Static	[150]
Wolfe *et al.*	Electrospun PDO	Low thrombogenic potential	Monocyte	Static	[159]
PEUU					
Wagner, Vorp, *et al.*	Thermally induced phase separation and electrospun PEUU	Cell attachment, proliferation, and mechanical properties	SMC and Pericytes	Static and Vacuum Seeding	[151, 154-158]

Collagen

Collagen is the most abundant protein in the human body, a key element of the ECM, and imparts structural integrity and tensile strength to tissues. Tissue disruption following injury requires collagen for the repair and restoration of structure and function. Excessive collagen deposition at a wound site results in loss of anatomical structure, function and fibrosis. Conversely, if insufficient amounts of collagen are deposited, the wound is weak and may rupture [160]. This confers directly towards vascular tissue engineering; a vascular graft can be initially strong due to a synthetic polymer, however, once degradation occurs to a point where that strength is lost, there must be something to take over the mechanical requirements. In this case, not enough collagen remodeling will cause the graft to develop an aneurysm and rupture.

Collagen has been used in a variety of tissue engineering applications because of its predominance in the ECM, non-immunogenicity and available methods of isolation from a variety of sources (Table 2.4). However, the typical procedures used to isolate and

reprocess this natural scaffolding into an engineered material may compromise many of its biological and structural properties [5]. Collagen fibers also possess some unique structural properties important for tissue engineering: they transmit forces, dissipate energy, prevent premature mechanical failure and provide biological signals to adjacent cells that regulate functional responses. Additionally, collagen is resorbable, has high water affinity, low antigenicity, very good cell compatibility and ability to promote tissue regeneration [161]. These factors combine to make collagen one of the most ideal biopolymers available for tissue engineering applications.

In vascular tissue engineering, collagen alone has been used in a number of applications. In 1986, Weinberg and Bell were the first to pioneer the idea of living blood vessels produced *in vitro* using cell seeded collagen gel tubes [36]. The Weinberg and Bell arterial graft consisted of an adventitia of bovine FBs embedded in a collagen gel; a media of gelled collagen and bovine SMCs, and a lumen lined by ECs. One of the main limitations of this approach was the lack of mechanical strength, demonstrating a burst pressure of only 90 mmHg. Investigators thereafter have attempted a number of other strategies to increase burst pressure strength, and maintain the biological aspect using ECs and SMCs. Berglund *et al.* mixed collagen and human dermal FBs together in the form of gels, which were subsequently crosslinked under different conditions to impart higher mechanical strength, resulting in a burst pressure over 600 mmHg [162]. Cummings *et al.* performed a similar experiment using the same manufacturing protocol, but with higher concentrations of collagen and no cross-linking [163]. Matthews *et al.* forewent the collagen gel construct and used electrospinning. Cells were well incorporated into cylindrical collagen constructs placed in a 55 mL bioreactor with aortic

SMCs [164]. Collagen by itself provides a construct that is advantageous for cellular seeding, but comes with drawbacks mechanically. Therefore, synthetic biodegradables are highly desired to provide mechanical stability for collagen-based grafts. PCL and collagen constructs have been studied extensively and have been produced mostly through the form of electrospinning [165-167]. Each of the studies found that when PCL and collagen were combined, collagen provided increased cellular attachment and proliferation for FBs, ECs, and SMCs. Additionally, Ju *et al.* found that fiber diameter highly affected SMC penetration of the PCL/collagen scaffolds under static culture. Other synthetics that have been investigated include electrospun PDO/collagen [148], surface modified electrospun PLLA-co-CL with an air plasma coating of collagen [168], a porous collagen mold with electrospun PLGA [169], and a combined collagen gel/particulate leached PLCL graft [170], where each study has clearly shown the cellular benefits associated with the addition of collagen. Collagen is a very attractive protein to add to vascular grafts, increasing adhesive properties and cellular infiltration and penetration. However, mechanically it can add significant stiffness to the material; therefore the proper amounts of collagen need to be paid special attention when utilizing it.

Elastin

In vivo, elastin is a chemically inert, highly insoluble polymer composed of covalently cross-linked molecules of its precursor, tropoelastin, a soluble, non-glycosylated and highly hydrophobic protein. Tropoelastin expression and subsequent elastin synthesis typically occurs in FBs, vascular SMCs, ECs, and chondrocytes [171]. During the process of elastogenesis, tropoelastin is synthesized, preventing its premature

intracellular aggregation and protecting it from proteolytic degradation by binding a 67 kDa galactoectin (elastin binding protein, EBP). This association lasts until the complex is excreted into the extracellular space. EBP then interacts with galactosugars of the microfibrils, dramatically decreasing its own affinity for tropoelastin. In order for proper elastogenesis to occur, the interaction of the N-terminal part of the microfibrillar-associated glycoprotein with the C-terminal end of tropoelastin is required. Once aligned, lysyl oxidase deaminates and oxidizes the lysyl residues to allysine following the action of Cu^{2+}. Cross-links are then formed by the reaction of the allysines with themselves or with an unmodified lysine [171-173].

As a biomaterial, elastin is becoming more and more popular for tissue engineering applications as one of the main structural components of the vascular ECM (Table 2.4). The incorporation of elastin into biomaterials has been used in several different forms, including insoluble elastin occurring in autografts, allografts, xenografts, decellularized ECM, and in purified elastin preparations where the insoluble elastin is hydrolyzed to a soluble form of α, β, and κ elastin [174]. Although insoluble elastin in its different graft forms could be considered a more "natural state," there is an advantage to its solubility which makes handling and analysis of the material more straightforward. Additionally, elastin peptides influence signaling, chemotaxis, proliferation, and protease release via the elastin receptor [175]. Daamen *et al.* not only found that solubilized elastin induced angiogenesis, but also increased elastic fiber synthesis and displayed no signs of calcification when compared to grafts containing its insoluble form [176]. Leach *et al.* created α-elastin discs using a diepoxy crosslinker, finding that vascular SMCs adhered

well to the substrates [177]. This is one of many studies that have proven soluble elastin to be an advantageous biopolymer.

As stated previously, tropoelastin provides the necessary building blocks to form native elastin *in vivo*. Li *et al.* demonstrated that recombinant human tropoelastin could be electrospun to form both nanofibers and microfibers, depending on the delivery rate [178]. In their study, both tropoelastin and solubilized α-elastin were electrospun. The parameters were optimized and the final products were compared through microscopy, mechanical tensile moduli, and cellular activity with human embryonic palatal mesenchymal cells. Welsh *et al.* manufactured crosslinked elastin-like polypeptide films, and performed tensile testing where stress-strain curves produced the low stress toe region of native tissue J-curves [179]. Again, like collagen, elastin by itself will fail to perform properly under the physiological stresses imposed by the vasculature. Investigators have looked into the combination of elastin and synthetic materials. As mentioned previously, PDO/elastin grafts were electrospun and tested mechanically to find that certain blends emerged as comparable to native artery [20]. This study subsequently led to another blending PDO and elastin in a layered fashion with PDO sutures as reinforcement between each layer [145]. Elastin-like polypeptide has also been implemented into vascular tissue engineering. Nicol and Urry explored the possibility of incorporating cell recognition peptide sequences into ELPs in order to promote EC adhesion, finding that too small an amount of RGD sequence significantly decreased cellular attachment [180]. More recently, tropoelastin was combined with PCL to form a bi-layered vascular scaffold with pure electrospun tropoelastin on the inner layer and combined PCL/tropoelastin on the outer layer [181]. Results displayed enhanced EC

interaction, improved blood compatibility, excellent mechanical properties, and full cell penetration of the scaffold structure when implanted *in situ*. While elastin is known as an essential, key factor in vascular arteries, its addition to scaffold materials comes with both advantages and disadvantages. Mechanically, elastin enhances compliance and distensibility of scaffold material. From the cellular perspective, it has come with mixed results where specific types of elastin are conducive to cellular attachment and others are not. These factors must be considered when working with elastin as a biomaterial.

Combined Elastin and Collagen

As collagen and elastin are two of the most prevalent protein constituents in native vessel, it is only logical that they are often used in concert as tissue engineering scaffolds for vascular applications (Table 2.4). Berglund *et al.* looked to take their previous collagen gel study and enhance its biomechanical properties through the incorporation of organized intact elastin to form hybrid constructs [182]. Histological staining from the study revealed that both the collagen gel control and the collagen/elastin hybrid exhibited dense layers of cells along their outer walls. Additionally, elastin incorporation increased mechanical properties by 11 fold. Boland *et al.* [38], in an attempt to create a biomimicking layered vascular structure, first electrospun an 80/20 collagen type I/elastin tube on a 4 mm diameter mandrel. This tube was subsequently seeded with both FBs and SMCs. Another tubular scaffold of 30/70 collagen type I/elastin was electrospun on a 2 mm diameter mandrel. This electrospun scaffold was then inserted into the 4 mm diameter scaffold and the lumen was filled with a SMC suspension. After 3 days in culture, a suspension of human umbilical vascular

endothelial cells (HUVEC) was injected into the lumen, and the entire construct was cultured for 2 more days. Histological examination revealed complete cellular infiltration into the three-layered construct after 21 days. The artificial intima was covered by morphologically mature ECs and SMCs were present throughout the media, and had begun to align circumferentially around the axis of the scaffold. The FBs and SMCs in the adventitia created a dense population throughout the outermost wall. This study proved that an electrospun scaffold that mimics the native ECM is highly beneficial in the field of vascular tissue engineering. However, the lack of synthetic polymers in the tubular structures did not allow for sustained mechanical viability.

In a study by Buttafoco *et al.* [183], soluble collagen type I from calf skin and soluble elastin from bovine neck ligament were electrospun from aqueous acidic solutions in order to avoid the use of organic solvents. To ensure continuous and homogenous fibers, poly(ethylene oxide) (PEO) and sodium chloride (NaCl) was added. Meshes composed of fibers with diameters ranging from 220 to 600 nm were obtained by spinning the collagen/elastin solutions. Scaffolds completely devoid of PEO and NaCl were obtained by cross-linking with 1-ethyl-3-(3-dimethylaminopropyl)carbodiimide (EDC) and N-hydroxysuccinimide (NHS). SMC were successfully cultured on cross-linked scaffolds and a confluent layer of cells was observed after 14 days on the surface of the different scaffolds.

Combinations of collagen and elastin with synthetic polymers have also been used in order to create scaffold and graft materials with desirable mechanical properties, bioactivity, and sustained mechanical integrity. Nanofiber grafts were fabricated using a mixture of 40% collagen type I, 15% elastin and 45% PLGA by weight electrospun onto

a 4.75 mm diameter cylindrical mandrel. Compliance testing results showed that the diameter change was approximately 9% for native vessels and 12–14% for electrospun grafts under a physiologic pressure range. *In vitro* cell proliferation of SMC and EC showed an average of 82% of SMCs and 72% of ECs survived on the grafts [184].

In a similar study, an array of synthetic materials with 45% collagen, 15 % elastin, and 40% biodegradable synthetic (PLGA, poly(L-lactide) (PLLA), PCL, and poly(D,L-lactide-*co*-ε-caprolactone) (PLCL)) were electrospun. Tubular grafts were characterized through SEM, uniaxial tensile testing, and biocompatibility. Once again it was demonstrated that graft mechanical properties were improved with the addition of synthetic polymers. This study also demonstrated that in order for a graft to remain patent when using biopolymers such as collagen and elastin, the addition of a synthetic is necessary for sustained stability [185]. Recently studies have come out that have looked to mimic the natural architecture of blood vessels with the use of synthetic polymers, collagen, and elastin. McClure *et al.* used electrospun PCL, elastin, and collagen in different ratios to develop a cross-linked mechanically tunable vascular graft characterized by compliance, tensile properties, suture retention, and burst pressure strength [186]. Thomas *et al.* performed a similar study with the use of an uncross-linked, electrospun polyglyconate, elastin, and gelatin, demonstrating a distinctive tri-layered design [187]. Working with the natural polymers and architecture that are provided by Mother Nature could prove to be an advantageous method for vascular tissue engineering.

Table 2.4. Collagen, Elastin, and Collagen/Elastin Blends.

Biopolymer	Manufacturing Method	Improvement	Cell Seeded	Culture Condition	Ref
Collagen					
Weinberg and Bell	Collagen gel	Cell proliferation	SMC, FB, and EC	Static	[36]
Berglund *et al.*	Crosslinked collagen gel	Mechanical strength	FB	Static	[162]
Cummings *et al.*	High concentration collagen gel	Mechanical strength	SMC	Cyclic mechanical stimulation	[163]
Matthews *et al.*	Electrospun collagen	Collagen nanofibers for cell attachment and proliferation	SMC	Rotary Bioreactor	[164]
Elastin					
Leach *et al.*	Crosslinked elastin discs	Cell attachment	SMC	Static	[177]
Li *et al.*	Electrospun tropoelastin	Mechanical elasticity and cell attachment	Meschymal Stem Cell	Static	[178]
Welsh *et al.*	Elastin-like polypeptide film	Stress-strain curve	—	—	[179]
Collagen and Elastin					
Berglund *et al.*	Collagen and elastin gel	Mechanical properties and cell proliferation	FB	Static	[182]
Boland *et al.*	Electrospun collagen and elastin in three layers	Cell proliferation and native arterial architecture	FB, SMC, EC	Rotary Bioreactor	[38]
Buttafoco *et al.*	Electrospun collagen and elastin with PEO and NaCl additives	Cell attachment and proliferation	SMC	Static	[183]
McClure *et al.*	Crosslinked electrospun PCL, collagen, and elastin	Mechanical compliance and burst pressure with tunable properties	—	—	[186]
Thomas *et al.*	Uncrosslinked electrospun elastin, gelatin, polyglyconate	Tunable properties	—	—	[187]

Decellularized Vessels

One obvious choice for vascular tissue engineering is finding a hollow tissue with the appropriate extracellular matrix components and removing cells from the construct (Table 2.5). Several types of decellularized tissues have already been developed including human veins [188], bovine ureters [189], canine arteries [190], and small intestine submuscosa (SIS) [191]. Results found varying signs of proximal and distal hyperplasia with a varying patency rate between 40 and 100%. Lantz *et al.* grafted dog jejunal submucosa as an autologous vascular graft and found that after 28 days the graft was histologically similar to native vessel [192]. More recently, Gui *et al.* developed a

decellularized human umbilical artery with a compliance of 4.3%/100 mmHg and a max burst pressure of 970 mmHg [193]. As most of the aforementioned decellularized matrices were collagen-based, there are some groups who have looked into elastin-based products. Lu *et al.* utilized the Rasmussen protocol [194] on aorta samples to obtain an elastin network [195]. The advantage of elastin-based scaffolds is their distensibility, which, according to the experiment, remained the same as native aorta and significantly higher than collagen-based aorta tested under the same conditions; however, tensile strength was severely decreased. Additionally, hDF studies revealed that elastin based scaffolds had a higher degree of cellular infiltration after 28 days in rotary culture. Berglund *et al.* used the Starcher and Galione extraction method [196] with carotid arteries [182]. These elastin grafts were repopulated using cells encapsulated in a collagen gel, cultured, and then tested mechanically. Positive aspects of decellularized tissues include a more "off the shelf" type graft with no maturation time. However, despite a readily available supply of artificial arteries is attractive, drawbacks include the inability to tailor the matrix content and architecture.

Fully Biological Grafts

The concept of a completely biological living graft implies the ability to remodel, grow, self-repair and respond to the immediate environment (Table 2.5). The graft would also contain enough collagen and elastin proteins to display desirable viscoelastic properties, and would lack any synthetic foreign material that would initiate chronic inflammatory responses or be susceptible to infection [67]. L'Heureux developed an approach to biological scaffolds using human FBs and vascular SMCs in sheet form,

which were subsequently wrapped around a PTFE coated mandrel [197]. The assembled constructs required an 8 week maturation period and were then seeded with human ECs, resulting in burst pressures able to withstand 2000 mmHg. Recently, L'Heureux and associates have performed a human trial using rolled cell sheets for radial artery, A-V shunts, and lower limb indications. This study demonstrated grafts that were able to withstand burst pressures in excess of 3000 mmHg while retaining an average compliance of 8.8%/100 mmHg after 6 months implantation [198]. Campbell *et al.* produced another graft through an inflammatory reaction, where a silastic tube was placed in the peritoneal cavity of rats and rabbits for 2 weeks and was covered in a layered fashion with myoFBs, collagen matrix, and a single layer of mesothelium [94]. Lengths of myoFB-rich tubes were then grafted by end-to-end anastomoses into the carotid artery of a rabbit and the abdominal aorta of a rat. *In situ*, cells responded to local environmental cues, remodeled, and produced structures similar to those of native vessel. More recently, Stickler *et al.* aimed to assess the possibility to strengthen these peritoneal cavity grafts, shortening the time for development [199]. This was achieved through the use of an implantable device which consisted of an inner stretchable tub, a perforated external tube and a transabdominal tube. So, as tissue grew onto the device, it was subjected to cyclic stretch to enhance growth. Mechanically, pulsed tubes displayed a significantly higher failure strength and failure strain compared to unpulsed tissue. This was most likely attributed to the higher organization of collagen in the circumferential direction. While work in the area of fully biological grafts has demonstrated promise in vascular tissue engineering, there are still some drawbacks to the process, including

culture time, risk of infection during the culture period, and a prolonged maturation time that takes away from "off the shelf" capabilities.

Table 2.5. Decellularized and Fully Biological Grafts.

Biopolymer	Manufacturing Method	Improvement	Cell Seeded	Culture Condition	Ref
Decellularized					
Lantz *et al.*	Jejunal submucosa	Histologically similar	—	Canine implant	[200]
Gui *et al.*	Umbilical artery	Compliance and burst pressure	—	—	[193]
Lu *et al.*	Aorta with elastin network	Higher cell penetration	FB	Rotary Bioreactor	[195]
Berglund *et al.*	Carotid artery with collagen gel	Mechanical properties	FB	Static	[182]
Fully Biological Graft					
L'Heureux *et al.*	Rolled SMC sheets	Mechanical properties and autologous cell use	SMC	Static	[197]
Campbell *et al.*	Silastic tube in peritoneal cavity	Structure similar to native vessel	—	Rat Implant	[94]
Stickler *et al.*	Silastic tube in peritoneal cavity with cylic strain	Mechanical properties	—	—	[199]

Drug Delivery for Improved Vascular Grafts

Delivery of growth factors from scaffolds has been gaining interest as a therapy for a variety of tissue engineering applications, including vascular graft regeneration (Table 2.6). Growth factors play a critical role in the communication and information transfer between cells and their environment by binding to specific receptors on cell surfaces. They modulate a variety of cell activities, including proliferation, differentiation, migration, adhesion, and gene expression. Due to their ability to play such a key role in cell activity, cell fate, tissue development, and repair, especially in the vascular system, it is no surprise that their use in therapies has been proposed. However, their success in clinical applications has been limited, partly due to the cost related to the purchasing of recombinant or isolated proteins. In addition, the delivery of one, or several, factors in clinical therapies is complicated, as there is limited knowledge behind

the signaling and release of growth factors that occurs between cells and the physiological environment. In addition, there are several parameters that must be considered, including the delivery vehicle, the quantity/concentration of factor to deliver, the duration of the delivery, and the ability to control the release both temporally and spatially [201-205]. Furthermore, the route of travel by the growth factor(s)/drug(s) once it is delivered is also an important parameter, particularly if there could be a potential detrimental effect downstream.

Growth factors that play key roles in the angiogenic process necessary for vascular graft regeneration include VEGF, FGF, platelet derived growth factor-BB (PDGF-BB), stromal cell-derived factor-1α (SDF-1α), TGF-β, and angiopoietins-1 and 2 (Ang-1 and 2). VEGF and bFGF are heparin-binding growth factors involved in the initiation of the process, promoting EC proliferation and migration. PDGF-BB recruits SMCs and pericytes which, along with TGF-β, promote ECM deposition to stabilize neovessels [202]. SDF-1 plays an important role in angiogenesis as well by recruiting EPCs from the bone marrow [206]. For vascular applications, numerous studies have been performed on the delivery of these growth factors, either alone, or in concert with one or two others, with the use of different delivery vehicles, as well as different delivery methods.

Table 2.6. Biopolymers and Synthetic Polymers for Drug Delivery.

Drug Delivery	Drug Additive	Improvement	Cell Seeded	Culture Condition	Ref
Biopolymers					
Pang *et al.*	R136K to bind to collagen scaffolds	Lower thrombogenic properties	—	—	[207]
Wissink *et al.*	Immobilized heparin onto collagen scaffolds	Increased amounts of bFGF to material and cell proliferation	EC	Static	[208]
Synthetic Polymers					
Thevenot *et al.*	PLGA salt-leached scaffold injected with SDF-1α	Cell proliferation, angiogenesis, lower inflammatory response	EPC and MSC	Mouse Implant	[209]
Mooney *et al.*	VEGF and PDGF-BB released from PLGA scaffolds	Increased angiogenesis and maturation	—	Hindlimb Ischemia Model	[210]
Saif *et al.*	VEGF, HGF, Ang-1 released form PLGA scaffolds	Increased angiogenesis and maturation	EPC	Hindlimb Ischemia Model	[211]

Delivery Methods and Vehicles

Traditionally, growth factors are administered systemically (transdermal), orally, or intravenously. However, these methods of delivery are likely to be ineffective due to the short half-lives of the growth factors, their relatively large size, slow tissue penetration, and their potential toxicity at high systemic levels [202, 203]. For these reasons, polymeric materials, both natural and synthetic, are frequently used as delivery vehicles. Using polymers for this application allows for a more timely and spatially controlled delivery. Biomaterials used for this function must be nonimmunogenic, have degradation products that are soluble and nontoxic, and must be able to be produced sterile and free of infectious pathogens [204]. While natural polymers are beneficial due to their bioactive factor for cell recognition and degradation, synthetic polymers have very controlled and reproducible chemical and physical properties. Another attractive feature of natural polymers are that some have specific binding sequences for and intermolecular interactions with many angiogenic growth factors [212].

Natural Derived Polymers

Natural polymers that have been previously used for delivery vehicles include alginate [213-215], agarose [216], chitosan [217, 218], gelatin [219, 220], fibrin [221], and collagen [222-225]. They are often formed as a gel, or as microspheres, and are usually processed by freeze-drying or cross-linking in an aqueous solution [226].

Often, fibrin glue, which is a mixture of fibrinogen and thrombin, is used therapeutically, as it serves as a temporary platform for the gradual development of granulation tissue. Clinical application of fibrin glue has been studied as a carrier of angiogenic growth factors to create a confluent endothelium on the luminal surface of synthetic vascular grafts [221, 227]. After coating e-PTFE grafts with fibrin glue and FGF-1, it was found to produce better EC retention and expansion after seeding, eliminating graft thrombogenicity and improving graft patency [228]. Recently, Pang *et al.* studied the affinity and distribution of a fusion protein consisting of R136K, a relatively thrombin-resistant mutant derivative of FGF-1, and a collagen-binding domain, to 3-D collagen scaffolds [207]. They found that R136K-collagen binding domain had a greater affinity for collagen scaffolds than either R136K or FGF-1, demonstrating a 1.7 fold lower release rate.

To suppress initial burst release often seen in hydrogel-type delivery systems, and still permit longer retention in the delivery carrier, heparinization has been proposed, either by covalent conjugation of heparin molecules, or the encapsulation of growth factor together with heparin-binding material within the delivery vehicle. Modifying the network structure, such as cross-linking with glutaraldehyde, has also been done, so as to couple the rate of release to the rate of matrix degradation [229, 230]. Other studies have

used EDC and NHS to cross-link collagen and heparin, or collagen and heparin sulfate, enhancing growth factor capture within the hydrogel, enhancing HUVEC expansion onto the graft [208], and producing a strong and stable vascularization throughout the hydrogel in a subcutaneous implant [231].

Synthetic Derived Polymers

Synthetic matrices that studies have reported on have been composed of poly(vinyl alcohol) (PVA), poly(alpha-hydroxyester)s including poly(ethylene glycol) (PEG) [232], PLGA [233-238], PLLA, or PCL [239], polyanhydrides, and polyorthoesters [220, 240]. They are typically processed into porous grafts that provide mechanical support for cells or microspheres for injection and are fabricated by techniques such as solvent casting, gas foaming, particulate leaching, double emulsion, electrospinning, and rapid prototyping [226]. Synthetic matrices for this application must completely degrade and be resorbed into the body, and must temporarily act as mechanical support to allow cells to infiltrate and produce native ECM.

A PLGA salt-leached scaffold injected with SDF-1α was implanted subcutaneously into mice to determine the ability of the scaffold to promote stem cell recruitment, reduce inflammatory response and fibrosis, and enhance angiogenic processes [209]. MSC migration and EPC engraftment near the SDF-1α incorporated scaffold were found to be enhanced after 7 days over a PLGA control scaffold. In addition, there was decreased inflammatory cell recruitment, with reduced fibrotic capsule formation and proinflammatory cytokines around the scaffold. Histological analysis illustrated improved angiogenesis by EPCs throughout the SDF-1α incorporated

scaffold over a PLGA control scaffold, with vessel-like formations occurring at the interface of the scaffold. The results from this study demonstrate the potential for these SDF-1α incorporated scaffolds to be used in vascular graft applications, as they elicit improved tissue response and regeneration.

Angiogenesis and tissue survival after implantation is essential for the survival of any implant, including tissue engineered vascular grafts. Dual growth factor delivery from synthetic grafts was first reported by Mooney's group, where both VEGF and PDGF-BB were released with distinct kinetics from grafts of PLGA fabricated by a high-pressure carbon dioxide process [210]. In looking at blood vessel size and distribution in a hindlimb ischemia model, relative to either growth factor delivered individually, both vessel size and distribution were improved when the delivery of the two growth factors were together. This demonstrates that therapies involving growth factor delivery for angiogenesis would benefit from the actions of multiple growth factors over just a single delivery. For this study, VEGF was responsible for the increase in blood vessel density, whereas PDGF contributed to the maturation and size of the blood vessels. Another study fabricated PLGA grafts from gas foaming and particulate leaching with VEGF and PDGF incorporated into different layers of the graft [241]. This layered graft system allowed compartmentalization of VEGF and PDGF and controlled spatial and temporal presentation of the growth factors.

Saif *et al.* took it a step further and incorporated three growth factors into a scaffold for delivery. In a murine hindlimb ischemia model, PLGA microparticles were fabricated containing VEGF, hepatocyte growth factor (HGF), and Ang-1 using a double emulsion technique [211]. These microparticles, along with cord blood-derived vascular

progenitor cells, were coadministered into the hindlimb of a mouse. This resulted in a robust enhancement of vascularization, superior to any single growth factor administered. Including increased muscular capillary density and enhanced number of conductant vessels, with sufficient vessel stabilization and maturation.

In the presence of TGF- β1, SMCs cultured on adhesive ligand-modified glass surfaces, specifically Arg-Gly-Asp-Ser (RGDS)-modified surfaces, increased matrix production. In addition, tethering TGF- β1 to PEGdiacrylate hydrogel with RGDS resulted in a significant increase in matrix production over the same amount of soluble, unmodified TGF- β1 incorporated into scaffolds, most likely due to the diffusion of the soluble growth factor into the culture medium [232].

The authors of this paper have successfully electrospun lyophilized PRP with PCL to form nanofibrous grafts [242]. As PRP contains various supraphysiologic, autologous growth factors and cytokines that enhance healing, its addition to a synthetic construct has the potential to increase the bioactivity of the graft and enhance regeneration through the release of growth factors contained within the PRP. Results from a protein assay have demonstrated successful release from the electrospun grafts for 35 days, as well as quantifiable release of PDGF-BB over 14 days. The PRP containing grafts were also chemotactic towards macrophages, and significantly enhanced proliferation of adipose derived stem cells over synthetic grafts. These results are promising for the use of electrospun grafts incorporated with PRP as an improved therapeutic strategy for tissue engineering applications such as vascular grafts.

Other growth factors/drugs used to improve scaffolds for vascular graft applications include heparin [243], a known anticoagulant, insulin [244], nitric oxide

[245, 246], a known vasodilator and mediator of EC growth and function, cyclosporine [247], a potent immunosuppressive that inhibits SMC proliferation and intimal hyperplasia, and other antibiotics. A study by Javerliat *et al.* implanted vascular grafts preloaded with antibiotics, rifampin and tobramycin, into the infrarenal aortas of dogs [248]. The grafts implanted were: gelatin-sealed knitted polyester grafts used as controls, and antiobiotic-bonded gelatin-sealed knitted polyester grafts loaded with rifampin and tobramycin at normal doses, and twice the normal doses. After 21 days, histological analysis of the grafts revealed complete patency of all grafts, with no signs of local toxic response to the antiobiotics. Healing of the preloaded grafts, whether at standard or twice standard loading of antibiotics, was always similar to that of the conventional gelatin-sealed grafts, with no signs of poor healing. These results are encouraging, seeing as how vascular prosthetic infections still remain a serious complication of vascular surgery.

Conclusion

Despite the many obstacles to overcome in the creation of a successful vascular graft, research from the last 10 years has exponentially increased our knowledge and understanding of what is required of a vascular substitute. Biohybrid and tissue engineered vascular grafts have been investigated using material properties, complex tissue culture, and cell seeding techniques. Investigators have looked at several approaches to the issues that still prevent an ideal graft from being designed. At the present time, both *in vivo* and *ex vivo* solutions have significant drawbacks; however, through the combination of bioresorbables, biopolymers, drug delivery, and cells, we can surmount the setbacks and ameliorate these problems.

Chapter 3: SCAFFOLD CHARACTERIZATION OF AN ELECTROSPUN NOVEL CO-POLYMER

Preface: The following manuscript is in Journal of Engineered Fibers and Fabrics. The included work demonstrates the capability of creating an electrospun nanofibrous structure from a novel copolymer and investigates the thermal and mechanical properties of the scaffolds. The scaffolds' mechanical and thermal characteristics are different, depending on the ratio of monomers used to form the copolymer and can be tailored for different tissue engineering applications.

Characterization of Electrospun Novel Poly(ester-ether) Copolymers: 1,4-Dioxan-2-one and D,L-3-Methyl-1,4-dioxan-2-one

Patricia S. Wolfe[1], Yemanlall Lochee[2], Dhanjay Jhurry[2], Archana Bhaw-Luximon[2], and Gary L. Bowlin[1]

[1]Department of Biomedical Engineering, Virginia Commonwealth University, Richmond, Virginia 23284-3067
[2]Polymer Group, Department of Chemistry, University of Mauritius, Réduit, Mauritius

Abstract

Because tissue engineering scaffolds serve as a temporary environment until new tissue can be formed, their mechanical performance, thermal properties, and biocompatibility are critical for maintaining their functionality. The goal of this study was to electrospin scaffolds from copolymers containing varying amounts of 1,4-Dioxan-2-one (DX) and D,L-3-Methyl-1,4-dioxan-2-one (DL-3-MeDX), and characterize their

mechanical and thermal properties. Image tool analysis of scanning electron micrographs revealed the presence of DL-3-MeDX causes the fiber diameter of the scaffold to decrease as compared to PDO. Uniaxial tensile testing revealed increasing amounts of DL-3-MeDX in the copolymer decreases scaffold peak stress, strain at break and toughness. Modulated differential scanning calorimetry was used for thermal analysis of the scaffolds and showed that increasing amounts of DL-3-MeDX causes a decrease in the melting as well as crystallization temperatures. Based on the results of the mechanical and thermal properties of these copolymer scaffolds, it is evident that these constructs could be functional in a variety of biomedical engineering applications.

Introduction

The combination of materials science and engineering with tissue engineering aims to restore, repair or replace diseased or damaged tissue. The design and fabrication of scaffolds are an essential task for functional, engineered tissue. A scaffold serves as a temporary cell adhesion and proliferation microenvironment until natural ECM biomacromolecules (proteins and proteoglycans) are generated by inoculated cells to form a tissue morphology resembling that of a native tissue. Electrospinning is a well known technique to fabricate micro to nanometer-scale scaffolds [249], and because it is relatively inexpensive, it has become increasingly popular. In the development of new scaffolding for tissue regeneration, there are several requirements that must be fulfilled. In addition to surface morphology, porosity, and sufficient mechanical performance and thermal properties, the material must be biocompatible and support cell adhesion, growth and differentiation. Amongst the most investigated biomaterials, PDO, a poly(ester-ether)

originally developed for use as a wound closure suture, has attracted a lot of interest because of its superior degradation rate of 6-12 months [144, 250]. PDO has shown higher strength retention, slower absorption rates and lower inflammatory response as compared to PGA (Dexon®) and PLGA (Vicryl®). In addition to its biocompatibility, its unique shape memory makes PDO particularly suitable for vascular tissue engineering [5].

Previously, the thermal properties (glass transition, melting and crystallization temperatures) of various electrospun polymers have been reported. The first study to use differential scanning calorimetry (DSC) was published by Kim *et al.* [251]. This study concluded that the electrospinning of poly(ethylene terephthalate) (PET), poly(ethylene naphthalate) (PEN), and blends of PET and PEN caused an increase in crystallinity, but a decrease in glass transition temperature (T_G) and crystallization temperature (T_C). According to the authors, this was due to the thermal degradation (i.e. decrease in molecular weight resulting in decrease of chain entanglements) after spinning, and exchange reactions in the melt blends. Zong *et al.* investigated the thermal properties of electrospun poly(L-lactic acid) (PLLA) from dimethyl formamide using DSC [252]. It was reported that the electrospun PLLA nanofibers had lower T_G, T_C, and T_M (melting temperature) compared to the corresponding values for PLLA resin. The study concluded that the electrospun PLLA scaffolds were non-crystalline, but had highly ordered polymer chains, and thus, the crystallization of PLLA was obstructed by the electrospinning process. Ramdhanie, *et al.* have previously reported on the mechanical and thermal properties of virgin and electrospun PGA, polylactic acid (PLA), and blends of these polymers [253]. It was found that the electrospinning process lowered the

crystallization temperature for both polymers; PLA decreased from 108 to 72 – 77 °C and PGA decreased from 68 to 49 °C. The glass transition and melting temperatures of the electrospun polymers and polymer blends remained the same as the virgin polymers, except for one of the blended ratios (PLA 25%:PGA 75%).

To improve the processability of PDX, 1,4-dioxanone (DX) has often been copolymerized with glycolide (GA) or lactide (LA) and much of this work is covered in patents [254-257]. Using aluminium triisopropoxide ($Al(O^iPr)_3$) as initiator, block poly(*ε*–caprolactone)-poly(1,4-dioxan-2-one) (PCL-PDX) copolymers have been prepared by Raquez *et al*. through sequential polymerization [258]. Thermal analysis of the copolymer revealed two glass transition temperatures (-65 °C for the PCL and -10 °C for the PDX), confirming immiscibility of the two blocks with each other. Poly(trimethylenecarbonate-co-*ε*-caprolactone)-block-poly(1,4-dioxan-2-one) [(PTMC)-*co*-(PCL)]-*b*-(PDX) was prepared using the (PTMC)-*co*-(PCL) unit as macroinitiator in the presence of $Sn(Oct)_2$ as a catalyst [259-261]. As soft segments, caprolactone (CL) and trimethylenecarbonate (TMC) moieties endow the PDX chain with enhanced flexibility and degradability, and excellent handling characteristics. Analysis of this copolymer revealed a lower T_G and decreased mechanical properties compared to that of PDX, which can be explained by the decrease in crystallinity. Using dihydroxyterminated PEO of different molar masses as a macroinitiator, the triblock (PDX)-b-(PEO)-b-(PDX) has been previously formed in the presence of $Sn(Oct)_2$ [262-265]. The addition of the PEO chains did not affect the thermal properties of the triblock. It is noteworthy that most of the above copolymers have not been subjected to electrospinning except the one recently reported by Shin *et al.* [261].

Lochee *et al.* recently reported on the synthesis of a derivative of DX monomer, *R,S*-3-methyl-1,4-dioxan-2-one (3-MeDX) using a novel synthetic route [266] and provided a detailed account of the homopolymerization of 3-MeDX, using a range of initiators including tin(II) octanoate. The same authors also reported on the preparation of a range of random copoly(ester-ether)s by the non-sequential polymerization of 1, 4-dioxan-2-one with DL-3-methyl-1,4-dioxan-2-one using various initiator systems [266]. The stiffness of PDX can now be reduced by introducing small amounts of DL-3-MeDX. Indeed, the thermal properties of the copoly(ester-ether)s changed significantly with the percentage of MeDX units incorporated. For instance, a copolymer with 8 % (mole percent) of MeDX units exhibits a T_M of 95.5 °C; this is about 15 °C lower than PDO homopolymer. Thus, the ability to tailor the PDO composition and subsequent properties (i.e. mechanical properties, biocompatibility, and degradation rates) will allow for the design of the next generation of tissue engineering scaffolds for application in regenerating such tissues as arteries, peripheral nerve, and bone. Overall, it is hoped that these novel compositions would allow for a significant enhancement of the current state of the field.

This chapter reports for the first time on the successful electrospinning of fibers from a new family of poly(ester-ether)s obtained by random copolymerization of 1,4-Dioxan-2-one (DX) and DL-3-methyl-1,4-dioxan-2-one (DL-3-MeDX) and on their mechanical and thermal characterization. The hypothesis of this study is that the addition of DL-3-MeDX will have an affect on the mechanical and thermal properties of the electrospun scaffolds.

Materials and Methods

Copolymerization

For polymerization, solvents used were purchased from Sigma Aldrich® or Fischer Scientific, and were purified prior to use. DX and DL-3-MeDX were synthesized according to procedures previously described [266]. Briefly, freshly distilled DX and DL-3-MeDX at various masses were transferred in a quick-fit tube under argon inside a glove box. 100 µL of a 2-ethyl tin (II) hexanoate solution in toluene (1.26×10^{6} mol; 500 ppm Sn) was added to the monomers via a syringe. The tube was placed in a preheated oil bath at 80 °C outside the glove box and polymerization was allowed to take place. After 24 hours, the reaction was quenched through freezing in liquid nitrogen and the crude sample was dissolved in 1,1,1,3,3,3 hexafluoro-2-propanol (HFIP) followed by precipitation in tetrahydrofuran (THF). The precipitate was washed several times with THF and dried under vacuum at room temperature before characterization. The composition and reduced viscosities of the copolymers synthesized are listed in Table 3.1.

Table 3.1. DX:DL-3-MeDX copolymer ratios and viscosities.

Mole percentage of comonomeric units in purified copolymer [a] (%)		η_{red} [b] [dLg^{-1}]
DX	DL-3-MeDX	
100	0	1.16
94	6	0.93
93	7	0.77
91	9	0.88
88	12	0.82
80	20	0.95

[a] Determined by ^{1}H NMR
[b] Reduced viscosity determined using $CHCl_3$, concentration=0.2 $g.dL^{-1}$

Electrospinning

Varying compositions of P(DX:DL-3-MeDX) (80:20, 88:12, 91:9, 93:7, 94:6), as well as PDO (100:0 DX:DL-3-MeDX) were all dissolved in HFIP (TCI America Inc.) at different concentrations, ranging from 100-220 mg/ml, depending upon their optimal fiber forming ranges. For the electrospinning, 3 mL of each solution was loaded into a 3 mL Becton Dickinson syringe, and placed in a KD Scientific syringe pump (model number 100) for dispensing at a specific rate (depending on ratio of copolymer). The positive voltage lead of a power supply (Spellman CZE1000R; Spellman High Voltage Electronics Corp.) was set to a certain voltage according to the copolymer ratio and was attached to a blunt 18 gauge needle on the syringe. A grounded mandrel (1.5 cm wide x 7.6 cm long x 0.5 cm thick; 303 stainless steel) was placed a certain distance away from the needle tip and was rotated at 500 rpm and translated at 7.5 cm/s over 15 cm distance for collection of the fibers. Table 3.2 displays the different parameters used to electrospin the various ratios of copolymers.

Table 3.2. Electrospinning parameters for different DX:DL-3-MeDX copolymer ratios.

Copolymer ratio (DX:DL-3-MeDX)	**Electrospinning concentrations (mg/ml)**	**Pump rate (ml/hr)**	**Airgap distance (cm)**	**Voltage (kV)**
100:0	100, 160, 220	2.5	20	22
94:6	100, 160, 200	2		
93:7				
91:9				
88:12	120, 160, 200	0.5	28	20
80:20	120, 160			

Scaffold Characterization

Scanning electron microscopy

Fiber diameter characterization was accomplished using SEM (Zeiss EVO 50 XVP) of each scaffold. Samples from each scaffold were mounted on an aluminum stub and sputter coated with gold for imaging. The average fiber diameter of each electrospun structure was determined from the SEM using UTHSCSA ImageTool 3.0 software (Shareware provided by University of Texas Health Science Center in San Antonio). Fiber diameter averages and standard deviations were calculated by taking the average of 60 random measurements per micrograph.

Uniaxial tensile testing

Mechanical testing was performed on the electrospun scaffolds using a MTS Bionix 200 system (MTS Systems Corp., Eden Prairie, MN). Using a template, "dog bone" shaped samples (2.75 mm, 11.25 mm gauge length, thicknesses ranging from 0.025 – 0.432 mm, n=3) were punched from the different constructs and were hydrated in phosphate buffered saline for one hour before testing. Peak stress, elastic modulus and strain at break values were determined for each scaffold. In addition, toughness was calculated in Matlab™ using the stress and strain data.

Differential scanning calorimetry

Modulated DSC was performed on the virgin and electrospun copolymers and PDO using TA Instruments Q1000 Differential Scanning Calorimeter. Samples (2-5 mg) of the copolymers were placed into separate aluminum pans and the temperature was programmed using Thermal Advantage for Q Series™ software (TA Instruments). Each sample was heated (±0.5 °C/40 sec) from -50 °C to 250 °C at a rate of 3 °C/min and then

cooled from 250 °C to -50 °C at the same rate. Data was then analyzed using Universal Analysis 2000 (TA Instruments).

Statistical Analysis

Statistical analysis was performed using JMP IN 4 statistical software (SAS Institute, Inc.) to determine significant differences between the results of mechanical testing of the electrospun copolymers. All analysis was based on a Kruskal-Wallis one-way analysis of variance on ranks and a Tukey-Kramer pairwise multiple comparison procedure ($\alpha < 0.05$). The results are presented as mean ± standard deviation.

Results and Discussion

Scanning Electron Microscopy

In this study, copolymers of DX and DL-3-MeDX in varying compositions (80:20, 88:12, 91:9, 93:7 and 94:6) and PDO were successfully electrospun from HFIP to form nano- to micron sized fibrous, non-woven mats (Figure 3.1A). For all copolymer scaffolds, the analysis of SEM verifies a linear relationship between polymer concentration and fiber diameter (Figure 3.1B). This relationship is expected, as it has been demonstrated in previous studies [5, 38, 144, 253, 267]. It should be noted that because only two concentrations of 80:20 DX:DL-3-MeDX were electrospun (120 and 160 mg/ml), only two fiber diameters were calculated, and therefore, the degree at which the fiber diameter values fit the linear regression line (R^2 value) could not be determined for this scaffold ratio.

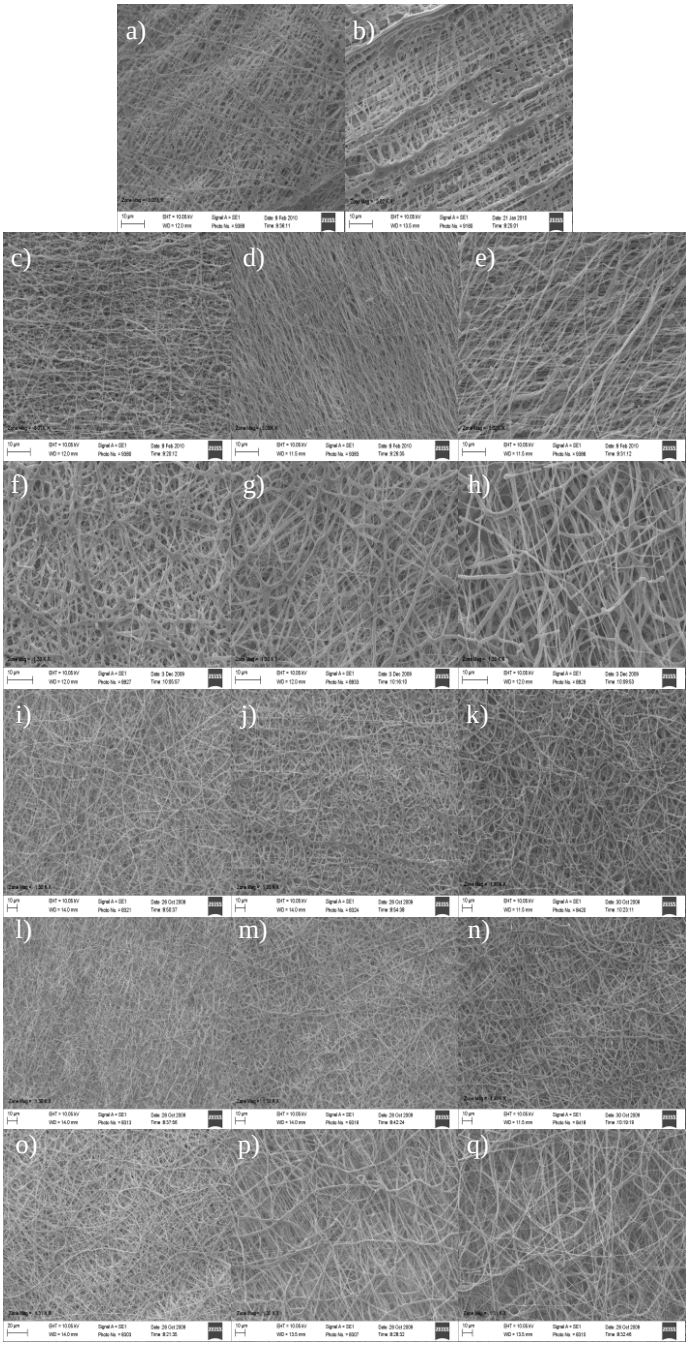

Figure 3.1(a). SEM of electrospun a) 120 mg/ml 80:20 DX:DL-3-MeDX, b) 160 mg/ml 80:20 DX:DL-3-MeDX, c) 120 mg/ml 88:12 DX:DL-3-MeDX, d) 160 mg/ml 88:12 DX:DL-3-MeDX, e) 200 mg/ml 88:12 DX:DL-3-MeDX, f) 100 mg/ml 91:9 DX:DL-3-MeDX, g) 160 mg/ml 91:9 DX:DL-3-MeDX, h) 200 mg/ml 91:9 DX:DL-3-MeDX, i) 100 mg/ml 93:7 DX:DL-3-MeDX, j) 160 mg/ml 93:7 DX:DL-3-MeDX, k) 200 mg/ml 93:7 DX:DL-3-MeDX, l) 100 mg/ml 94:6 DX:DL-3-MeDX, m) 160 mg/ml 94:6 DX:DL-3-MeDX, n) 200 mg/ml 94:6 DX:DL-3-MeDX, o) 100 mg/ml PDO, p) 160 mg/ml PDO, q) 220 mg/ml PDO. Magnification 3000x for SEM a) – e). Magnification 1300x for SEMs f) – q).

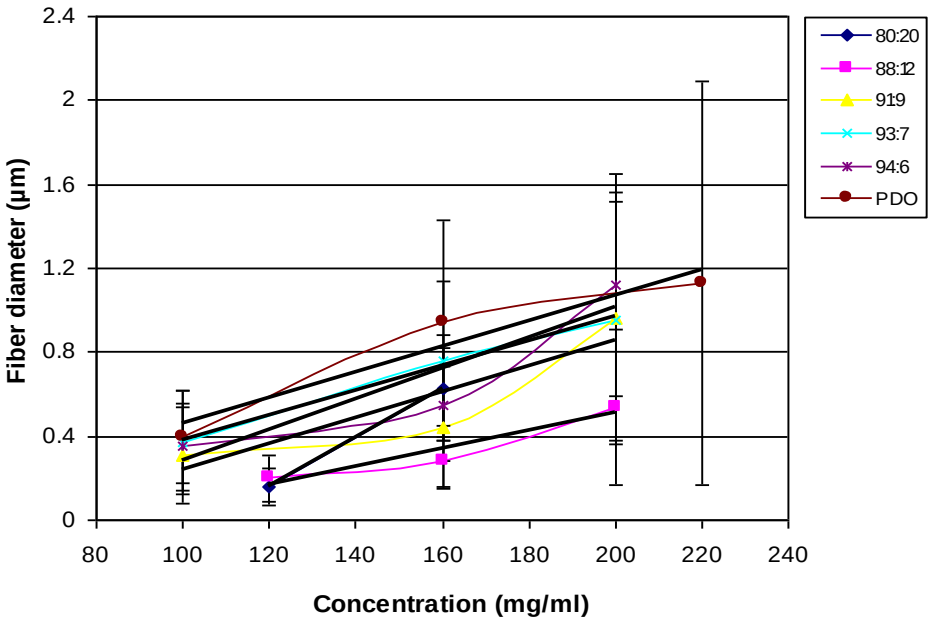

Figure 3.1(b). Fiber diameter of the electrospun constructs as a function of polymer concentration illustrating the linear relationship between solution concentration and fiber diameter. $R^2 = 0.915$ for 88:12 DX:DL-3-MeDX, $R^2 = 0.812$ for 91:9 DX:DL-3-MeDX, $R^2 = 0.993$ for 93:7 DX:DL-3-MeDX, $R^2 = 0.859$ for 94:6 DX:DL-3-MeDX, $R^2 = 0.929$ for PDO.

Table 3.3. Fiber diameters (µm) of electrospun DX:DL-3-MeDX and PDO scaffolds.

Concentration / **DX: DL-3-MeDX**	100 or 120 mg/ml	160 mg/ml	200 or 220 mg/ml
80:20	0.16±0.09	0.63±0.25	-
88:12	0.20±0.11	0.28±0.12	0.54±0.37
91:9	0.31±0.23	0.44±0.29	0.96±0.60
93:7	0.37±0.25	0.76±0.38	0.95±0.57
94:6	0.35±0.21	0.55±0.27	1.12±0.53
100:0	0.40±0.22	0.94±0.49	1.13±0.96

Figure 3.1B also shows that the fiber diameter decreases with increasing content of DL-3-MeDX. For instance, copolymer 88:12 (DX:DL-3-MeDX) has a fiber diameter as low as 0.2 µm. The unexpected high fiber diameter of 160 mg/ml 80:20 DX:DL-3-

MeDX most probably results from its higher reduced viscosity and therefore higher molar mass compared to the other copolymers.

Uniaxial Tensile Testing

As mechanical properties are an extremely important characteristic of any biomedical material, the modulus, peak stress, strain at break, and toughness of the DX:DL-3-MeDX and PDO electrospun scaffolds were determined. Results from uniaxial tensile testing revealed the addition of DL-3-MeDX does alter the mechanical properties of the constructs, as illustrated in Figure 3.2.

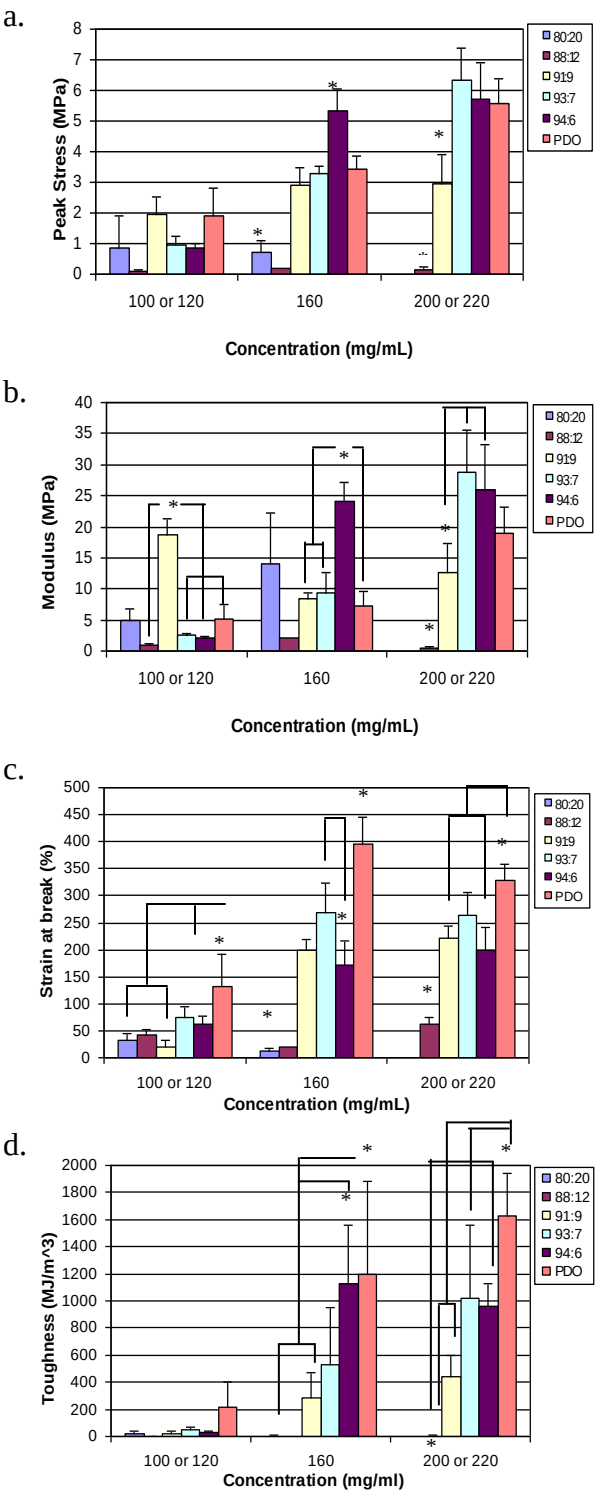

Figure 3.2. Results of peak stress (a), modulus (b), strain at break (c), and toughness (d) of electrospun constructs of different ratios illustrating mechanical properties increase with increasing electrospinning concentrations, but decrease with increasing DL-3-MeDX concentrations (with the exception of modulus, which does not follow a trend). *

represents statistical significance when compared to all other co-polymer ratios within the same electrospinning concentrations ($p<0.05$).

Figure 3.2(a) reveals peak stress (Table 3.4) values for electrospun scaffolds of 80:20 and 88:12 (DX:DL-3-MeDX) were 2-6 times lower compared to PDO. Statistical analysis of this data indicates no significant differences in peak stress values for scaffolds of 100 or 120 mg/ml. Peak stress results for 160 mg/ml 94:6 and 80:20 (DX:DL-3-MeDX) constructs were significantly different from each other and from all other 160 mg/ml scaffolds. In addition, peak stress results for 200 mg/ml 91:9 and 88:12 (DX:DL-3-MeDX) copolymer scaffolds indicated significant differences from each other and from all other 200 and 220 mg/ml electrospun constructs. In summary, the peak stress increases with increasing DX content.

In comparison to other electrospun polymers, scaffolds of different DX:DL-3-MeDX ratios have peak stress values similar to those of other polymers that have been previously electrospun in our lab. For electrospun PGA:PLA blends of varying ratios, and PDS (polydioxanone II violet monofilament sutures), peak stress values fell in the range of 4.50 – 10.0 MPa and 4.50 – 5.50 MPa, respectively [144, 253]. Natural polymers have also been electrospun and mechanically tested in our lab including PDO:collagen blends, PDO:elastin blends, and fibrinogen; these scaffolds exhibited peak stresses of 4.60 – 6.70 MPa, 2.70 MPa, and 0.400 MPa, respectively [147, 148, 267].

Results of modulus (Table 3.4) reveal there to be no obvious trends relating DX:DL-3-MeDX ratio with scaffold modulus (Figure 3.2(b)). Statistical analysis of modulus values for the electrospun copolymers and PDO reveals 100 mg/ml 91:9 DX:DL-3-MeDX is significantly different from all other 100 and 120 mg/ml electrospun

scaffolds, with the exception of 120 mg/ml 80:20 (DX:DL-3-MeDX). 160 mg/ml 94:6 DX:DL-3-MeDX scaffolds have a modulus that is significantly different from 160 mg/ml 91:9 DX:DL-3-MeDX, 93:7 DX:DL-3-MeDX, and PDO. The modulus results from electrospun constructs of 200 mg/ml 88:12 DX:DL-3-MeDX are significantly different from all other 200 and 220 mg/ml scaffolds. In addition, the moduli of 200 mg/ml 91:9 DX:DL-3-MeDX scaffolds are statistically different from the moduli of 200 mg/ml 93:7, 94:6, and 88:12 DX:DL-3-MeDX.

Table 3.4. Peak Stress, modulus, strain at break, and toughness values for DX:DL-3-MeDX and PDO scaffolds.

Scaffold	Peak Stress (MPa)	Modulus (MPa)	Strain at break (%)	Toughness (MJ/m^3)
120 mg/ml 80:20	1.11 ± 0.64	12.2 ± 8.13	21.0 ± 3.80	15.2 ± 9.95
160 mg/ml 80:20	0.74 ± 0.38	14.0 ± 8.29	13.0 ± 3.31	2.87 ± 2.29
120 mg/ml 88:12	0.09 ± 0.03	0.91 ± 0.34	42.4 ± 8.68	1.85 ± 0.75
160 mg/ml 88:12	0.19	1.99	19.9	2.76
200 mg/ml 88:12	0.16 ± 0.06	0.57 ± 0.15	61.0 ± 13.1	4.45 ± 2.04
100 mg/ml 91:9	1.94 ± 0.61	18.6 ± 2.64	20.3 ± 11.6	21.7 ± 17.3
160 mg/ml 91:9	2.90 ± 0.56	8.32 ± 1.01	198 ± 19.9	280. ± 187
200 mg/ml 91:9	2.95 ± 0.94	12.5 ± 4.76	221 ± 23.9	440. ± 155
100 mg/ml 93:7	0.97 ± 0.27	2.47 ± 0.23	74.8 ± 18.5	50.1 ± 22.6
160 mg/ml 93:7	3.30 ± 0.24	9.38 ± 3.32	268 ± 56.7	532 ± 417
200 mg/ml 93:7	6.31 ± 1.08	28.8 ± 6.69	264 ± 42.3	1020 ± 534
100 mg/ml 94:6	0.87 ± 0.14	2.06 ± 0.21	63.3 ± 14.8	28.5 ± 6.85
160 mg/ml 94:6	5.32 ± 0.72	24.2 ± 2.99	173 ± 44.8	1130 ± 430.
200 mg/ml 94:6	5.71 ± 1.19	26.0 ± 7.24	199 ± 40.9	965 ± 162
100 mg/ml PDO	1.89 ± 0.92	5.23 ± 2.16	132 ± 59.7	218 ± 187
160 mg/ml PDO	3.44 ± 0.44	7.21 ± 2.27	397 ± 47.7	1190 ± 695
220 mg/ml PDO	5.55 ± 0.82	18.9 ± 4.17	328 ± 29.0	16300 ± 316

The wide range of modulus results of the electrospun DX:DL-3-MeDX ratios were lower than most synthetic electrospun polymers that have previously been tested in

our lab, but similar to the moduli of the natural electrospun polymers. Electrospun PGA:PLA blends, and PDS scaffolds had moduli of 30.0 – 140. MPa and 8.00 – 15.0 MPa, respectively [253]. Electrospun PDO:collagen had a moduli between 7.60 and 18.0 MPa, 50:50 PDO:elastin had a modulus of 6.10 MPa and electrospun fibrinogen had a modulus of 0.300 MPa [147, 148, 267].

Figure 3.2(c) reveals that strain at break values (Table 3.4) of electrospun DX:DL-3-MeDX constructs were approximately 8 times lower than those of electrospun PDO. Statistical analysis concludes strain at break of 100 mg/ml PDO is significantly different from 120 mg/ml 80:20 and 100 mg/ml 91:9 DX:DL-3-MeDX. Strain at break values for scaffolds of 160 mg/ml 80:20 DX:DL-3-MeDX and 160 mg/ml PDO are statistically different from each other and from all other 160 mg/ml scaffolds. In addition, strain at break for 160 mg/ml 94:6 DX:DL-3-MeDX scaffolds are significantly different than 160 mg/ml 93:7 DX:DL-3-MeDX, 80:20 DX:DL-3-MeDX, and PDO. Results of strain at break reveal 200 mg/ml 88:12 DX:DL-3-MeDX scaffolds are significantly different than all other 200 and 220 mg/ml electrospun constructs. In addition, 220 mg/ml PDO scaffolds have significantly different strain at break values than 200 mg/ml 88:12, 91:9, and 94:6 DX:DL-3-MeDX. Results from mechanical testing conclude that with increasing amounts of DL-3-MeDX, there is a decrease in strain at break.

Results of strain at break for the DX:DL-3-MeDX scaffolds also covered a wide range, and therefore, were similar to the strains at break found for previously electrospun synthetic and natural polymers at certain ratios. PGA, PLA and their copolymer blends had strains at break ranging from 90.0 – 200 % and electrospun PDS had strains at break of 170 % [144, 253]. PDO:collagen blends had strain to failure values between 56.5 –

186 %, electrospun 50:50 PDO:elastin exhibited strains at break of 80 %, and electrospun fibrinogen scaffolds had strains at break of 134 % [147, 148, 267].

Results from Figure 3.2(d) indicates toughness values of electrospun DX:DL-3-MeDX were about 110 – 350 times lower than electrospun PDO scaffolds (Table 3.4). Statistical analysis reveals there is no significant difference in toughness between scaffolds of 100 and 120 mg/ml. Values of toughness for 160 mg/ml PDO are significantly different from those of 160 mg/ml 80:20 and 91:9 (DX:DL-3-MeDX). In addition, the toughness of 160 mg/ml 94:6 DX:DL-3-MeDX is significantly different from that of 160 mg/ml 91:9 and 80:20 DX:DL-3-MeDX. 220 mg/ml PDO has statistically different toughness from 200 mg/ml 91:9 and 88:12 DX:DL-3-MeDX, and 200 mg/ml 88:12 has significantly different toughness from 200 mg/ml 93:7 DX:DL-3-MeDX, 94:6 DX:DL-3-MeDX , and 220 mg/ml PDO. It should be noted that because of the fragility of the 160 mg/ml 88:12 DX:DL-3-MeDX scaffold, only one sample was tested, and therefore, statistical significance for this scaffold could not be determined. To conclude, as the amount of DL-3-MeDX increases, toughness decreases for all electrospinning concentrations.

Differential scanning calorimetry

In this study, we used modulated DSC to analyze the glass transition, melting, and crystallization temperatures of virgin and electrospun DX:DL-3-MeDX copolymers of different ratios, as well as PDO (Figures 3.3 and 3.4).

The addition of DL-3-MeDX does not affect the T_G, but does cause the T_M and T_C of the copolymers to decrease. T_G values of copolymers ranged from -22.5 to -8.60 °C.

Increasing DL-3-MeDX content (6 – 20 %) decreased T_C of copolymers from 78.1 – 81.2 °C for 100 % DX to 48.0 – 50.9 °C for 80:20 DX:DL-3-MeDX. T_M showed a similar trend decreasing from 106 – 107 °C for 100% DX to 71.0 – 74.4 °C for 80:20 DX:DL-3-MeDX. According to literature, our results for the T_G and T_M of electrospun PDO were as expected [250].

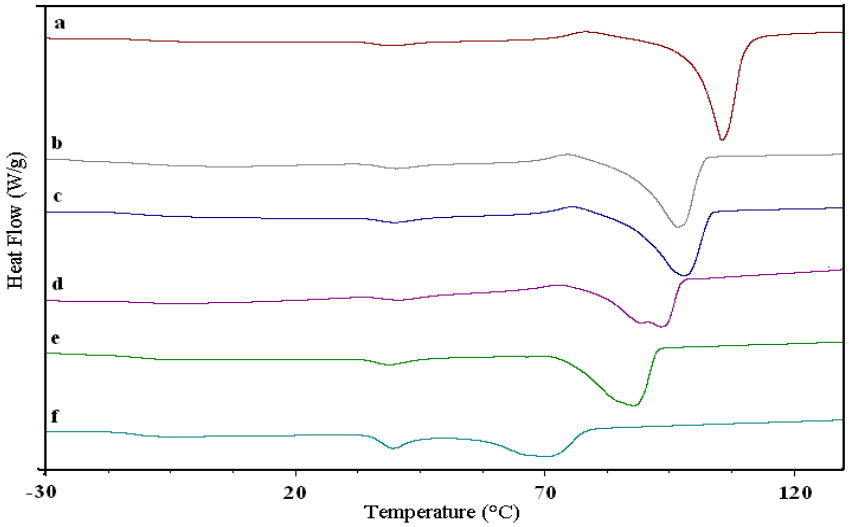

Figure 3.3. Modulated DSC thermograms for 160 mg/ml a) PDO b) 94:6 DX:DL-3-MeDX c) 93:7 DX:DL-3-MeDX d) 91:9 DX:DL-3-MeDX e) 88:12 DX:DL-3-MeDX f) 80:20 DX:DL-3-MeDX.

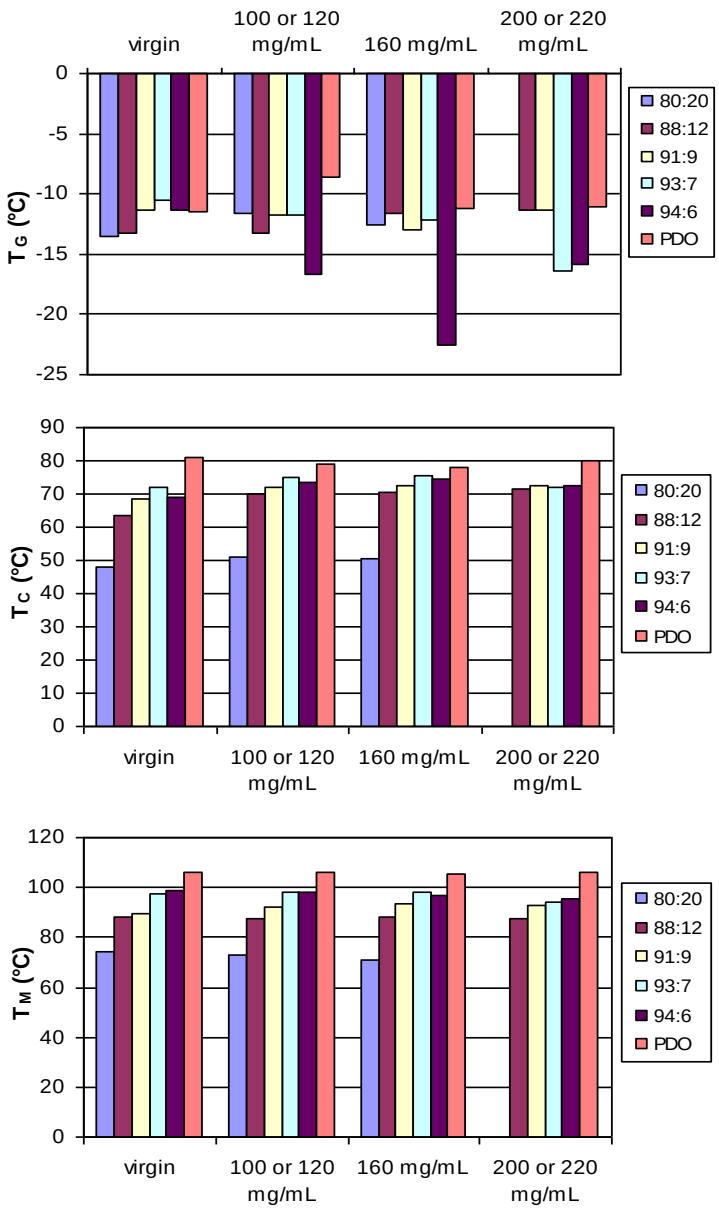

Figure 3.4. Graphical depiction of the glass transition temperatures (T_G, top), crystallization temperatures (T_C, middle) and melting temperatures (T_M, bottom) for the different copolymer ratios and PDO illustrating the addition of DL-3-MeDX does not affect the T_G, but does cause the T_M and T_C of the copolymers to decrease.

The decrease in melting and crystallization temperatures is due to the increasing amorphous character of the copolymer as the DL-3-MeDX content increases. Indeed, the latter units disrupt the crystallinity of the polymer chains. It is well established that an increase in crystallinity leads to an increase in tensile strength and modulus [268]. Based

on the results from this study, it appears there is a linear relationship between the crystallinity of the electrospun fibers and their fiber diameter for copolymers with comparable molar masses: the greater the percent crystallinity, the larger the fiber diameter (Figure 3.5). Again, we note the peculiar behavior of copolymer 80:20 which, as depicted in Figure 3.5 (b), shows the lowest crystallinity but quite a high fiber diameter. As explained previously, this is due to the antagonist effects of reduced crystallinity and molar masses on fiber diameter. It has been explained that the enhancement of polymer-polymer interactions can promote fiber formation due to the presence of inter-chain hydrogen bonding [269, 270]. Thus, enhanced crystallinity may imply increased chain-chain interaction; the larger number of chains per unit volume directly translates to larger fiber diameters due to lower chain extensibility.

a.

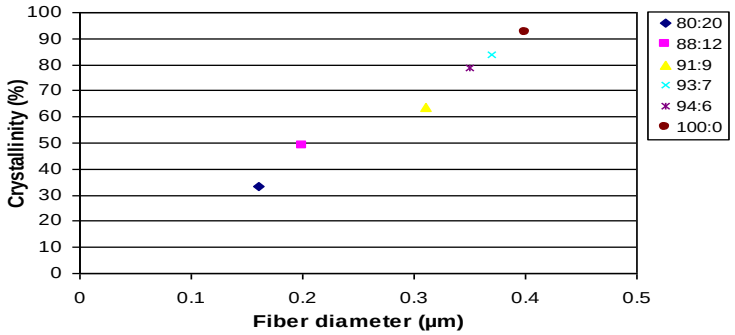

b.

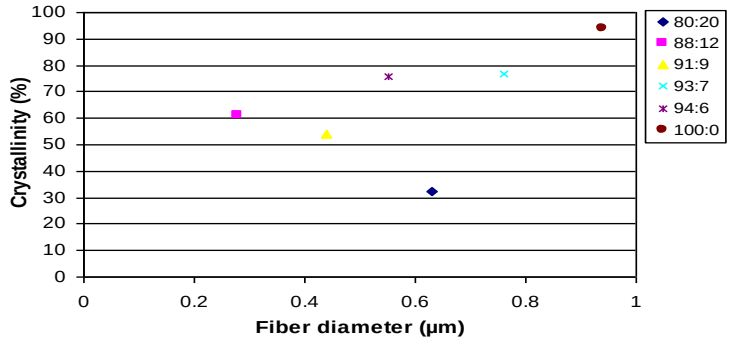

c.

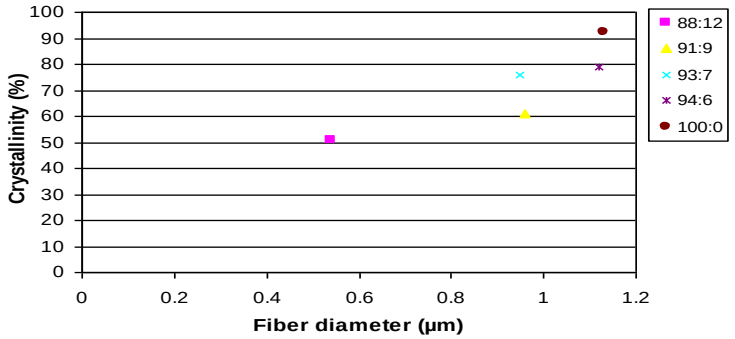

Figure 3.5. Effects of DX:DL-3-MeDX copolymer ratio and fiber diameter on percent crystallinity for scaffolds of 100 and 120 mg/ml (a), 160 mg/ml (b), and 200 and 220 mg/ml (c).

It should also be noted that the electrospinning process, as well as the different concentrations of electrospinning solution, did not affect the thermal properties of the DX:DL-3-MeDX and PDO scaffolds compared to their virgin counterparts, as illustrated in Figure 3.4.

In comparison to other electrospun synthetic copolymers, such as PLA, PGA, PLLA, PET and PEN, the electrospun DX:DL-3-MeDX scaffolds have glass transition temperatures lower than that of the other copolymers. PLA and PGA have T_G of 30.0 – 35.0 °C, PLLA has a T_G around 60.0 °C, and PET and PEN have T_G ranging from 70.0 – 123 °C. Crystallization temperatures of electrospun DX:DL-3-MeDX (50.0 – 80.0 °C) are around the same range as or lower than other copolymers. PLA and PGA have T_C of 72.0 – 77.0 °C and 49.0 °C, respectively, PLLA has a T_C of 103 °C, and PET and PEN have T_C ranging from 130 – 219 °C. Melting temperatures for electrospun DX:DL-3-MeDX (70.0 – 106 °C) are lower than that of other electrospun synthetic copolymers. Electrospun PLA and PGA have melting temperatures of 171 °C and 220 °C, respectively, PLLA has a T_M around 150 °C, and electrospun PET and PEN have T_M ranging from 252 – 272 °C [251-253].

Conclusion

In this study, 1,4-Dioxan-2-one (DX) and DL-3-methyl-1,4-dioxan-2-one (DL-3-MeDX) monomers were synthesized and copolymerized in varying ratios. The copolymers, as well as PDO, were dissolved in HFIP at different concentrations and electrospun to form scaffolds of different fiber diameters. These scaffolds were analyzed, and their fiber diameters, mechanical properties, and thermal properties were compared to those of PDO. The copolymerization of monomers can be beneficial in tissue engineering applications because of the ability to vary their mechanical, chemical, thermal and biological properties. The hypothesis stated at the beginning of this chapter was proven; the addition of DL-3-MeDX did affect the fiber diameter of the scaffold, as

well as the mechanical and thermal properties. To summarize, the fiber diameter of the electrospun fibers and their mechanical performance increased with increasing polymer concentration, polymer molar masses and crystallinity. The wide range of fiber diameters, as well as mechanical and thermal properties should allow for the construction of scaffolds to meet a variety of biomedical engineering applications, including bone regeneration and vascular graft design. More specifically, the mechanical properties of many of the copolymer ratios determined in this study fall within the range of the mechanical properties of native bone and femoral artery [20, 271]. In addition, PDO is known to have excellent shape memory, which may be a positive aspect for vascular grafts, as it can provide rebound and kink resistance [144]. Although mechanical properties are an important aspect of vascular grafts, other characteristics, such as biocompatibility, were not taken into consideration in this study, and should be evaluated in the future to confirm these materials could be used in vascular graft applications. Copolymers consisting of increasing MeDX content possess a lower crystallinity as compared to PDO and should allow for the control of biodegradability properties. This characteristic is useful in applications such as growth factor delivery [272]. Future analysis will include performing copolymer degradation studies and biocompatibility testing.

Acknowledgement

The authors wish to thank the Department of Chemical and Life Science Engineering at Virginia Commonwealth University for the use of the TA Q1000 Differential Scanning Calorimeter.

Chapter 4: EVALUATION OF THROMBOGENIC POTENTIAL OF ELECTROSPUN VASCULAR GRAFT MATERIALS

Preface: The following manuscript appeared in Journal of Biomedical Materials Research-Part A, 92(4), 1321-1328, 2009. The work included investigates the thrombogenic potential of various vascular graft materials by evaluation of tissue factor expression from monocytes using an In Cell Western assay.

Evaluation of Thrombogenic Potential of Electrospun Bioresorbable Vascular Graft Materials: Acute Monocyte Tissue Factor Expression

Patricia S. Wolfe[1], Parthasarathy Madurantakam[1], Koyal Garg[1], Scott A. Sell[1], Matthew Beckman[2], and Gary L. Bowlin[1]

[1] Department of Biomedical Engineering
Virginia Commonwealth University
Richmond, VA 23284-3067

[2] Department of Biochemistry
Virginia Commonwealth University
Richmond, VA 23298-0709

Abstract

The purpose of this study was to quantify the acute expression of tissue factor (TF) by monocytes upon interaction with electrospun bioresorbable constructs. A

minimal expression of TF will demonstrate the potential for scaffolds to be used as a vascular graft without enhanced risk of failure from acute thrombotic occlusion. Polydioxanone (PDO) (60, 80, 120, and 160 mg/mL) and polycaprolactone (PCL) (80, 10, and 160 mg/mL) dissolved in 1,1,1,3,3,3 hexafluoro-2-propanol (HFIP) were electrospun to form fibrous scaffolds. Circular discs (10 mm diameter) of each scaffold were disinfected and seeded with human monocytes (50,000 cells/well). The discs were statically cultured under standard conditions (37ºC and 5% CO_2), and removed after 24 hours for TF analysis with an In-cell Western assay. Fiber diameter was calculated through ImageTool analysis of scanning electron micrographs. Acute monocyte interaction with scaffolds of PCL (120 mg/mL) resulted in the lowest amount of TF expressed (4 ng/disc), whereas scaffolds of 160 mg/mL PDO elicited the highest amount of TF expressed (51 ng/disc). TF levels expressed on all scaffolds were comparable to the amount expressed on e-PTFE (20 ng/disc). Preliminary data for TF expression on scaffolds of silk (70 mg/mL and 150 mg/mL) and silk:PCL (100 mg/mL, v/v) blends (50:50 and 70:30) resulted in values of TF expression ranging from 0-24 ng. Results from this study reveal electrospun grafts composed of PDO and PCL provide no greater risk of failure from an acute thrombotic occlusion due to TF expression when compared to that of the standard e-PTFE graft.

Introduction

Tissue factor (TF) is a 47 kDa membrane glycoprotein identified as the initiator of the coagulation cascade and more recently, has been shown to induce angiogenesis [273-275]. Monocytes are known to be the cell of origin of tissue factor, and can be activated

by endotoxins, mitogens, antigens, aggregated immunoglobulins, and adherence to different surfaces [276, 277]. The binding of TF to factor VII of the coagulation cascade is the critical factor in the initiation of thrombosis. From here, factor X is either directly activated through the intrinsic pathway, or indirectly activated through factor IX of the extrinsic pathway, thereby causing the activation of factor IIa, cleaving fibrinogen to fibrin [273]. These fibrin monomers accumulate and the ending result is a clot, or thrombus. Within small diameter vascular prosthetics, this thrombus can grow large enough to occlude the lumen, and in worse cases, become fatal.

Limited literature on the role of TF in inducing angiogenesis states that it may occur from two different methods. One mechanism is through the induction of signal transduction, specifically through the activation of p42/p44 MAP kinase [278], p38 MAP kinase and c-Jun-terminal kinase (JNK) [274, 279]. The MAP kinase family has been associated with cell proliferation, so TF:factor VIIa interaction may stimulate cell division, and thus, contribute to angiogenesis, although this explanation is ambiguous. Another possibility is that TF:factor VIIa interaction leads to RNA synthesis of FGF-5, heparin-binding EGF (hbEGF), interleukin-1β (IL-1β), MIP2a, LIF and interleukin-8 (IL-8). hbEGF is a mediator of angiogenesis, IL-1β stimulates production of VEGF (a potent angiogenic growth factor) in vascular smooth muscle cells and IL-8 is a chemoattractant for many angiogenic cell types including monocytes, macrophages and smooth muscle cells [280]. IL-8 also induces proliferation of ECs [281]. In addition, the interaction between TF and factor VIIa causes an enhanced increase in cell protein synthesis, which may increase the production of those angiogenic factors as well [274].

Several methods for analyzing TF expression from monocytes have been used previously, including fluorescence-based assays, such as fluorescence confocal microscopy and fluorescence-activated cell sorter analysis, and immunoassays, such as protein immunoblotting and enzyme-linked immunosorbent assays [282-284]. A previous study done by Egorina *et al.* [285] proved tissue factor expression by monocytes could be quantified using an In-Cell Western (ICW) assay and is the motivation for this study. More specifically, in our lab, we are interested in quantifying the amount of TF expressed by monocytes during their interaction with electrospun bioresorbable vascular graft materials using an ICW assay. A minimal expression of TF produced by monocytes will demonstrate the potential for these materials to be used as a vascular graft without enhanced risk of failure from acute thrombotic occlusion.

The graft materials that were chosen for analysis were electrospun scaffolds of PDO and PCL. Although these polymers are synthetic and lack the bioactivity needed for ECM-cell signaling, their mechanical integrity and slow degradation rate make them attractive for use as tissue engineering constructs. Because of their synthetic nature and lack of bioactivity, the possibility of an over expression of TF by inflammatory cells is possible, and thus, there is an increased potential for acute thrombotic events. This is one complication that can arise when an electrospun construct is implanted as a vascular graft [286-288]. For this reason, we quantified the amount of TF expressed by monocytes at a 24 hour time point to determine this risk. These levels were compared to the clinical standard, e-PTFE, which is a fairly non-thrombogenic synthetic vascular graft that is still being used after 50 years.

Because of the angiogenic role TF can have, the levels of TF expression produced by monocytes during their interaction with the electrospun scaffolds should ideally be angiogenic, and not have thrombogenic effects.

One option of providing more bioactivity to electrospun scaffolds without compromising its mechanical integrity is to blend natural polymers with the synthetic polymers. Our lab has accomplished this with many natural polymers including collagen, elastin, fibrinogen, and silk [5, 20, 38, 289]. The hypothesis of this study is that electrospun scaffolds fabricated from synthetic and natural polymers will not have an enhanced expression of TF from monocytes compared to that of e-PTFE.

Preliminary studies have been conducted to quantify monocyte TF expression during their interaction with electrospun silk and silk:PCL blended scaffolds and will be briefly discussed in this article.

Materials and Methods

Electrospinning

For this study, PDO (Ethicon, Inc.) was dissolved in HFIP (TCI America Inc.) at concentrations of 0.06, 0.08, 0.12, and 0.16 g/mL to produce scaffolds of different fiber diameters. PCL (Sigma Aldrich Co., 65kDa) was dissolved in HFIP at concentrations of 0.08, 0.12, 0.16 g/mL for the same reasons as stated above.

Silk was extracted from the cocoons of *Bombyx mori* silkworms (The Yarn Tree) using a protocol previously described by Jin *et al.* [290]. The silk was dissolved in HFIP at concentrations of 0.07 and 0.15 g/mL. Blends of PCL (0.1 g/mL) and silk (0.1 g/mL) were combined at ratios of 50:50 and 70:30 (v/v, silk:PCL).

For electrospinning, 5 mL of each solution was loaded into a Becton Dickinson syringe, and placed in a KD Scientific syringe pump for dispensing at a rate of either 4 or 8 mL/h (4 mL/h for silk and silk blends, 8 mL/h for PDO and PCL). The positive voltage lead of the power supply (Spellman CZE1000R; Spellman High Voltage Electronics Corp.) was set to 22 kV and was attached to a blunt 18 gauge needle on the syringe. A grounded mandrel (2.5cm wide x 10.2cm long x 0.3 cm thick; 303 stainless steel) was placed 6 inches from the needle tip and was rotated at 500 rpm and translated at 7.5 cm/s over 15 cm distance for collection of the fibers.

Scaffold Characterization

Scaffold characterization was accomplished using SEM (Zeiss EVO 50 XVP) of each scaffold type. The average fiber diameter of each electrospun structure was determined from the SEM using ImageTool 3.0 software (Shareware provided by University of Texas Health Science Center in San Antonio). Fiber diameter averages and standard deviations were calculated by taking the average of 60 random measurements per micrograph image.

Scaffold seeding and culture

For scaffold seeding, 6 discs of 10 mm diameter of each scaffold type, along with the clinical standard, e-PTFE (Impra, Inc.), were punched out and disinfected by rinsing the discs in Ethanol for 10 minutes. Discs were then washed three times in sterile phosphate buffered saline for 3 minutes each rinse. The scaffolds were then placed flat in a 48-well culture plate and 8 mm cloning rings were placed on top of the scaffolds to

retain the cells during scaffold seeding. Human peripheral blood monocytes (ATCC CRL 9855) were seeded on 5 of the 6 scaffolds at a density of 50,000 cells/well and 400 µL of macrophage serum-free medium supplemented with 0.5% penicillin – streptomycin (10 U/mL) (Gibco) was added to each well (50 µL of cells in media incubated for 45 minutes, followed by the addition of 350 µL of media). For each scaffold type, three scaffolds were used as experimental samples, two scaffolds accounted for background fluorescence, and one unseeded scaffold with media added was used as a negative control. Scaffolds were statically cultured in standard conditions (37°C and 5% CO_2) in an incubator for 24 hours before they were fixed in 10% formalin for quantification of TF expression.

Quantitative immunofluorescence assay (ICW assay)

In order to begin the ICW assay, after 24 hours of allowing monocytes to adhere to scaffold surfaces, the cells and control scaffolds were fixed with 10% formalin for 20 minutes. Scaffolds were carefully removed from the well plate they were cultured in and placed in a different well plate to avoid obtaining TF expression from cells that were not interacting with the scaffolds. Free aldehyde groups were quenched with three washes of 25 mM glycine in PBS. All scaffolds were blocked using Odyssey Blocking Buffer (LI-COR Biosciences) for 1.5 hours at room temperature.

Standards used to quantify TF expression from monocytes consisted of purified full-length recombinant human coagulation factor III/TF (rhF3, 224 amino acids, purchased from R&D Systems, Inc.) spotted on an Immobilon-FL PVDF membrane (Millipore Corporation) at the amounts of 500, 250, 125, 62.5, 31.25, 15.63, 7.81, 3.91,

and 0 ng, diluted in 20 µL of sterile water. The membrane was blocked for 1 hour at room temperature using Odyssey Blocking Buffer.

After blocking, the scaffolds and membrane were washed five times with 0.1% Tween-20 in PBS and four scaffolds of each material (three experimental samples plus one negative control scaffold), along with the membrane, were incubated with polyclonal anti-human TF antibody (R&D Systems, Inc.) diluted in Odyssey Blocking Buffer overnight at 4ºC. Scaffolds and membrane were washed four times with 0.1% Tween-20 in PBS, after which the signal from goat anti-human TF polyclonal antibody was detected with IRDye 800CW-conjugated donkey antigoat polyclonal antibody (Rockland, Inc.). To account for antibody background fluorescence, each sample was incubated in duplicate with secondary antibody only. Scaffolds and membrane were treated with the IR sensitive secondary antibody for 1 hour at room temperature without exposure to light. After washing, scaffolds and membrane were scanned using the 800 nm channel of the Odyssey Infrared Imaging System (LI-COR Biosciences, Lincoln, NE) at an intensity of 4.0. Fluorescence intensities were measured using circular gates that completely surrounded the scaffolds. Background fluorescence that was obtained from scaffolds incubated with secondary antibody only was subtracted from the signal intensities of the samples incubated with both primary and secondary antibodies.

Statistical Analysis

Statistical analysis was performed using JMP IN 4 statistical software (SAS Institute, Inc.) to determine significant differences between the amounts of TF expressed by monocytes on different electrospun materials. All analysis was based on a Kruskal-

Wallis one-way analysis of variance on ranks and a Tukey-Kramer pairwise multiple comparison procedure (α=0.05). The results are presented as mean ± SE.

Results

Scaffold Characterization

The results of electrospinning PDO at different concentrations are shown in Figures 4.1 and 4.2. For scaffolds of PDO, the analysis of the SEM verifies a linear relationship (R^2 = 0.99) between polymer concentration and fiber diameter. For a concentration of 0.06 g/mL PDO, fiber diameters are 0.29 ± 0.14 µm. PDO scaffolds of 0.08 g/mL result in fiber diameters of 0.69 ± 0.45 µm, 0.12 g/mL concentration exhibits fiber diameters of 1.39 ± 0.61 µm, and PDO concentrations of 0.16 g/mL produce fibers of 2.13 ± 0.66 µm.

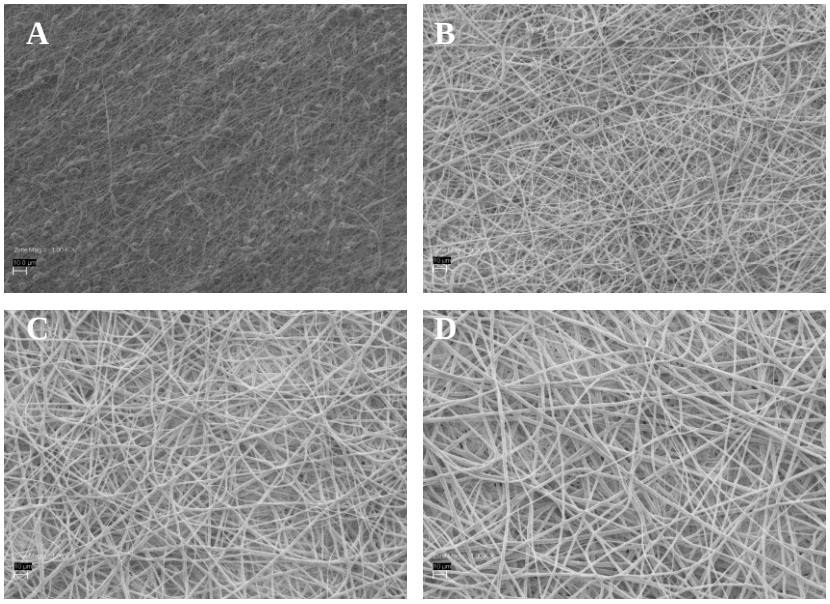

Figure 4.1. Micrographs of random electrospun structures produced from 0.06 g/mL (A), 0.08 g/mL (B), 0.12 g/mL (C), and 0.16 g/mL (D) PDO in HFIP. All images taken at 1000x magnification and an inserted scale bar is 10µm.

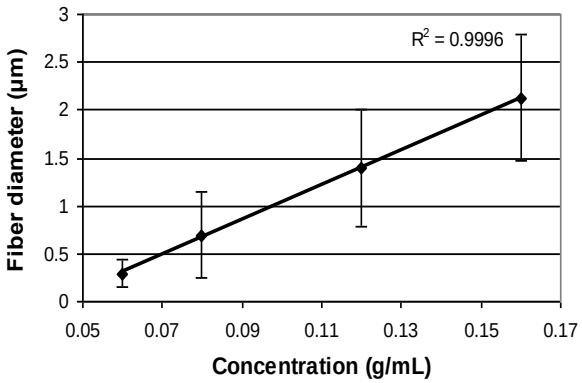

Figure 4.2. Results of fiber diameter analysis versus PDO concentration illustrating the linear relationship between fiber diameter and polymer concentration.

Figures 4.3 and 4.4 present the results of electrospinning PCL at concentrations of 0.08, 0.12, and 0.16 g/mL. Analysis of scaffolds reveals fiber diameters of 0.29 ± 0.14 µm, 0.48 ± 0.49 µm, and 0.94 ± 0.88 µm for scaffold concentrations of 0.08, 0.12, and 0.16 g/mL respectively. Like scaffolds of PDO, a linear relationship exists (R^2 = 0.9456) between polymer concentration and fiber diameter.

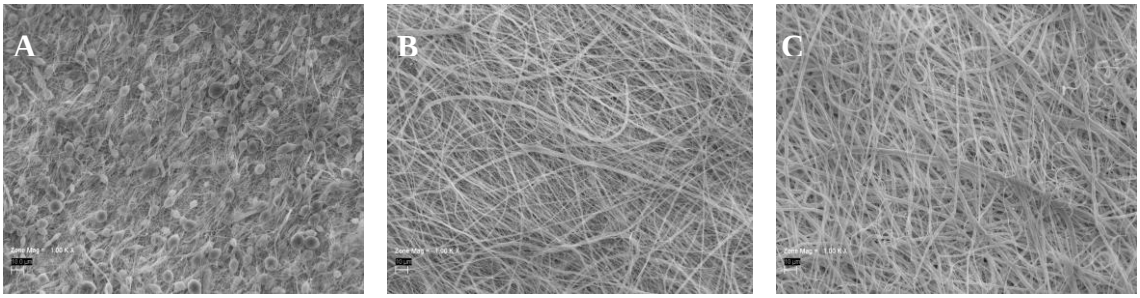

Figure 4.3. Micrographs of electrospun PCL scaffolds produced from 0.08 g/mL (A), 0.12 g/mL (B), and 0.16 g/mL (C) in HFIP at 1000x magnification. The scale bar represents 10µm.

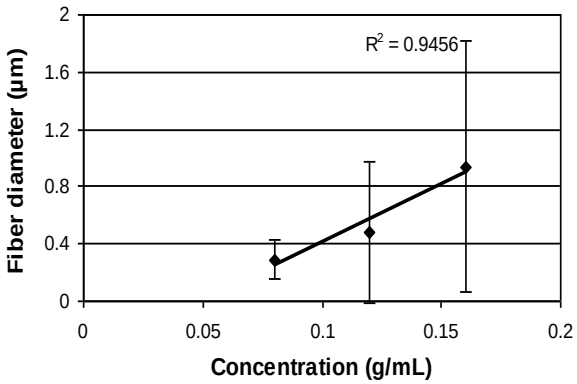

Figure 4.4. ImageTool analysis of PCL scaffolds reveal a linear relationship between polymer concentration and fiber diameter.

Scaffold characterization of electrospun silk reveals fiber diameters of 0.72 ± 0.45 µm and 3.46 ± 2.29 µm for concentrations of 0.07 and 0.15 g/mL. As silk concentration increases from 0.07 g/mL to 0.15 g/mL, fiber diameter increases. SEM are shown in Figure 4.5, along with fiber diameter analysis shown in Figure 4.6. Silk:PCL blended scaffolds reveal fiber diameters of 0.63 µm for 50:50 and 0.99 µm for 70:30. Although it appears there may be a linear relationship between increasing silk volume and increasing fiber diameter, more ratios will need to be analyzed to confirm this (Figure 4.6). SEM images are shown in Figure 4.5.

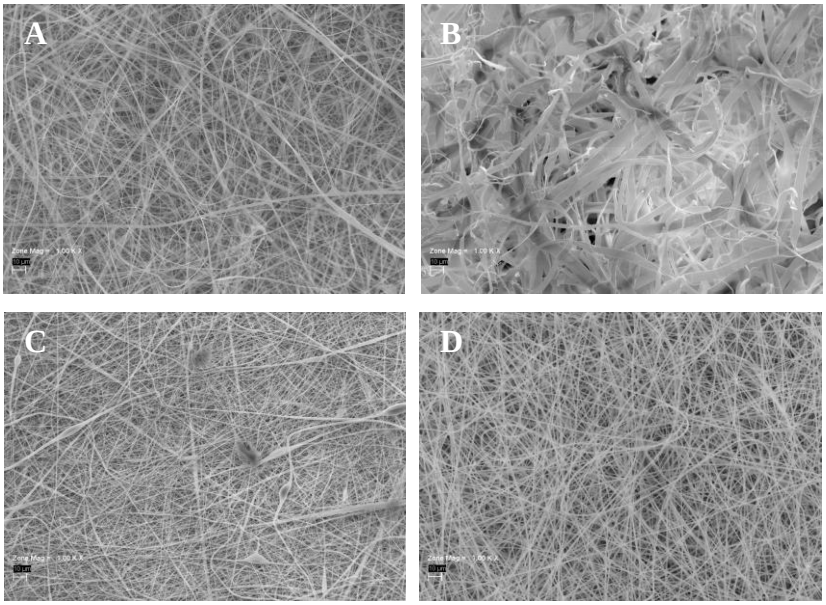

Figure 4.5. SEM images of silk and silk:PCL scaffolds at 0.07 g/mL silk (A), 0.15 g/mL silk (B), 50:50 silk:PCL (C), 70:30 silk:PCL (D) at 1000x magnification. Scale bar represents 10 µm.

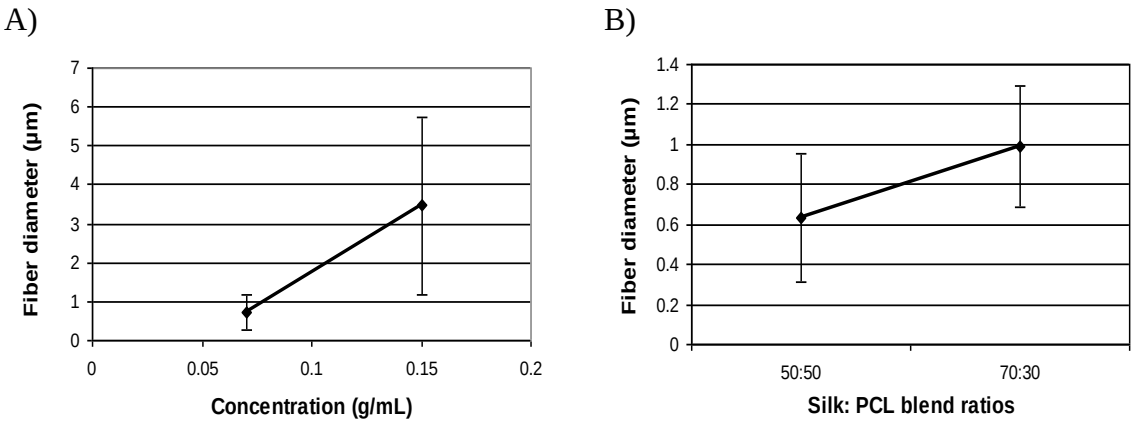

Figure 4.6. Fiber diameter analysis of scaffolds of different silk concentrations (A) and silk:PCL ratios (B).

ICW Assay Results

To quantify the amount of TF expression present on the surface of monocytes, the PVDF membrane that was spotted with 0 to 500 ng of rhTF was scanned by the Odyssey system and fluorescent intensities were acquired. A standard curve was plotted and displays a linear relationship ($R^2 = 0.9324$, $y = 0.102x+0.25$). These results are illustrated

in Figure 4.7 below. With the equation acquired from the standard curve, a quantified amount of TF expression was calculated for each scaffold concentration.

A)

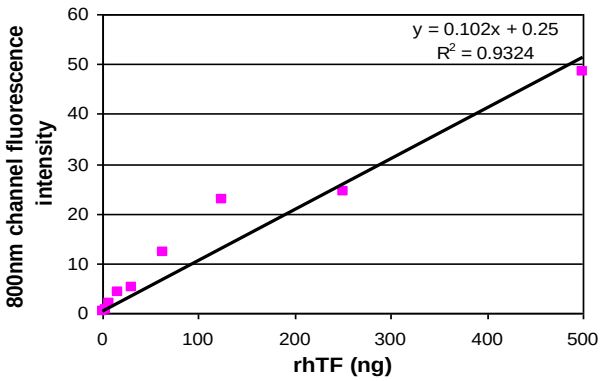

B)

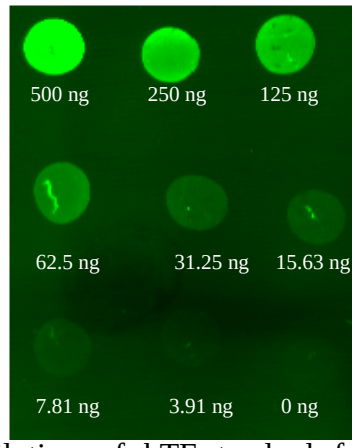

Figure 4.7. (a) Linear curve (R^2 = 0.9324) obtained from dilutions of rhTF standards for ICW assay. (b) Fluorescent intensity image of standards spotted on PVDF membrane from Odyssey Infrared System.

ICW Assay Results for PDO and e-PTFE

The amount of TF expressed on scaffolds of PDO and e-PTFE ranged from 13.5 – 84.9 ng. Specifically, e-PTFE scaffolds amounted in 13.5 ± 20.6 ng, 0.06 g/mL PDO resulted in 26.2 ± 18 ng, 0.08 g/mL PDO exhibited 22.8 ± 18.5 ng, 0.12 g/mL PDO expressed 54.9 ± 13.9 ng, and 0.16 g/mL PDO resulted in 84.9 ± 51.8 ng TF. PDO concentrations of 0.16 g/mL exhibited the highest amount of TF expressed by monocytes, and e-PTFE resulting in the lowest expression. These results are shown in Figure 4.8. Scaffolds of 0.08 g/mL PDO was the only concentration to result in a significantly different amount of TF expressed from that of 0.16 g/mL. TF expressions on all scaffolds of PDO were not significantly different from TF expression on scaffolds of e-PTFE.

A) B)

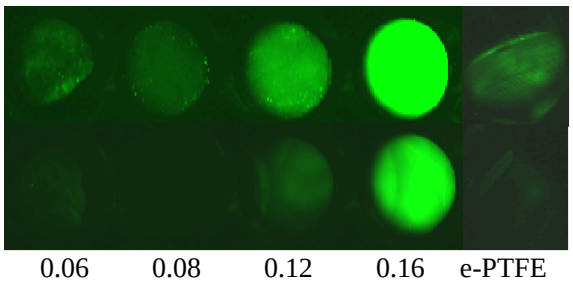

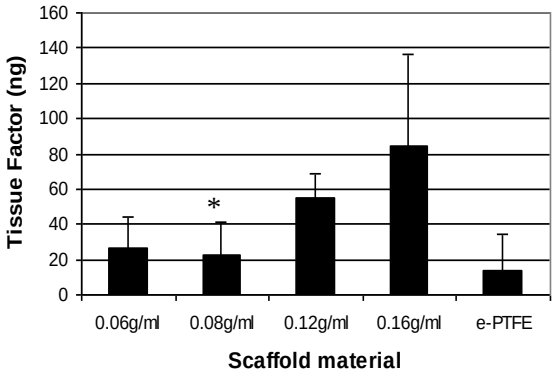

Figure 4.8. (a) TF fluorescence intensity of PDO and ePTFE scaffolds taken at 800nm, 4.0 intensity. Numbers under scaffolds of PDO are represented in g/mL. Top row displays fluorescence of experimental samples, while bottom row displays background fluorescence control scaffolds. (b) Quantified TF expression on scaffolds of PDO and e-PTFE. (*) denotes statistically different TF amount from that of 0.16 g/mL PDO.

ICW Assay Results for PCL Scaffolds

Scaffolds of the highest concentration of PCL, 0.16 g/mL, resulted in the highest expression of TF from monocytes (10.2 ± 19.9 ng), while 0.12 g/mL PCL exhibited the lowest amount (4.2 ± 5.6 ng). PCL scaffolds of 0.08 g/mL resulted in TF expression of 7.48 ± 0.57 ng. These results are shown in Figure 4.9. From statistical analysis, scaffolds of 0.08 g/mL and 0.12 g/mL PCL resulted in significantly different amounts of TF expressed from those of 0.16 g/mL PDO scaffolds.

A) B)

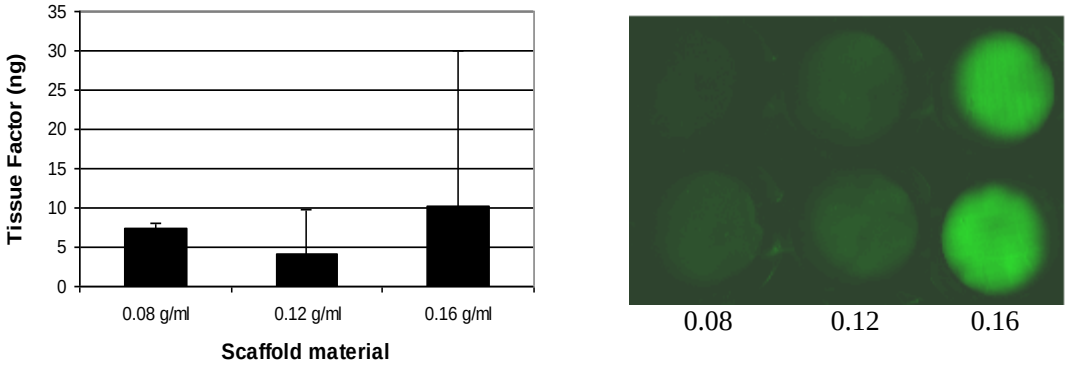

Figure 4.9. (a) Quantified TF expression on scaffolds of PCL. (b) TF fluorescence intensity of PCL scaffolds taken at 800nm, 4.0 intensity. Numbers under PCL scaffolds are represented in g/mL. Top row displays fluorescence of experimental samples, bottom row displays background fluorescence from control scaffolds.

Preliminary Results for Scaffolds of Silk and Silk:PCL Blends

Scaffolds of silk at a concentration of 0.07 g/mL appear to cause no expression of TF from monocytes in 24 hours. Silk scaffolds of 0.15 g/mL result in 6.4 ng of TF expression, while silk:PCL blends at ratios of 50:50 and 70:30 exhibit 5.4 and 24.2 ng of TF, respectively. These results are shown in Figure 4.10.

A) B)

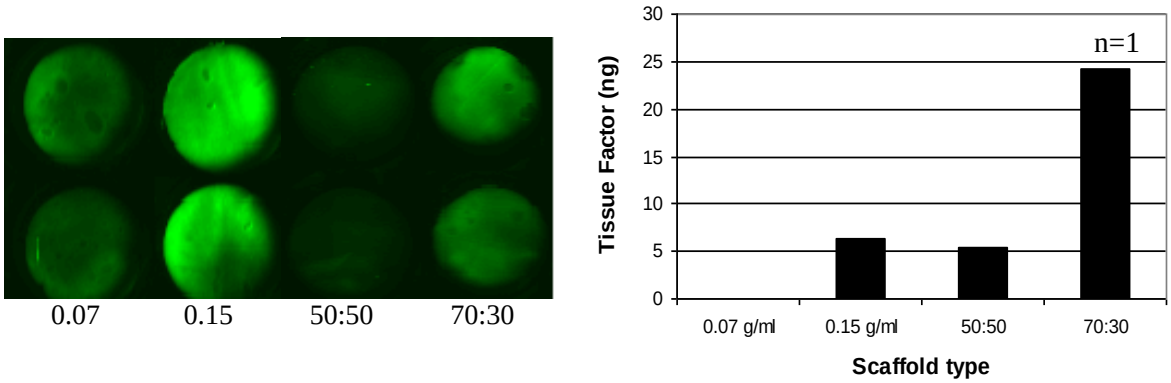

Figure 4.10. (a) Fluorescent intensity image obtained from Odyssey Infrared System at 800 nm, 4.0 intensity. Numbers below scaffolds of silk represent concentrations in g/mL. Top row illustrates fluorescence of experimental samples, while bottom row displays background fluorescence from control samples. (b) Graph displays quantified amount of TF expression from scaffolds of silk and silk:PCL blends.

Discussion

In this study, acute TF expression from the surface of monocytes during their interaction with electrospun constructs was successfully quantified using an ICW assay. Fiber dimension analysis from SEMs using ImageTool 3.0 revealed a linear relationship between polymer concentration and electrospun fiber diameter. These results are shown in Figures 4.2, 4.4, and 4.6. Although the quantified amount of TF expressed on different scaffold materials did not follow a specific trend, it can be concluded that scaffolds of larger fiber diameters caused higher amounts of TF expression, while electrospun constructs of smaller fiber diameters resulted in lower amounts of TF expressed. These results can be seen in Figures 4.8, 4.9, and 4.10.

The amount of TF expressed by monocytes on scaffolds of PDO ranged from 22.8 - 84.9 ng (Figure 4.8). PCL scaffolds elicited TF expression in the amounts of 4.2-10.2 ng (Figure 4.9). Preliminary results acquired for TF expression on scaffolds of silk and silk:PCL blends revealed levels ranging from 0 - 24.2 ng (Figure 4.10). While the formation of acute thrombotic occlusions are a risk of implanted electrospun vascular grafts, the data from this study reveals electrospun scaffolds of PDO and PCL provide no greater risk from an acute thrombotic occlusion than that of the current standard, e-PTFE. Statistical analysis validates that the amount of TF expressed on scaffolds of PDO and PCL is not significantly different compared with that of e-PTFE. The addition of natural polymers to synthetic based grafts provides more bioactivity to the graft, reducing the potential for thrombotic events to occur. Further analysis will need to be completed to verify the preliminary results of the low expression of TF on scaffolds of silk and silk:PCL blends.

Angiogenic properties of TF have recently been declared. TF may educe upregulation of specific angiogenic chemokines and growth factors as well as migration and differentiation of endothelial cells. *In vitro* experiments have shown levels of TF around 3.6-60 µg to be angiogenic [275]. The levels of acute TF expressed on the electrospun scaffolds from this experiment are below these limits, confirming that they may be non- thrombogenic. Further experimentation will need to be done to determine if the levels of TF expressed on electrospun scaffolds are angiogenic.

The ICW assay was performed using a sensitive fluorescent based antibody that is detectable by infrared. The sensitivity of the technique is remarkable in that it can pick up signals from as little as 10^4 cells. Scanning in the infrared region of the spectrum also greatly diminishes the biological auto-fluorescence, which may be a potential issue in the visible region. This reduced auto-fluorescence increases the signal-to-noise ratio and makes the assay more accurate.

Conclusion

This study provides a positive insight for the ability of electrospun grafts to be successfully used in tissue engineering applications without an increased risk of failure due to an acute thrombotic occlusion compared to that of the current vascular graft material used clinically. The hypothesis of this study was proven: TF expression from monocytes cultured on electrospun scaffolds was not significantly enhanced compared to TF expression from monocytes cultured on e-PTFE scaffolds. However, results from this study do not confirm that these electrospun materials would not elicit the formation of a thrombosis, and further testing needs to be completed to determine this possibility.

Overall, 0.16 g/mL PDO scaffolds caused the highest expression of TF (84.9 ± 51.8 ng) from monocytes, while scaffolds of 0.07 g/mL silk expressed the lowest expression (0 ng). The results from silk scaffolds will need to be investigated further, as this is preliminary data. The results from this *in vitro* experiment will need to be further correlated with *in vivo* models to confirm the reduced potential for thrombotic events to occur from these electrospun constructs.

Chapter 5: CREATION OF ELECTROSPUN PLATELET-RICH PLASMA NANOFIBERS

Preface: The following manuscript appeared in Journal of Tissue Science and Engineering, 2(2), 1-7, 2011. The work included demonstrates the feasibility of enhancing the bioactivity of a bioresorbable vascular graft by electrospinning nanofibers from platelet-rich plasma. Various aspects of the electrospun structures are investigated, including scaffold characterization and cellular interaction.

The Creation of Electrospun Nanofibers from Platelet Rich Plasma

Patricia S. Wolfe[1*], Scott A. Sell[1,2*], Jeffery J. Ericksen[2,3], David G. Simpson[4], and Gary L. Bowlin[1,#]

[1] Department of Biomedical Engineering
Virginia Commonwealth University
401 W. Main St., Richmond, VA 23284, USA

[2] Physical Medicine and Rehabilitation Service
Hunter Holmes McGuire VA Medical Center
1201 Broad Rock Blvd., Richmond, VA 23249, USA

[3] Department of Physical Medicine and Rehabilitation
Virginia Commonwealth University, Richmond, VA 23298, USA

[4] Department of Anatomy and Neurobiology
Virginia Commonwealth University, Richmond, VA 23298, USA

*Authors contributed equally

Abstract

Activated platelet rich plasma (aPRP) contains supraphysiologic amounts of autologous growth factors and cytokines known to enhance wound healing and tissue regeneration. Here we report the first results of electrospinning nanofibers from aPRP to create fibrous scaffolds that could be used for various tissue engineering applications. Human PRP was created, activated by a freeze-thaw-freeze process, and lyophilized to form a powdered preparation rich in growth factors (PRGF). It was dissolved in HFIP at different concentrations to form fibers with average diameters of 0.3 – 3.6 μm. A sustained release of protein from the PRGF scaffolds was demonstrated up to 35 days, and cell interactions with the PRGF scaffolds confirmed cell infiltration after just 3 days. As electrospinning is a simple process, and PRGF contains naturally occurring growth factors in physiologic ratios, creating nanofibrous structures from PRGF has the potential to be beneficial for a variety of tissue engineering applications.

Introduction

The creation of tissue engineering scaffolds through the process of electrospinning has yielded promising results for the field of regenerative medicine over the last decade. These scaffolds can replicate the sub-micron scale topography of the native ECM, through the creation of nanoscale, non-woven fibers, using a number of natural and synthetic polymers. Using the process of electrospinning it is also possible to control the alignment and orientation of the created fibers, creating scaffolds that can be easily customized for nearly any tissue in the body. This control over fiber orientation,

coupled with the diverse array of polymers conducive to being electrospun, allows for the tissue engineer to create structures with tailorable mechanical properties. Additionally, these scaffolds exhibit high surface area-to-volume ratios, high porosities, and variable pore-size distributions that mimic the native ECM and effectively create a dynamic structure capable of sustaining the passive transport of nutrients and waste throughout the structures [5, 100, 291-295].

However, despite the porosity and flexibility afforded by the electrospinning process, it is still considered to be quite challenging to promote cellular penetration into the depth of an electrospun structure, with cells preferring to proliferate and migrate across the surface of the scaffold rather than venture inside it [296-299]. While a number of rather novel techniques have been employed to increase cellularization of electrospun scaffolds [154, 297, 299], nothing has been proven to be useful for tissue engineering applications, nor to date become common practice in the field. The incorporation of growth factors into electrospun matrices for tissue engineering has the potential to enhance scaffold bioactivity, by supplying appropriate physical and chemical cues to promote cellular proliferation and migration, thereby increasing the cellularization of the structures [291, 300, 301]. By replicating the role of the native ECM in the normal wound healing cascade, that is serving as a reservoir of soluble growth factors critical to regeneration and providing a template for tissue repair, it may be possible to accelerate cellularization and tissue repair [292, 300].

PRP is a supraphysiologic concentration of platelets suspended in plasma intended to serve as an autologous source of concentrated growth factors and cytokines. The use of PRP has been growing rapidly in the clinical world, as activated-PRP (aPRP)

has been proven effective in accelerating healing in a number of tissues: osteochondral defects [302-304], tendon/ligament injuries [302-308], and chronic skin wounds (diabetic and pressure ulcers) [303, 304, 309, 310]. The creation of aPRP is a relatively simple procedure that can be performed bedside, typically involving a blood draw and centrifugation to concentrate the platelet portion, followed by a platelet activation step and the delivery of the aPRP to the site of injury. There have been several methods reported in the literature on successfully activating and delivering aPRP to an injury site, with most involving the creation of a platelet gel using thrombin [302-304, 311] or $CaCl_2$ [302-304, 312]. These aPRP gels can then be easily applied to wound sites through injection or topical application.

The basis behind the use of these aPRP gels is that through the activation of the platelets, the alpha and dense granules contained within the platelets release an array of growth factors and cytokines critical to mediating normal wound healing [302, 304, 312-314]. The milieu of growth factors and cytokines released from the aPRP are in physiologically relevant ratios, albeit in concentrations several times higher than that of normal blood due to the linear relationship between platelet and growth factors concentrations [315]. Activated PRP has been shown to contain platelet derived growth factor (PDGF), transforming growth factor-β (TGF-β), VEGF, fibroblast growth factor (FGF), epidermal growth factor (EGF), and others in elevated concentrataions [302, 304, 305, 309, 312-314]. Activated PRP has also been shown to contain a number of macrophage and monocyte mediators such as RANTES (Regulated upon Activation, Normal T-cell Expressed, and Secreted), lipoxin, and an array of interleukins capable of

mediating inflammation [313]. In addition, the plasma portion of the PRP contains the proteins albumin, fibrinogen, a number of immunoglobulins, and more [316-318].

While the incorporation of growth factors and cytokines into electrospun scaffolds to modify cellular response is not new, the majority of studies have previously investigated single or multiple growth factors from isolated or recombinant sources. This method can be prohibitively expensive and difficult to deliver physiologically relevant concentrations [301, 302, 319], while aPRP has proven an efficient and cost-effective method for acquiring a number of highly concentrated factors. The purpose of this study was to create an electrospun scaffold that would harness the reparative potential and bioactivity found in aPRP, namely the growth factor and cytokine milieu contained within, by lyophilizing aPRP and creating PRGF suitable for electrospinning. Utilizing the plasma proteins contained within the PRGF, namely fibrinogen which has been successfully electrospun in the past [21, 289, 320, 321], it was hypothesized that pure lyophilized PRGF could be electrospun into a stable scaffolding material for tissue engineering applications. Such a scaffold, containing a concentration of multiple growth factors and cytokines, would have the potential to promote cellularization of the structure while providing a sustained release of growth factors capable of providing a chemotactic gradient for cellular recruitment.

Methods

Creation of aPRP and PRGF

Fresh human whole blood from 3 donors was purchased (Biological Specialty Corp., Colmar, PA, USA), pooled, and used in a SmartPReP® 2 (Harvest Technologies

Corp., Plymouth, MA, USA) centrifugation system to create PRP per manufacturers protocol. A small aliquot of both pooled whole blood and PRP were sent to the Harvard Immune Disease Institute's Blood Research laboratory to determine their respective platelet concentrations. PRP was then subjected to a freeze-thaw-freeze (FTF) cycle for platelet lysis and activation. Briefly, PRP was placed in a -70° C freezer for 24 hrs followed by a 37° C waterbath for 1 hr, and then returned to the -70° C freezer for 24 hrs. This method has previously been found to contain the same, and in some cases, higher levels of bFGF and VEGF as thrombin and $CaCl_2$ aPRP (data not published). Frozen aPRP was then lyophilized for 24 hrs to create a dry PRGF powder which was finely ground in a mortar and pestle prior to use.

Creation of Electrospun PRGF Scaffolds

PRGF was dissolved in HFIP (TCI America Inc., Portland, OR, USA) at different concentrations, ranging from 80-280 mg/ml, to determine the optimum fiber forming concentration range. HFIP was used as the solvent because, not only is it the most widely used solvent in our lab, but it also is very versatile in creating nanofibrous scaffolds from a variety of natural and synthetic polymers without much difficulty. In addition, previously published studies performed by our lab, as well as many others, have shown electrospun scaffolds fabricated from HFIP are biocompatible [20, 38, 106, 144, 242, 299, 320, 322]. Once in solution, PRGF was loaded into a 3 mL Becton Dickinson syringe, and placed in a KD Scientific syringe pump (model number 100, Holliston, MA, USA) for dispensing at a rate of 2.5 ml/hr. A blunt 18 gauge needle was placed on the syringe, and the positive voltage lead of a power supply (Spellman CZE1000R; Spellman

High Voltage Electronics Corp., Hauppauge, NY, USA) was attached to the needle and set to 25 kV. A grounded mandrel (1.9 cm wide x 7.6 cm long x 0.5 cm thick; 303 stainless steel) was placed 15 cm away from the needle tip and was rotated at 500 rpm and translated at 7.5 cm/s over 15 cm distance for collection of the fibers.

Scaffold Characterization

SEM and Fiber Diameter

Fiber diameter characterization was accomplished using SEM (Zeiss EVO 50 XVP, Peabody, MA, USA) of each scaffold. Samples from each scaffold were mounted on an aluminum stub and sputter coated with gold for imaging. The average fiber diameter of each electrospun structure was determined from the SEM images using UTHSCSA ImageTool 3.0 software (Shareware provided by University of Texas Health Science Center in San Antonio). Fiber diameter averages and standard deviations were calculated by taking the average of 60 random measurements per micrograph.

Protein Release Kinetics

From scaffolds of 100, 150, and 200 mg/ml PRGF, 10 mm diameter discs were punched, disinfected with a 30 minute soak in ethanol, followed by three 10 minute rinses in PBS, and placed in a 48 well plate with 500 µl of PBS. On days 1, 4, 7, 10, 14, 21, 28 and 35, PBS was retained and kept in a -70 °C until ready for evaluation. A generic protein assay (BCA Protein Assay, Thermo Scientific Pierce, Rockford, IL, USA) was performed on samples to quantify the concentration of total protein released from the PRGF scaffolds.

Gel Electrophoresis

Gel electrophoresis was performed to analyze the molecular weight of the proteins in PRGF, platelet poor plasma (PPP), and electrospun PRGF scaffolds and compare them to those of fibrinogen (FBG, Sigma Aldrich, St. Louis, MO, USA) and bovine serum albumin (BSA, Sigma Aldrich, St. Louis, MO, USA) controls. Briefly, 2 mg BSA, FBG, PRGF, and 100, 150, 200 mg/ml PRGF scaffolds were solubilized in a reducing agent containing laemmeli buffer with 5 % β-mercaptoethanol. Samples were boiled for 3-5 minutes to further ensure they were solubilized, and 10 µL of each sample was placed in duplicate in each lane of 4-15% polyacrylamide 18-well gels (Criterion Bio-Rad, Hercules, CA, USA). A molecular weight protein ladder (20 µL, Sigma Aldrich, St. Louis, MO, USA) was run to provide a molecular weight basis for protein identification and comparison. Samples were run at constant voltage of 120 V over 2 hours. After the 2 hours, the gels were stained with Coomassie Blue, and evaluated by the Bio-Rad Gel Doc™ 2000 system.

Fluorescent Based Assay

FBG concentration was quantified in the PRGF electrospun scaffolds, as well as in aPRP, blood and PPP by using a fluorescent based assay. Scaffolds of 100, 150, and 200 mg/ml electrospun PRGF (10 mm diameter discs, n=4) were placed in a 48 well plate and blocked with Odyssey Blocking Buffer (LI-COR Biosciences, Lincoln, NE, USA) for 1 hour at room temperature. Simultaneously, human FBG from reference plasma (Fisher Scientific, Pittsburgh, PA, USA) was diluted in DI water at concentrations of 76, 38, 19, 9.5, 4.75, 2.38, 1.19, 0.59, and 0 mg/dl and was blotted on a PVDF membrane, along with aPRP, PPP, blood, and PRGF diluted in water at 10, 5, and 1 mg/ml. The membrane

was blocked in Odyssey Blocking Buffer for one hour at room temperature. After blocking, standards and samples were incubated in anti-human fibrinogen antibody (Millipore, Billerica, MA, USA) at room temperature for 1.5 hours. All samples and standards were then washed four times with 0.1% Tween-20 in PBS, after which the signal from mouse anti-human fibrinogen antibody was detected with goat anti-mouse IgG secondary antibody tagged with a fluorescent 800 nm marker (ThermoScientific, Pittsburgh, PA, USA). To account for antibody background fluorescence, each scaffold was incubated with secondary antibody only. Samples and standards were incubated in the secondary antibody for 1 hour at room temperature without exposure to light. After washing, the samples were scanned using the 800 nm channel of the Odyssey Infrared Imaging System (LI-COR Biosciences, Lincoln, NE) at an intensity of 3.5. Fluorescence intensities were measured using circular gates that completely surrounded the scaffolds and well plates. Background fluorescence that was obtained from samples incubated with secondary antibody only was subtracted from the signal intensities of the samples incubated with both primary and secondary antibodies.

Evaluation of Cell Interaction

To determine the interaction of human cells on electrospun PRGF scaffolds, 10 mm diameter discs were punched from scaffolds of 100, 150, and 200 mg/ml PRGF, disinfected (30 minute soak in ethanol followed by three 10 minute rinses in PBS), and placed in a 48 well plate. A sterile Pyrex cloning ring (10 mm outer diameter, 8 mm inner diameter) was placed on top of each scaffold to prevent them from floating, and to ensure all cells stayed on the surface of the scaffold during culture. Each scaffold was seeded

with either 100,000 human adipose derived stem cells (hADSC) isolated from medical waste lipoaspirate [323] in 500 µl of complete media (DMEM low glucose supplemented with 10% FBS and 1% penicillin/streptomycin, Invitrogen, Carlsbad, CA, USA) or 100,000 human umbilical artery smooth muscle cells (hSMC, Lonza, Basel, Switzerland) in 500 µl of complete media (SMGM-2 bullet kit, Lonza, Basel, Switzerland). Controls consisted of scaffolds in complete media without cells. Media was changed every third day, and on days 3 and 10, scaffolds were fixed in 10% Formalin and cryosectioned for 4',6-diamidino-2-phenylindole (DAPI) staining.

Statistical Analysis

Statistical analysis was performed using JMP®IN 8.0 statistical software (SAS Institute, Inc., Cary, NC, USA) and was based on a Kruskal-Wallis one-way analysis of variance on ranks and a Tukey-Kramer pairwise multiple comparison procedure (α=0.5). Graphical depictions of mean data were constructed with Microsoft Excel 2007, with error bars representing standard deviations.

Results and Discussion

Creation of aPRP and PRGF

It was determined by Harvard Immune Disease Institute's Blood Research Laboratory that the PRP created by the SmartPReP® 2 centrifugation system resulted in a 5.5 fold increase in platelets compared to the pooled whole blood used in this study (955 x 10^3 platelets/µl versus 175 x 10^3 platelets/µl). This result is in agreement with published data [324], and based upon the linear relationship between platelet count and

growth factor concentration, a resulting similar fold increase should present in platelet derived growth factor concentrations [315].

Electrospun Scaffold Characterization

SEM and Fiber Diameter

SEM characterization of the electrospun PRGF scaffolds is shown in Figure 5.1. The micrographs illustrate the nanofibrous structures of each scaffold starting around 100 mg/ml, with the appearance of a large range of fiber diameters for the different PRGF concentrations, as well as increased void space as PRGF concentration increases. Fiber diameters for the scaffolds range from 0.28 ± 0.29 μm for 100 mg/ml PRGF to 6.37 ± 4.81 μm for 280 mg/ml PRGF (Figure 5.2). Statistical analysis reveals the average fiber diameters for 100 and 175 mg/ml PRGF are significantly different from all other scaffolds, with the exception of 125 and 150 mg/ml PRGF. Average fiber diameters for scaffolds of 200, 220, and 250 mg/ml PRGF are significantly different from all other scaffolds, but not each other. Scaffolds of 280 mg/ml PRGF have significantly greater fiber diameters from those of all other scaffolds. This linear relationship between polymer concentration and fiber diameter is expected, as it has been well established previously [5, 21, 38, 144, 325]. The broad range of fiber diameters produced during the electrospinning process allows for flexibility in the fabrication of electrospun scaffolds for different tissue engineering applications.

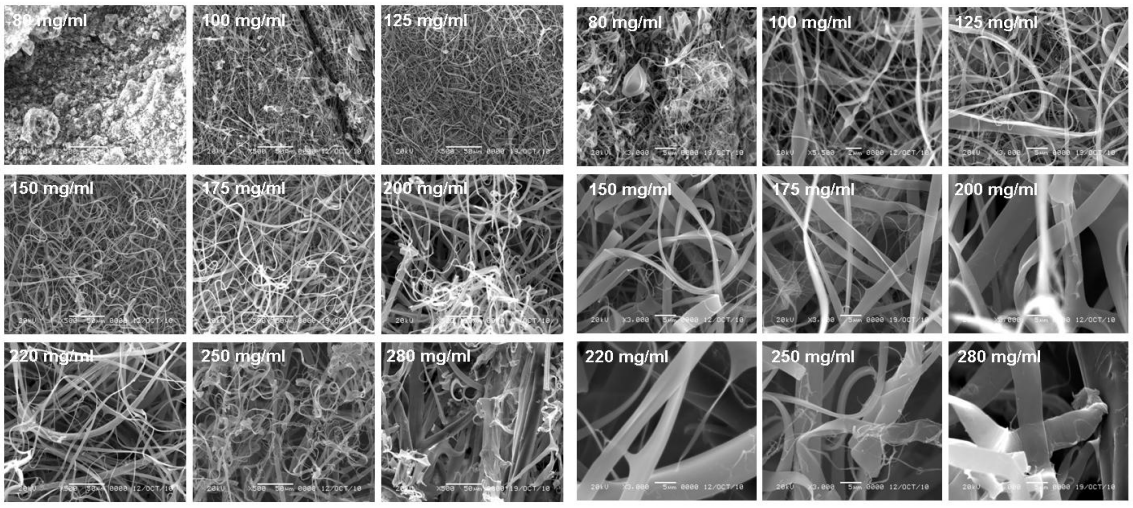

Figure 5.1. (Left) SEM of electrospun PRGF scaffolds taken at 500x, scale bar represents 50 µm. (Right) SEM of electrospun PRGF scaffolds taken at 3000x, scale bar represents 5 µm.

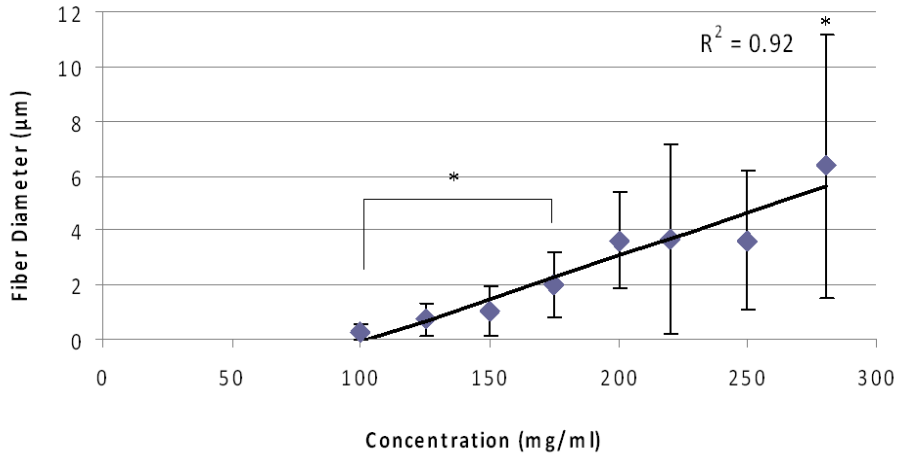

Figure 5.2. Graph of mean fiber diameters for electrospun PRGF scaffolds of different concentrations illustrating the linear relationship between PRGF concentration and fiber diameter. * denotes statistical significance.

Protein Release Kinetics

The quantified protein release results from electrospun PRGF scaffolds are shown in Figure 5.3, demonstrating protein release from PRGF scaffolds was detectable over 35 days. The release kinetics illustrates a peak release of protein on day 1 for all scaffold concentrations, followed by a distinct decrease in release for days 4-21. Unexpectedly, at

day 28, protein release increases for all scaffolds. By day 35 protein release has decreased, however, compared to days 4-21, overall release has increased. Surprisingly, 100 mg/ml PRGF scaffolds had the highest release of protein over the 35 days compared to the other scaffolds, releasing 370 µg/ml of protein at day 1 and 175 µg/ml by day 35. Scaffolds of 150 and 200 mg/ml PRGF had similar release kinetics over the 35 days (185 – 49 µg/ml and 194 – 96 µg/ml for the 150 and 200 mg/ml PRGF scaffolds, respectively). The initial burst release from scaffolds at day 1 is expected, as PRGF from the surface of the scaffolds is released. The high protein release from scaffolds of 100 mg/ml PRGF over the other scaffolds may be explained by the scaffold's smaller fiber diameters. Although not specifically investigated in this study, other previously published studies have demonstrated similar results, and explain that with smaller fiber diameters there is less distance for molecules to traverse to reach the fiber surface, hence, more protein release from the fibers over time [326-329]. The rise in protein release after day 21 may be due to fiber degradation of the PRGF scaffolds occurring around 28-35 days and subsequent release of entrapped proteins. Although degradation may have started to occur around day 28, the electrospun scaffolds were still very much intact at 35 days. This outcome was unexpected, as most electrospun natural polymers degrade rapidly in solution and need to be cross-linked or co-spun with a synthetic polymer to increase their stability [147]. Statistical analysis revealed protein release at day 1 and day 28 from all PRGF scaffolds was significantly greater than protein release from those respective scaffolds at all other time points (days 4, 7, 10, 14, 21, and 35). For scaffolds of 100 mg/ml PRGF, protein release at days 1, 4, and 35 was significantly different from that at all other time points for that respective scaffold (days 7, 10, 14, and 21).

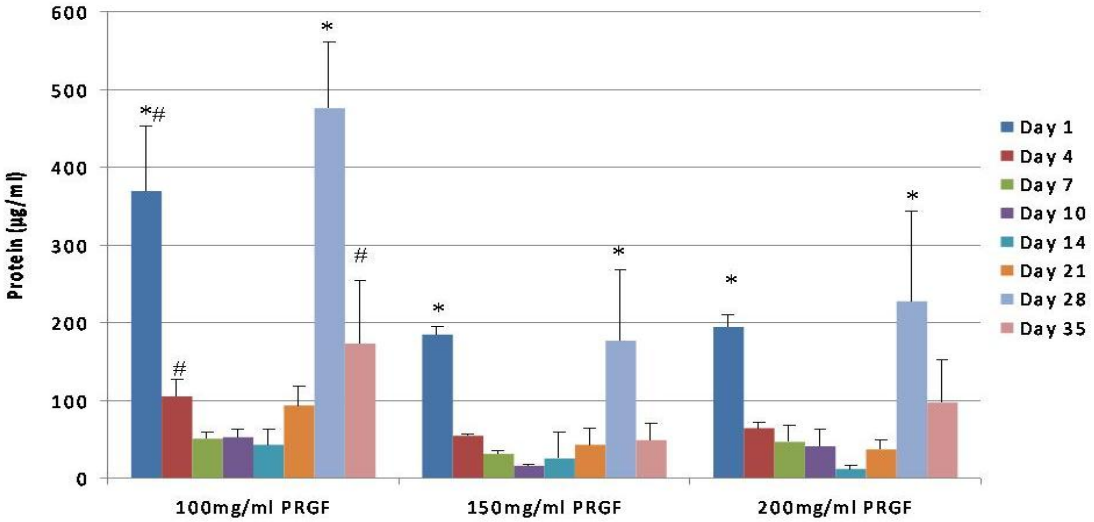

Figure 5.3. Quantification of generic protein released from pure PRGF scaffolds over 35 days. * indicates significant differences, $p < 0.05$, for days 1 and 28 when compared to all other time points for each material, but not each other. # indicate statistically significant differences, $p < 0.05$, between days 1, 4, and 35 when compared to other time points, but not each other. Minimum level of detection was 17 µg/ml.

Gel Electrophoresis

The results from the gel electrophoresis technique are illustrated in Figure 5.4. The electrophoretic pattern of FBG appears as expected, as it has been previously determined that the alpha, beta and gamma chains have average molecular weights of around 68, 58 and 50 kDa, respectively [330]. BSA also exhibits a pattern that would be expected, with a distinct band around 67 kDa [318, 331, 332]. The electrophoresis results of PRGF resembles those of BSA and the FBG alpha chain, with a distinct band around 68 kDa. This band is also likely to be representative of hemoglobin, which has a molecular weight of 68 kDa. PRGF also illustrates a faint band around 80 kDa, which is representative of different glycoprotiens, including transferrin, and plasminogen, and a distinct thick band at 14 kDa, indicating the presence of multiple chains of haptoglobin and transthyretin [318]. These results are not surprising, due to the fact that plasma

contains large amounts of these proteins. Interestingly, PPP has a similar electrophoretic pattern to that of both FBG and BSA, with the triple banding that is typically seen with FBG and the distinct band at 70 kDa that is characteristic of BSA. Additionally, PPP has additional banding around 80, 25, 18, and other faint bands between 25 – 50 kDa. These bands most likely represent a multitude of components, including different kinds of glycoproteins (similar to PRGF), various IgG light chains, multiple haptoglobin chains and various lipoproteins (both LDL and HDL) [318]. The fact that PPP is made up of mostly albumin, fibrinogen, and immunoglobulins is understandable, due to the fact that these components are the most prevalent proteins in blood.

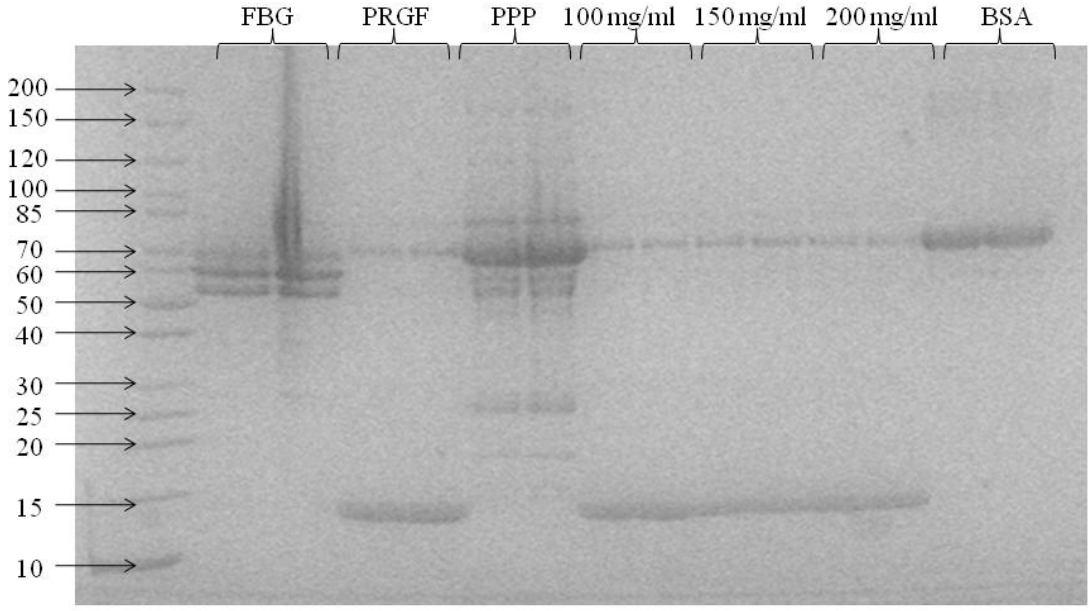

Figure 5.4. Electrophoretic patterns of molecular weight standards, FBG, PRGF, PPP, PRGF scaffolds of 100, 150, and 200 mg/ml and BSA in the 4-20% polyacrylamide gels.

Fluorescent Based Assay

The PVDF membrane that was spotted with 0 to 76 mg/dl of human FBG was scanned by the Odyssey system and fluorescent intensities were acquired. The standard

curve obtained is shown in Figure 5.5, illustrating a linear relationship (R^2 = 0.96, y = 1.58x +13.8). Using the standard curve equation, the amount of FBG in each sample was determined.

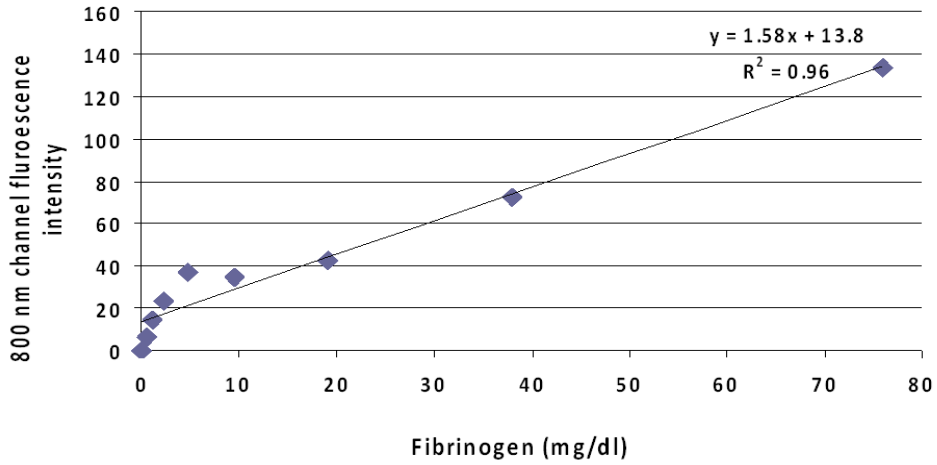

Figure 5.5. Linear curve (R^2 = 0.96) obtained from dilutions of human FBG standards for fluorescent assay.

The amount of FBG expressed on scaffolds of pure PRGF ranged from 30-51 mg/dl (Figure 5.6, right). Specifically, 100 mg/ml PRGF amounted in 51 mg/dl FBG, 150 mg/ml PRGF contained 43 mg/dl FBG, and 200 mg/ml PRGF had 30 mg/dl FBG. PRGF diluted in water at 10, 5 and 1 mg/ml resulted in 67, 37, and 21 mg/dl FBG, respectively. Blood and PPP contained the highest amount of FBG (423 and 440 mg/dl, respectively), while aPRP contained only 234 mg/dl FBG. The values of FBG that were quantified in blood, aPRP, and PPP were expected, and are consistent with previously published data [324, 333, 334]. The reason behind why 200 mg/ml PRGF contained less amounts of FBG than 100 mg/ml PRGF is not completely understood, and will need to be investigated further in future studies.

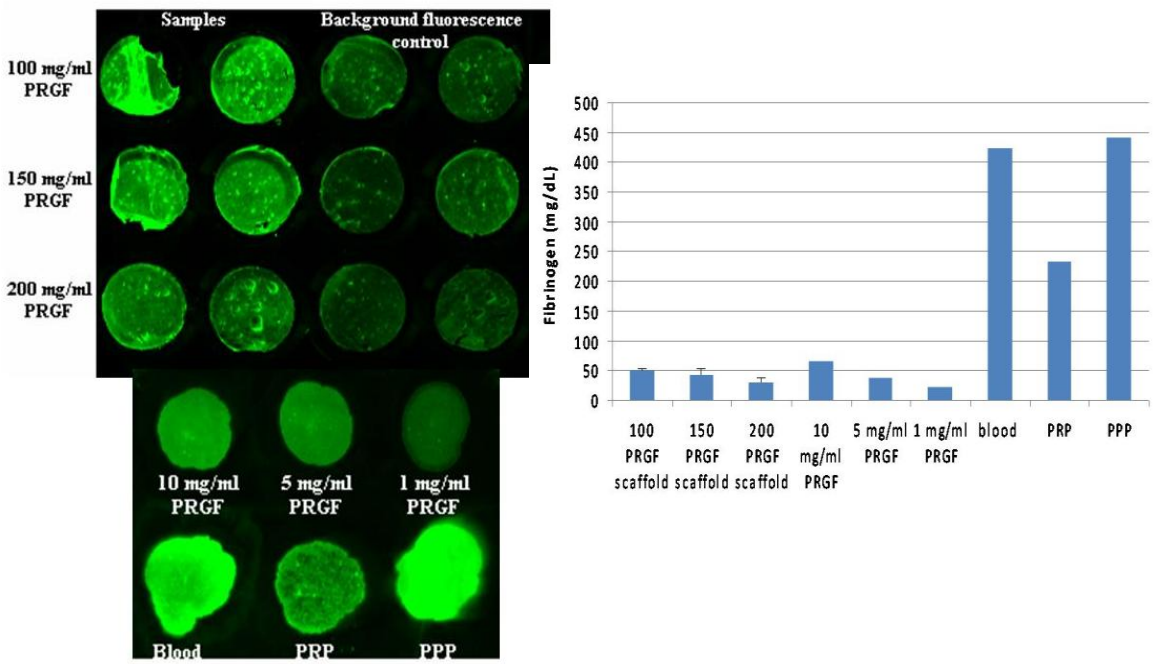

Figure 5.6. (Left) FBG fluorescence intensity of 100, 150, and 200 mg/ml pure PRGF scaffolds, 10, 5, and 1 mg/ml PRGF in PBS and blood, aPRP and PPP taken at 800 nm, 3.5 intensity. (Right) Quantified FBG expression on scaffolds, PRGF in water, blood, aPRP and PPP.

The authors speculate the presence of FBG and hemoglobin in PRGF may be the reason why this protein is stable enough to form electrospun nanofibers. More specifically, Factor XIII, a stabilizing enzyme of the blood coagulation system that cross-links fibrin, may explain why the electrospun PRGF scaffolds were still intact during the protein release study, even after 35 days in culture. This speculation is based on previous studies, which have demonstrated the ability of FBG and hemoglobin to form electrospun nanofibers from HFIP [21, 335]. In addition to the methods presented in this study, the presence of FBG, albumin, and hemoglobin in electrospun PRGF scaffolds was further confirmed by mass spectrometry.

Cell Interaction

Results from DAPI staining of hADSCs cultured on pure PRGF scaffolds reveals cell penetration into the scaffolds after as little as 3 days (Figure 5.7). As PRGF electrospinning concentration increases from 100 to 200 mg/ml, it appears there is greater cell migration into the scaffolds, potentially due to the increase in average fiber diameter and subsequent increase in scaffold void space. Regardless, after 10 days it is evident hADSCs have migrated through the entire thickness of the PRGF scaffolds for all concentrations.

hSMC interaction with PRGF scaffolds is shown in Figure 5.8, demonstrating after only 3 days there is cell migration throughout the entire 200 mg/ml PRGF scaffold. 100 mg/ml PRGF scaffolds demonstrated little penetration of hSMC into the scaffold, with most cells remaining on the surface of the scaffold even after 10 days. Scaffolds of 150 and 200 mg/ml PRGF had complete cellular migration throughout the entire scaffold by day 10. Surprisingly, hSMC cultured on 150 mg/ml PRGF completely migrated from the surface of the scaffold into the middle region in only 10 days.

The reason for this rapid migration of cells into the scaffold may be two-fold: the presence of an array of chemokines and growth factors found in concentrated amounts in aPRP is most likely chemotactic towards multiple cell types, and the increased void space as PRGF electrospinning concentration increases allows cells to easily migrate into the scaffold. Although not investigated in this manuscript, a previous study conducted by the authors has confirmed the release of RANTES and PDGF-BB from electrospun PRGF fibers (data not published). The release of these growth factors and cytokines, as well as many others contained within PRGF that have been previously shown to be chemotactic

and induce cell proliferation, is most likely the reason for enhanced cell infiltration within the scaffolds. Although it was not directly analyzed in this study, from the SEMs it appears the difference in fiber diameters between the PRGF concentrations affects the porosity of the scaffolds, with increased void space occurring as PRGF concentration increases.

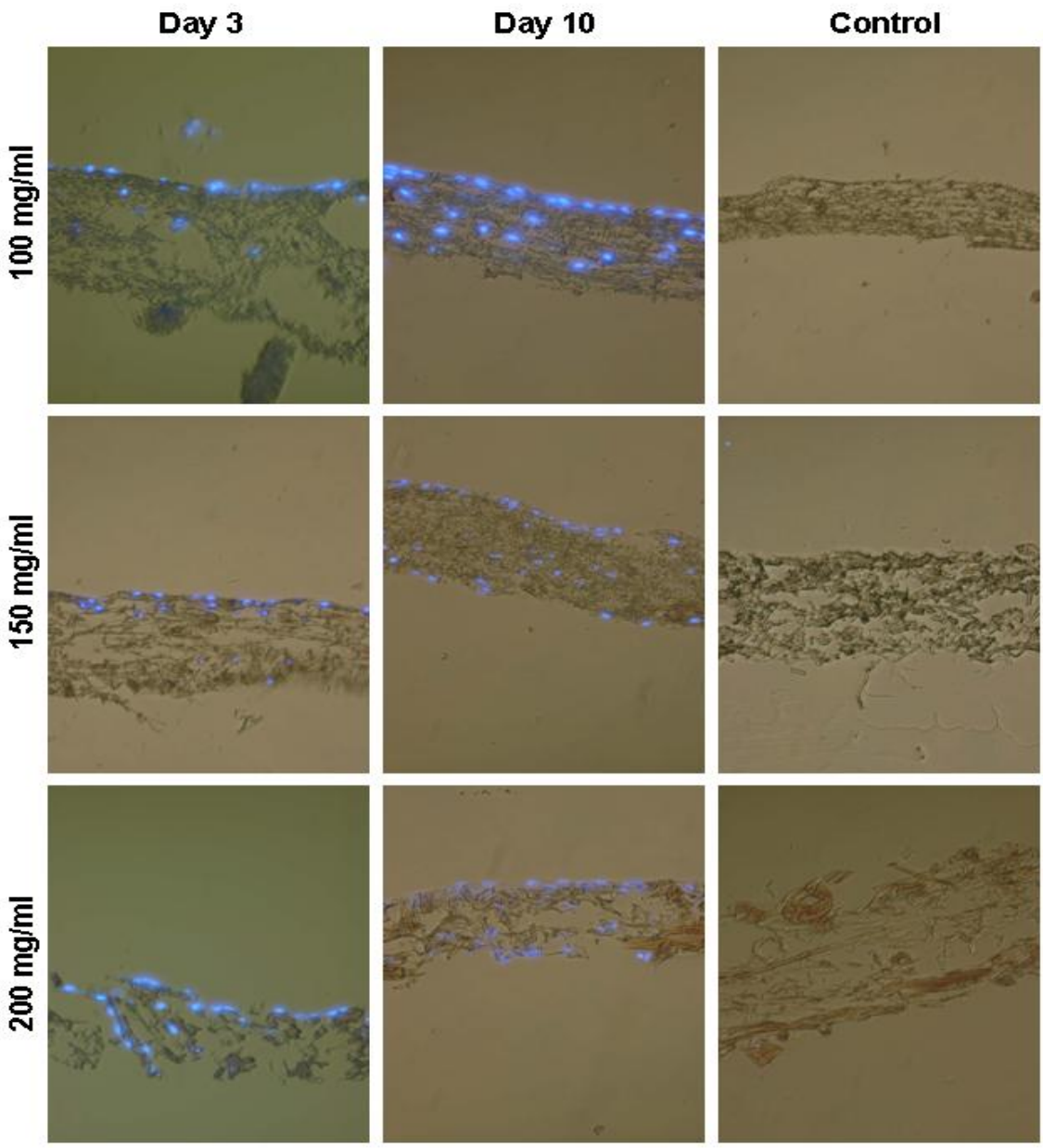

Figure 5.7. DAPI staining of ADSCs cultured on electrospun scaffolds of pure PRGF at days 3 and 10. Images at 20x.

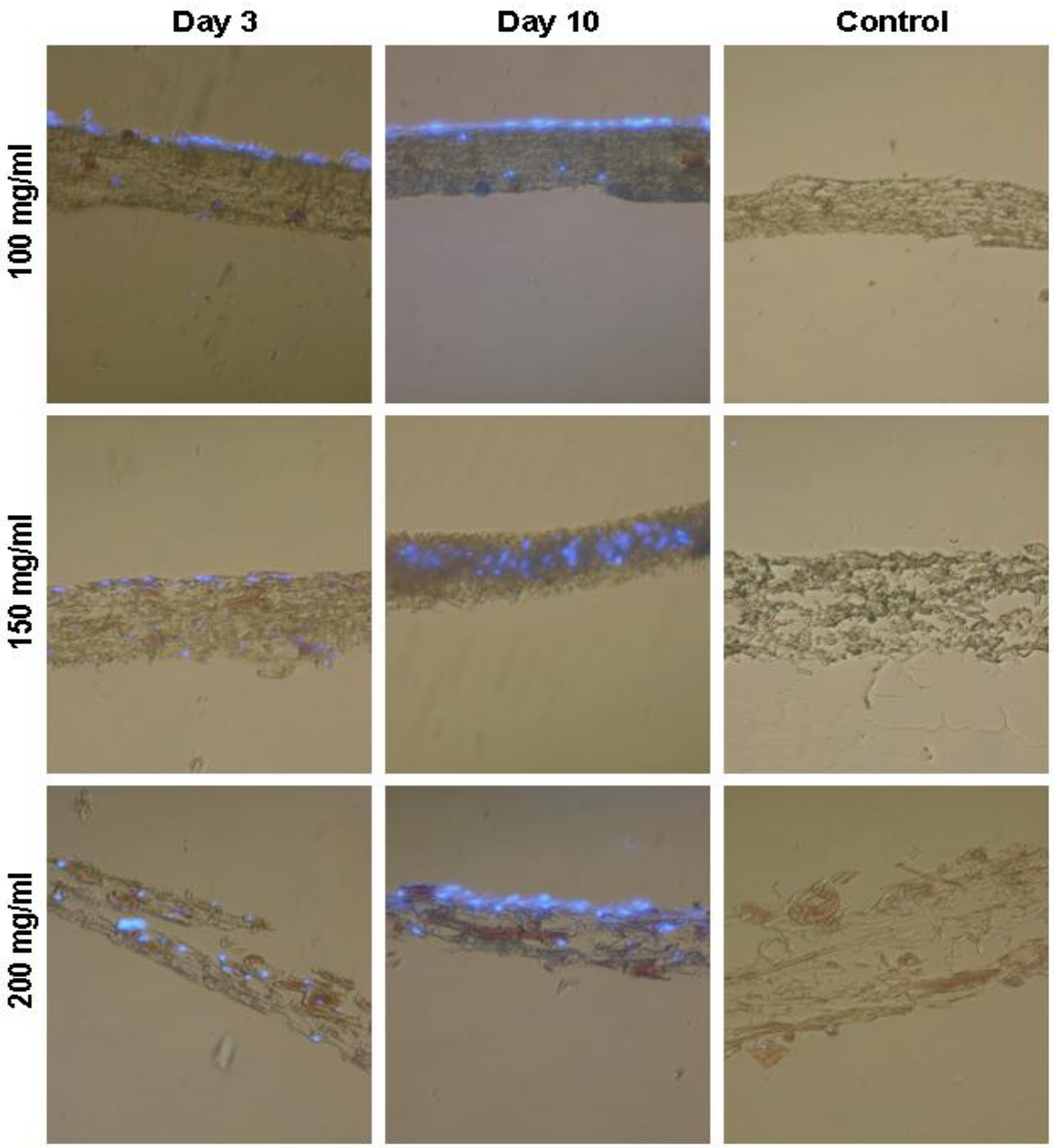

Figure 5.8. DAPI staining of SMC cultured on electrospun scaffolds of pure PRGF at days 3 and 10. Images at 20x.

Conclusion

This manuscript demonstrates, for the first time, the feasibility of creating a nanofibrous scaffold from aPRP. As PRP has gained recent popularity in the clinical

setting due to its ability to enhance healing and promote regeneration in an array of tissues clinically, it may prove beneficial when used as a tissue engineering scaffolding material. Not only was the hypothesis proven that pure lyophilized, electrospun PRGF scaffolds could be stable for extended periods of time *in vitro*, but they also exhibited a sustained release of proteins known to be important for tissue regeneration for up to 35 days. Additionally, despite the fact that electrospinning is often criticized for its perceived lack of cellular penetration, electrospun PRGF scaffolds promoted rapid cellular infiltration due to the presence of a milieu of growth and chemotactic factors inherent to aPRP. While this preliminary evaluation of electrospun PRGF demonstrated its tissue engineering potential in an *in vitro* setting, its true benefit may be seen in an *in vivo* scenario where multiple regenerative cell types can act concomitantly on the scaffolds in a manner similar to the natural healing cascade through the sustained chemotactic and growth factor gradients eluted.

Acknowledgements

The authors would like to thank Drs. Sherwin Kevy and May Jacobsen from the Harvard Immune Disease Institute's Blood Research Laboratory for conducting platelet counts on pooled whole blood and PRP. The authors would also like to thank Dr. Kristina Nelson from the Virginia Commonwealth University Chemical and Proteomic Mass Spectrometry Core Facility for performing mass spectrometry on electrospun PRGF. Cryosectioning of PRGF scaffolds for DAPI staining was performed at the Virginia Commonwealth University Department of Anatomy and Neurobiology Microscopy Facility.

Chapter 6: INCORPORATION OF PLATELET-RICH PLASMA INTO ELECTROSPUN SCAFFOLDS

Preface: Parts of the following chapter are taken from the manuscript "Incorporating Platelet-Rich Plasma into Electrospun Scaffolds for Tissue Engineering Applications" appearing in Tissue Engineering: Part A, 17(21 and 22), 2011. The complete manuscript can be found in Appendix A. This chapter investigates the potential to create, lyophilize, and incorporate platelet-rich plasma into electrospun PCL scaffolds to create a delivery vehicle for a number of growth factors and cytokines known to enhance regeneration and wound healing without compromising scaffold mechanical properties.

Incorporating Platelet-Rich Plasma into Electrospun Scaffolds for Tissue Engineering Applications

Scott A. Sell[1, 2*], Patricia S. Wolfe[2*], Jeffery J. Ericksen[1, 3], David G. Simpson[4], and Gary L. Bowlin[2#]

[1]Physical Medicine & Rehabilitation Service
Hunter Holmes McGuire VA Medical Center, Richmond, VA 23249

[2]Department of Biomedical Engineering
Virginia Commonwealth University, Richmond, VA 23284

[3]Department of Physical Medicine and Rehabilitation
Virginia Commonwealth University, Richmond, VA 23298

[4]Department of Anatomy and Neurobiology, Virginia Commonwealth University, Richmond, VA 23298

[*]Authors contributed equally

Abstract

PRP therapy has seen a recent spike in clinical interest due to the potential that the highly concentrated platelet solutions hold for stimulating tissue repair and regeneration. The purpose of this study was to incorporate PRP into a well-known electrospun polymer to determine the effect on scaffold mechanical properties and to show the release kinetics of growth factors eluted from the structures. PRP underwent a freeze-thaw-freeze process to lyse platelets, followed by lyophilization to create a powdered PRGF, which was subsequently added to the electrospinning process. Release of protein from scaffolds over time was quantified, along with unaxial tensile testing. Protein assays demonstrated a sustained release of protein from PRGF containing scaffolds at up to 35 days in culture. Mechanical integrity of the scaffold was not affected by the addition of PRGF at certain concentrations, and was retained over a 28 day period. The incorporation of PRGF into electrospun structures may prove beneficial in a number of tissue engineering applications.

Introduction

PRP therapy is a method of collecting and concentrating autologous platelets, through centrifugation and isolation, for the purpose of activating and releasing their growth factor-rich α- and dense granules. The discharge of these concentrated granules releases a number of growth factors and cytokines in physiologically relevant ratios, albeit in concentrations several times higher than that of normal blood, that are critical to tissue regeneration and cellular recruitment. Some of the more highly concentrated

factors found within PRP include PDGF, TGF-β, VEGF, FGF, EGF [302, 304, 305, 309, 312-314].

Clinically, PRP therapy has been used to stimulate tissue growth and regeneration in a number of different tissues; effectively accelerating the healing response in patients suffering from osteochondral defects [302-304], tendon/ligament injuries [302-308], and chronic skin wounds (diabetic and pressure ulcers) [303, 304, 309, 310]. Typically, these procedures involve a blood draw and centrifugation to concentrate the platelet portion, followed by a platelet activation step and the delivery of the activated PRP to the site of injury. There have been several methods reported in the literature on successfully activating and delivering PRP to an injury site, with most involving the creation of a platelet gel using thrombin [302-304, 311] or $CaCl_2$ [302-304, 312]. These PRP gels can be easily applied to wound sites through injection or topical application.

However, studies have shown that the use of thrombin as a clotting agent can result in a rapid activation of platelets and a bolus release of growth factors, with 70% of growth factors released within 10 minutes of clotting, and nearly 100% released within 1 hour [302]. This "dumping" method fails to maximize the cell stimulating potential of the PRP growth factors as most are cleared before they can take effect [336]. Growth factor release from PRP gels can be slowed when the gel is formed with $CaCl_2$ rather than thrombin. The addition of $CaCl_2$ to PRP results in the formation of autogenous thrombin from prothrombin and the eventual formation of a loose fibrin matrix that will secrete growth factors over 7 days [302].

Other techniques have been evaluated for further sustaining the release of growth factors from PRP and include the use of gelatin gel microspheres [337], lyophilized PRP

[338-341], and alginate beads [336]. The injection of PRP gelatin gel microspheres in a mouse ischemic hind limb model demonstrated sustained release of the PRP potent angiogenic components as illustrated by an increase in perfusion, capillary density, and mature blood vessel density [337]. Alginate beads were shown to be successful in delivering (based on cell proliferation) PRP-derived growth factors and cytokines over the course of 14 days [336]. The use of freeze-dried PRP in a dermal wound has been shown to significantly increase cellular proliferation (up to 21 days), tissue regeneration and angiogenesis in a mouse dermal wound [338-341]. Collectively, these studies demonstrate the importance of keeping PRP-derived growth factors and cytokines in the wound site and slowly releasing them as the wound site becomes infiltrated with reparative cells.

While a number of individual growth factors and/or cytokines have been used previously in an array of sustained release tissue engineering and regenerative medicine applications with positive results, the use of either single or multiple isolated growth factors/cytokines is often prohibitively expensive, and it can be difficult to replicate physiologically relevant quantities [302]. The purpose of this study was to attempt to harness the reparative potential found in PRP, namely the growth factor and cytokine milieu contained within, and apply it to tissue engineering through the creation of a PRP eluting electrospun scaffold. It was hypothesized that the inclusion of lysed and lyophilized PRP would create an effective PRGF capable of being introduced into the electrospinning process to create a scaffold capable of a sustained release of growth factors, without compromising mechanical properties.

Materials and Methods

Creation of PRP and PRGF

Fresh human whole blood from 3 donors was purchased (Biological Specialty Corp.), pooled, and used in a SmartPReP® 2 (Harvest Technologies Corp.) centrifugation system to create PRP per manufacturers protocol. A small aliquot of both pooled whole blood and PRP were sent to the Harvard Immune Disease Institute's Blood Research laboratory to determine their respective platelet concentrations. PRP was then subjected to a freeze-thaw-freeze (FTF) cycle in a -70° C freezer for cell lysis and activation. Centrifuge tubes containing PRP were placed in a -70° C freezer for 24 hrs followed by a 37° C waterbath for 1 hr, and then returned to the -70° C freezer for 24 hrs. The degree of activation of the FTF lysed PRP, and thrombin (Recothrom, ZymoGenetics Inc.) and 10% $CaCl_2$ (American Regent) activated PRP was quantified through an enzyme-linked immunosorbent assay (ELISA) analysis of VEGF and bFGF (Antigenix America Inc.). Frozen PRP was then lyophilized for 24 hrs to create a dry PRGF powder which was finely ground in a mortar and pestle prior to use.

Creation of PRGF Incorporated Electrospun Scaffolds

Polycaprolactone (PCL, Lakeshore Biomaterials, 125 kDa) was dissolved in 1,1,1,3,3,3 hexafluoro-2-propanol (HFIP, TCI America Inc.) at a concentration of 100 mg/ml. PRGF was then added in concentrations of 10 or 100 mg of PRGF per ml of electrospinning solution (PCL:PRGF(10) and PCL:PRGF(100), respectively) and allowed to dissolve completely into solution. As a means to reduce the thrombogenicity of the

electrospun material and to slow the release of growth factors from the fibers, sodium heparin salt from porcine submucosa (Sigma Aldrich) was dissolved in distilled water at 0.05% or 0.5% (wt.:vol. of electrospinning solution), which correlates to around 100 U/ml or 1000 U/ml, respectively, of electrospinning solution, and then added to PCL electrospinning solutions with and without PRGF [342, 343]. As PRGF can be successfully electrospun by itself from HFIP at a concentration of 200 mg/ml [344], PRGF fibers were also integrated into PCL scaffolds using two separate syringes of PCL and PRGF electrospinning solutions at 90° from each other targeting the same collection mandrel (PCL:PRGF). Heparin was also added to the PCL:PRGF scaffold solutions separately, so there was an equivalent amount of heparin as the other scaffolds overall. Control scaffolds contained no PRGF and no heparin.

All solutions were electrospun onto a grounded rectangular stainless steel mandrel (1.9 cm wide x 7.5 cm long x 0.5 cm thick) rotating at 400 RPM and translating at 6 cm/s over a distance of 12 cm, using a Becton Dickinson syringe fitted with a blunt tip 18 gauge needle and a KD Scientific syringe pump. PCL solutions with and without PRGF and heparin were electrospun using a charging voltage of +22 kV, an air gap distance of 15 cm, and a flowrate of 5 ml/hr. PCL:PRGF used charging voltages of +22 and +25 kV for the PCL and PRGF solutions, respectively, an air gap distance of 15 cm from each syringe to the collecting mandrel, and a flowrate of 2.5 ml/hr for each solution.

Scaffold Characterization

Samples from each of the electrospun constructs was characterized through SEM (Zeiss EV050) to ensure the fibrous nature of the structures. Average fiber diameters and

pore areas were calculated by taking 60 random fiber measurements or pore area measurements from the SEM image using ImageTool 3.0 software (Shareware provided by UTHSCSA).

Uniaxial tensile testing was performed on dog-bone shaped samples (overall length of 20 mm, 2.67 mm at its narrowest point, gage length of 7.5 mm, n=5) punched from each of the electrospun scaffolds. All specimens were cultured in complete media (DMEM low glucose supplemented with 10% FBS and 1% penicillin/streptomycin) at standard conditions (37°C, 5% CO_2) for 1, 7, 14, 21, or 28 days. At each time point, samples were uniaxially tested to failure at a rate of 10 mm/min (1.33 min^{-1} strain rate) using an MTS Bionix 200 testing system with a 100 N load cell (MTS Systems Corp.). Peak stress, modulus, and strain at break were calculated using TestWorks version 4.

Endotoxin levels of the scaffolds were detected using a Limulus Amebocyte Lysate Endosafe® Endochrome-k kit (Charles River Laboratories). From each of the electrospun materials, 6 mm diameter discs were punched (n=3), disinfected (30 minute soak in ethanol followed by three 10 minute rinses in PBS), and placed in a 96 well plate in 100 µL reagent water (provided by the kit). Samples were cultured in standard conditions overnight, after which the reagent water was aspirated and analyzed for endotoxin levels.

Quantification of Protein Release Kinetics

To determine the effect heparin had on the protein release kinetics from the scaffolds, 10 mm diameter disks were punched (n=3), disinfected (30 minute soak in ethanol followed by three 10 minute rinses in PBS), and placed in a 48-well plate with

500 µl of PBS. The PBS was changed and retained for evaluation on days 1, 4, 7, 10, 14, 21 and 28. In addition, 500 µl of PBS with PRGF (1 mg/ml) and heparin (0.05% and 0.5%) was placed in a 48-well plate and retained after 1 day for analysis. Samples at each time point were subjected to a generic protein assay (BCA Protein Assay, Thermo Scientific Pierce) to quantify the concentration of total protein released.

Based upon these results, specific ELISAs (TGF-β (Promega), PDGF-BB (Antigenix America Inc.), RANTES (Antigenix America Inc.), VEGF (Antigenix America Inc.), Lipoxin (LXA_4, Neogen), and SDF-1α (Antigenix America Inc.)) were run on the retained samples (days 1, 4, 7, 10, 14, and 21) to detect proteins found in PRP.

Statistical Analysis

All statistical analysis was based on a Kruskal–Wallis one-way ANOVA on ranks and a Tukey–Kramer pairwise multiple comparison procedure ($\alpha = 0.05$) performed with the JMP®IN 8.0 statistical software package (SAS Institute, Inc.). Graphical depictions of mean data were constructed with Microsoft Excel 2007, with error bars representing standard deviations.

Results

Creation of PRP and PRGF

Based upon the platelet counts performed at the Harvard Immune Disease Institute's Blood Research laboratory, it was determined that the pooled whole blood used for this study contained 175 x 10^3 platelets/µl, while the PRP created with the

SmarPReP^2 system yielded 955 x 10^3 platelets/µl. This 5.5 fold increase in platelets is consistent with published data [324], and should result in a similar fold increase in growth factor concentration based upon the linear relationship between platelet and growth factor concentration [315].

The results of the bFGF and VEGF ELISAs (Figure 6.1) reveal the FTF method of activation, essentially lysing platelets to release their α and dense granule contents, to be as effective, if not more so, than the traditional PRP activation techniques of thrombin and $CaCl_2$ for releasing growth factors. The FTF activation method resulted in average growth factor concentrations of 0.4 ng/ml for bFGF, and 1.6 ng/ml for VEGF. Using the traditional $CaCl_2$ and thrombin activation methods bFGF values were 0.8 and 0 ng/ml, respectively, while the VEGF values were 0.3 and 0.7 ng/ml, respectively. While there were few statistical differences between the different methods in the bFGF ELISA, with only the $CaCl_2$ activated different from the thrombin activated, the VEGF ELISA results demonstrated clearly that the FTF method was significantly greater than the other activation methods. It should be noted that the thrombin activation method resulted in an instantaneous gel, making it difficult to obtain liquid samples for ELISA analysis. The $CaCl_2$ activated PRP contained visible floating thrombi, but was mostly liquidous, while the FTF activated PRP was completely liquid with no evidence of thrombus formation.

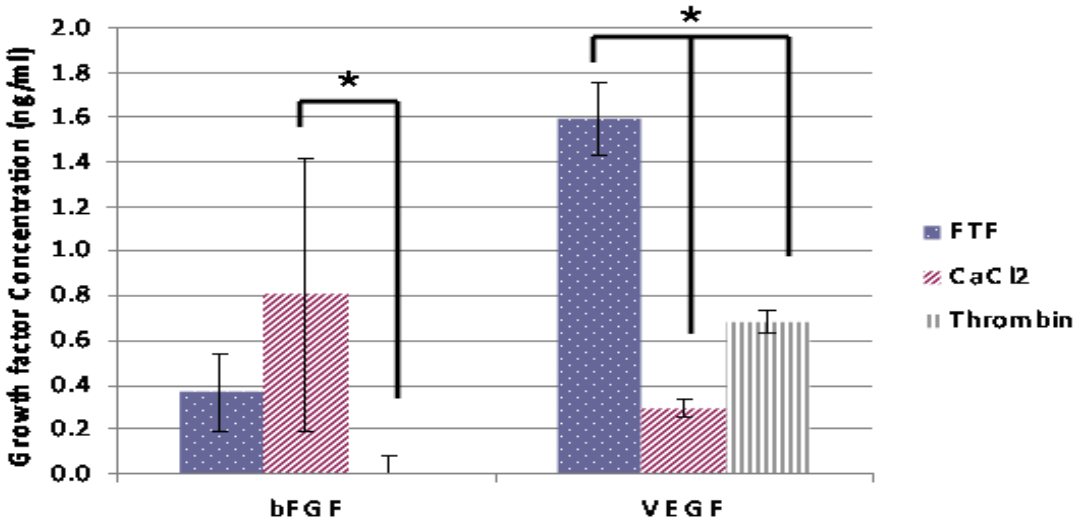

Figure 6.1. Results of PRP activation method on bFGF and VEGF concentration. * indicates significant differences between activation methods, $p < 0.05$. Minimum levels of detection for bFGF and VEGF were 0.11ng/ml and 0.04 ng/ml.

Characterization of Electrospun Structures

Scanning Electron Microscopy

SEM images of the scaffolds are displayed in Figure 6.2, illustrating the fibrous nature of the scaffolds with and without the incorporation of PRGF and heparin. Mean fiber diameters for these scaffolds are depicted in Figure 6.3, and range from 0.25 µm for PCL scaffolds with 0.05% heparin to 0.92 µm for PCL control scaffolds. The addition of PRGF alone did not have a significant effect on fiber diameter, however, when heparin was added at 0.05% or 0.5%, PCL:PRGF(100) scaffolds had significantly larger fiber diameters than other scaffolds containing heparin. With the exception of scaffolds with 100 mg/ml PRGF, the addition of heparin (both 0.05% and 0.5%) resulted in significantly smaller fiber diameters compared to scaffolds without heparin. The significant decrease in fiber diameter is most likely accredited to an increase in charge density on the surface of the ejected polymer jet during electrospinning. The increased charge density of heparin

(as Na^+ salt) causes greater elongation and thinning forces on the jet as it travels through the electric field, resulting in smaller fiber diameters [342]. It is evident from the images that with increasing amounts of PRGF added, there are both large and small fiber diameters present. This divergent population of fiber diameters in scaffolds with PRGF is also illustrated through the large standards of deviation that were determined for those structures. While the addition of PRGF to the scaffolds does not have an affect on fiber diameter, it does have a linear affect on average pore area; as PRGF content is increased, pore area increases as well (Figure 6.3). The addition of 100 or 200 mg/ml PRGF to PCL scaffolds resulted in significantly increased pore areas over the control and 10 mg/ml PRGF containing samples. With the addition of heparin (both 0.05% and 0.5%), scaffolds with 100 mg/ml PRGF had significantly increased pore areas over all other scaffolds with heparin. PCL control scaffolds and PCL:PRGF scaffolds not containing heparin had significantly greater pore areas than their heparin incorporated counterparts. In previous electrospinning studies, the correlation between average pore area and average fiber diameter has been well documented [144, 321, 325]. This same correlation is observed here for the PCL:PRGF(100) scaffolds: as fiber diameter increased, pore area increased.

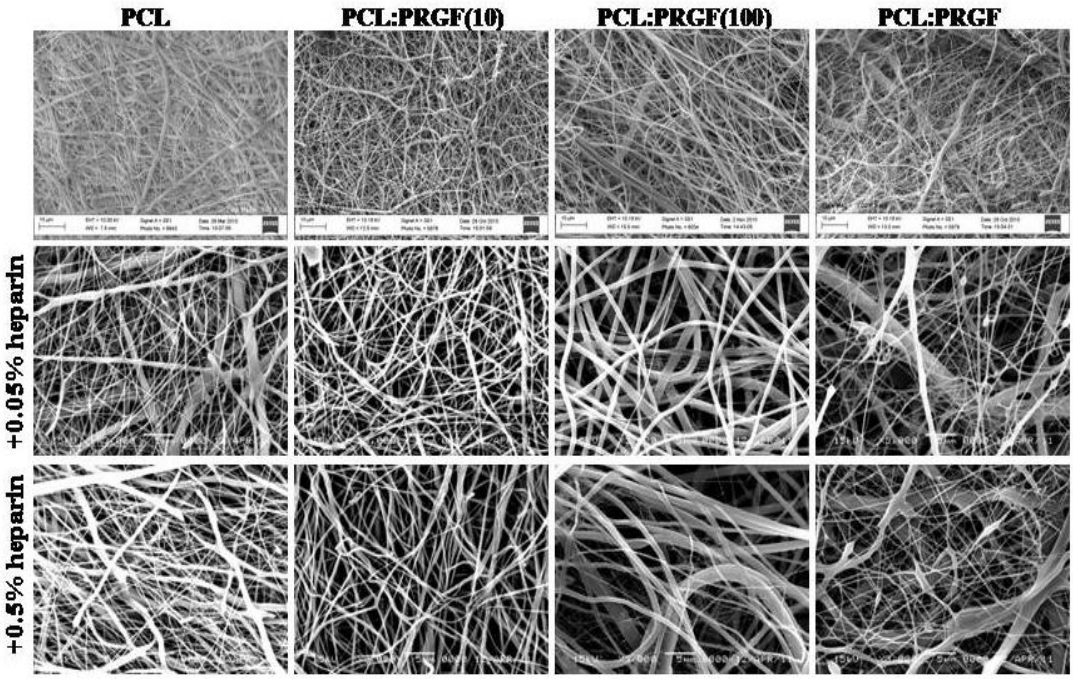

Figure 6.2. SEM images of PCL scaffolds with and without heparin and PRGF. Magnification is 3000X.

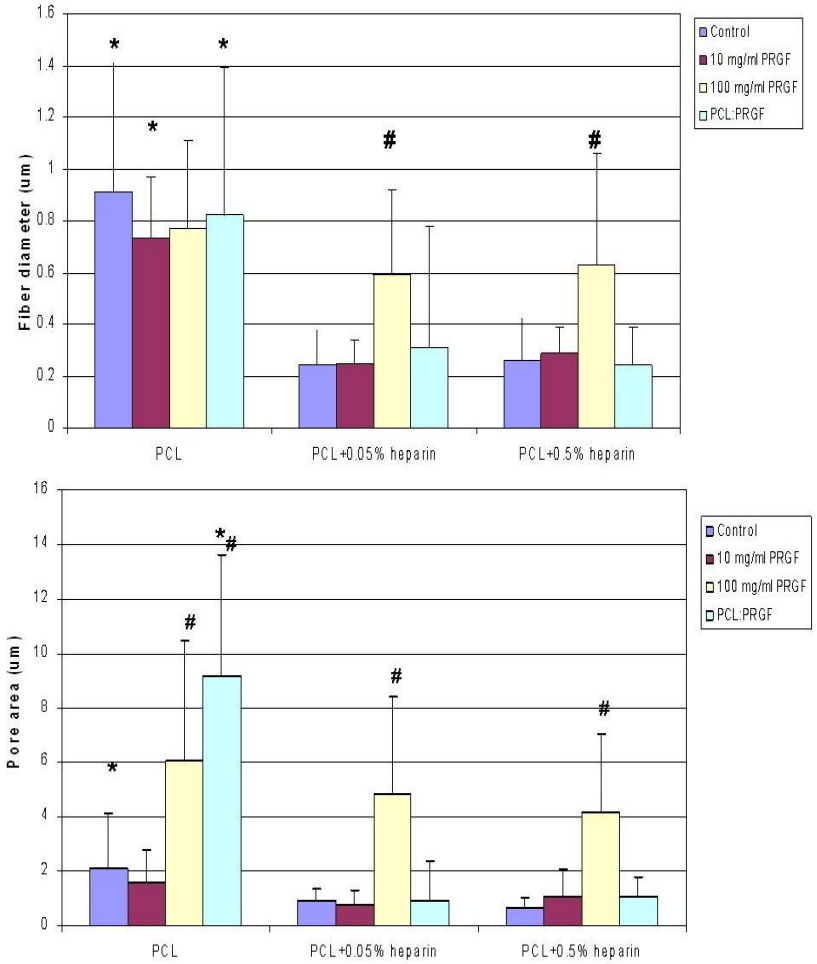

Figure 6.3. (Top) Average fiber diameters of PCL and PRGF incorporated scaffolds with and without heparin. * indicates statistical significance ($p<0.05$) between scaffolds with and without heparin. # indicates statistically significant differences, $p<0.05$, between PCL:PRGF(100) scaffolds with 0.05% or 0.5% heparin and other scaffolds with 0.05% or 0.5% heparin. (Bottom) Average pore areas for PCL scaffolds containing PRGF and heparin. * indicates statistical significance ($p<0.05$) between scaffolds with and without heparin. # indicates statistically significant differences, $p<0.05$, between PCL:PRGF(100), PCL:PRGF scaffolds and all other scaffolds without heparin, and between scaffolds of PCL:PRGF(100) with 0.05% or 0.5% heparin and all other scaffolds with 0.05% or 0.5% heparin.

Uniaxial tensile testing

The results from the uniaxial tensile testing performed on scaffolds incorporated with PRGF are depicted in Figure 6.4. Peak stress ranged from approximately 0.25 MPa

for scaffolds of PCL:PRGF(100) to 3.5 MPa for scaffolds of PCL:PRGF(10). The addition of PRGF did not affect the peak stress of the structures, except when added at 100 mg/ml. These results were not surprising, as traditionally the combination of biologic proteins in large concentrations (collagen, elastin, fibrinogen, etc.) with electrospun polymers regarded for their tensile strength typically results in significantly reduced mechanical strength [20, 148, 345]. Surprisingly, there were no differences in peak stress values for any of the structures over the 28 days. This result, although opposite of what normally occurs over time when a natural component or polymer is added to electrospinning solutions, is encouraging, and may indicate these materials will retain their mechanical integrity *in vivo* as well.

The modulus for the PCL and PRGF containing scaffolds ranged from approximately 2.5 MPa for structures containing 100 mg/ml PRGF to about 13 MPa for PCL scaffolds. Similar to the results of peak stress, in general, the addition of PRGF did not affect the modulus of the constructs, except when added at 100 mg/ml. PCL scaffolds did have a significantly higher modulus at day 1 and 7 than that of PRGF containing scaffolds at those time points (except PCL:PRGF at day 7). In addition, modulus did not significantly decrease over the 28 day time point for any of the scaffolds, illustrating the ability of the PCL and PRGF incorporated scaffolds to retain their mechanical strength over time. Strain at break values for the scaffolds ranged from 30% for PCL:PRGF(100) to around 140% for scaffolds of PCL:PRGF(10). Again, in general, with the exception of PCL:PRGF(100), the addition of PRGF did not have a significant effect on the strain at break and all scaffolds had a consistent strain at break over the 28 days. Scaffolds of PCL:PRGF(10) had significantly higher strain at break than all other scaffolds at all other

time points, except PCL:PRGF(10) scaffolds at day 1. PCL:PRGF(100) constructs had a significantly different strain of break at day 1 than at day 28.

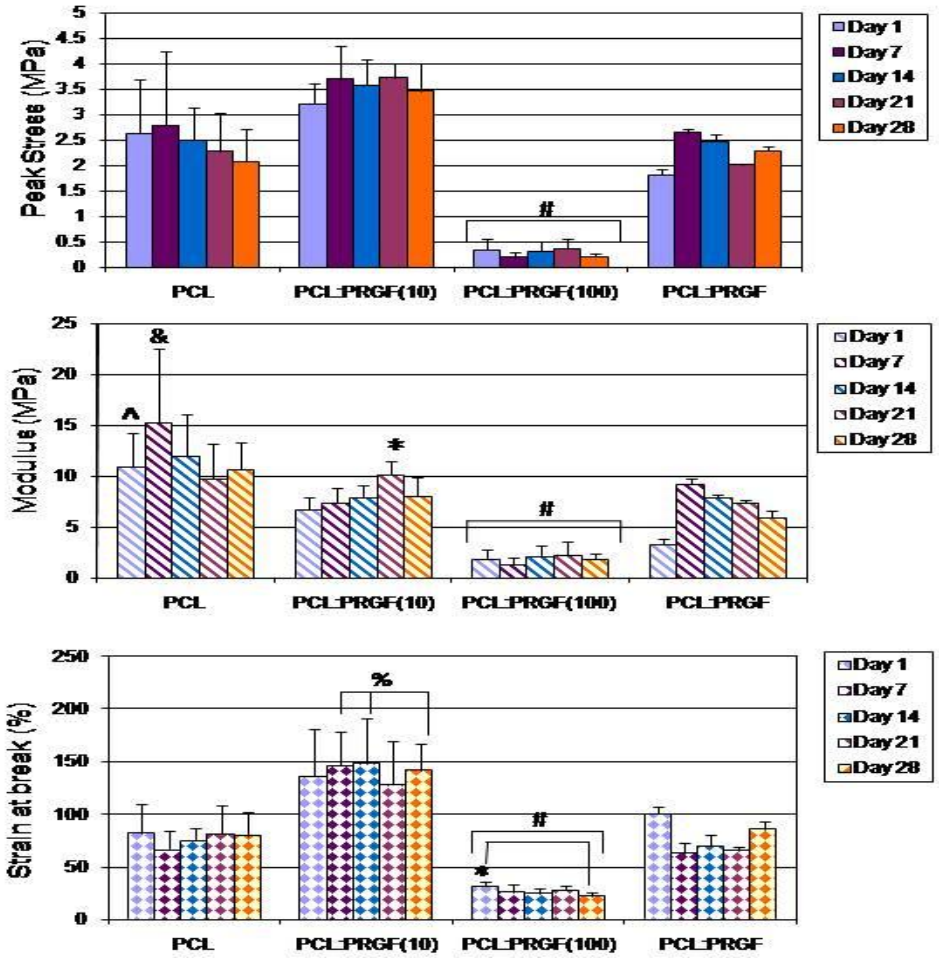

Figure 6.4. Results of peak stress (top), modulus (middle), and strain at break (bottom) for PCL and PRGF incorporated scaffolds. For peak stress, # indicates statistically significant differences, $p < 0.05$, between PCL:PRGF(100) scaffolds and all other scaffolds at all other time points, except for PCL:PRGF at day 1. For modulus, ^ indicates statistically significant differences ($p<0.05$) between PCL (day 1) and all other PRGF incorporated scaffolds at day 1. & indicates statistical significance ($p<0.05$) between PCL scaffolds at day 7 and all other scaffolds at day 7 time point, except PCL:PRGF. # denotes statistically significant differences, $p < 0.05$, between PCL:PRGF(100) scaffolds and all other scaffolds at all other time points. For strain at break, % denotes statistical significance ($p<0.05$) between scaffolds of PCL:PRGF(10) at days 7, 14 and 28 over all other scaffolds at all other time points, except PCL:PRGF(10) scaffolds at day 1. # indicates statistically significant differences ($p<0.05$) between PCL:PRGF(100) scaffolds and PCL:PRGF(10) scaffolds at all time points. * indicates statistical significance ($p<0.05$) between PCL:PRGF(100) scaffolds at day 1 versus day 28.

Uniaxial tensile testing results from that performed on scaffolds with and without heparin are shown in Figure 6.5 (a-d). Over all, the results for peak stress, modulus and strain at break for all scaffolds revealed the addition of heparin did not significantly affect the mechanical integrity of the scaffolds. For PCL:PRGF, the addition of heparin did significantly decrease the peak stress and modulus of the scaffolds, while for PCL:PRGF(100) scaffolds, the addition of heparin significantly increased the peak stress and strain of break of the constructs. Similar to scaffolds without heparin, electrospun PCL and PRGF incorporated structures with 0.05% or 0.5% heparin did not significantly lose their mechanical strength over the 28 day time period, indicating little to no degradation was occurring over the time course of the experiment. The peak stress, modulus and strain at break for PCL scaffolds with heparin (0.05% and 0.5%) are similar to those for PCL scaffolds without heparin (Figure 6.5(a)), with no statistically significant differences observed. Additionally, scaffolds incorporated with heparin retained their mechanical strength over the 28 days, with statistical analysis revealing no significant differences for peak stress, modulus, or strain at break between the different time points tested for each scaffold type.

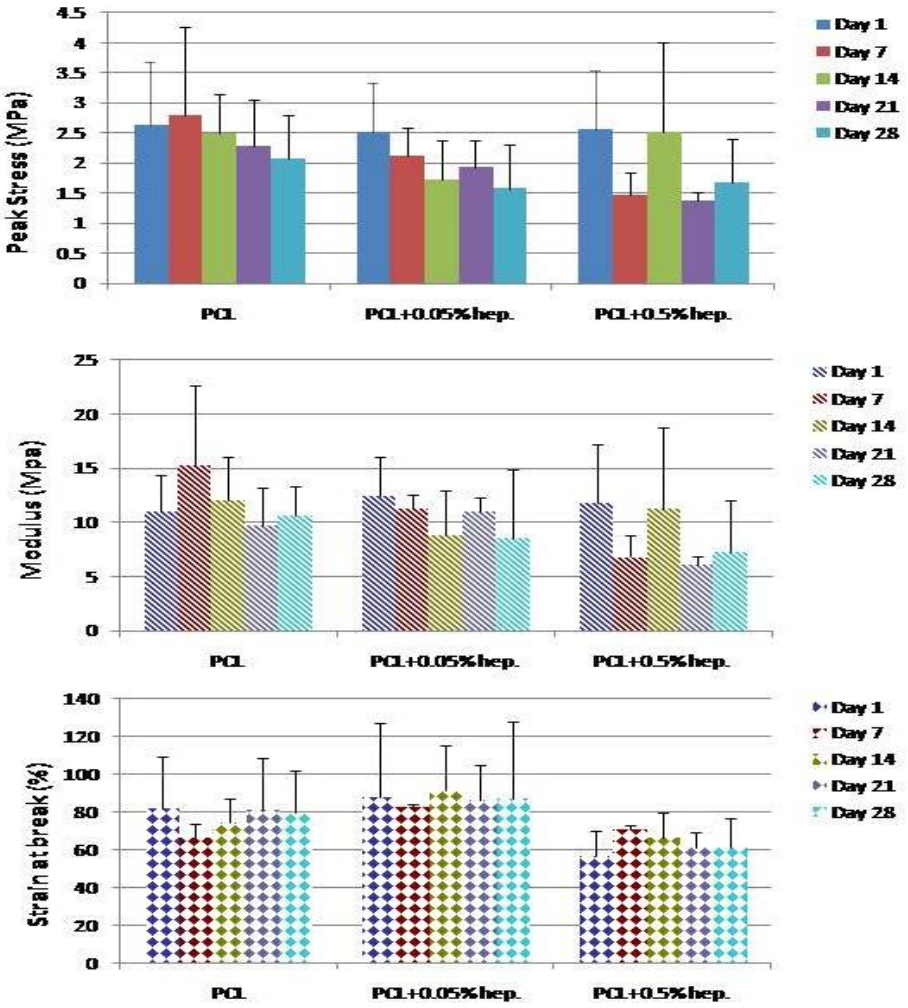

Figure 6.5(a). Results of peak stress (top), modulus (middle), and strain at break (bottom) for PCL scaffolds incorporated with and without heparin (0.05% and 0.5%).

Figure 6.5(b) shows the mechanical testing results for scaffolds of PCL:PRGF(10) with and without 0.05% and 0.5% heparin. Similar to PCL scaffolds, for peak stress, modulus and strain at break, there were no significant differences between scaffolds with and without heparin tested at the same time point, as well as between days 1-28 for each scaffold type.

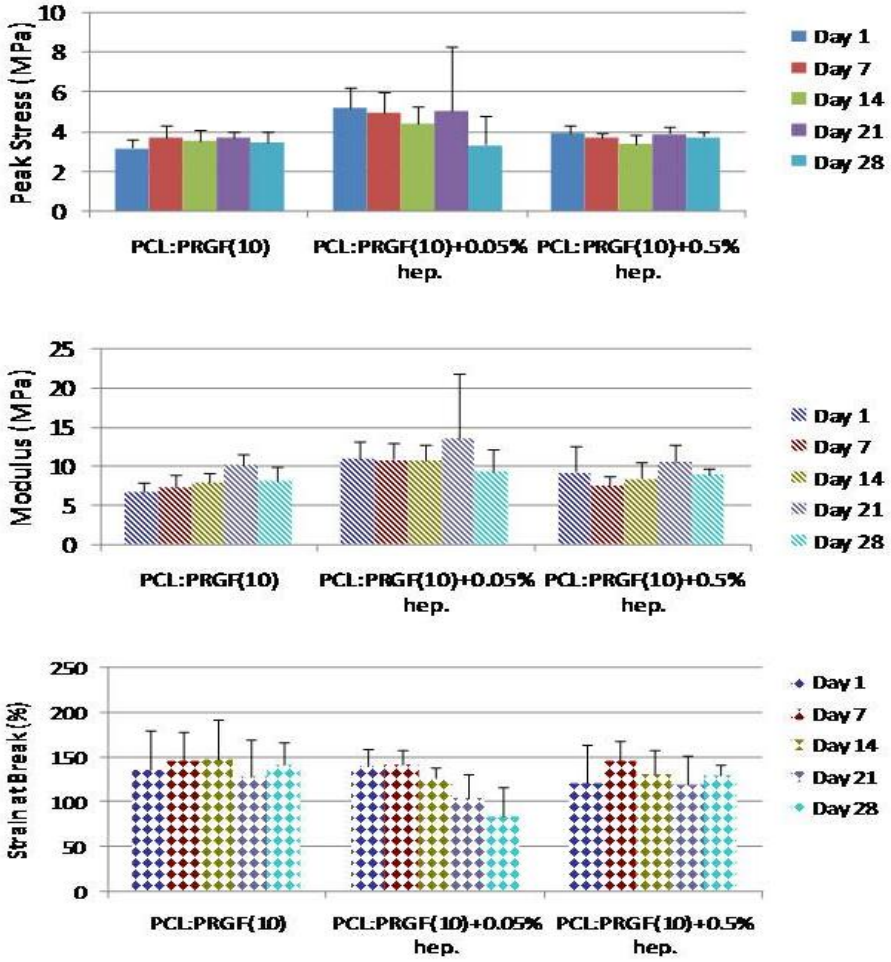

Figure 6.5(b). Unaxial tensile testing results for PCL:PRGF(10) scaffolds with and without heparin (0.05% and 0.5%) illustrating peak stress (top), modulus (middle), and strain at break (bottom).

Results from uniaxial tensile testing of PCL:PRGF(100) scaffolds with and without heparin (0.05% and 0.5%) are displayed in Figure 6.5(c). Statistical analysis revealed PCL:PRGF(100) scaffolds without heparin have a significantly lower peak stress at all time points than those equivalent scaffolds with 0.05% and 0.5% heparin (except PCL:PRGF(100)+0.05% heparin scaffolds at days 14 and 21). Analysis of modulus results revealed no significant differences between scaffolds with and without 0.05% and 0.5% heparin. Scaffolds with 0.05% and 0.5% heparin tested at day 28 had a

significantly higher strain at break than PCL:PRGF(100) scaffolds without heparin tested at all time points (except day 1). For peak stress, modulus and strain at break, however, there were no significant differences observed between the different time points tested for each scaffold type, illustrating their ability to retain their mechanical strength over 28 days.

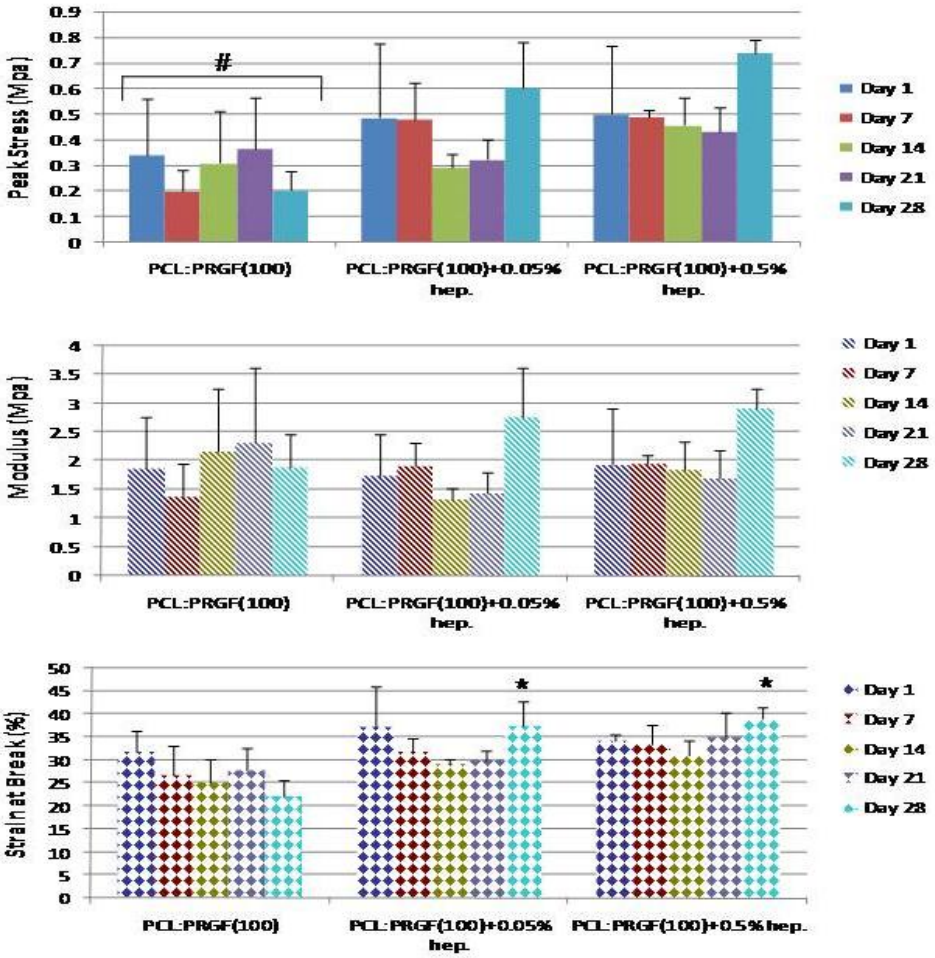

Figure 6.5(c). Peak stress (top), modulus (middle), and strain at break (bottom) results for scaffolds with 100 mg/ml PRGF incorporated with and without heparin (0.05% and 0.5%). # denotes statistical significance ($p<0.05$) between PCL:PRGF(100) scaffolds without heparin and PCL:PRGF(100) scaffolds with heparin (except PCL:PRGF(100)+0.05% heparin at days 14 and 21). * signifies statistically significant differences between PCL:PRGF(100) scaffolds with heparin (0.05% and 0.5%) tested at day 28 and PCL:PRGF(100) scaffolds without heparin at all time points tested, except day 1.

The values determined for the peak stress, modulus and strain at break of PCL:PRGF scaffolds are shown in Figure 6.5(d). PCL and PRGF co-spun scaffolds without heparin exhibited significantly increased peak stress over the same scaffolds with heparin for their respective time points, with the exception of PCL:PRGF scaffolds tested at days 1 and 21. Similar results were seen with modulus; scaffolds without heparin had significantly increased modulus over PCL:PRGF scaffolds with heparin between the specific time points tested, except PCL:PRGF scaffolds at days 1 and 28. No significant differences were observed between the time points tested of each type of scaffold for the peak stress and modulus. Strain at break results revealed no statistically significant differences between PCL and PRGF co-spun scaffolds with and without heparin for their respective time points (except PCL:PRGF scaffolds and PCL:PRGF+0.5% heparin tested at day 28). In looking at differences between days 1 – 28, PCL:PRGF+0.5% heparin scaffolds tested at day 28 had significantly decreased strain at break than PCL:PRGF+0.5% heparin scaffolds tested at day 1 and 7.

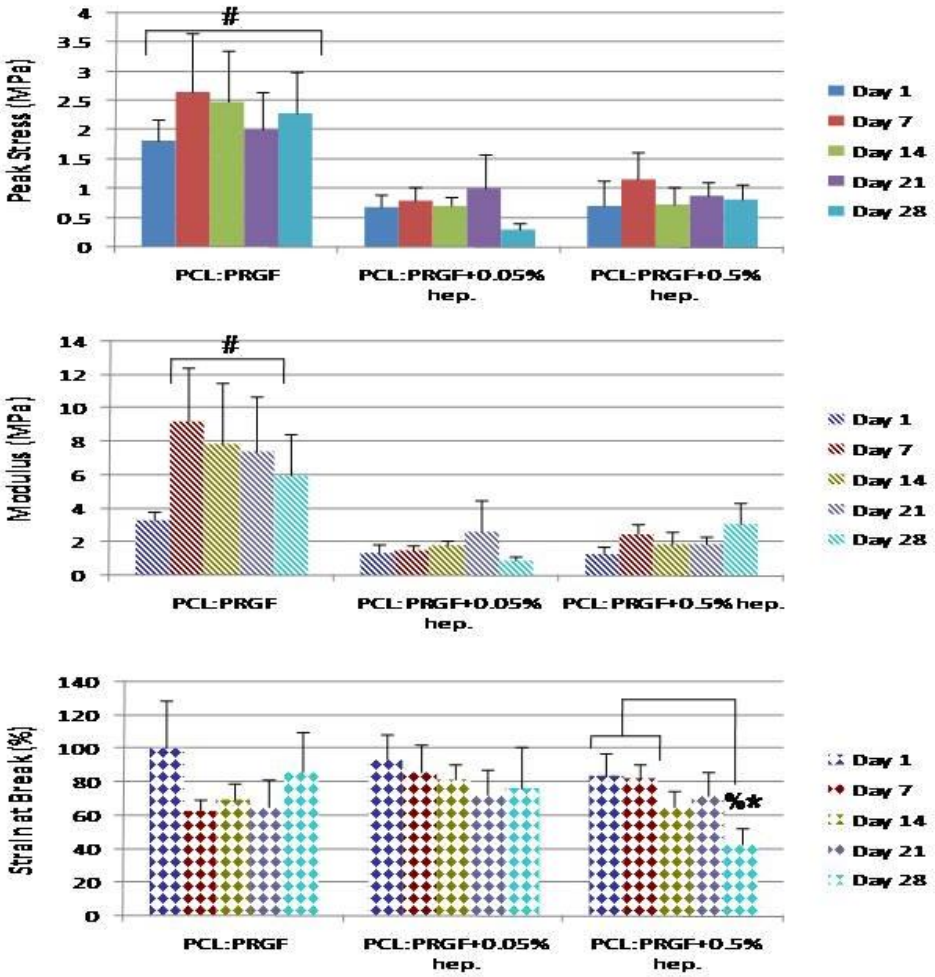

Figure 6.5(d). Unaxial tensile testing results for PCL and PRGF co-spun scaffolds with and without heparin (0.05% and 0.5%) illustrating peak stress (top), modulus (middle), and strain at break (bottom). # denotes statistically significant differences ($p<0.05$) between scaffolds with and without heparin (0.05% and 0.5%) for peak stress and modulus (except for scaffolds of PCL:PRGF tested at days 1 and 21, and days 1 and 28, respectively). * signifies significant differences, $p<0.05$, between PCL:PRGF scaffolds with 0.5% heparin and without heparin tested at day 28. % represents statistical significance between PCL:PRGF+0.5% heparin scaffolds tested at day 28 and those tested at days 1 and 7.

Table 6.1 shows a comparison of the range of mechanical properties determined for the electrospun materials in this study to that of a native femoral artery and e-PTFE. The table illustrates that electrospun PCL constructs incorporated with PRGF and heparin

are comparible to that of the native femoral artery, and therefore, could withstand physiological pressure if implanted as a vascular graft.

Table 6.1. Mechanical properties of electrospun PCL:PRGF:heparin scaffolds compared to native femoral artery [346, 347] and e-PTFE [348].

Graft Material	Peak Stress (MPa)	Modulus (MPa)	Strain at Break (%)
Femoral artery	1 – 2	9 – 12	63 – 76
e-PTFE	6 – 15	42 – 60	20 – 30
PCL	1.5 – 2.5	1 – 1.5	60 – 90
PCL:PRGF(10)	3 – 5	6 – 12	100 – 150
PCL:PRGF(100)	0.2 – 0.7	1.5 – 2.9	25 – 40
PCL:PRGF	0.5 – 2.5	2 – 8	40 – 90

Endotoxin levels

Levels of endotoxin detected for PCL and PRGF incorporated scaffolds with and without 0.05% and 0.5% heparin are displayed in Figure 6.6 and are below the acceptable levels of endotoxin for standard clinical applications as determined by the U.S. Pharmacopeia (0.5 Endotoxin units (EU)/ml) [349]. It should be noted that the endotoxin levels for PRGF and heparin in water are above the standard acceptable limit for medical devices; however, several proteins and anticoagulants contained within the PRGF (including citrate dextrose, fibrinogen and globulins), as well as heparin itself, have separate acceptable endotoxin limits, of which the levels displayed in Figure 6.6 all fall below [349]. Furthermore, the levels of endotoxin detected for PCL and PRGF incorporated scaffolds with and without heparin are far below (1800 fold less) that used to activate macrophages (100 ng/ml lipopolysaccharide (LPS) which corresponds to 1100 EU/ml).

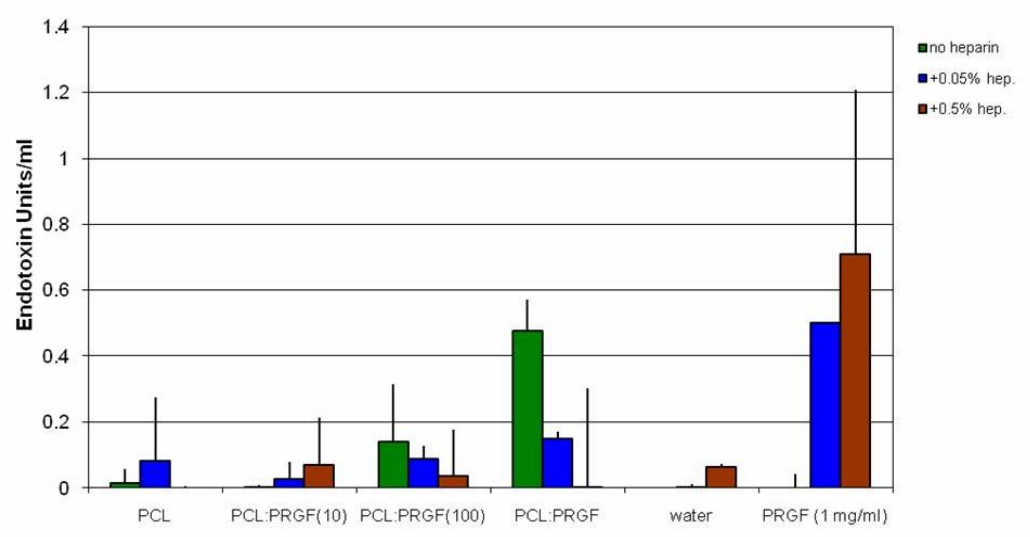

Figure 6.6. Endotoxin levels detected for PRGF and heparin incorporated scaffolds, heparin in water and in PRGF in water (0.05% and 0.5%).

Quantification of Release Kinetics from PRGF and Heparin Incorporated Scaffolds

Protein release

The results of quantified protein release from PRGF containing scaffolds are shown in Figure 6.7. The results of this study demonstrated that scaffolds containing high concentrations of PRGF (PCL:PRGF(100) and PCL:PRGF) released detectable amounts of protein over 35 days in culture. The protein release from PRGF containing scaffolds peaked at day 1, decreased by about half on days 4 and 7, and reached a plateau that was sustained for the remainder of the duration. PCL:PRGF(100) had the highest release of protein at all time points (0.22 mg/ml – 0.05 mg/ml). Surprisingly, PCL:PRGF scaffolds released a lower amount of protein over the 35 days, even though the concentration of PRGF incorporated was the same as that of PCL:PRGF(100) scaffolds. Minimal protein release was detected for PCL control scaffolds and scaffolds containing 10 mg/ml PRGF

over the 35 days, indicating that the protein detected was in fact due to PRGF release and not simply an artifact of scaffold degradation.

Statistical analysis revealed protein release at day 1 from scaffolds of PCL:PRGF(100) to be significantly greater than protein release from those respective scaffolds at all other time points (day 4-35). Additionally, scaffolds of PCL:PRGF(100) had significantly greater release at day 4 than day 35. The initial burst of release from the scaffolds at day 1 was expected as PRGF from the surface of the scaffolds was released. Remarkably, after the first day there was still a sustained release of protein from scaffolds of PCL:PRGF(100) that continued throughout the 35 days, presumably due to the degradation of the polymer scaffolds and subsequent release of entrapped proteins.

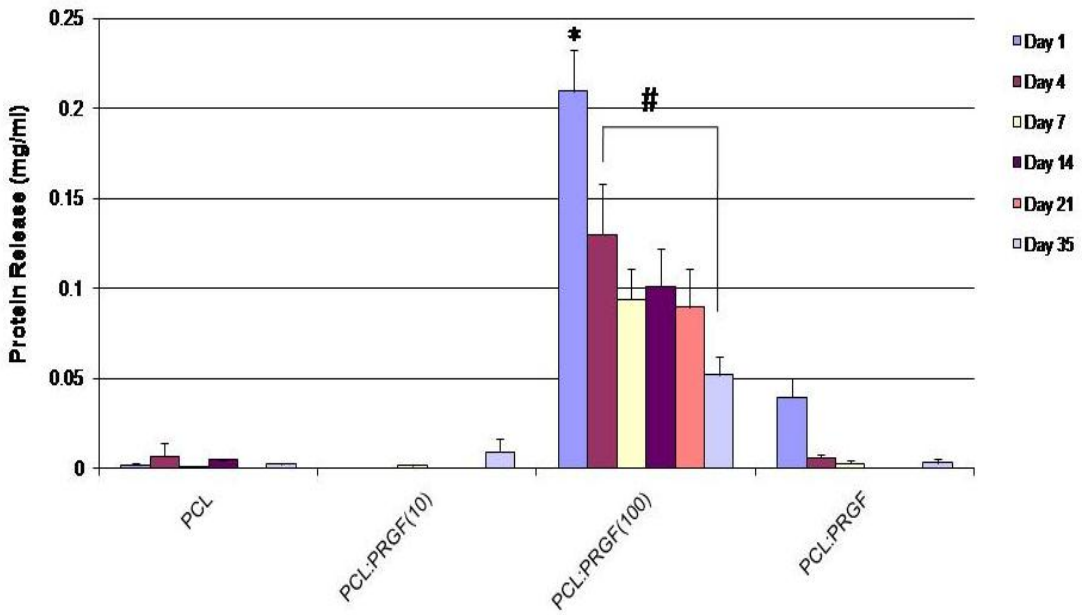

Figure 6.7. Quantification of generic protein released from PRGF containing scaffolds over 35 days. * indicates a significant difference, $p < 0.05$, for day 1 when compared to all other time points for each material. # indicate statistically significant differences, $p < 0.05$, between day 4 and day 35 of PCL:PRGF(100). Minimum level of detection was 14.3 µg/ml.

The results from the BCA protein assay to determine the effect the addition of heparin had on protein detection from PRGF in PBS and protein release from scaffolds are illustrated in Figure 6.8. The addition of heparin to PRGF dissolved in PBS at 1 mg/ml did have a significant effect on amount of protein detected. The addition of heparin at increasing amounts to 1 mg/ml PRGF had a linear effect on the amount of protein detected; with increasing amounts of heparin incorporated, protein detection was decreased (Figure 6.8, Day 1). Statistical analysis revealed the addition of heparin at 0.5% to 1 mg/ml PRGF resulted in a statistically significant difference in protein detection compared to that of 1 mg/ml PRGF without heparin. These results indicate heparin may bind to specific growth factors contained within PRGF, thereby hindering their release and overall detection.

In contrast to the results seen from PRGF dissolved in PBS at 1 mg/ml, the addition of heparin at 0.05% and 0.5% to electrospun PRGF incorporated scaffolds does not appear to affect the amount of protein released from the constructs over 21 days (Figure 6.8). With the exception of PCL:PRGF and PCL:PRGF(100) scaffolds at days 1 and 4, respectively, there were no statistically significant differences in amount of protein released from PRGF containing scaffolds with and without heparin. On day 1, unexpectedly, PCL:PRGF scaffolds with 0.05% heparin had a significant increase in protein release compared to PCL:PRGF scaffolds without heparin. On day 4, PCL:PRGF(100) scaffolds without heparin had significantly higher protein release than those same scaffolds with heparin incorporated at both 0.05% and 0.5%. These results may imply heparin was not incorporated into the electrospun scaffolds consistently, thereby producing contradictory results from that explained above.

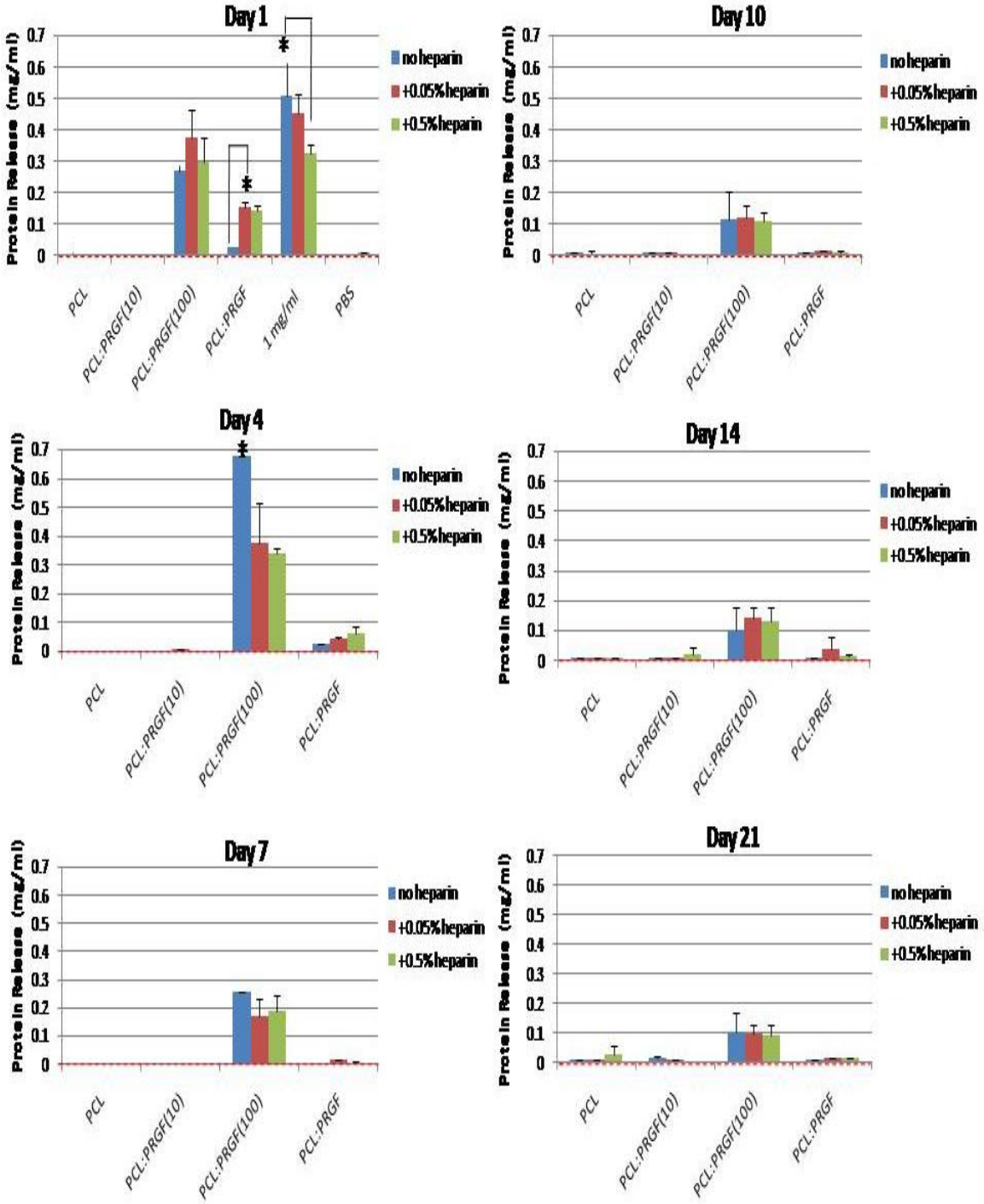

Figure 6.8. Protein release from PRGF dissolved in PBS (1 mg/ml) and PRGF incorporated scaffolds with and without 0.05% and 0.5% heparin over 21 days. * denotes statistical significance ($p<0.05$) between PRGF with and without heparin and when comparing the same type of scaffold with and without heparin. Minimum levels of detection were 0.001 mg/ml for protein detected at days 1, 4 and 7 and 0.009 mg/ml for protein detected at days 10, 14 and 21 (red dashed line).

Growth factor release

Quantification of TGF-β, RANTES, and PDGF-BB from the PRGF containing scaffolds revealed detectable cumulative release over 21 days (Figure 6.9(a)) with kinetics similar to those of the protein assay results described previously. These growth factors were also detectable in whole blood (WB), PRP, PPP and PRGF dissolved in PBS at 10 mg/ml, 5 mg/ml and, for TGF-β and RANTES, 1 mg/ml. TGF-β release was highest from scaffolds of PCL:PRGF(100). Release at day 1 was 0.5 ng/ml, with cumulative release increasing thereafter until day 21. Release from PCL:PRGF scaffolds increased from day 1 to day 7, but plateaued throughout the rest of the 21 days. Cumulative TGF-β release from scaffolds was not significantly different over the 21 days.

Much like the release of TGF-β from the scaffolds, PDGF-BB release was highest from scaffolds of PCL:PRGF(100), with release at day 1 of 0.15 ng/ml, and increasing cumulatively thereafter. PCL:PRGF scaffolds elicited PDGF-BB release of 0.03 ng/ml at day 1, but was not released at any time points thereafter. PDGF-BB release at day 1 from scaffolds of PCL:PRGF(100) was significantly higher than release from those same scaffolds at all other time points (days 4-21). For PCL:PRGF(100), PDGF-BB release at day 4 was significantly higher than that of days 10-21, and release at day 7 was significantly different from that of all other time points, except day 10.

Scaffolds of PCL:PRGF(100) had the highest release of RANTES, with 3 ng/ml released at day 1, with gradual increase in release thereafter. RANTES release from PCL:PRGF scaffolds had a peak of 0.5 ng/ml at day 1, but did not release any detectable amounts after day 4. Statistical analysis revealed no significant differences between RANTES release over the 21 days from PRGF incorporated scaffolds. It is unusual that

the level of PDGF-BB and RANTES found in WB and PRP was found to be similar, as growth factors in PRP should be around 5 times more than that of WB. One reason for this may be due to the storage of the PRP at 2-8°C over 24-48 hours. Because many of the growth factors have a short half life, they may have become inactivated over that time.

Similar to the protein assay results, TGF-β, PDGF-BB, and RANTES were undetectable from both the PCL control scaffolds and the scaffolds containing 10 mg/ml PRGF at all time points. The results of the statistical analysis illustrated that in general, the release of RANTES and TGF-β that occurred at all time points is not significantly different, demonstrating a sustained release of growth factors from the scaffolds over the 21 day period as the polymer fibers begin to degrade. This is also true for PDGF-BB release after day 7.

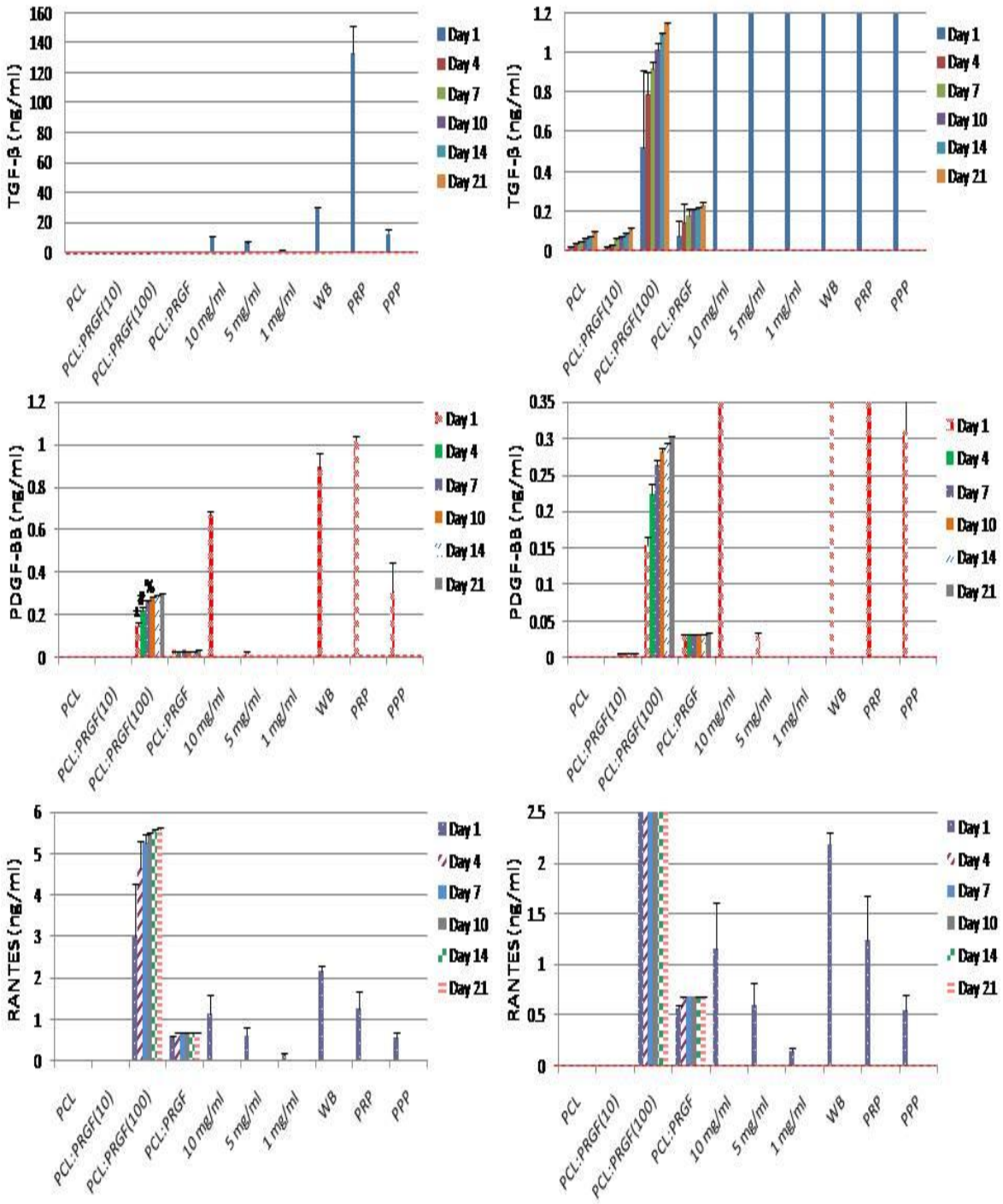

Figure 6.9(a). Cumulative release of TGF-β, PDGF-BB, and RANTES from PRGF incorporated scaffolds. Minimum levels of detection for TGF-β, PDGF-BB and RANTES were 0.011 ng/ml, 0.003ng/ml and 0.001ng/ml, respectively (red dashed line). * and # indicate statistically significant differences, $p < 0.05$, between day 1 and day 4, respectively, and all other time points. % indicates statistical significance, $p < 0.05$, between day 7 and all other time points, except day 10.

In contrast to TGF-β, PDGF-BB and RANTES, VEGF, SDF-1α, and LXA_4 release from PRGF incorporated scaffolds was not detectable at any time point (Figure 6.9(b)). This result may be explained by the fact that these growth factors are contained in PRP in smaller concentrations, and therefore, their release from electrospun scaffolds is most likely lower than the ELISA kits' minimum levels of detection [313, 337]. VEGF, SDF-1α and LXA_4 levels in PRP were 0.458 ng/ml, 0.130 ng/ml, and 0.246 ng/ml, respectively. These values are in agreement with previously published data. PRGF dissolved at 10 mg/ml and 5 mg/ml contained detectable levels of all three growth factors, while only LXA_4 was detectable in 1 mg/ml PRGF.

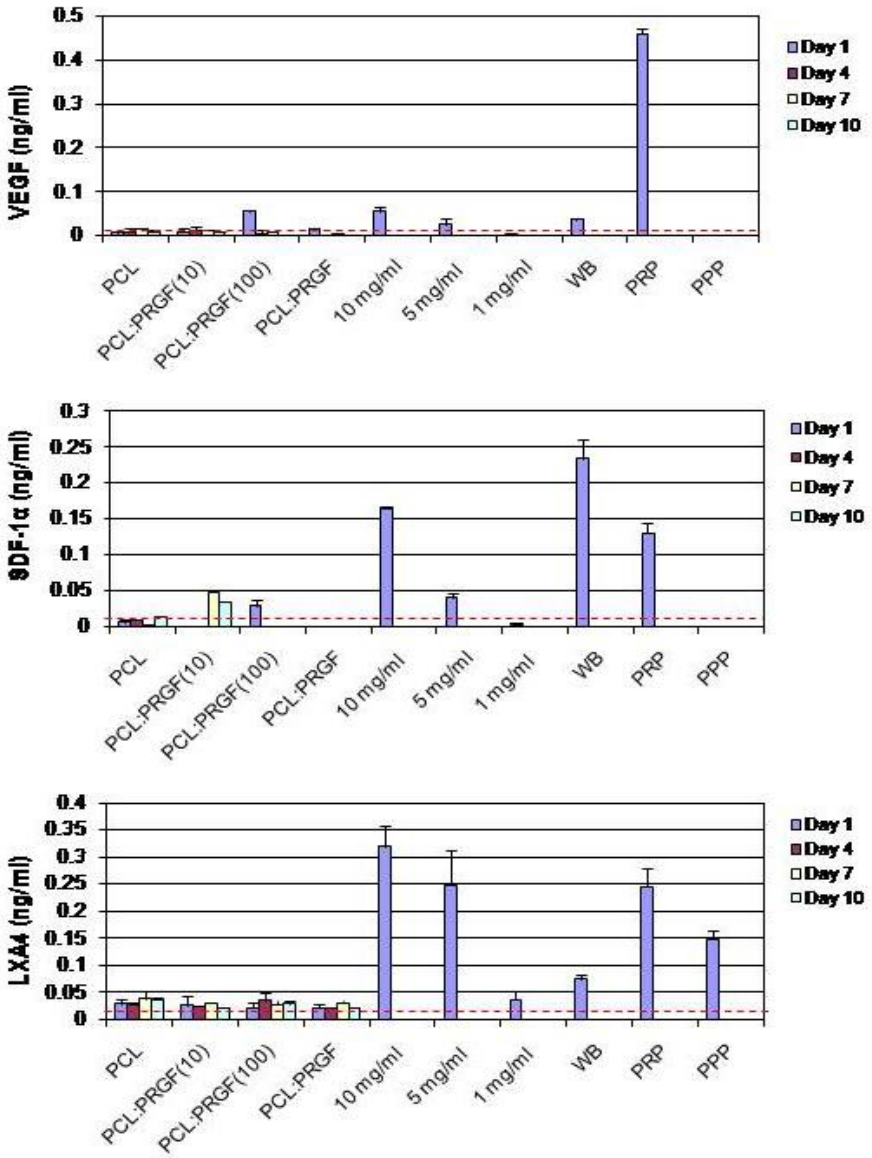

Figure 6.9(b). Levels of VEGF, SDF-1α, and LXA_4 from PCL and PRGF incorporated scaffolds, PRGF in media (10, 5 and 1 mg/ml), WB, PRP and PPP. Minimum levels of detection (dashed red line) are 0.011 ng/ml, 0.013 ng/ml, and 0.013 ng/ml for VEGF, SDF-1α and LXA_4, respectively.

Discussion

This present study provides a proof-of-principle for the incorporation of a powdered PRGF derived from human PRP into electrospun scaffolds of PCL. Through a number of evaluation methods, we were able to demonstrate that PRGF retained its

physiologic activity after lyophilization and through the electrospinning process, subsequently releasing a number of growth factors while retaining scaffold mechanical integrity over 28 days.

The use of PRP in clinical applications has been gaining in popularity as a means to stimulate tissue repair and regeneration with very minimal risk to the patient. However, the "black box" approach taken by many of the clinicians utilizing PRP leaves much to be done in the realm of basic science to fully understand and standardize the practice. To date, the collection of whole blood and the concentration and isolation of platelets to make PRP has been proven effective *in vitro* for stimulating cellular activity in a number of formats, both in liquid [311, 350-356] and in lyophilized PRGF form [338-341].

To the best of the authors' knowledge, this manuscript serves as the first instance of a powdered PRGF being incorporated into an electrospun tissue engineering scaffold to serve as a controlled release vehicle for such a concentrated growth factor and cytokine milieu. While electrospun scaffolds have been used as growth factor delivery systems in the past [301, 319, 357-360], they have typically been limited to the incorporation of only a small number of growth factors due in part to the cost associated with purchasing the recombinant or isolated proteins [357]. The incorporation of a cost-effective PRGF protein array into an electrospun structure has the potential to deliver a multitude of growth factors, cytokines, and chemokines in physiologically relevant ratios. Such a platelet-based growth factor cocktail would essentially replicate the necessary factors found in a site of normal wound healing and promote the formation of healthy tissue through the stimulation of the healing cascade [300]. The results presented in this

manuscript demonstrated the potential of such a sustained release vehicle through the detection of various growth factors. Heparin was also incorporated as a means to bind to different growth facors and interleukins and modulate their release from the PRGF incorporated electrospun constructs.

With the creation of individual PRGF fibers within the electrospun scaffolds containing high concentrations of PRGF (PCL:PRGF(100)), the loss of mechanical strength was not surprising. These PRGF fibers, consisting of natural proteins, lack inherent mechanical strength [344]. Similar in composition to electrospun collagen or fibrinogen [321, 345], which performs best mechanically when blended with synthetic polymers, and the presence of which can significantly decrease scaffold mechanical strength, the PRGF fibers may be best utilized in a role of enhancing scaffold bioactivity rather than load bearing. Surprisingly, even with the incorporation of large amounts of PRGF and/or heparin, the electrospun scaffolds were able to retain their mechanical integrity over the 28 days, demonstrating little to no degradation occurring. The addition of a natural polymer generally causes a quicker degradation of a scaffold; however, because PRGF consists mainly of a fibrinogen backbone, this may be assisting in fiber stabilization [361]. This stability of the PRGF fiber was also demonstrated in the PCL:PRGF co-spun scaffold, where even when PRGF was incorporated in large amounts, the mechanical properties fell in between that of PCL and PCL:PRGF(100) scaffolds. The mechanical properties of these scaffolds were found to be comparible to those of native femoral artery, illustrating these scaffolds may withstand physiological pressures if implanted as a vascular graft.

As demonstrated in the protein release assays conducted herein, detectable levels of proteins were released from the electrospun scaffolds for up to 35 days *in vitro*. The addition of heparin, while not affecting protein release from electrospun PRGF containing constructs, did have a reverse effect on protein detection in 1 mg/ml PRGF; a significant decrease in protein detection was observed with increasing amounts of heparin. This result was expected, and can be explained by the binding of growth factors by heparin. With more heparin added, more growth factors become bound, hindering their release and detection by the assay.

While it can be assumed that a large percentage of the released proteins were in fact albumin and other blood proteins, not growth factors, the fact that RANTES, PDGF-BB, and TGF-β were detectable in electrospun materials at up to 21 days attests to the sustained release nature of the structures. VEGF, SDF-1α, and LXA_4 release from electrospun constructs was not detectable, however, quantification of these growth factors in PRP as well as in PRGF dissolved in PBS alludes to the fact that their release from electrospun scaffolds may be too small to detect by ELISAs, but may still be sensed by cells. RANTES, PDGF-BB, and TGF-β release were analyzed as they are three of the more highly concentrated proteins contained within PRP/PRGF[313], however, it can be interpolated that other factors such as PDGF-ab, FGF, and EGF will be released in the same fashion. The nature of the release demonstrated from the electrospun scaffolds may prove to be effective in proposed *in vitro* and *in vivo* follow-up studies at enhancing migration of cells from surrounding tissues, with a large burst of protein creating a substantial chemotactic gradient, followed by a sustained release of protein to promote cell proliferation, and scaffold infiltration and remodeling. The incorporation and

subsequent release of albumin, while seemingly inconsequential, may in fact serve as a protectant for the cytokines and chemokines included in the PRGF. The hydrophilic albumin molecules have been demonstrated in the literature to have the potential to encapsulate smaller proteins, and effectively shield them from potential denaturation [362, 363]. However, it is important to note that the electrospinning process may alter the molecular structures of the different components in PRP, thereby effecting growth factor bioactivity. In performing TGF-β ELISAs, TGF-β was only detectable in PRGF and PRP after performing an acid activation technique, while it was detectable in electrospun constructs without activation. Although this ELISA was the only one to specifically detect this change, other growth factors are likely to be effected by the electrospinning process as well, and may not have been detected by ELISAs. Further analysis of the components contained with electrospun PRGF incorporated scaffolds, PRP and PRGF, either by performing gel electrophoresis or a similar technique, may confirm this explanation.

In conclusion, this study demonstrated proof of the hypothesis in that PRP was able to be subjected to a FTF process, lyophilized to create PRGF, and incorporated into electrospun scaffolds of PCL. In addition, this PRGF was released from the electrospun scaffolds in a controlled fashion over a period of 35 days in culture, and the scaffolds retained their mechanical strength *in vitro*. In addition, endotoxin levels were not elevated by the addition of PRGF or heparin above the acceptable limit for standard clinical applications as determined by the U.S. Pharmacopeia. Additional studies are needed to determine what effect the presence of PRGF will have *in vivo* on the release of growth factors and mechanical stability of the electrospun structures.

Acknowledgments

The authors would like to thank Drs. Sherwin Kevy and May Jacobsen from the Harvard Immune Disease Institute's Blood Research laboratory for conducting platelet counts on pooled whole blood and PRP. SEM was performed at the Virginia Commonwealth University Department of Anatomy and Neurobiology Microscopy Facility, supported, in part with funding from NIH-NINDS Center core grant (5P30NS047463-02).

Chapter 7: EVALUATION OF ANGIOGENIC POTENTIAL OF INCORPORATED PLATELET-RICH PLASMA SCAFFOLDS

Preface: Parts of the following chapter are taken from the manuscript "Incorporating Platelet-Rich Plasma into Electrospun Scaffolds for Tissue Engineering Applications" appearing in Tissue Engineering: Part A, 17(21 and 22), 2011. The complete manuscript can be found in Appendix A. The included work investigates the potential for incorporated PRP/PRGF scaffolds with and without heparin to enhance scaffold bioactivity and promote regeneration and angiogenesis through cellular migration, proliferation, and sprout formation.

Incorporating Platelet-Rich Plasma into Electrospun Scaffolds for Tissue Engineering Applications

Scott A. Sell[1, 2*], Patricia S. Wolfe[2*], Jeffery J. Ericksen[1, 3], David G. Simpson[4], and Gary L. Bowlin[2#]

[1]Physical Medicine & Rehabilitation Service
Hunter Holmes McGuire VA Medical Center, Richmond, VA 23249

[2]Department of Biomedical Engineering
Virginia Commonwealth University, Richmond, VA 23284

[3]Department of Physical Medicine and Rehabilitation
Virginia Commonwealth University, Richmond, VA 23298

[4]Department of Anatomy and Neurobiology, Virginia Commonwealth University, Richmond, VA 23298

[*]Authors contributed equally

Introduction

When an artery is injured, similar to any tissue, a complex set of events takes place, beginning with clot formation and acute inflammation, development of granulation tissue, and in ideal cases, ending with complete tissue regeneration, but in most cases, scar formation [364]. After a biomaterial has been implanted into the body, a different response is elicited. First, a nonspecific adsorption of proteins takes place on the surface of the implant, ranging from natural to denatured conformations, causing the foreign body reaction to begin. Several cell types that are normally present during wound healing are chemoattracted to the biomaterial, including platelets, monocytes and macrophages, and adhere to the surfaces. Because these graft implants are significantly larger than the macrophages themselves, they are unable to phagocytose the foreign material, and reside at the implant sight, often times forming into multinucleated foreign body giant cells. While these macrophages reside at the wound site, interaction with these biomaterials and the environment drives them towards different phenotypes, with very different characteristics (Figure 7.1). Pro-inflammatory macrophages, also called classical macrophages, or M1s, were first established as being activated by interferon-gamma (IFN-γ), an angiogenesis inhibitor chemokine. The M1 macrophage has been shown to act pro-inflammatory, immunogenic and pro-destructive [365-368] and secrete copious amounts of inflammatory cytokines, including, but not limited to IL-23 and TNF-α [369, 370]. M2, or alternative activated macrophages, were first described by Gordon *et al.*, and are characterized as anti-inflammatory, tolerogenic, inflammation resolving, and tissue restorative. They possess the ability to facilitate tissue repair and regeneration, and in addition, promote angiogenesis and tissue remodeling [367, 369-371] by releasing pro-

angiogenic growth factors (FGF, TGF-β, granulocyte macrophage-colony stimulating factor (GM-CSF), VEGF) and cytokines (IL-1, IL-6, IL-8), that chemoattract additional pro-regenerative cells, such as ECs [365, 368]. Alternative activated macrophages are stimulated by, and also produce, high levels of IL-4, IL-10, and IL-13, which are all down regulators of pro-inflammatory properties of macrophages. M2 macrophages also produce large amounts of arginase, an amino acid whose end degradation products function to mediate the production of collagen, enhance tissue repair, and induce cell proliferation [366, 368, 372-376]. Their inflammation resolving capabilities are thought to be due to LXA_4 in the environment.

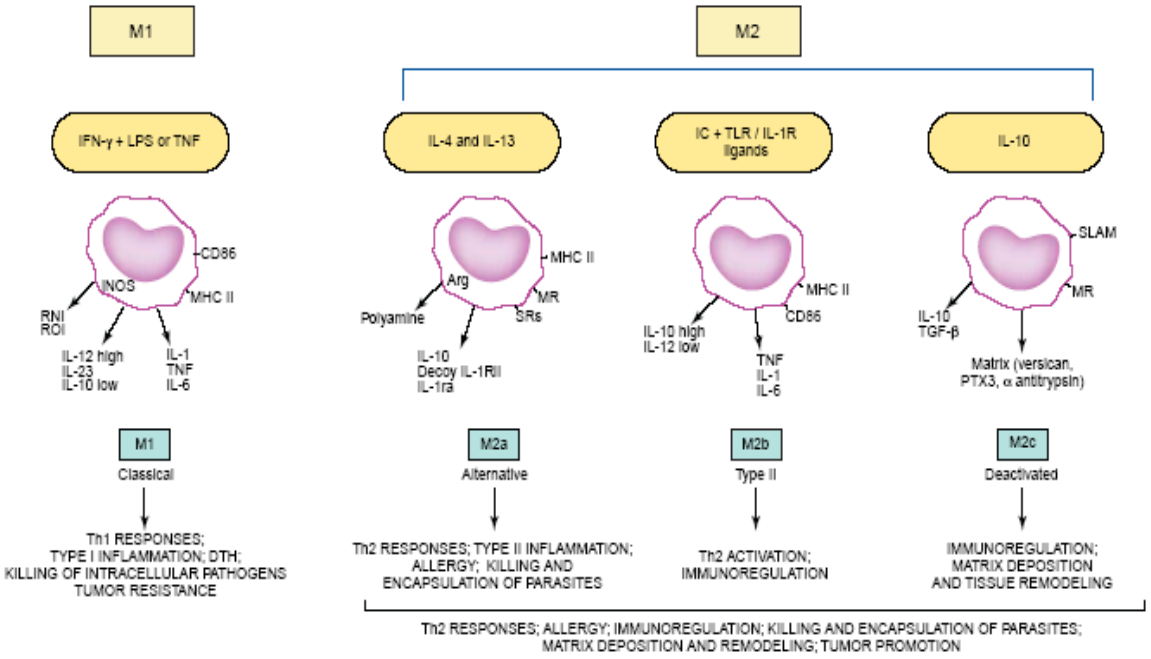

Figure 7.1. Schematic describing macrophage phenotypes and their roles in inflammation and wound healing. Reprinted from [369].

In previous studies, macrophage phenotype has been directly correlated to the healing outcome of an implanted biomaterial; an implant that is dominated by M1s has resulted in chronic inflammation and the formation of a fibrotic capsule, while a wound

site that promotes an M2 response results in immunoregulation and constructive tissue remodeling [370, 371]. Although it may appear that the ideal scenario would be to have all M2s residing at a wound site, it has been demonstrated that macrophage activation is plastic, rapid and fully reversible under the influence of different microenvironments, suggesting there is a balance in macrophage activation of both phenotypes that allows for wound resolution [368, 376].

Angiogenesis

Angiogenesis, or the formation of new vessels from pre-existing vessels, is a complex process that involves the interaction between vascular cells and the surrounding ECM. In wound healing, angiogenesis serves to restore vascular perfusion to damaged tissues. This process is critical in order for tissue regeneration and healing to take place, especially that of an implanted electrospun bioresorbable vascular graft. As stated previously, angiogenesis begins indirectly through the release of factors from inflammatory cells, as they are the first cell type to the site of implantation. The secretion of growth factors and chemokines initiate the wound healing process, recruiting various pro-angiogenic cells to the implant site where, in order for angiogenesis to take place, they must be able to migrate and infiltrate through capillaries or tunnels that have been created through by macrophages. ECs are the main cell type involved in angiogenesis and repair of vascular implants, as they penetrate the basement membrane and migrate into the graft where they form functional new vasculature in response to stimuli from inflammatory cells. This involves extravasation through the graft wall, proliferation, sprout and lumen formation and branching of sprouts to form networks [377]. Capillaries

that are formed vascularize the construct, providing a blood supply to deliver oxygen and nutrients through the graft, so further regeneration can occur [378]. In addition, ECs from the periphery of the graft must migrate through to the luminal side, aiding other EPC and EC from the blood stream in creating an EC lining. It is important to recognize that angiogenesis is more than a simple response by one cell type to growth factors, but rather, results from an intricate and complex balance between inflammatory and vascular cells in response to pro- and antiangiogenic agents, whose expression might vary between neighboring microenvironments [379].

In this study we investigate the potential for electrospun PCL incorporated with and without PRGF and heparin to promote EC proliferation, migration (chemotaxis), and sprout formation. In addition, macrophage phenotype, as determined by TNF-α and IL-10 release, in response to electrospun bioactive vascular graft materials was investigated over time. The hypothesis of this study is that the release of PRGF from electrospun scaffolds will chemoattract pro-regenerative type macrophages; the corollary to this being that the PRGF incorporated scaffolds will promote proliferation and migration of ADSCs *in vitro*. The ability of macrophages to be driven towards a pro-regenerative phenotype on these structures, and the preliminary investigation of EC sprout formation in the presence of PRGF, will provide insight into the potential for this vascular graft to become successfully regenerated.

Materials and Methods

Creation of PRP and PRGF

The same PRP/PRGF that was created and used in Chapter 7 was also used for this study.

Chemotactic Effect of PRGF

To determine the role that powdered PRGF had on macrophage and EC chemotaxis, and to demonstrate that lyophilized PRGF retained viable chemotactic proteins, PRGF was dissolved in either macrophage media (RPMI 1640, supplemented with 10% FBS, 1% pennicillin/streptomycin) or complete EC medium (M199 Media supplemented with 10% FBS, 1% penicillin/streptomycin, Glutamax 100x, G418, heparin sodium salt (50 µg/ml), and endothelial cell growth supplement (ECGS, 50 µg/ml)) in a range of concentrations (0, 0.1, 1, 5, and 10 mg/ml). Using a 24-well Transwell plate with 8 µm diameter pores (Corning, Inc.), 600 µl of PRGF containing media was placed in the bottom wells, while the top insert was seeded with 50,000 murine peritoneal macrophages (ATCC, TIB 186) or human pulmonary microvascular endothelial cells (HPMEC, received generously from Dr. C.J. Kirkpatrick) in 200 µl of control media for 72 or 168 hours (n=3). Following the duration of the experiment, an MTS assay (Promega) was performed to determine the average number of cells that had migrated to the bottom well.

Chemotactic Effect of PRGF and Heparin Incorporated Scaffolds

To determine the role that the electrospun PRGF constructs with and without heparin had on macrophage and EC chemotaxis, 10 mm diameter disks were punched,

disinfected (30 min. soak in ethanol followed by three 10 min. rinses in PBS) and placed in the bottom of a 24-well Transwell plate (8 µm diameter pores, Corning, Inc.). The bottom wells consisted of 600 µl macrophage or EC media, along with control media with and without 1 mg/ml PRGF and 0.05% or 0.5% filtered heparin. The top insert was seeded with 50,000 murine peritoneal macrophages or HPMEC in 200 µl of control media for 72 or 168 hours (n=3). Following the time duration, the average numer of cells that had migrated was determined by performing an MTS assay (Promega).

Proliferative Effect of PRGF on Endothelial Cells

To determine the effect PRGF had on EC proliferation, PRGF was dissolved in complete EC medium in a range of concentrations (0, 0.1, 1, 5, and 10 mg/ml). HPMEC were seeded at a density of 50,000 cells/well in 500 µL media (n=3). At days 1, 4 and 7, an MTS assay (Promega) was performed to determine the average cell number.

Effect of PRGF and Heparin Incorporated Scaffolds on Cell Proliferation

To determine the mitogenic potential of PRGF and heparin incorporated scaffolds on macrophages, 10 mm diameter disks were punched from each scaffold, disinfected (30 min. soak in ethanol followed by three 10 min. rinses in PBS) and placed in a 48-well plate (n=3). Each scaffold was seeded with 50,000 murine peritoneal macrophages (ATCC, TIB 186) in 500 µl macrophage media. Control wells consisted of macrophages cultured on tissue culture polystyrene (TCPS) in media with and without 1 mg/ml PRGF (TCPS:PRGF). On days 1, 4 and 7, macrophage proliferation was analyzed using an MTS assay (Promega).

This study was then replicated with HPMEC. Similar to the macrophages, disinfected 10 mm diameter disks of each scaffold were placed in a 48-well plate and were seeded with 25,000 cells/well in 500 µl complete EC media. HPMEC proliferation was determined by performing an MTS assay at days 1, 4 and 7.

Released PRGF Effect on Cell Proliferation

To determine the mitogenic potential of the PRGF released from the electrospun scaffolds that were cultured in the presence or absence of macrophages on HPMECs and ADSCs, 10 mm diameter disks of each electrospun material were punched, disinfected (30 min, soak in ethanol followed by three 10 min. rinses in PBS), and placed in a 48-well plate (n=3). Each well was then seeded with 300,000 human peripheral blood macrophages (ATCC, CRL9855) in 500 µl MSFM, as well as in a control TCPS well containing MSFM with and without 1 mg/ml PRGF added (TCPS:PRGF). The macrophage conditioned media was removed daily and used as a media supplement for HPMECs and ADSCs (200 µl MSFM with 300 µl HPMEC media or ADSC media (DMEM low glucose, 10% FB, 1% penicillin/streptomycin, (Invitrogen)) cultured on TCPS (25,000 cells/well) in a separate 48-well plate. HPMEC and ADSC proliferation was analyzed using an MTS Assay (Promega) at days 1, 4, and 7.

This study was then replicated without the use of macrophage conditioned media to isolate the impact of the released PRGF on HPMEC and ADSC proliferation. That is, disinfected 10 mm diameter disks of each electrospun material were placed in a 48-well plate with 500 µl HPMEC or ADSC culture media. Media was removed daily and used as

a supplement for HPMECs or ADSCs cultured at 25,000 cells/well. HPMEC and ADSC proliferation was determined with an MTS Assay (Promega) at days 1, 4, and 7.

Evaluation of Cell Interaction

To determine the response of human cells on the PRGF containing scaffolds, 10 mm diameter disks from each electrospun scaffold were punched, disinfected (30 min. soak in ethanol followed by three 10 min. rinses in PBS), and placed in a 48-well plate. Each scaffold was then seeded with 25,000 HPMEC in 500 µl EC media or 50,000 human ADSC cultured in 500 µl ADSC culture media. Media was changed every third day, and HPMEC samples were removed from culture and fixed in 10% buffered formalin at day 14 for DAPI staining, while ADSC samples were removed from culture and fixed in buffered formalin on days 7 and 21 for Hematoxylin and Eosin (H&E) staining.

Effect of PRGF and Heparin Incorporated Scaffolds on Chemokine Release from Macrophages

To determine the release of M1 and M2 chemokines from macrophages cultured on the PRGF and heparin containing scaffolds, 10 mm diameter discs were punched, disinfected, and placed in a 48-well plate. Each scaffold was then seeded with 50,000 murine peritoneal macrophages in 500 µl macrophage media. In addition, macrophages were also seeded on TCPS without and with 1 mg/ml PRGF (TCPS:PRGF) and 0.05% and 0.5% heparin. For positive controls, macrophages were cultured on TCPS in media containing 100 ng/ml lipopolysaccharide (LPS, Sigma-Aldrich) plus 20 ng/ml IFN-γ

(PeproTech, for M1 polarization) or 20 ng/ml IL-4 (PeproTech, for M2 polarization). Macrophages were cultured in standard conditions (37°C, 5% CO_2) and supernatant was collected on days 1, 4, 7, and 14. Simultaneously, an MTS assay was performed to determine macrophage number on days 1, 4, 7, and 14. TNF-α (Antigenix America, Inc.) and IL-10 (PeproTech) ELISAs were performed per manufacturer's protocol to quantify the amount of M1 (pro-inflammatory, TNF-α) and M2 (pro-regenerative, IL-10) chemokine being released. These results were normalized to amount of chemokine released (ng/ml) per 10,000 cells.

***In vitro* angiogenesis bead assay**

A preliminary *in vitro* angiogenesis bead assay was performed, similar to that of Chen, *et al.* [380]. After Cytodex® microcarrier beads (Sigma) were autoclaved and hydrated overnight, 10 µl of bead solution was placed in a 15 ml tube and rinsed three times with complete EC medium before being mixed with approximately 1 million HPMEC. The tube was incubated in standard conditions (37° C, 5% CO_2), with inversion of the tube occurring every half hour over 3 hours to ensure cells attached to the beads. The media was then removed from the centrifuge tube, placed in a flask and incubated overnight. After incubation, beads were rinsed in PBS and transferred back to a 15 ml tube. Once the beads had settled to the bottom, any remaining media was removed, and beads were washed once more with PBS. After allowing the beads to settle to the bottom of the tube a second time, the beads with adherent cells were resuspended in a collagen gel solution (80% liquid Purecol with 10% 0.1M NaOH and 10% 10X PBS) containing 1000 KIU/ml aprotinin (Sigma). Simultaneously, 250 µl of collagen gel solution with

aprotinin was placed in the bottom of a 24 well plate and incubated at standard conditions until gelation occurred. Once the first layer was gelled, 250 µl of cell suspension was placed on the first collagen gel layer and was incubated for 2 hours to again allow for gelation. PRGF was then dissolved in EC media (0, 0.1, 1, 5 and 10 mg/ml) and 500 µl was placed on top of the gel solution containing the cell covered beads and incubated in standard conditions for 6 days. At days 1, 4 and 6, images were captured using a Nikon Eclipse TE200 microscope with a Dage-MTS digital camera. Three images were taken for each PRGF concentration at each time point. To quantify the percentage of HPMEC sprouts per bead, a circular grid was overlayed onto each bead, dividing it into 36 sections. All sprouts extending from the surface of the beads were counted, summed, and divided by 36 to determine the percentage of sprouts for each bead. In addition, the length of each sprout extending from the surface of the beads was quantified using ImageTool 3.0 software (Shareware provided by UTHSCSA). Results are presented as average sprout length per bead (n=3).

Statistical Analysis

All statistical analysis was based on a Kruskal–Wallis one-way ANOVA on ranks and a Tukey–Kramer pairwise multiple comparison procedure ($\alpha = 0.05$) performed with the JMP®IN 8.0 statistical software package (SAS Institute, Inc.). Graphical depictions of mean data were constructed with Microsoft Excel 2007, with error bars representing standard deviations.

Results

Chemotactic Effect of PRGF on Macrophages and HPMEC

The results of macrophage chemotaxis in response to a dose of PRGF dissolved in media are shown in Figure 7.2. Macrophage chemotaxis increased with the amount of PRGF, except for 0.1 mg/ml. While a trend is somewhat apparent, the only value that was significantly different from the group was the 10 mg/ml PRGF concentration, potentially indicating an ideal concentration for stimulating macrophage chemotaxis.

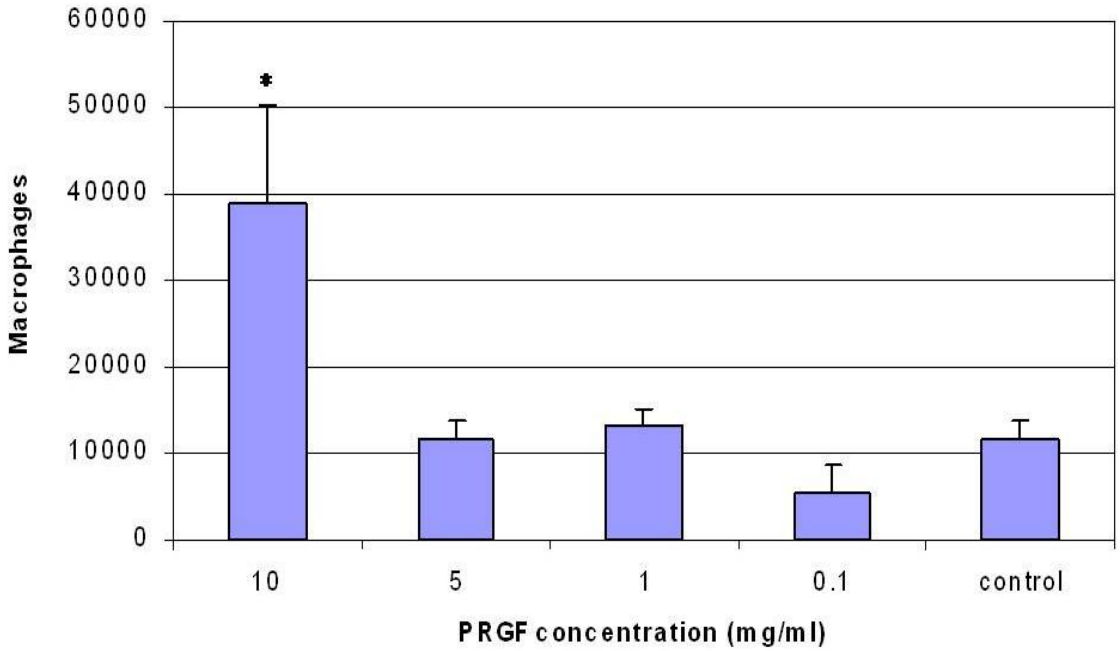

Figure 7.2. Results of macrophage chemotaxis in response to PRGF dose. * indicates statistically significant differences, $p < 0.05$, compared to all other groups.

HPMEC chemotaxis results in response to different concentrations of PRGF dissolved in media are illustrated in Figure 7.3. With the exception of 1 mg/ml, HPMEC chemotaxis appeared to significantly increase with increasing concentrations, however, the results obtained from the MTS assay for the amount of HPMECs that did migrate for

10 mg/ml and 5 mg/ml PRGF seems questionable. Compared to the 50,000 cells that were originally seeded on the insert, the fact that 250,000 HPMECs migrated to the bottom wells seems almost impossible. The reason for this may have been due to excess PRGF left in the well at the time of the experiment, which may have skewed the results of the MTS assay.

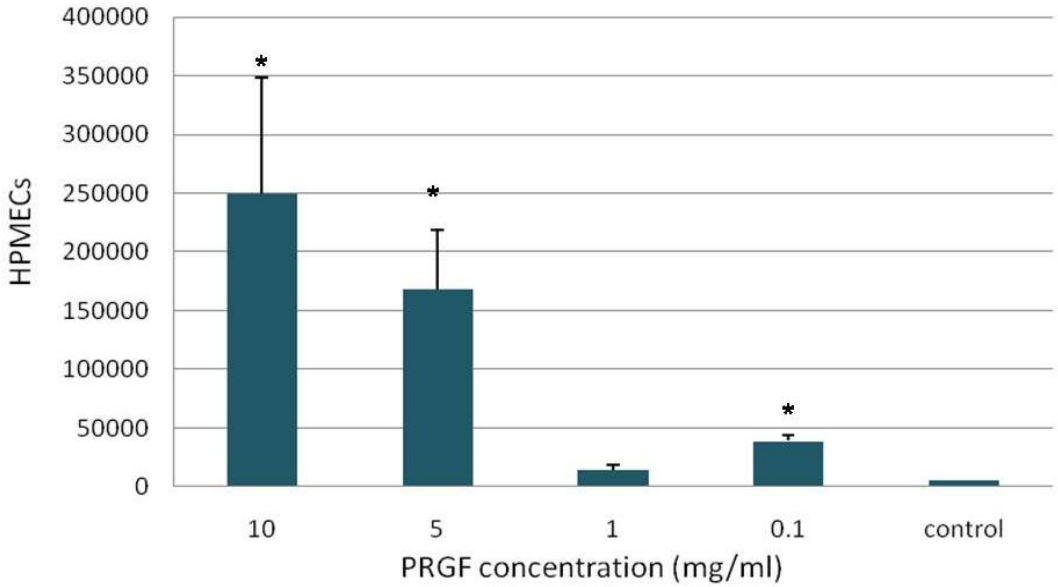

Figure 7.3. HPMEC chemotaxis to PRGF dissolved in media at different concentrations. *signifies statistical significance, $p<0.05$, compared to all other concentrations.

Chemotactic Effect of PRGF and Heparin Incorporated Scaffolds

Results from the Transwell assay to determine the chemotactic effect of heparin and PRGF incorporated scaffolds on macrophages is illustrated in Figure 7.4. PRGF containing scaffolds did not have a significant chemotactic effect on macrophages over PCL control scaffolds. This may be due to the duration of the experiment; because of limited amounts of nutrients in the top inserts of the Transwells, cells may have migrated to the bottom wells within the 72 hours regardless of PRGF concentration. In contrast, the

addition of heparin at 0.05% and 0.5% did have a significant effect on macrophage chemotaxis. Specifically, macrophage chemotaxis was significantly decreased for TCPS with heparin compared to TCPS without heparin. Surprisingly, PCL:PRGF(10) scaffolds not containing heparin had a significantly lower chemotactic effect than those same scaffolds with 0.05% heparin. As mentioned previously, the increase in chemotaxis of the PCL:PRGF(10) heparin containing scaffolds may be due to the inconsistent inclusion of heparin throughout the scaffolds.

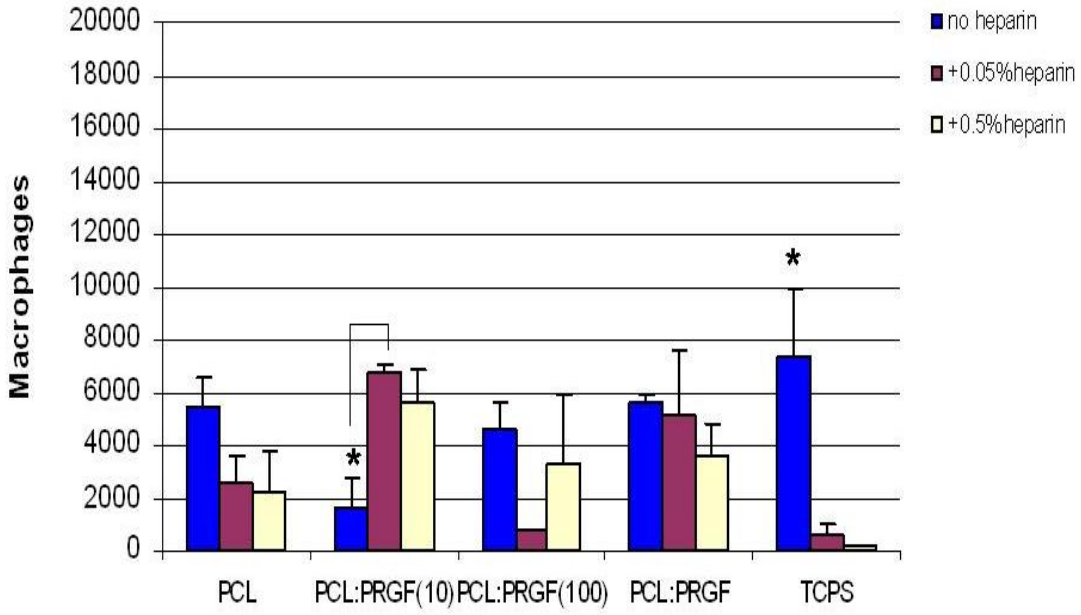

Figure 7.4. Effect of heparin and PRGF on macrophage chemotaxis. * denotes statistical significance ($p<0.05$) between material groups with and without heparin.

The results of HPMEC chemotaxis in response to heparin and PRGF containing scaffolds over 168 hours is displayed in Figure 7.5 and illustrates there are no significant differences in chemotaxis between scaffolds and TCPS with and without heparin. Additionally, there were no significant differences in chemotaxis for scaffolds with and

without PRGF, alluding to the fact that electrospun PRGF and heparin containing scaffolds may not be chemoattractant towards HPMECs.

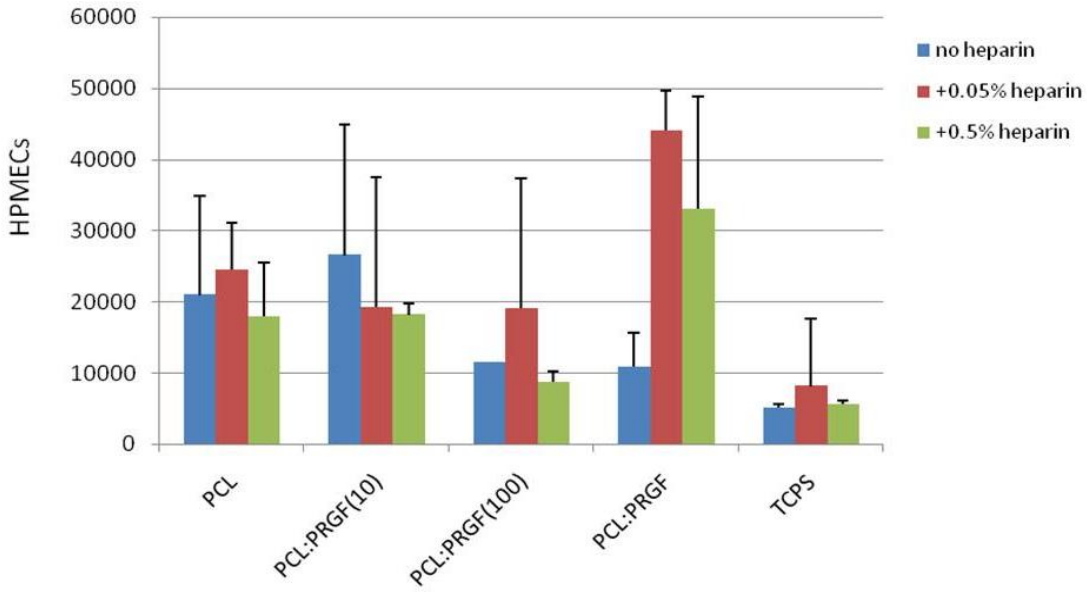

Figure 7.5. HPMEC chemotaxis in response to PRGF and heparin.

Proliferative Effect of PRGF on Endothelial Cells

Results from the MTS assay performed to determine the effect of PRGF on endothelial cell proliferation are illustrated in Figure 7.6. At day one, there are no differences in cell proliferation, however, at day 4, HPMECs cultured in PRGF at 5 and 10 mg/ml are statistically different from those cultured in media control. By day 7, HPMECs cultured in 0.1, 1, and 5 mg/ml PRGF are significantly different than cells cultured in media control.

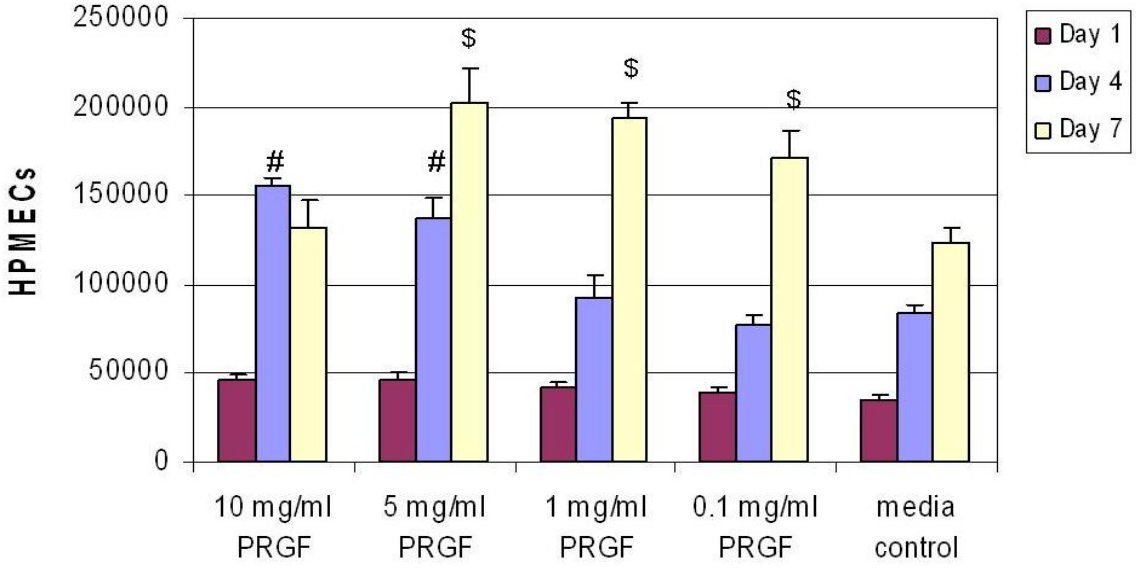

Figure 7.6. Results of HPMEC proliferation over 7 days when cultured in PRGF in media at different concentrations. # and $ signifies statistical significance in proliferation over media control at day 4 and day 7, respectively ($p<0.05$).

PRGF and Heparin Incorporated Scaffolds' Effect on Cell Proliferation

Proliferation of macrophages when cultured on PCL and PRGF incorporated scaffolds with and without heparin are shown in Figure 7.7. There were no significant differences comparing macrophages cultured on PRGF incorporated scaffolds versus PCL control over the 14 days (Figure 7.7, top). Cells cultured on TCPS with 1 mg/ml PRGF had significantly greater proliferation at day 4 than those cultured on TCPS control at day 4. Although PRGF caused a significantly higher proliferation of macrophages at day 4, PRGF incorporated scaffolds as well as TCPS:PRGF did not cause significantly greater proliferation than their controls, implying PRGF may not have an impact on macrophage proliferation.

The incorporation of heparin at different concentrations had some effect on macrophage proliferation, as illustrated in Figure 7.7, bottom (represented by $, ^, @, +);

however, it was inconsistent between the two different amounts of heparin. At day 1, PCL+0.05% heparin and PCL:PRGF(10)+0.5% heparin scaffolds had significantly increased proliferation over PCL+0.5% and PCL:PRGF(10)+0.05% heparin scaffolds. At day 4, PCL and TCPS:PRGF with 0.05% heparin had significantly higher proliferation over their substrate counterparts with 0.5% heparin. PCL:PRGF(10) and PCL:PRGF scaffolds with 0.05% heparin had statistically significant proliferation at day 7 over their scaffold counterparts with 0.5% heparin. At day 14, TCPS:PRGF+0.5% heparin had significantly higher proliferation than TCPS:PRGF+0.05% heparin. There were significant differences (denoted by *, #, %, &) in cell proliferation when comparing macrophages cultured on PRGF incorporated scaffolds and TCPS:PRGF with heparin to cells cultured PCL control scaffolds and TCPS, however, there were no consistent significant increases or decreases in proliferation between any of the PRGF incorporated scaffolds and TCPS and control groups. Macrophages cultured on PCL:PRGF(100) scaffolds with heparin had significantly lower proliferation at days 1 and 4 then PCL control scaffolds with heparin. TCPS:PRGF with heparin (0.05% and 0.5%) had significantly greater proliferation at day 14 than those cultured on TCPS control with heparin. These results demonstrate the incorporation of PRGF and/or heparin to PCL scaffolds does not have a direct effect on the proliferation of macrophages. In both cases, there were no consistent increases or decreases in macrophage number over the 14 day time period.

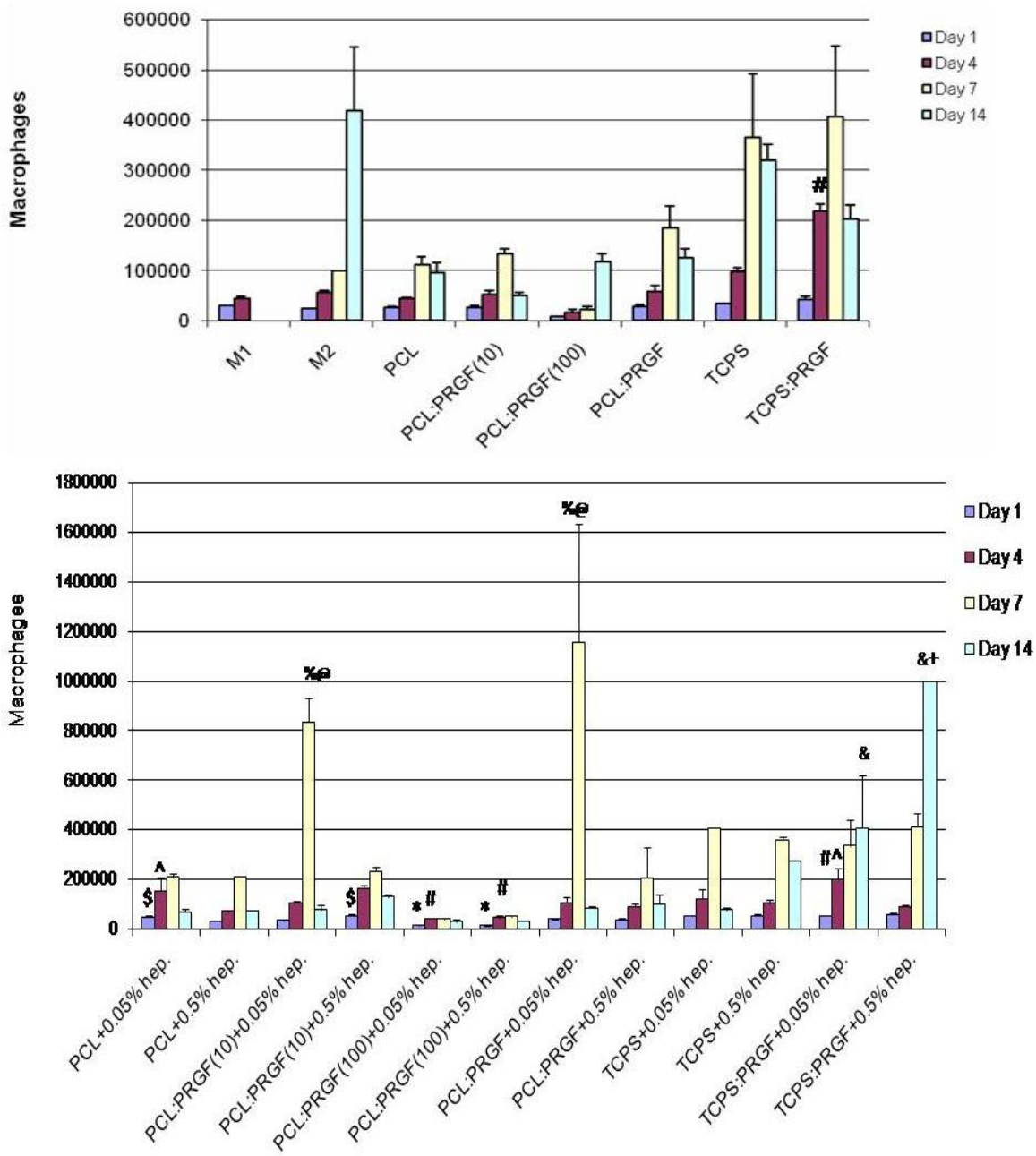

Figure 7.7. Top: Proliferation of macrophages cultured on PCL and PRGF containing scaffolds over 14 days. # signifies statistical significance, $p<0.05$, between cells cultured on TCPS and TCPS:PRGF at day 4. Bottom: Macrophage proliferation results when cultured on PCL and PRGF incorporated scaffolds with heparin (0.05% and 0.5%). *, #, %, & denotes statistical significance ($p<0.05$) of cell proliferation between scaffolds and TCPS incorporated with PRGF and heparin and PCL and TCPS with heparin control groups at days 1, 4, 7 and 14 respectively. $, ^, @, + signifies statistical significance, $p<0.05$, between scaffolds of the same material groups with 0.05% or 0.5% heparin for days 1, 4, 7, and 14 respectively.

Results of HPMEC proliferation are illustrated in Figure 7.8. Statistical analysis revealed cells cultured on scaffolds with 100 mg/ml or 200 mg/ml PRGF had significantly lower proliferation than those cultured on PCL control scaffolds on days 1, 4 and 7 (Figure 7.8, top). Also on day 7, HPMECs cultured on TCPS with 1 mg/ml PRGF in media had significantly higher proliferation than those cultured on TCPS control, while at day 14, cells cultured in TCPS:PRGF had significantly lower proliferation than those cultured on TCPS. HPMEC proliferation on scaffolds incorporated with PRGF at high concentrations may be explained by increased cell infiltration into the scaffolds (investigated in Figure 7.13 below). If cells have penetrated into electrospun scaffolds, the MTS solution does not have adequate time to diffuse into the cells within the scaffolds, and therefore, the assay does not provide accurate results. Additionally, activated TGF-β1 present in the electrospun PRGF incorporated scaffolds may also be the reason for low HPMEC proliferation. TGF-β1 has been shown to be inhibitory to EC proliferation at levels ranging from 10 pg/ml – 10 ng/ml [381] and the electrospun PCL:PRGF(100) scaffolds analyzed in Chapter 6 had detectable TGF-β1 levels ranging from 0.6 – 1 ng/ml over 21 days (Figure 6.8(a)). Although TGF-β1 was also detectable in PRP and PRGF in media, this was only possible after subjecting the PRP and PRGF to an acid activation treatment (data not published). The significantly lower proliferation that was observed with cells cultured in TCPS:PRGF over those cultured in TCPS at day 14 may be due to cell apoptosis caused by a loss of nutrients because of cell confluency.

The addition of heparin at different amounts to electrospun scaffolds did not have a significantly consistent effect on HPMEC proliferation over the 14 days (Figure 7.8, Bottom). There were no significant differences at day 1 between scaffolds of the same

type with different amounts of added heparin. At day 4, PCL:PRGF(10)+0.5% heparin scaffolds and TCPS+0.05% heparin elicited significantly higher proliferation than their counterparts with 0.05% and 0.5% heparin. At day 7, PCL+0.05% heparin and PCL:PRGF(10) and TCPS:PRGF with 0.5% heparin added resulted in significantly greater proliferation than their same substrate counterparts with 0.5% or 0.05% heparin. By day 14, only scaffolds of PCL:PRGF(10)+0.5% heparin had significantly enhanced cell proliferation over PCL:PRGF(10)+0.05% heparin. Compared to PCL controls at day 1, PCL:PRGF(100) scaffolds with heparin had significantly lower proliferation. At day 4, PCL:PRGF(100) scaffolds with heparin and PCL:PRGF+0.05% heparin scaffolds elicited significantly lower proliferation then PCL control scaffolds, while TCPS:PRGF with heparin elicited significantly higher proliferation over TCPS control with 0.5% heparin. On day 7, PCL:PRGF(100) and PCL:PRGF scaffolds with heparin both resulted in significantly decreased proliferation over PCL control scaffolds with heparin, whereas TCPS:PRGF with heparin elicited significantly higher proliferation compared to TCPS control with heparin. PCL:PRGF(100) scaffolds with heparin resulted in significantly lower proliferation at day 14 compared to PCL+0.05% heparin control scaffolds. The decrease in proliferation seen on scaffolds with a high concentration of PRGF, again, is most likely due to the activated TGF-β1 being released. The fact that PCL:PRGF(10) scaffolds with 0.5% heparin had significantly increased proliferation over their counterparts with 0.05% heparin may be explained by the large amount of heparin available to bind to more growth factors, and therefore, more growth factors available for cells to detect. However, that is the only scaffold type that followed that trend. Previous studies that have investigated the effect of heparin on EC proliferation have reported

varying results as well. One study concluded that the proliferative effect of heparin on ECs was variable between 7 identical experiments: EC proliferation was stimulated in four of the experiments, but was unaffected in the other three [382]. Heparin ranging from 5 U/ml – 500 U/ml has been shown to enhance EC proliferation in other studies, but only when bound with a growth factor such as FGF-1, or ECGS [383, 384]. In the instance where heparin was bound to FGF-1, mitogenic activity only took place when the bond between the FGF-1 and heparin was broken [383]. Seeing as how the heparin added to scaffolds in this study was around 100 U/ml and 1000 U/ml, and was most likely bound to several growth factors in the PRGF, one might expect an increase in HPMEC proliferation on scaffolds with 0.5% heparin. The inconsistency in proliferation, however, was not specifically investigated, and further studies will need to be completed to determine the effects of heparin on HPEC proliferation.

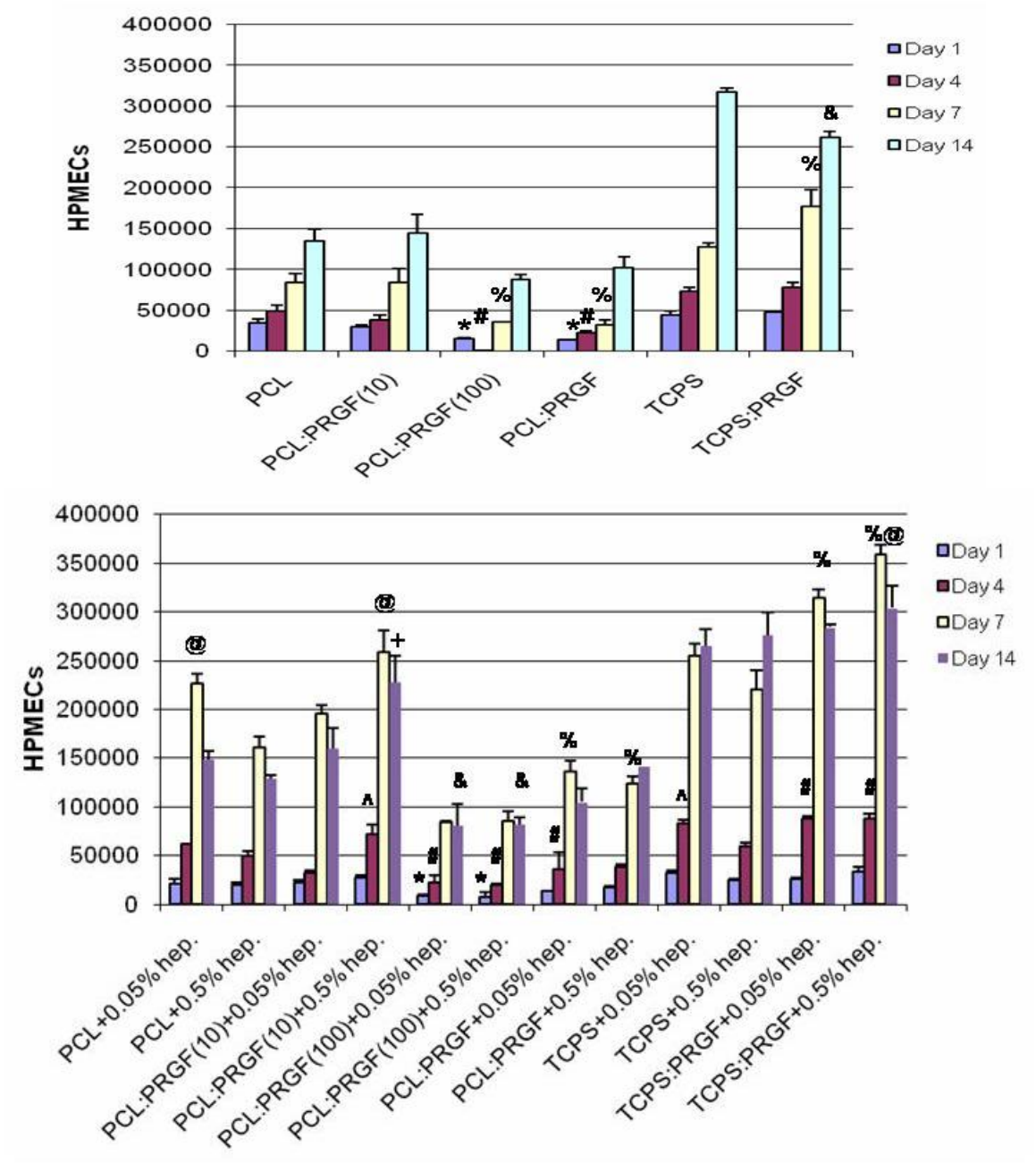

Figure 7.8. Top: Proliferation of HPMECs when cultured on PCL and PRGF containing scaffolds without heparin. *, #, %, & denotes statistical significance ($p<0.05$) of HPMEC proliferation when compared to PCL or TCPS control for days 1, 4, 7 and 14, respectively. Bottom: Proliferation of HPMECs when cultured on PCL and PRGF incorporated scaffolds with 0.05% or 0.5% heparin. *, #, %, & indicates significant differences, $p<0.05$, compared to cell proliferation on PCL and TCPS control substrates with heparin on days 1, 4, 7 and 14 respectively. $, ^, @, + signifies statistical significance, $p<0.05$, between scaffolds of the same material groups with 0.05% or 0.5% heparin for days 1, 4, 7, and 14 respectively.

Released PRGF Effect on Cell Proliferation

To determine the role that PRGF had in the secretion of macrophage growth factors, HPMEC and ADSCs were cultured in media conditioned by macrophages exposed to released PRGF. The effect of macrophage conditioned medium on HPMEC proliferation is shown in Figure 7.9. HPMEC cultured in preconditioned media from macrophages that were cultured on PRGF incorporated scaffolds proliferated as expected, increasing over the 7 days. Statistical analysis revealed there to be no significant differences between cells cultured in media from different material groups on days 1, 4 and 7. However, HPMEC cultured in preconditioned media from macrophages cultured on PRGF incorporated scaffolds exhibited higher proliferation by day 7 over that from PCL control scaffolds, with the highest proliferation occurring in media from PCL:PRGF scaffolds.

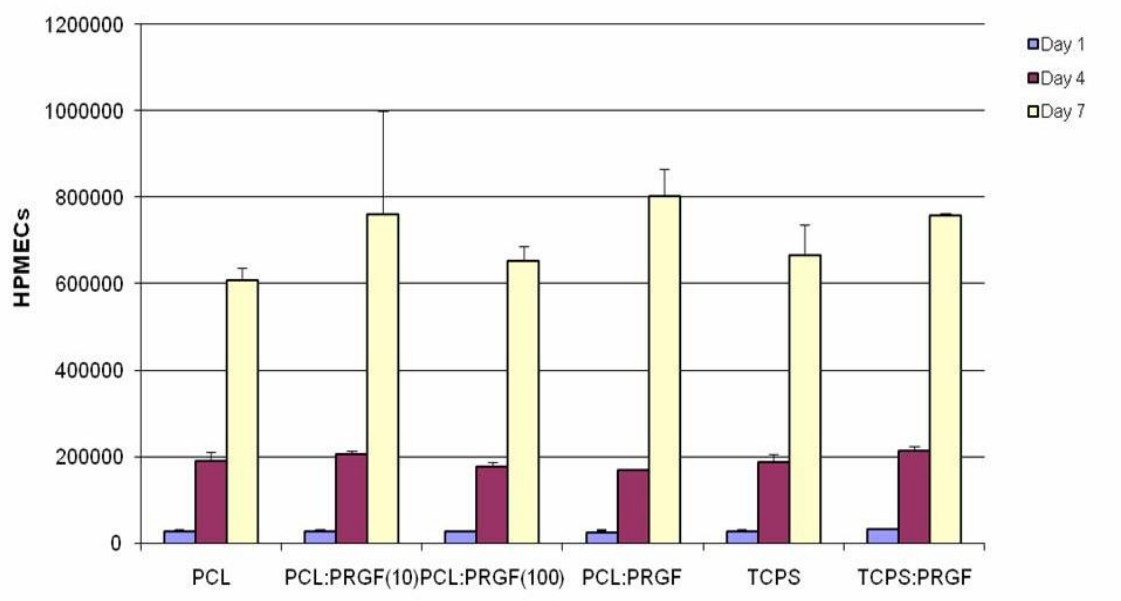

Figure 7.9. Results of HPMEC proliferation when cultured with macrophage preconditioned medium.

HPMEC proliferation when cultured in preconditioned media without macrophages is shown in Figure 7.10. At days 1 and 4, with the exception of cells cultured in medium from PCL:PRGF scaffolds, there no significant differences in cell proliferation. Surprisingly, cells cultured in conditioned medium from PCL:PRGF scaffolds had significantly lower numbers than cells cultured in medium from PCL scaffolds at days 1 and 4. By day 7, cells cultured in conditioned medium from PCL control scaffolds and TCPS had significantly higher proliferation than cells cultured in conditioned medium from PRGF incorporated scaffolds and TCPS:PRGF. In comparing the results of HPMEC proliferation in conditioned media with macrophages versus conditioned media without macrophages, it is very clear that HPMEC proliferation is very much affected by macrophage interaction with PRGF scaffolds. When HPMEC are cultured in conditioned media without macrophages their proliferation rate is decreased, almost 3 times as much.

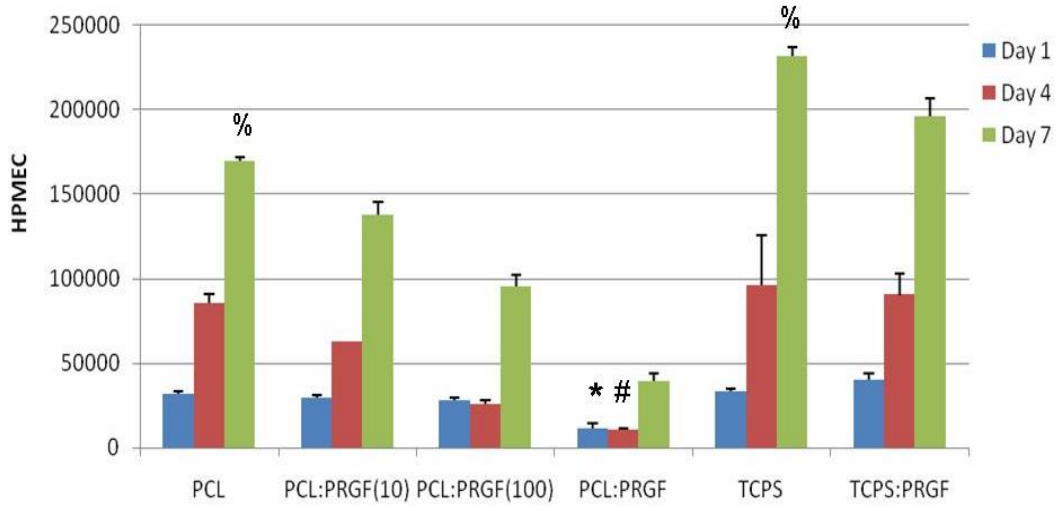

Figure 7.10. HPMEC MTS assay results when cultured without macrophage preconditioned medium. * signifies statistical significance ($p<0.05$) compared to PCL control scaffolds at day 1. # indicates statistical significance, $p<0.05$, compared to PCL control scaffolds at day 4. % denotes significant differences ($p<0.05$) at day 7.

The results of ADSC proliferation, when cultured in macrophage conditioned media, demonstrated no significant differences in proliferation at day 1. However, by day 4 ADSCs cultured in macrophage conditioned media from scaffolds of PCL:PRGF(100) had significantly greater proliferation than ADSCs cultured in macrophage conditioned media from the PCL and TCPS control, as well as all other scaffolds (Figure 7.11). By day 7, there was significantly greater ADSC proliferation in macrophage conditioned media from scaffolds of PCL:PRGF(100) and TCPS:PRGF than ADSCs cultured in conditioned media from PCL and TCPS control, as well as all other scaffolds. This was expected, as it had previously been demonstrated that PRGF, as well as growth factors secreted by macrophages, enhanced fibroblast, mesenchymal and stromal stem cell proliferation [302, 352, 354-356, 385]. In general, ADSC proliferation in all preconditioned media increased from day 1 to day 4, however, by day 7 it appeared that proliferation slowed, and in some cases cell number even decreased, potentially due to induced contact inhibition as the cells became confluent in the wells, or died off following exhaustion of media nutrients. This may also have been due to the fact that the conditioned media used for the ADSCs was macrophage serum free media, which is unfavorable over the long-term for ADSC growth, or due to harmful factors expressed during macrophage apoptosis [386]. From the results in Figure 7.7, it is evident that the effect of macrophages on ADSC proliferation was due to macrophage interaction with PRGF containing scaffolds, and not merely macrophage number.

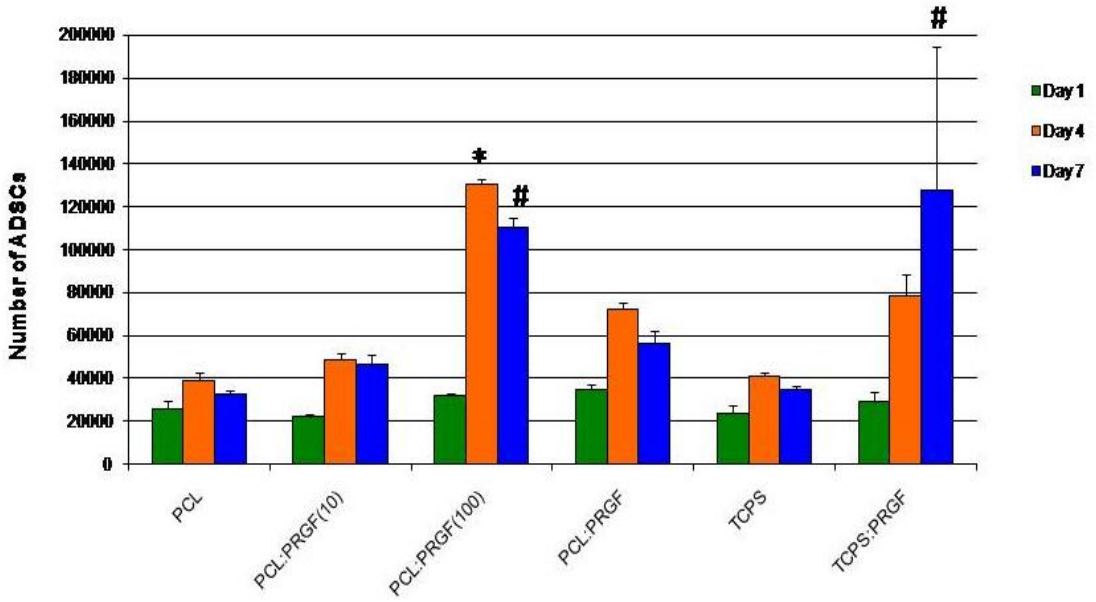

Figure 7.11. Results of ADSC MTS assay when cultured with macrophage conditioned media. * and # indicate statistically significant differences, $p < 0.05$, between material groups at day 4 and day 7, respectively.

ADSC proliferation when cultured in PRGF conditioned media without macrophages is displayed in Figure 7.12. Overall, ADSCs proliferated from day 1 to day 4 (with a few exceptions), and from day 4 to day 7, as expected. After day 1 and 4, there were no significant differences in ADSC proliferation for any scaffold. By day 7, compared to ADSCs cultured in media from the TCPS control, cells cultured in media from PCL:PRGF scaffolds had significantly greater proliferation. These results suggest that the presence of PRGF does impact ADSC proliferation, and corroborates previously published work [302, 352, 354-356]. It is clearly evident from these studies that the proliferation of ADSCs, cultured in conditioned media, is different depending on the presence or absence of macrophages and macrophage secreted factors over the 7 day study duration, and will be discussed further in the following section.

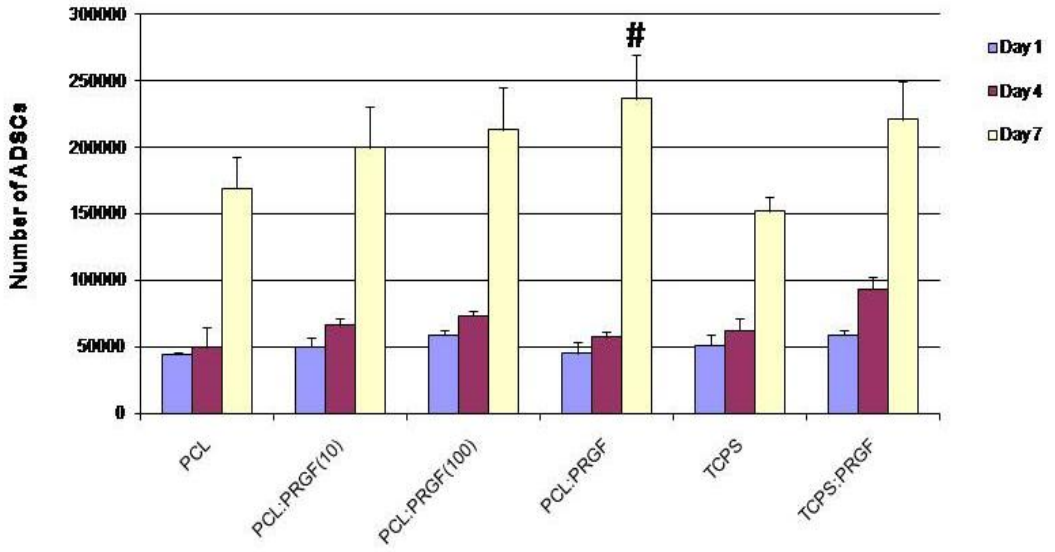

Figure 7.12. Results of ADSC MTS assay when cultured without macrophage conditioned media. # indicates statistically significant differences, $p < 0.05$, between PRGF containing scaffolds and the TCPS control at day 7.

EC Interaction on PRGF scaffolds

In order to elucidate the results from the MTS assay for HPMECs, scaffolds were fixed, sectioned, and stained for DAPI at the end of the 14 day time period. Figure 7.13 displays HPMECs cultured on PCL and PRGF containing scaffolds with and without heparin. Cells cultured on PCL and PCL:PRGF(10) scaffolds with and without 0.05% and 0.5% heparin appear to remain on the surface of the scaffolds after 14 days, with minimal to no infiltration occurring. In contrast, scaffolds incorporated with PRGF at 100 mg/ml and 200 mg/ml exhibit HPMEC infiltration, particularly throughout those scaffolds without heparin. This outcome may explain why there was decreased cell proliferation, as determined by the MTS assay, in scaffolds incorporated with high amounts of PRGF both with and without heparin.

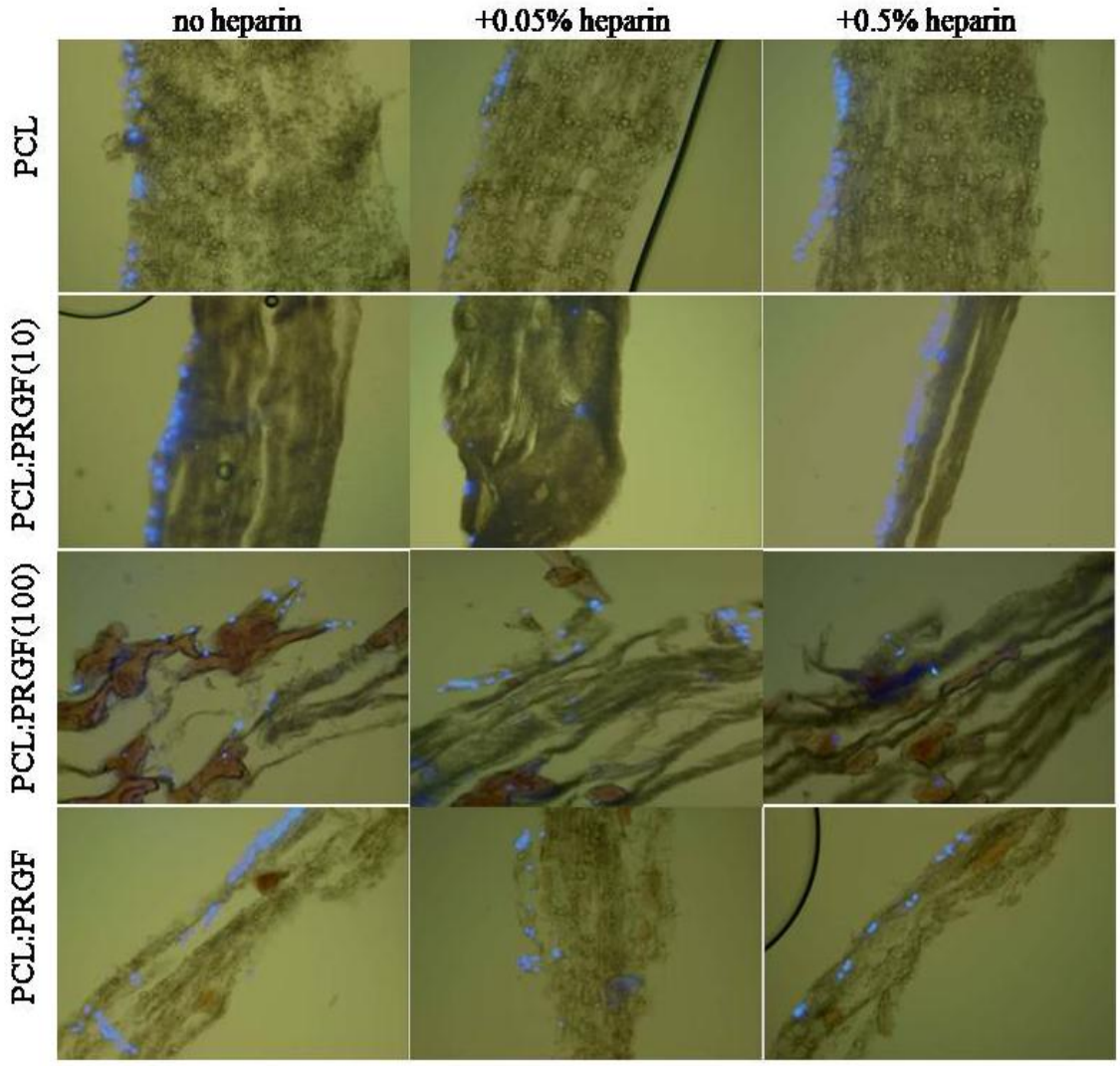

Figure 7.13. DAPI staining of HPMECs cultured on PCL and PRGF containing scaffolds with and without heparin. Images taken at 20X.

Evaluation of ADSC Interaction

The results of the H&E staining are shown in Figure 7.14. H&E staining revealed confluent layers of ADSCs on the surfaces of the control scaffolds by day 7, while increased PRGF content resulted in increased cellular penetration into the scaffold. Surprisingly, after only 7 days ADSCs had migrated through a quarter of the thickness of the PCL:PRGF scaffold. By day 21 this trend was even more apparent, with clear cell

migration through nearly the entire thickness of the PCL:PRGF scaffold (Figure 7.12). The PCL:PRGF(100) scaffold demonstrated a similar result, with the electrospun synthetic PCL material traditionally being difficult to cellularize *in vitro* [297-299], as it too exhibited increased cellular penetration when compared to the PCL scaffold containing no PRGF.

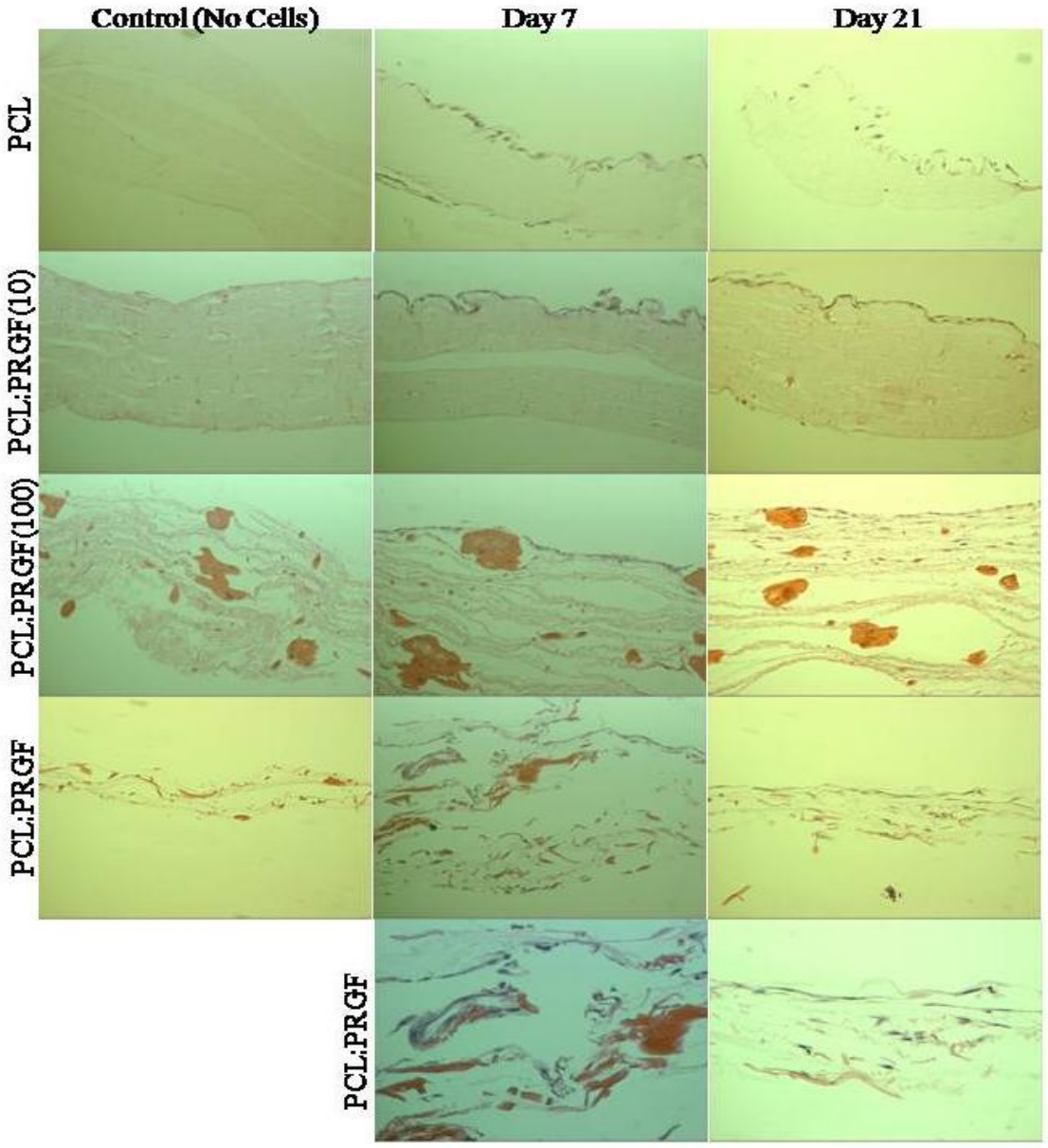

Figure 7.14. H&E staining of PCL scaffolds at day 7 and 21. Images at 20x. High magnification (40x) images of PCL:PRGF scaffolds shown in bottom row, demonstrating significant cellular penetration.

Effect of PRGF and Heparin on Macrophage Phenotype

Figure 7.15(a) below shows the results of IL-10 release from macrophages cultured on PCL and PRGF incorporated scaffolds and TCPS with and without 1 mg/ml PRGF. With the exception of day 7, in most cases, IL-10 release from macrophages

increased throughout the 14 days. At days 1, 4, and 7 there were no significant differences between the different scaffold types and control groups. However, by day 14, scaffolds with increased amounts of PRGF (PCL:PRGF(10), PCL:PRGF(100), PCL:PRGF) elicited higher IL-10 release from macrophages over control groups (PCL scaffolds and M2s), and was significantly different for PCL:PRGF(10) scaffolds. Another point worth noting is that, in general, IL-10 release was higher from macrophages cultured on electrospun scaffold materials than it was for the positive control (M2) at all time points. These results indicate PRGF, as well as electrospun structures overall, may have the ability to enhance the release of IL-10 from macrophages, possibly driving them towards the M2 phenotype.

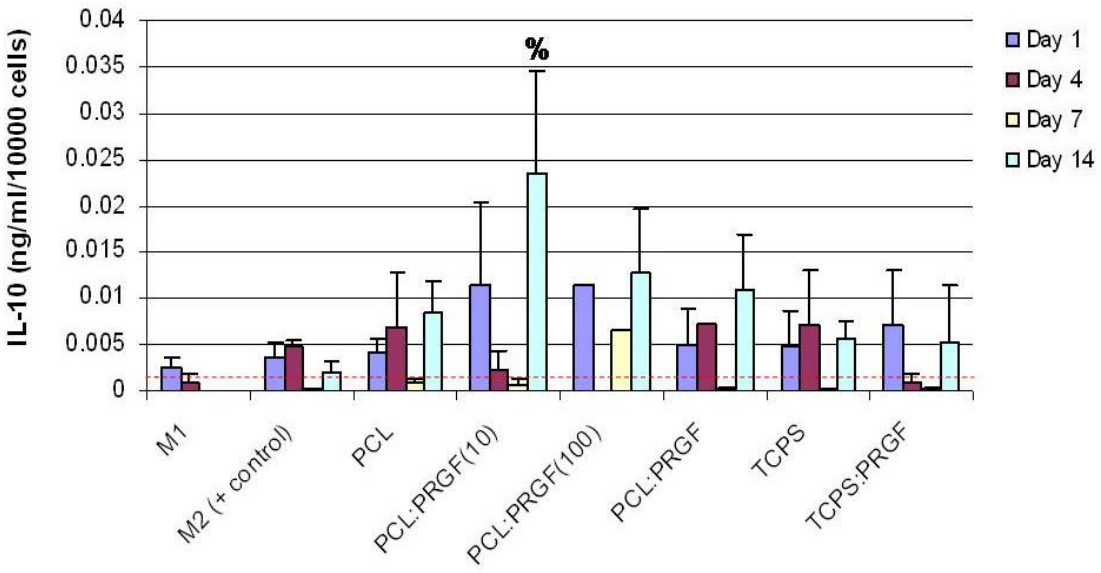

Figure 7.15(a). Macrophage IL-10 release when cultured on PRGF incorporated scaffolds, TCPS and media supplemented with 1 mg/ml PRGF (TCPS:PRGF). Results are normalized to amount of IL-10 released (ng/ml) per 10,000 cells. % denotes statistical significance ($p<0.05$) over PCL and M2 control at day 14. Minimum level of detection is 0.002 ng/ml (dashed line).

The results of IL-10 release from macrophages cultured on PRGF and heparin incorporated scaffolds and TCPS with and without 1 mg/ml PRGF and 0.05% and 0.5% heparin are shown in Figure 7.15(b). In general, IL-10 release from macrophages cultured on PRGF and heparin-containing scaffolds appeared to be highest at early time points (days 1 and 4), and decreased thereafter. Overall, the addition of heparin to scaffolds in different amounts did not elicit significant differences in IL-10 release from macrophages, with the exception of PCL:PRGF(100)+0.05% heparin and TCPS:PRGF+0.5% heparin. In both cases, there was a significantly greater release of IL-10 when compared to PCL:PRGF(100)+0.5% heparin and TCPS:PRGF+0.05% heparin. IL-10 release at day 4 was significantly higher from macrophages cultured on PCL:PRGF(100) scaffolds with 0.05% heparin compared to PCL control scaffolds with

same amounts of heparin, as well as TCPS:PRGF+0.5% heparin compared to TCPS control with 0.05% and 0.5% heparin. At day 7, scaffolds with 100 mg/ml PRGF and heparin elicited significantly higher IL-10 release compared to PCL control scaffolds and at day 14, PCL:PRGF(100) scaffolds with 0.5% heparin had significantly higher IL-10 release than PCL control scaffolds with the same amount of heparin. In comparing IL-10 levels from figure 7.15(a), the addition of heparin, in general, appeared to increase the release of IL-10 from macrophages over all, with higher levels released at early stages, and decreased thereafter. These results may suggest macrophages cultured on heparin incorporated scaffolds may begin as M2s, but over time may undergo a change in phenotype.

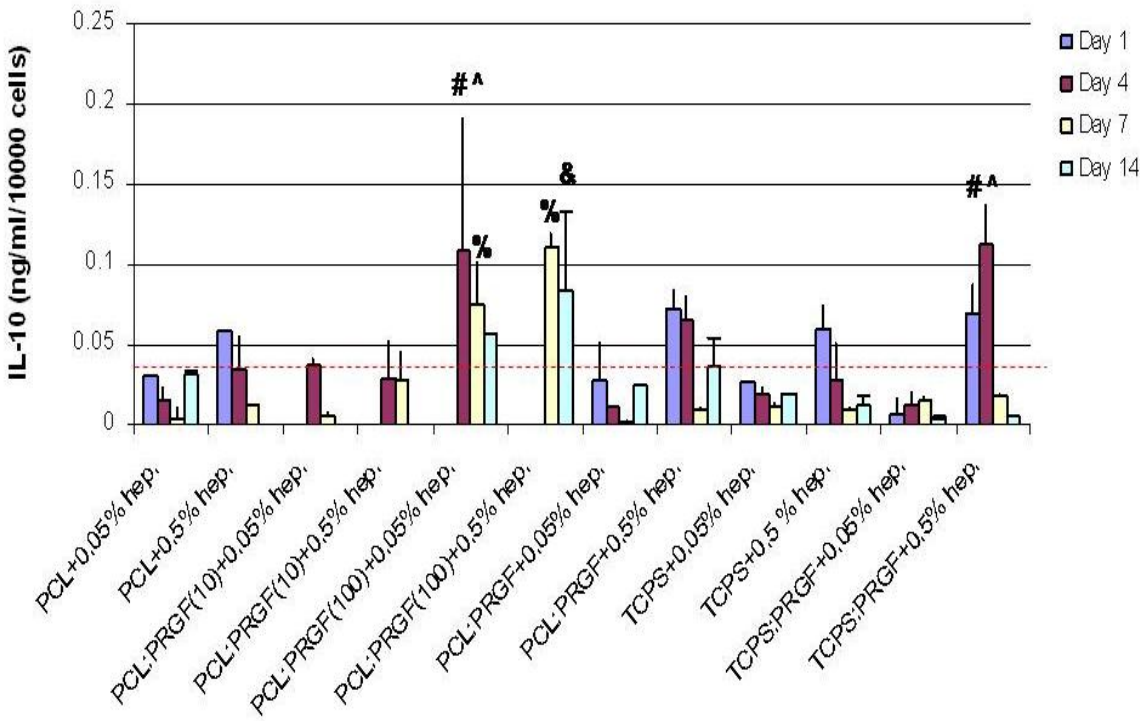

Figure 7.15(b). IL-10 release from macrophages cultured on PRGF incorporated scaffolds, TCPS, and TCPS with 1 mg/ml PRGF with the addition of 0.05% or 0.5% heparin. Results are normalized to amount of IL-10 released (ng/ml) per 10,000 cells. # denotes statistical significance ($p<0.05$) between PRGF incorporated scaffolds and PCL control scaffolds with same amounts of heparin, as well as TCPS:PRGF+0.5% heparin and TCPS control with 0.05% and 0.5% heparin at day 4. ^ denotes statistical significance, $p<0.05$, between the different amounts of heparin for the same type of material substrate for day 4. % indicates statistical significance ($p<0.05$) at day 7 between scaffolds with PRGF and heparin and PCL control scaffolds. & signifies statistical significance, $p<0.05$, for day 14 between PRGF containing scaffolds and PCL control scaffolds with the same amount of heparin. Minimum level of detection is 0.04 ng/ml (dashed line).

Figure 7.16(a) shows the results of TNF-α release from macrophages cultured on PCL scaffolds with and without PRGF. At days 1 and 4, only the positive M1 control had detectable TNF-α release. By days 7 and 14, release on all scaffold types was detectable, with statistical significance on PCL:PRGF(10) scaffolds at day 14. Although there was no release from the positive M1 control at days 7 and 14 (due to cell apoptosis), the amount of TNF-α released on electrospun scaffolds at days 7 and 14 was much lower

than that from the positive control at days 1 and 4. Also worth noting is that at day 14, TNF-α release from macrophages cultured on all scaffold types was less than that of IL-10 release at day 14 (except for PCL). These results indicate PRGF and electrospun structures overall, did not enhance the release of TNF-α from macrophages over the positive control, and may be driving cells towards the M2 phenotype over the M1 phenotype (as indicated by amount of chemokine released per 10,000 cells).

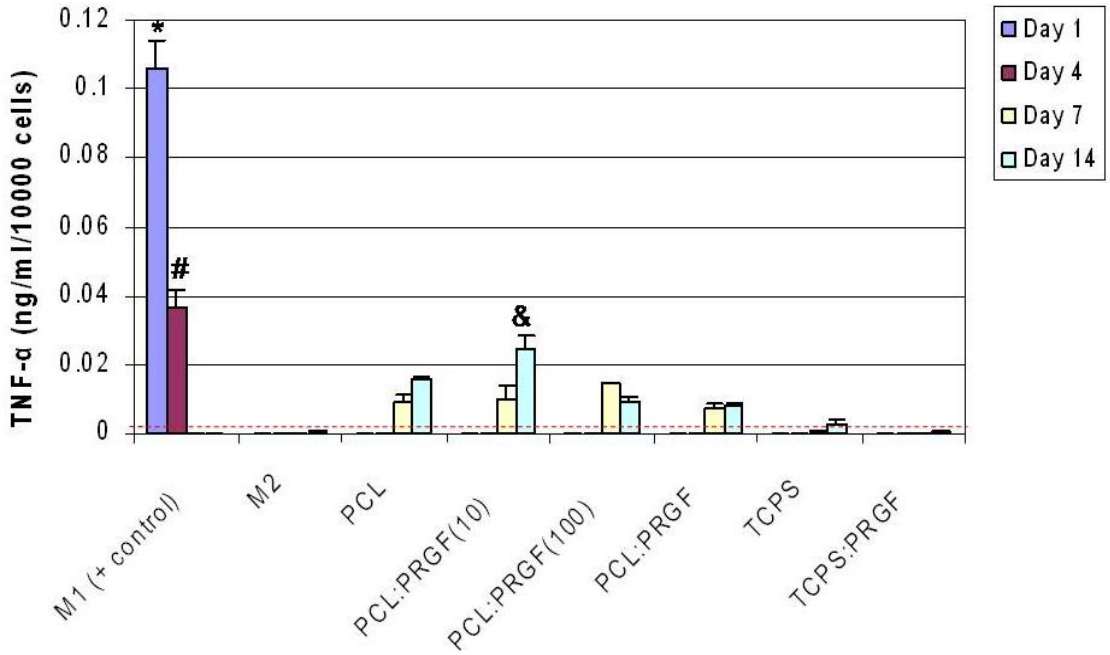

Figure 7.16(a). Macrophage TNF-α release when cultured on PCL and PRGF containing scaffolds, TCPS, and media supplemented with 1 mg/ml PRGF. Results are normalized to amount of TNF-α released (ng/ml) per 10,000 cells. *, #, & indicates significant differences, $p<0.05$, between all other scaffolds at days 1, 4 and 14 respectively. Minimum level of detection is 0.0025 ng/ml (red dashed line).

Figure 7.16(b) shows the results of TNF-α release from macrophages cultured on PRGF incorporated scaffolds with heparin. With the exception of PCL:PRGF(100) scaffolds with heparin, release of TNF-α from macrophages cultured on scaffolds was low at days 1-7, and increased by day 14. Release from cells cultured on TCPS and TCPS:PRGF with heparin appeared constant over the 14 days. Similar to IL-10, the

addition of heparin in different amounts did not appear to have a significant affect on TNF-α release between substrates. In comparing TNF-α levels from figure 7.16(a), the addition of heparin, in general, elicited a higher release of TNF-α over the 14 day time period. Based on the results shown, because IL-10 release decreased throughout the 14 days and TNF-α release increased throughout 14 days, heparin may be driving macrophages from the M2 phenotype towards the M1 phenotype.

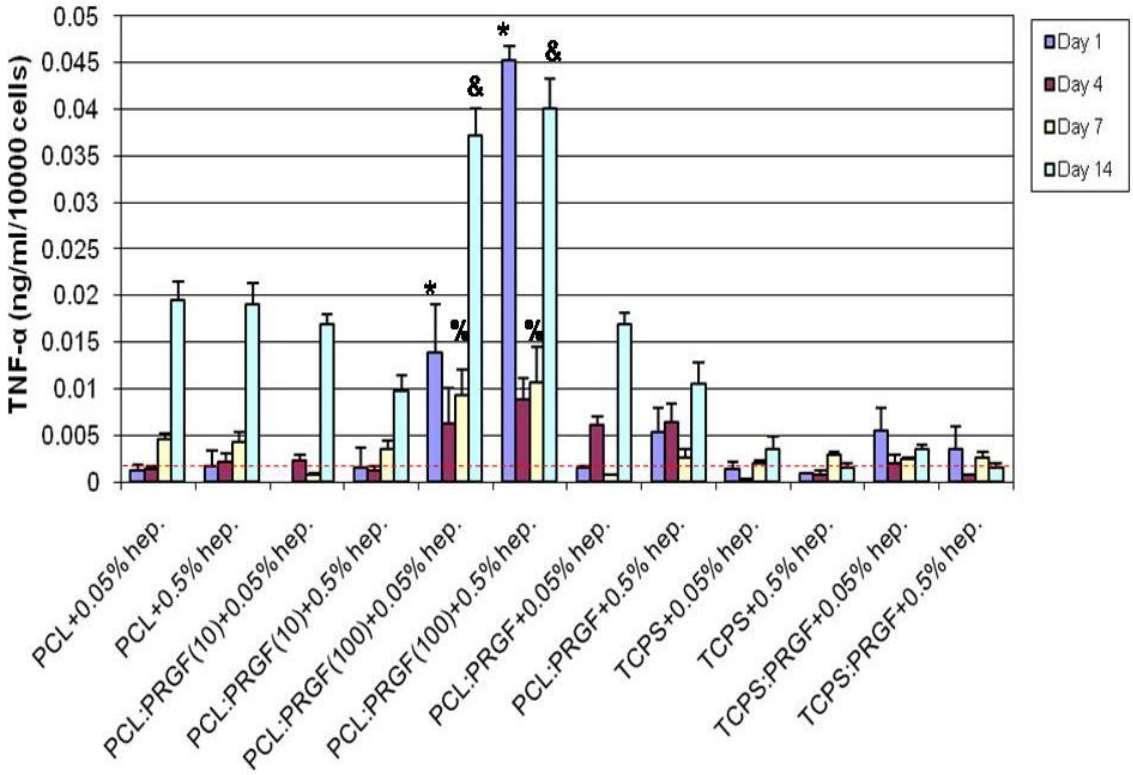

Figure 7.16(b). TNF-α release from macrophages when cultured on PRGF incorporated scaffolds, TCPS, and TCPS with 1 mg/ml PRGF with 0.05% or 0.5% heparin. * indicates statistically significant differences, $p<0.05$, compared to all other material groups at day 1. % indicates TNF-α release on scaffolds of PCL:PRGF(100)+0.05% and 0.5% heparin is significantly different ($p<0.05$) from that of other scaffolds at day 7 (but not each other). & indicates a significant difference, $p<0.05$, of TNF-α released compared to all other materials at day 14 (but not each other). Minimum level of detection is 0.0025 ng/ml (red dashed line).

EC Angiogenesis Bead Assay

To determine the ability of PRGF to induce HPMEC sprouting, an *in vitro* angiogenesis assay was performed. Figure 7.17 illustrates the images of HPMEC covered beads cultured in media with PRGF at different concentrations, with results of percentage of sproutage and sprout length shown in Figures 7.18. At day 1, there was minimal sprouting occurring for cells cultured in all PRGF concentrations, with no significant differences over media control for percentage of sprouts and length of sprouts. By day 4, there were more sprouts visible, as well as an increase in sprout length, however, no significant differences were observed for sprout length or percentage of sprouts. At day 6, in general, percentage of sprouts did not increase; however, sprout length did increase. HPMEC covered beads cultured in 1 mg/ml PRGF elicited a significantly higher percentage of sprouts, while HPMEC cultured in 5 mg/ml PRGF revealed a significantly higher length of sprouts, compared to that of media control. PRGF dissolved in media at high concentrations (10 mg/ml) started clotting over the 6 day time period, making sprouts difficult to visualize. This explains why there were no results obtained for percentage of sprouts and sprout length for HPMEC cultured in 10 mg/ml PRGF at day 6.

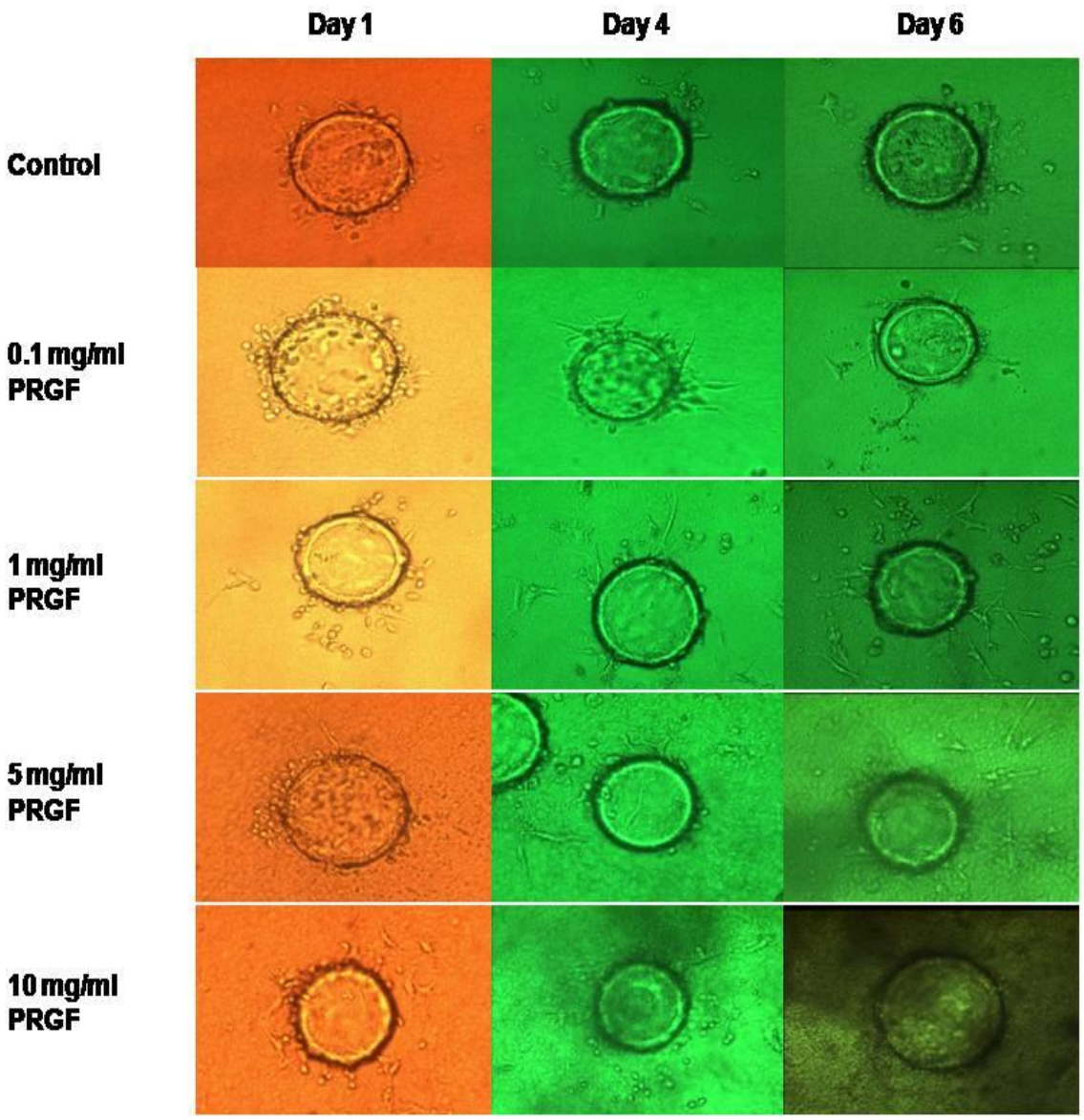

Figure 7.17. Sprout formation of HPMEC cultured in media with PRGF (0, 0.1, 1, 5, 10 mg/ml) at days 1, 4 and 6. Images taken at 20X.

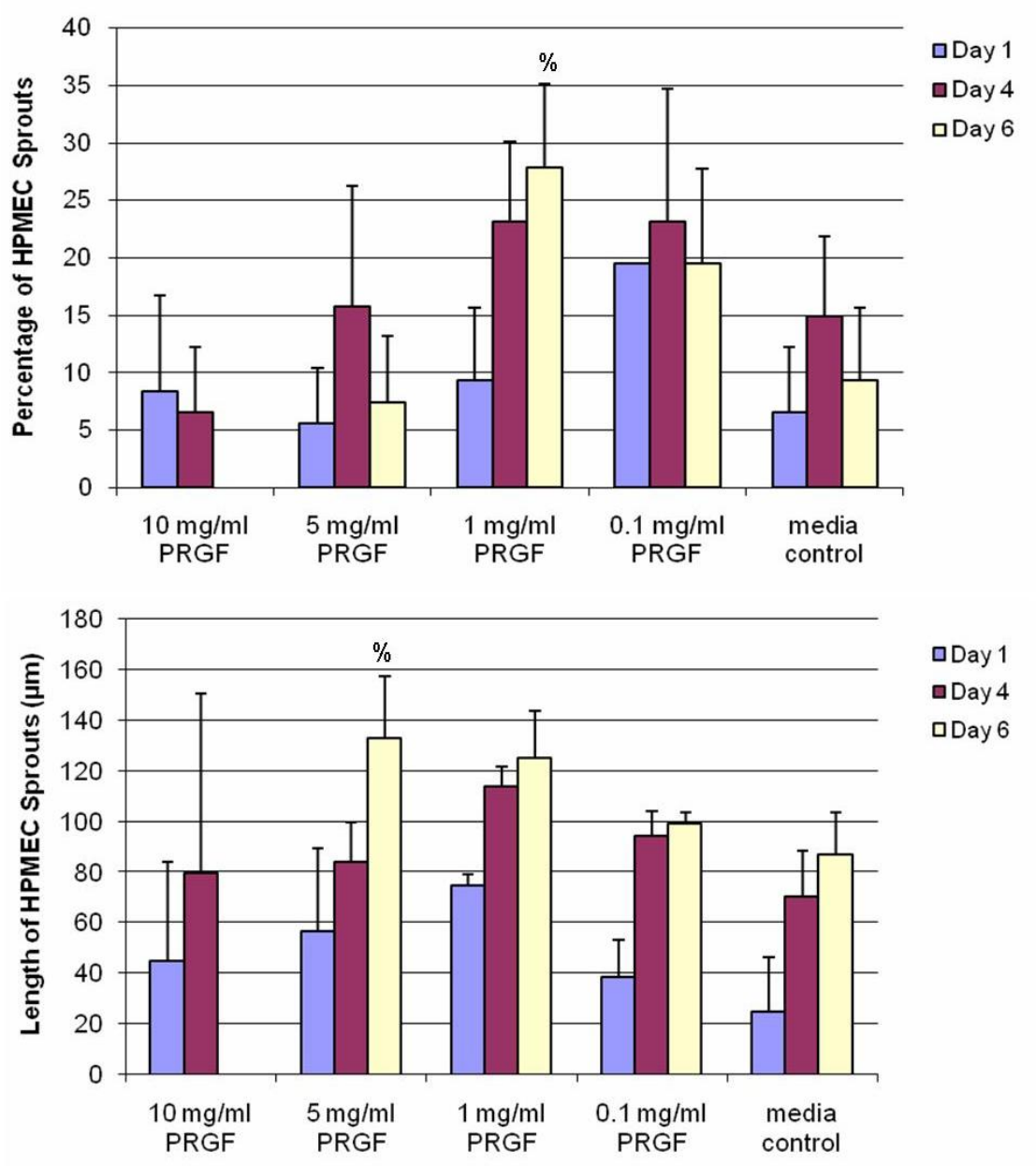

Figure 7.18. Results of percentage of HPMEC sprouts (Top) and length of HPMEC sprouts (Bottom) when cultured in different concentrations of PRGF in media over 6 days. % signifies statistically significant differences, $p<0.05$, at day 6 over media control.

Discussion

This study provided insight into the potential for PRGF and/or heparin to enhance the regenerative capacity of electrospun synthetic scaffolds. Cellular proliferation of

HPMEC and ADSC, migration of macrophages, and sprout formation by HPMEC confirmed that PRGF did enhance the bioactivity of the electrospun scaffolds. In addition, IL-10 release by macrophages, indicative of an M2 phenotype, was enhanced over time on PRGF incorporated scaffolds, indicating the potential for the bioresorbable vascular graft materials to stimulate a tissue restorative environment.

PRP has previously been used clinically, and has shown promising results in promoting regeneration and angiogenesis *in vitro*, as well as *in vivo*, although the mechanism behind the success of PRP in this regard has not yet been fully understood. Previous studies have shown that PRP can induce proliferation, chemotaxis and tube formation in pro-regenerative cell types (mesenchymal stem cells, bone marrow stromal stem cells, ECs, SMCs, ADSCs) [354, 387, 388], and enhance the release of pro-angiogenic growth factors in inflammatory cell types (macrophages). Additionally, specific components within PRP (LXA_4 and RANTES) have been shown to drive macrophages to towards the pro-regenerative phenotype [313]. In a murine model of hind limb ischemia, PRP improved perfusion and neovascularization, providing evidence for its benefit *in vivo* [337]. The use of heparin has been previously investigated as a way to reduce the thrombogenicity of the graft surface and as a way to regulate EC and SMC proliferation. Studies have shown heparin does prevent coagulation build-up from occurring on graft surfaces, as well as a reduction of intimal hyperplasia at the anastomoses of the graft [343, 389, 390]. In addition, binding of heparin to various growth factors has been reported to protect growth factors from inactivation, thereby maintaining their biological activity. Conclusions from the literature demonstrate the use of PRGF, and/or heparin, may be beneficial for vascular graft applications, as it may lead

to graft vascularization in a more timely manner while reducing the risk of thrombosus formation or intimal hyperplasia.

Macrophage and HPMEC chemotaxis was significantly increased when PRGF was dissolved in media at certain concentrations; however, electrospun PRGF incorporated scaffolds did not elicit a chemotactic response over PCL control scaffolds. These results were most likely due to the duration of the experiment, as well as lack of nutrients available to the macrophages in the Transwells, and not the effect of the PRGF. For HPMECs specifically, chemotaxis may have been hindered because of the TGF-β present in the scaffolds. Much like EC proliferation, it has also been previously reported that TGF-β1 has an inhibitory effect on EC migration at certain concentrations in assays such as the Boyden chamber assay [381]. One way to verify this observation would be to add an anti-human TGF-β1 antibody to the EC media, which would specifically block the TGF-β1 in the PRGF containing scaffolds. An increase in HPMEC proliferation and chemotaxis when cultured on PRGF incorporated scaffolds would prove this theory. The results obtained in this study of HPMEC migration towards PRGF in media seem questionable, and requires further investigation to determine the true chemotactic effect of PRGF on HPMECs.

Macrophage proliferation was not affected by the addition of PRGF, both dissolved in media and incorporated into scaffolds, which is not seen as necessarily a negative outcome; during wound healing, macrophages are a critical cell type needed for regeneration; however, too many macrophages could result in a pro-inflammatory environment and hinder regeneration. Heparin did hinder the migration of macrophages at both concentrations (0.05% and 0.5%) over the 72 hours. This same phenomenon has

been observed in *in vivo* settings as well; heparin coated xenografts implanted in rabbits elicited less macrophage infiltration and proliferation, and subsequently, a reduction in intimal hyperplasia, than the nonheparin-coated grafts up to 3 weeks. This inhibitory effect of heparin on macrophage infiltration and proliferation, and succeeding release of MCP-1, at early time points was predicted to be one of the main reasons behind the decrease in intimal hyperplasia that was observed [390].

The present study demonstrated PRGF does enhance the proliferation of HPMEC when dissolved in media at certain concentrations, but not when incorporated into electrospun scaffolds, most likely due to the activated TGF-β being released from the PRGF incorporated scaffolds. The addition of heparin in different amounts to electrospun PCL and PRGF incorporated scaffolds did not have a consistent effect on HPMEC proliferation overtime. Conclusions stated in the literature vary as well, indicating the mechanism by which heparin affects HPMEC proliferation remains to be elucidated.

Although the hindrance of HPMEC proliferation by PRGF incorporated scaffolds may be looked at as a negative, their proliferative response to conditioned media from macrophages cultured on PRGF incorporated scaffolds proves these constructs may be beneficial in promoting regeneration, and may even serve as a better illustration of what would occur *in vivo*. HPMEC proliferation was not enhanced over the 7 days when cultured in conditioned media from scaffolds containing PRGF, however, in the presence of macrophages, their proliferation was enhanced. The fact that HPMEC proliferation resulted in very different outcomes when cultured in conditioned media with and without macrophages makes it clear that HPMEC proliferation was affected the interaction of macrophages with PRGF containing scaffolds.

In contrast to results seen for HPMEC cultured in conditioned media with and without macrophages, ADSC proliferation was enhanced over 7 days when cultured in conditioned media from scaffolds containing PRGF versus those not containing PRGF in the presence and absence of macrophages. The existence of several growth factors within PRGF, and those that were detected from the electrospun constructs, known to induce cell proliferation (VEGF, PDGF, IGF, FGF, and EGF, etc.) is most likely the reason for enhanced proliferation [302]. Like HPMEC proliferation, ADSC proliferation was different throughout the 7 days depending on the inclusion or exclusion of macrophages, alluding to the fact that ADSC proliferation was also affected by the interaction of macrophages with PRGF containing scaffolds. It is evident from this study that macrophage number is not the most critical factor in HPMEC and ADSC proliferation; however, the specific mechanism by which macrophage interaction with the scaffolds affects HPMEC and ADSC proliferation still remains to be explained. The authors hypothesize that the HPMEC and ADSC proliferation seen in this study might be due, in part, to the various growth factors and cytokines secreted by the macrophages. It has been shown previously that macrophages cultured on electrospun scaffolds have the ability to produce high levels of VEGF and FGF [150], and in the presence of PRGF, produce additional pro-angiogenic growth factors and cytokines, including those which enhance cell proliferation [313]. Additional experiments, whereby specific growth factor and cytokine ELISAs are performed on supernatant from macrophages cultured on PRGF incorporated scaffolds, would be valuable to validate this explanation. Although ADSC proliferation appeared to stop by day 7 when cultured in macrophage conditioned media, this was not perceived as a negative effect brought about by the presence of PRGF, rather

most likely due to media mismatch and/or harmful factors produced during macrophage apoptosis induced by a lack of nutrient supply in the conditioned media [386].

Cellular migration and penetration was enhanced in scaffolds containing high amounts of PRGF by both HPMEC and ADSC. While historically the ability for cells to migrate into a synthetic electrospun structure has been viewed as a challenge, and one of the major downfalls of standard blood vessel replacements [297-299], the inclusion of PRGF yielded structures that were readily infiltrated. The specific reason for this rapid infiltration is not yet fully understood, and will need further examination. The presence of an array of chemotactic proteins found in large quantities in PRP may be the most logical explanation [337, 388]. It may also be an affect of the change in scaffold mechanical properties; as shown in Chapter 6, scaffolds with higher PRGF content exhibited decreased mechanical properties which may have allowed for cellular migration into the scaffold to occur more readily. The presence of PRGF fibers intermingled amongst the polymer fibers of the scaffolds, particularly in the case of PCL:PRGF structures, may have also provided paths of easy entry into the thicknesses of the structures. These fibers of varying diameter had an apparent impact on the porosity of the scaffolds, and as verified in Chapter 6, void space within the scaffold increased as PRGF concentration increased.

This enhanced cellular infiltration, regardless of its root cause, may allow for a vascular graft to be more rapidly remodeled with native collagen extracellular matrix; the production of which would readily supplement the strength of the scaffolds and encourage incorporation into surrounding tissues. Although not investigated in this study, the many factors found in PRGF have been proven to increase collagen matrix production

in a number of cell types [302, 309, 350, 391]. TGF-β, one such well-known matrix production-related growth factor, was released by the electrospun scaffolds in detectable quantities (shown in Chapter 6), in some cases for up to 21 days. Should the presence of TGF-β and the other matrix production enhancing growth factors be actively taken up by the cells, it would be possible for accelerated matrix production to occur, and could therefore improve the mechanical strength of the weakened PRGF containing scaffolds. Specific ECM protein ELISAs, or assays, such as Sircol™ or hydroxyproline, would be interesting to complete after culturing matrix-producing cells on PRGF incorporated scaffolds, as this may provide insight into matrix production.

Macrophage phenotype, as analyzed by chemokine release, was found to be influenced by PRGF incorporated scaffolds, both with and without heparin. IL-10, a chemokine released mainly by M2s, was secreted by macrophages cultured on all scaffolds, increasing over time on PCL and PRGF heparin-free scaffolds, and decreasing over time on scaffolds containing heparin. Alternatively, TNF-α, a chemokine mainly secreted by pro-inflammatory (M1) macrophages, was not detectable in the early stages of the experiment, and only increased slightly by day 14. Regardless, TNF-α release by macrophages cultured on electrospun scaffolds and TCPS was 2 – 5 times less than that of the positive M1 control. Heparin containing scaffolds elicited a TNF-α release that increased over time. RANTES, a mediator of inflammatory process, was detected in PRGF containing scaffolds, and may play a role in shifting macrophages towards this pro-regenerative phenotype. In addition, although LXA_4 was not detectable by ELISAs from PRGF incorporated scaffolds, this resolving factor has also been shown to drive macrophages towards a tissue restorative phenotype [313, 392]. These results provide a

positive insight for PRGF incorporated scaffolds to be used in vascular graft applications. As macrophages will be one of the first cell types to the scene, their behavior during their interaction with these scaffolds is of utmost importance. The fact that these scaffolds do not enhance macrophage proliferation, but do promote macrophage chemotaxis and secretion of chemokines associated with the pro-regenerative macrophage is extremely beneficial in setting the stage to allow other pro-angiogenic cells to arrive to the graft site. Using specific phenotypic markers would allow for a more definitive analysis on quantifying macrophage phenotype when cultured on PRGF incorporated scaffolds. This can be done by immunohistochemically staining samples with a pan macrophage marker (CD68), an M1 phenotype marker (CCR7), or an M2 phenotype marker (CD163) and counting the number of immunopositive cells in each sample.

PRGF dissolved in media at specific concentrations also enhanced sprout development and sprout length by HPMEC within 4 days. This rapid sprout formation in the presence of PRGF is in agreement with results obtained in previously published studies, and may be due to the pro-angiogenic chemokines and growth factors that were detected in PRGF in this study, as well as others [393]. Although PRGF induced increased sprout formation by HPMECs over media control, the ability of these cells to form sprouts in control media could be due to the FBS and ECGS supplemented to the media. It would be interesting to replicate this experiment with ECs cultured in media without FBS or ECGS, as this would give a better depiction of the effect of PRGF alone. In addition, an experiment that would give a better representation of what may occur *in vivo* would be to analyze HPMEC sprout and lumen formation in the presence of other cells, such as fibroblasts and SMCs. Regardless, as the regeneration, and thus, success, of

an implanted bioresorbable vascular graft relies substantially on the ability of the graft to become vascularized by cells, the fact that PRGF induces sprout formation by HPMEC sheds a positive light on the potential for these scaffolds to be regenerated when used in vascular graft applications.

In looking at the release kinetics of growth factors from scaffolds reported in Chapter 6 and their effect on cell proliferation and sprout formation, it can be concluded that growth factor release may have a delayed effect on cell proliferation/sprout formation. There was a burst release of growth factors at day 1, and a tapering of this release thereafter, while cell proliferation, migration and sprout formation was not induced from PRGF and PRGF incorporated scaffolds until day 4. It appears there may be a delay in activity by cells in response to the growth factors being released.

Another important point to note is that electrospinning may alter the molecular structures of the different components in PRP, thereby effecting growth factor bioactivity. As it was briefly mentioned previously, TGF-β was only detectable in PRGF and PRP after performing an acid activation technique, while TGF-β was detectable in electrospun constructs without the activation. While this TGF-β ELISA was the only one to specifically detect a change in molecular structure after electrospinning, there are most likely other growth factors that undergo a change during the electrospinning process that may not have been detected by the ELISAs. This observation may also explain the differences seen in cell behavior when cultured with PRGF versus electrospun constructs. Further analysis of the components contained with electrospun PRGF incorporated scaffolds, PRP and PRGF, may confirm this explanation. By performing gel

electrophoresis, similar to what was done in Chapter 5, or a similar technique, this task could be accomplished.

In conclusion, the hypothesis stated at the beginning of this chapter for this study was proven. PRGF does positively influence the proliferation and sprout formation of HPMEC, as well as chemotaxis of macrophages at specific concentrations *in vitro*. HPMEC and ADSC migration into the electrospun constructs was enhanced, and although the addition of PRGF into the constructs may have been one reason for this outcome, PRGF cannot take full credit. As mentioned previously, increased pore area and decreased mechanical strength most likely lead to an increase in cell infiltration as well. The PRGF incorporated scaffolds promoted the release of regenerative chemokines from macrophages, illustrating their potential to encourage a pro-regenerative environment. As one of the major advantages of PRP, when used clinically, is its ability to deliver a milieu of growth factors and cytokines at the patients' bedside, the creation of an off-the-shelf electrospun vascular graft incorporating PRGF from pooled allogenic blood may have the same benefits. While the use of pooled blood is typically frowned upon in the United States, the use of allogenic PRP has been gaining popularity in a number of European studies with no mention of adverse immune reactions [394-396]. These studies illustrate PRGF incorporated scaffolds do have the potential to be used in vascular graft applications, however, future studies are needed to determine their ability to promote angiogenesis and become regenerated *in situ*.

Acknowledgement

The authors would like to thank Anatomic Pathology Research Services in the Department of Pathology at Virginia Commonwealth University for histological staining as well as Dr. C.J. Kirkpatrick from Johannes Gutenberg University Institute of Pathology for the generous donation of human pulmonary microvascular endothelial cells.

Chapter 8: Conclusions and Future Research

The creation of an ideal bioresorbable vascular graft has been sought after for over 50 years, however, the original Dacron and e-PTFE vascular grafts that were first used clinically are still the clinical standard. In small-diameter applications, this graft fails to perform optimally, illustrating the critical need for an improved vascular graft design. The ability for a tissue engineering scaffold to become completely regenerated is a daunting task, as it requires constructive interaction between the implant and host tissue in a timely manner. The graft material needs to be able to provide the complex and interrelated chemical, physical, and biological cues that are needed to affect remodeling.

Electrospinning is a popular fabrication method that has been used to create vascular graft conduits, as it has the ability to consistently produce nanofibrous constructs that mimic the native ECM. Furthermore, electrospinning is very versatile, and gives the tissue engineer the ability to alter a wide variety of scaffold properties, including the material make-up (natural versus synthetic polymers), mechanical strength, fiber diameter, pore area, material biocompatibility, etc. Although electrospinning has been used extensively in the design of vascular grafts, one of the main criticisms is the scaffold's inability to allow for cellular penetration, and hence, graft regeneration, while maintaining structural integrity throughout the remodeling phase. In this study we investigated different ways to alter the mechanical, biological, and regenerative

characteristics of an electrospun scaffold with the intention of creating an acellular bioresorbable vascular graft that would have the ability to become completely remodeled and develop into a fully functioning artery.

The first approach was to design a new copolymer whose mechanical and thermal properties could be altered to achieve those characteristics desireable for a vascular graft implant. DX and DL-3-MeDX were synthesized and copolymerized in different ratios and electrospun for the first time, forming nanofibrous scaffolds of different fiber diameters. Characterization of scaffold mechanical and thermal properties determined that fiber diameter and mechanical performance increased with increasing polymer concentration, polymer masses, and crystallinity. More specifically, increasing DL-3-MeDX content resulted in decreased peak stress, strain at break, and toughness, as well as melting and crystallization temperatures. Nevertheless, the mechanical properties of many of the electrospun scaffolds of DX:DL-3-MeDX at different ratios did fall within the range of mechanical properties of the native femoral artery. While this comparison does not necessarily predict whether these materials would have mechanical properties conducive for a small diameter vascular graft, it does give some insight into the strength and elasticity of the materials compared to native tissue. Further mechanical testing, such as burst strength and compliance would need to be done and compared to that of a small diameter coronary artery to really determine if the mechanical properties are sufficient. Additionally, because DX is comprised of PDO, these scaffolds exhibit rebound and kink resistance, another benefit in vascular graft design. The crystallinity of the copolymers was shown to change with different MeDX content as well, which would allow for controlled biodegradability and would be useful in growth factor delivery applications.

The creation of these novel electrospun copolymer scaffolds proved to have mechanical and thermal properties that could be conducive for vascular graft applications; however, the bioactivity and biocompatibility of these materials were not investigated in this study, and would need to be in the future before using these materials in vascular graft applications.

Following this, scaffolds were created from natural and synthetic polymers electrospun individually, or blended, and their potential to be used as vascular graft materials without an enhanced risk of failure from an acute thrombotic occlusion was investigated. Tissue factor expression by monocytes cultured on PDO, PCL, and PCL:silk scaffolds was quantified and compared to that of e-PTFE. Silk scaffolds resulted in the lowest amount of TF expression by monocytes, while PDO elicited the highest amount of TF expression. Expression of TF on electrospun scaffolds was lower, or as much as TF expression from monocytes cultured on e-PTFE. This study provided a positive insight for the ability of electrospun grafts of PDO, PCL, silk, or PCL:silk to be successfully used in tissue engineering applications without an increased risk of failure due to an acute thrombotic occlusion when compared to that of the standard e-PTFE graft. While this is a very important aspect to investigate for vascular graft implants, the experiments performed in this study do not clearly answer whether these electrospun scaffolds would or would not elicit the formation of an acute thrombosus, and therefore, future testing would need to be completed to confirm this.

Electrospun scaffolds were also created out of aPRP, a naturally occurring blood component, as a way to provide a sustained release of physiological proteins known to improve healing and regeneration and enhance overall scaffold bioactivity. Human PRP

was activated, lyophilized to form PRGF and electrospun for the first time to produce scaffolds which consisted of nano- to micron sized fibers. These scaffolds were stable for an extended period of time *in vitro*, which was found to be mainly because of the fibrinogen backbone, and exhibited a sustained release of proteins for up to 35 days. Additionally, these electrospun PRGF scaffolds promoted cellular infiltration within just 3 days. The presence of a variety of growth factors and chemokines inherent to PRP proved to enhance the bioactivity of the scaffolds, even after being dissolved in a harsh organic solvent and exposed to high voltages during the electrospinning process. These scaffolds could be beneficial if used in vascular graft applications, as the release of growth factors in PRP would most likely encourage wound healing and regeneration, however, to achieve the mechanical strength needed for a vascular graft they would need to be blended with synthetic polymers. Mechanical testing was not performed on pure PRGF constructs due to the fragility of the scaffolds after electrospinning.

Finally, incorporating PRP at different concentrations into electrospun scaffolds comprised of PCL was investigated as a way to enhance scaffold bioactivity while providing sufficient mechanical stability required of a blood vessel replacement. Heparin was also added to the scaffolds as a dual purpose: to reduce the thrombogenicity of the graft surface and to modulate the release of growth factors in PRP. Mechanical testing of these scaffolds proved that even with the addition of PRGF and heparin, with the exception of 100 mg/ml, these scaffolds have mechanical properties that are conducive to those needed for a vascular graft. A variety of growth factors known to be in PRP, including RANTES, PDGF-BB, TGF-β, were successfully detected to be released from the electrospun constructs, however, their molecular composition may undergo a change

during the electrospinning process. Additionally, VEGF, SDF-1α, and LXA_4 were detected when PRGF was dissolved in PBS. The release of these growth factors was shown to have an impact on cellular infiltration into the scaffolds by HPMEC and ADSC in as little as 7 to 14 days. Conditioned media from macrophages after being cultured on these scaffolds also proved to enhance HPMEC and ADSC proliferation. PRGF was also chemotactic towards macrophages at certain concentrations, and stimulated sprout formation by HPMEC, promoting an increase in number and length of sprouts over media controls in just 6 days. Evaluation of macrophage phenotype showed scaffolds without heparin drove macrophages towards a pro-regenerative type, while scaffolds with heparin elicited a change in macrophage phenotype, from pro-regenerative to pro-inflammatory over time. All in all, these scaffolds, specifically those of PCL:PRGF, have proven they could be used as a bioresorbable vascular graft, and would allow for cellular infiltration, sprout formation, and remodeling, while retaining mechanical strength over time.

The results of this study highlight some of the ways that electrospinning can be used to tailor the properties of scaffolds for vascular graft applications. Through simple solutions, like electrospinning natural and synthetic polymers with different mechanical and thermal characteristics, to adding bioactive factors, the requirements needed for the design of a successful vascular graft can be achieved. In considering one specific scaffold for use as a vascular graft, the PCL:PRGF scaffold may be the most successful. Mechanical properties were conducive to that of a vascular graft, endotoxin levels were not elevated above standard limits, release of regenerative and pro-angiogenic growth factors were detectable, cell infiltration was promoted, and macrophages exhibited enhanced release of regenerative chemokines. While these results do shed a positive light

on PCL:PRGF scaffolds and their use as a vascular graft, numerous other factors that were not addressed in this study may prove otherwise and should be considered. First, these grafts will be fabricated for use predominantly in elderly people. While mechanical properties were tested in this study, and were shown to be comparable to that of a femoral artery, the mechanical properties of the coronary arteries of the elderly is not only going to be different from that of a femoral artery, but is also going to vastly differ from one elderly person to the next. Some may be extremely fragile, while others may be hardened. Therefore, it is almost impossible to say what the ideal mechanical properties should be for a vascular graft, and if the properties observed in this study would suffice. This may possibly be one of the greatest roadblocks in the design of a vascular graft, and one limitation of the current vascular grafts used. How do we design an off-the-shelf product with mechanical properties that are adequate for each individual person? Although it may seem feasible to fabricate an electrospun vascular graft bedside, while a patient is undergoing surgery, to suit an individual's mechanical needs, this thought is not very realistic. Furthermore, cellular behavior in elderly patients is much different from that of the cells used in these *in vitro* experiments, and also from that of the young animal models frequently used in *in vivo* experiments. Another limitation of the current treatments is the lack of bioactivity and inability for cells to infiltrate the materials. While PCL:PRGF scaffolds do show enhanced bioactivity and cell infiltration, it may be more beneficial to conduct these cell experiments in harsh conditions for the cells (i.e. without FBS and ECGS), or with aged cells and/or animals. Overall, the addition of PRGF to an electrospun PCL scaffold does appear promising for use as a bioresorbable vascular graft, however, additional considerations and testing still remains to be done.

Future Research

Future work in this study will involve further investigation of the angiogenic potential of incorporated PRP and heparin scaffolds. The results obtained this study regarding HPMEC proliferation and macrophage chemokine release on heparin incorporated PRGF scaffolds did not provide definitive answers as to the effect of these scaffolds on promoting proliferation and driving macrophages towards a specific phenotype. Therefore, additional studies are needed to clarify these results. In regards to HPMEC proliferation, the addition of an anti-human TGF-β1 antibody to the EC media would specifically block the TGF-β1 in the PRGF containing scaffolds, and would provide an answer behind why PRGF incorporated scaffolds decrease HPMEC proliferation. Using specific phenotypic markers would allow for a more definitive analysis on quantifying macrophage phenotype when cultured on PRGF incorporated scaffolds. This could be done by immunohistochemically staining samples with a pan macrophage marker (CD68), an M1 phenotype marker (CCR7), or an M2 phenotype marker (CD163) and counting the number of immunopositive cells in each sample. Furthermore, as mentioned in the discussion section of Chapter 7, performing specific growth factor and cytokine ELISAs on supernatant from macrophages cultured on PRGF incorporated scaffolds would give insight into the growth factors secreted by macrophages during their interaction with PRGF containing scaffolds and may verify the results observed for HPMEC and ADSC proliferation.

Additionally, a more in depth look into these scaffolds' mechanical properties is needed. In addition to uniaxial tensile testing, burst strength and compliance testing should be performed, as these tests would provide insight in the ability of these grafts to

withstand physiological pressures. Also, mechanical properties of the grafts after being seeded with different cell types would be interesting to observe; macrophages may degrade the scaffold over time, and decrease the mechanical integrity of the constructs, while ECs and FBs may produce their own matrix, thereby enhancing the mechanical strength of the scaffolds. Quantification of matrix production by specific cell types cultured on PRGF incorporated scaffolds would also be of interest. As mentioned previously, specific ECM protein ELISAs, or assays, such as SircolTM or hydroxyproline, could be performed to determine matrix production.

Furthermore, while the preliminary work contained within demonstrated PRGF and heparin containing materials have the potential to promote sprout formation *in vitro*, the ability for PRGF to induce angiogenesis and regeneration *in vitro* is important. As mentioned previously, it would be interesting to replicate this experiment with ECs cultured in media without FBS or ECGS, as this would give a better depiction of the effect of PRGF alone. In addition, analyzation of HPMEC sprout and lumen formation in the presence of other cells, such as fibroblasts and SMCs would give a better depiction of what may occur *in vivo*.

The potential for these grafts to induce angiogenesis and regeneration needs to be evaluated *in vivo*. Implanting these materials subcutaneously into mice would help to examine the inflammatory responses and degradation behavior these scaffolds may elicit, as well as the ability for these constructs to promote vascularization *in vivo*. In addition, *in vivo* experiments, for example implanting the graft in the abdominal aorta of a rat, would be able to determine the scaffolds' true ability to be regenerated, as there would be multiple cell types working together, along with a variety of other molecules, growth

factors, and chemokines in the microenvironment that would play a role. Finally, the potential for these scaffolds to promote angiogenesis and regeneration *in situ* in a canine model needs to be investigated, as this would provide the most accurate results of what would happen if these graft materials were to be implanted in humans as blood vessel replacements.

Literature Cited

1. **Heineken, F.G. and R. Skalak, *Tissue engineering: A brief overview.* J Biomech Eng, 1991. 113: p. 111.**
2. **Langer, R., *Editorial: Tissue Engineering: Perspectives, Challenges, and Future Directions.* Tissue Engineering, 2007. 13(1): p. 1.**
3. **Langer, R. and J.P. Vacanti, *Tissue engineering.* Science, 1993. 260(5110): p. 920-926.**
4. **Palsson, B.O., and Sangeeta N. Bhatia, *Tissue Engineering*. 2004, Upper Sadle River, New Jersey: Pearson Prentice Hall.**
5. **Barnes, C.P., et al., *Nanofiber technology: Designing the next generation of tissue engineering scaffolds.* Advanced Drug Delivery Reviews, 2007. 59: p. 1413-1433.**
6. **Weigel, T., G. Schinkel, and A. Lendlein, *Design and preparation of polymeric scaffolds for tissue engineering.* Expert Reviews in Medical Devices, 2006. 3(6): p. 835-851.**
7. **Farach-Carson, M.C., R.C. Wagner, and K.L. Kiick, *Extracellular matrix: Structure, function, and applications to tissue engineering*, in *Tissue Engineering*, J.P. Fisher, A.G. Mikos, and J.D. Bronzino, Editors. 2007, CRC Press: Boca Raton, FL. p. 3-1 - 3-22.**
8. **Vacanti, J.P. and C.A. Vacanti, *The challenge of tissue engineering*, in *Principles of Tissue Engineering*, R. Lanza, R. Langer, and W. Chick, Editors. 1997, Academic Press: San Diego. p. 1-5.**
9. **Yoon, D.M. and J.P. Fisher, *Polymeric scaffolds for tissue engineering applications*, in *Tissue Engineering*, J.P. Fisher, A.G. Mikos, and J.D. Bronzino, Editors. 2007, CRC Press: Boca Raton, FL. p. 8-1 - 8-18.**
10. **Simpson, D.G. and G.L. Bowlin, *Tissue-engineering scaffolds: can we re-engineer mother nature?* Expert Rev Med Devices, 2006. 3(1): p. 9-15.**
11. **Huang, J.I., J.U. Yoo, and V.M. Goldberg, *Orthopedic applications of stem cells*, in *Essentials of Stem Cell Biology*, R. Lanza, et al., Editors. 2006, Elsevier Academic Press: Burlington, MA. p. 449-456.**
12. **Chamberlain, G., et al., *Concise Review: Mesenchymal stem cells: Their phenotype, differentiation capacity, immunological features, and potential for homing.* Stem Cells, 2007. 25: p. 2739-2749.**
13. **Bell, E., *Tissue engineering: a perspective.* J Cell Biochem, 1991. 45(3): p. 239-41.**
14. **Vacanti, J.P., et al., *Selective cell transplantation using bioabsorbable artificial polymers as matrices.* J Pediatr Surg, 1988. 23(1 Pt 2): p. 3-9.**

15. Martins-Green, M., *The Dynamics of Cell-ECM Interactions with Implications for Tissue Engineering*, in *Principles of Tissue Engineering*, R. Lanza, Robert Langer, and William Chick, Editor. 1997, R. G. Landes Company. p. 23-46.
16. Boland, E.D., P.G. Espy, and G.L. Bowlin, *Tissue engineering scaffolds*, in *Encyclopedia of Biomaterials and Biomedical Engineering*, G. Wnek, Bowlin G, Editor. 2004, Marcel Dekker, Inc.: New York. p. 1-9.
17. Agrawal, C.M. and R.B. Ray, *Biodegradable polymeric scaffolds for musculoskeletal tissue engineering.* Journal of Biomedical Materials Research, 2001. 55(2): p. 141-150.
18. Zong, X., et al., *Electrospun fine-textured scaffolds for heart tissue constructs.* Biomaterials, 2005. 26: p. 5330-5338.
19. Matthews, J.A., David G. Simpson, Gary E. Wnek, and Gary L. Bowlin, *Electrospinning of collagen nanofibers.* Biomacromolecules, 2002. 3: p. 232-238.
20. Sell, S.A., et al., *Electrospun polydioxanone-elastin blends: potential for bioresorbable vascular grafts.* Biomed Mater, 2006. 1(2): p. 72-80.
21. Wnek, G.E., et al., *Electrospinning of nanofiber fibrinogen structures.* Nano Letters, 2003. 3(2): p. 213-216.
22. Altman, G.H., et al., *Silk-based biomaterials.* Biomaterials, 2003. 24: p. 401-416.
23. Mooney, D.J., and Robert S. Langer, *Engineering Biomaterials for Tissue Engineering: The 10 - 100 Micron Size Scale*, in *Tissue Engineering*, B. Palsson, Jeffrey A. Hubbell, Robert Plonsey, and Joseph D. Bronzino, Editor. 2000, CRC Press.
24. Norman, J.J. and T.A. Desai, *Methods for fabrication of nanoscale topography for tissue engineering scaffolds.* Annals of Biomedical Engineering, 2006. 34(1): p. 89-101.
25. Zong, X., Harold Bien, Chiung-Yin Chung, Lihong Yin, Dufei Fang, Benjamin S. Hsiao, Benjamin Chu, and Emilia Entcheva, *Electrospun fine-textured scaffolds for heart tissue constructs.* Biomaterials, 2005. 26: p. 5330-5338.
26. Venugopal, J., and S. Ramakrishna, *Applications of Polymer Nanofibers in Biomedicine and Biotechnology.* Applied Biochemistry and Biotechnology, 2005. 125: p. 147-157.
27. Berry, C.C., Gordon Campbell, Antonio Spadiccino, Mary Robertson, Adam S.G. Curtis, *The influence of microscale topography on fibroblast attachment and motility.* Biomaterials, 2004. 25: p. 5781-5788.
28. Telemeco, T.A., C. Ayres, G. L. Bowlin, G. E. Wnek, E. D. Boland, N. Cohen, C. M. Baumgarten, J. Matthews, and D. G. Simpson, *Regulation of cellular infiltration into tissue engineering scaffolds composed of submicron diameter fibrils produced by electrospinning.* Acta Biomaterialia, 2005. 1(4): p. 377-385.
29. Levesque, S.G., Ryan M. Lim, and Molly S. Shoichet, *Macroporous interconnected dextran scaffolds of controlled porosity for tissue-engineering applications.* Biomaterials, 2005. 26: p. 7436-7446.

30. **Karande, T.S., Joo L. Ong, and C. Mauli Agrawal, *Diffusion in Musculoskeletal Tissue Engineering Scaffolds: Design Issues Related to Porosity, Permeability, Architecture, and Nutrient Mixing.* Annals of Biomedical Engineering, 2004. 32(12): p. 1728-1743.**
31. **Li, S., Joost R. De Wijn, Jiaping Li, Pierre Layrolle, and Klaas De Groot, *Macroporous Biphasic Calcium Phosphate Scaffold with High Permeability/Porosity Ratio.* Tissue Engineering, 2003. 9(3): p. 535-548.**
32. **Kannan, R.Y., Henryk J. Salacinski, Kevin Sales, Peter Butler, and Alexander M. Seifalian, *The roles of tissue engineering and vascularisation in the development of micro-vascular networks: a review.* Biomaterials, 2005. 26: p. 1857-1875.**
33. **Griffith, C.K., Cheryl Miller, Richard C. A. Sainson, Jay W. Calvert, Noo Li Jeon, Christopher C. W. Hughes, and Steven C. George, *Diffusion Limits of an in Vitro Thick Prevascularized Scaffold.* Tissue Engineering, 2005. 11(1/2): p. 257-266.**
34. **Sander, E.A., and Eric A. Nauman, *Permeability of Musculoskeletal Tissues and Scaffolding Materials: Experimental Results and Theoretical Predictions.* Critical Reviews in Biomedical Engineering, 2003. 31(1): p. 1-26.**
35. **Badylak, S., T. Gilbert, and J. Myers-Irvin, *The extracellular matrix as a biologic scaffold for tissue enigneering*, in *Tissue Engineering*, C. van Blitterswijk, et al., Editors. 2008, Academic Press: London. p. 121-143.**
36. **Weinberg, C.B. and E. Bell, *A blood vessel model constructed from collagen and cultured vascular cells.* Science, 1986. 231(4736): p. 397-400.**
37. **Rosamond, W., et al., *Heart disease and stroke statistics--2008 update: a report from the American Heart Association Statistics Committee and Stroke Statistics Subcommittee.* Circulation, 2008. 117(4): p. e25-146.**
38. **Boland, E.D., et al., *Electrospinning collagen and elastin: preliminary vascular tissue engineering.* Frontiers in Bioscience, 2004. 9: p. 1422-1432.**
39. **Buijtenhuijs, P., et al., *Tissue engineering of blood vessels: characterization of smooth-muscle cells for culturing on collagen-and-elastin-based scaffolds.* Biotechnol. Appl. Biochem., 2004. 39: p. 141-149.**
40. **Greenwald, S.E. and C.L. Berry, *Improving vascular grafts: the importance of mechanical and haemodynamic properties.* The Journal Of Pathology, 2000. 190(3): p. 292-299.**
41. **Kannan, R.Y., et al., *Current status of prosthetic bypass grafts: a review.* J. Biomed. Mater. Res., Part B, 2005. 74B(1): p. 570-581.**
42. **Tiwari, A., et al., *Improving the patency of vascular bypass grafts: the role of suture materials and surgical techniques on reducing anastomotic compliance mismatch.* Eur J Vasc Endovasc Surg, 2003. 25(4): p. 287-295.**
43. **Tiwari, A., et al., *New prostheses for use in bypass grafts with special emphasis on polyurethanes.* J. Cardiovasc. Surg., 2002. 10(3): p. 191-197.**
44. **Sarkar, S., et al., *Achieveing the ideal properties for vascular bypass grafts using a tissue engineered approach: a review.* Med Bio Eng Comput, 2007. 45: p. 327-336.**

45. Vara, D.S., et al., *Cardiovascular tissue engineering: state of the art.* Pathologic Biologie, 2005. 53: p. 599-612.
46. Thomas, A.C., G.R. Campbell, and J.H. Campbell, *Advances in vascular tissue engineering.* Cardiovascular Pathology, 2003. 12: p. 271-276.
47. Wang, X., et al., *Development of small-diameter vascular grafts.* World Journal of Surgery, 2007. 31: p. 682-689.
48. Xue, L. and H.P. Greisler, *Biomaterials in the development and future of vascular grafts.* Journal of Vascular Surgery, 2003. 37(2): p. 472-480.
49. Mitchell, S.L. and L.E. Niklason, *Requirements for growing tissue-engineered vascular grafts.* Cardiovascular Pathology, 2003. 12: p. 59-64.
50. Zarge, J.I., P. Huang, and H.P. Greisler, *Blood Vessels*, in *Principles of Tissue Engineering*, R. Lanza, R. Langer, and W. Chick, Editors. 1997, R.G. Landes Company: Austin, Texas. p. 349-364.
51. Walpoth, B.H. and G.L. Bowlin, *The daunting quest for a small diameter vascular graft.* Expert Review of Medical Devices, 2005. 2(6): p. 647-651.
52. Bohr, D.F., A.P. Somlyo, and H.V. Sparks, *The Cardiovascular System*, in *Handbook of Physiology*, S.R. Greiger, Editor. 1980, American Physiological Society: Bethesda. p. 1-31.
53. Pugsley, M.K. and R. Tabrizchi, *The vascular system. An overview of structure and function.* J Pharmacol Toxicol Methods, 2000. 44(2): p. 333-40.
54. Wagenseil, J.E. and R.P. Mecham, *Vascular extracellular matrix and arterial mechanics.* Physiol Rev, 2009. 89(3): p. 957-89.
55. Birukov, K.G., et al., *Intraluminal pressure is essential for the maintenance of smooth muscle caldesmon and filamin content in aortic organ culture.* Arterioscler Thromb Vasc Biol, 1998. 18(6): p. 922-7.
56. Harrison, D.G., *The shear stress of keeping arteries clear.* Nat Med, 2005. 11(4): p. 375-6.
57. Chatzizisis, Y.S., et al., *Role of endothelial shear stress in the natural history of coronary atherosclerosis and vascular remodeling: molecular, cellular, and vascular behavior.* J Am Coll Cardiol, 2007. 49(25): p. 2379-93.
58. Cummins, P.M., et al., *Cyclic strain-mediated matrix metalloproteinase regulation within the vascular endothelium: a force to be reckoned with.* Am J Physiol Heart Circ Physiol, 2007. 292(1): p. H28-42.
59. Hahn, C. and M.A. Schwartz, *Mechanotransduction in vascular physiology and atherogenesis.* Nat Rev Mol Cell Biol, 2009. 10(1): p. 53-62.
60. Younis, H.F., et al., *Hemodynamics and wall mechanics in human carotid bifurcation and its consequences for atherogenesis: investigation of inter-individual variation.* Biomech Model Mechanobiol, 2004. 3(1): p. 17-32.
61. Lehoux, S., Y. Castier, and A. Tedgui, *Molecular mechanisms of the vascular responses to haemodynamic forces.* J Intern Med, 2006. 259(4): p. 381-92.
62. Lip, G.Y., *Exacerbation of atherosclerosis by hypertension: potential mechanisms and clinical implications.* Arch Intern Med, 1997. 157(11): p. 1265-6.

63. **Wu, J.H., et al., *Aortic constriction exacerbates atherosclerosis and induces cardiac dysfunction in mice lacking apolipoprotein E.* Arterioscler Thromb Vasc Biol, 2002. 22(3): p. 469-75.**
64. **Li, C. and Q. Xu, *Mechanical stress-initiated signal transduction in vascular smooth muscle cells in vitro and in vivo.* Cell Signal, 2007. 19(5): p. 881-91.**
65. **Sawyer, P.N., *Modern Vascular Grafts*. 1987, New York: McGraw-Hill.**
66. **Wright, C.B., *Vascular Grafting: Clinical Applications and Techniques*. 1983, Boston: J. Wright, PSG Inc.**
67. **Chlupac, J., E. Filova, and L. Bacakova, *Blood vessel replacement: 50 years of development and tissue engineering paradigms in vascular surgery.* Physiol Res, 2009. 58 Suppl 2: p. S119-39.**
68. **Herring, M.B., et al., *Seeding arterial prostheses with vascular endothelium. The nature of the lining.* Ann Surg, 1979. 190(1): p. 84-90.**
69. **Kadletz, M., et al., *In vitro lining of fibronectin coated PTFE grafts with cryopreserved saphenous vein endothelial cells.* Thorac Cardiovasc Surg, 1987. 35 Spec No 2: p. 143-7.**
70. **Zilla, P., et al., *Use of fibrin glue as a substrate for in vitro endothelialization of PTFE vascular grafts.* Surgery, 1989. 105(4): p. 515-22.**
71. **Pratt, K.J., et al., *Kinetics of endothelial cell-surface attachment forces.* J Vasc Surg, 1988. 7(4): p. 591-9.**
72. **Shindo, S., A. Takagi, and A.D. Whittemore, *Improved patency of collagen-impregnated grafts after in vitro autogenous endothelial cell seeding.* J Vasc Surg, 1987. 6(4): p. 325-32.**
73. **Prendiville, E.J., et al., *Increased in-vitro incubation time of endothelial cells on fibronectin-treated ePTFE increases cell retention in blood flow.* Eur J Vasc Surg, 1991. 5(3): p. 311-9.**
74. **Ramalanjaona, G., et al., *The effect of fibronectin coating on endothelial cell kinetics in polytetrafluoroethylene grafts.* J Vasc Surg, 1986. 3(2): p. 264-72.**
75. **van Wachem, P.B., et al., *The influence of protein adsorption on interactions of cultured human endothelial cells with polymers.* J Biomed Mater Res, 1987. 21(6): p. 701-18.**
76. **Schneider, A., et al., *An improved method for endothelial cell seeding on polytetrafluoroethylene small caliber vascular grafts.* J Vasc Surg, 1992. 15(4): p. 649-56.**
77. **Lee, Y.S., et al., *Endothelial cell seeding onto the extracellular matrix of fibroblasts for the development of a small diameter polyurethane vessel.* Asaio J, 1993. 39(3): p. M740-5.**
78. **Bellon, J.M., et al., *Endothelial cell seeding of polytetrafluoroethylene vascular prostheses coated with a fibroblastic matrix.* Ann Vasc Surg, 1993. 7(6): p. 549-55.**
79. **Williams, S.K., et al., *Adult human endothelial cell compatibility with prosthetic graft material.* J Surg Res, 1985. 38(6): p. 618-29.**
80. **Kaehler, J., et al., *Precoating substrate and surface configuration determine adherence and spreading of seeded endothelial cells on polytetrafluoroethylene grafts.* J Vasc Surg, 1989. 9(4): p. 535-41.**

81. **Bowlin, G.L., et al., *The persistence of electrostatically seeded endothelial cells lining a small diameter expanded polytetrafluoroethylene vascular graft.* J Biomater Appl, 2001. 16(2): p. 157-73.**
82. **Bowlin, G.L., et al., *In vitro evaluation of electrostatic endothelial cell transplantation onto 4 mm interior diameter expanded polytetrafluoroethylene grafts.* J Vasc Surg, 1998. 27(3): p. 504-11.**
83. **Wesolowski, S.A., et al., *The compound prosthetic vascular graft: A pathologic survey.* Surgery, 1963. 53(1): p. 19-44.**
84. **Wesolowski, S.A., et al., *Arterial prosthetic materials.* Annals of The New York Academy Of Sciences, 1968. 146(1): p. 325-344.**
85. **Bowald, S., C. Busch, and I. Eriksson, *Arterial regeneration following polyglactin 910 suture mesh grafting.* Surgery, 1979. 86(5): p. 722-729.**
86. **Bowald, S., C. Busch, and I. Eriksson, *Absorbable material in vascular prostheses: A new device.* Acta Chir Scand, 1980. 146: p. 391-395.**
87. **Greisler, H.P., *Arterial regeneration over absorbable prostheses.* Archives of Surgery, 1982. 117: p. 1425-1431.**
88. **Greisler, H.P., et al., *Derivation of neointima in vascular grafts.* Circulation, 1988. 78(3, Part 2): p. I6-12.**
89. **Greisler, H.P., et al., *Arterial regeneration over polydioxanone prostheses in the rabbit.* Archives Of Surgery, 1987. 122(6): p. 715-721.**
90. **Campbell, G.R. and J.H. Campbell, *Development of tissue engineered vascular grafts.* Curr Pharm Biotechnol, 2007. 8(1): p. 43-50.**
91. **Asahara, T., et al., *Isolation of putative progenitor endothelial cells for angiogenesis.* Science, 1997. 275(5302): p. 964-7.**
92. **Asahara, T., et al., *Bone marrow origin of endothelial progenitor cells responsible for postnatal vasculogenesis in physiological and pathological neovascularization.* Circ Res, 1999. 85(3): p. 221-8.**
93. **Shin'oka, T., et al., *Midterm clinical result of tissue-engineered vascular autografts seeded with autologous bone marrow cells.* J Thorac Cardiovasc Surg, 2005. 129(6): p. 1330-8.**
94. **Campbell, J.H., J.L. Efendy, and G.R. Campbell, *Novel vascular graft grown within recipient's own peritoneal cavity.* Circ Res, 1999. 85(12): p. 1173-8.**
95. **Chue, W.L., et al., *Dog peritoneal and pleural cavities as bioreactors to grow autologous vascular grafts.* J Vasc Surg, 2004. 39(4): p. 859-67.**
96. **Nieponice, A., et al., *In vivo assessment of a tissue-engineered vascular graft combining a biodegradable elastomeric scaffold and muscle-derived stem cells in a rat model.* Tissue Eng Part A. 16(4): p. 1215-23.**
97. **Ma, Z., et al., *Potential of nanofiber matrix as tissue-engineering scaffolds.* Tissue Engineering, 2005. 11(1/2): p. 101-109.**
98. **Smith, L.A. and P.X. Ma, *Nano-fibrous scaffolds for tissue engineering.* Colloids and Surfaces. B: Biointerfaces, 2004. 39: p. 125-131.**
99. **Wen, X., D. Shi, and N. Zhang, *Applications of Nanotechnology in Tissue Engineering*, in *Handbook of nanostructured biomaterials and their applications in nanobiotechnology*, H.S. Nalwa, Editor. 2005, American Scientific Publishers: Stevenson Ranch, CA. p. 1-23.**

100. **Ramakrishna, S., et al., *Introduction to Electrospinning and Nanofibers*. 2005: World Scientific Publishing Company, Incorporated.**
101. **Alvarez-Cordero, R., et al., *Evaluation of polyglycolic acid sutures in vascular surgery.* J Surg Res, 1973. 15(1): p. 35-44.**
102. **Watts, D.R., S.H. Carr, and R.P. Hohf, *Poly(glycolic acid) sutures in canine vascular anastomoses.* J Biomed Mater Res, 1976. 10(6): p. 867-77.**
103. **Lauritzen, C., *Experimental studies on absorbable vascular grafts for microsurgery.* Scand J Plast Reconstr Surg, 1983. 17(2): p. 133-5.**
104. **Niklason, L.E., et al., *Functional arteries grown in vitro.* Science, 1999. 284(5413): p. 489-93.**
105. **Prabhakar, V., et al., *Engineering porcine arteries: effects of scaffold modification.* J Biomed Mater Res A, 2003. 67(1): p. 303-11.**
106. **Boland, E.D., et al., *Utilizing acid pretreatment and electrospinning to improve biocompatibility of poly(glycolic acid) for tissue engineering.* Journal of Biomedical Materials Research Part B: Applied Biomaterials, 2004. 71B: p. 144-152.**
107. **Iwasaki, K., et al., *Bioengineered three-layered robust and elastic artery using hemodynamically-equivalent pulsatile bioreactor.* Circulation, 2008. 118(14 Suppl): p. S52-7.**
108. **Stitzel, J.D., et al., *Arterial smooth muscle cell proliferation on a novel biomimicking, biodegradable vascular graft scaffold.* J Biomater Appl, 2001. 16(1): p. 22-33.**
109. **Wang, S., et al., *Fabrication and properties of the electrospun polylactide/silk fibroin-gelatin composite tubular scaffold.* Biomacromolecules, 2009. 10(8): p. 2240-2244.**
110. **Zhu, A., F. Zhao, and T. Ma, *Photo-initiated grafting of gelatin/N-maleic acyl-chitosan to enhance endothelial cell adhesion, proliferation and function on PLA surface.* Acta Biomater, 2009. 5(6): p. 2033-44.**
111. **Hibino, N., et al., *Late-term results of tissue-engineered vascular grafts in humans.* J Thorac Cardiovasc Surg. 139(2): p. 431-6, 436 e1-2.**
112. **Mooney, D.J., et al., *Stabilized polyglycolic acid fibre-based tubes for tissue engineering.* Biomaterials, 1996. 17(2): p. 115-124.**
113. **Wen, S.J., et al., *Human vascular smooth muscle cells and endothelial cells cocultured on polyglycolic acid (70/30) scaffold in tissue engineered vascular graft.* Chin Med J (Engl), 2007. 120(15): p. 1331-5.**
114. **Izhar, U., et al., *Novel synthetic selectively degradable vascular prostheses: a preliminary implantation study.* J Surg Res, 2001. 95(2): p. 152-60.**
115. **Roh, J.D., et al., *Construction of an autologous tissue-engineered venous conduit from bone marrow-derived vascular cells: optimization of cell harvest and seeding techniques.* J Pediatr Surg, 2007. 42(1): p. 198-202.**
116. **Allen, B.T., et al., *Reduction of platelet deposition on vascular grafts using an antiplatelet graft coating technique.* J Surg Res, 1984. 36(1): p. 80-8.**
117. **Lommen, E., et al., *Development of a neo-artery induced by a biodegradable polymeric vascular prosthesis.* Trans Am Soc Artif Intern Organs, 1983. 29: p. 255-9.**

118. van der Lei, B., et al., *Microporous, complaint, biodegradable vascular grafts for the regeneration of the arterial wall in rat abdominal aorta.* Surgery, 1985. 98(5): p. 955-63.
119. van der Lei, B., et al., *Regeneration of the arterial wall in microporous, compliant, biodegradable vascular grafts after implantation into the rat abdominal aorta. Ultrastructural observations.* Cell Tissue Res, 1985. 242(3): p. 569-78.
120. van der Lei, B., et al., *Sequential studies of arterial wall regeneration in microporous, compliant, biodegradable small-caliber vascular grafts in rats.* J Thorac Cardiovasc Surg, 1987. 93(5): p. 695-707.
121. Wang, S., et al., *Fabrication and properties of the electrospun polylactide/silk fibroin-gelatin composite tubular scaffold.* Biomacromolecules, 2009. 10(8): p. 2240-4.
122. Hibino, N., et al., *Late-term results of tissue-engineered vascular grafts in humans.* J Thorac Cardiovasc Surg, 2010. 139(2): p. 431-6, 436 e1-2.
123. Xu, C., et al., *In vitro study of human vascular endothelial cell function on materials with various surface roughness.* J Biomed Mater Res A, 2004. 71(1): p. 154-61.
124. Zhu, Y., C. Gao, and J. Shen, *Surface modification of polycaprolactone with poly(methacrylic acid) and gelatin covalent immobilization for promoting its cytocompatibility.* Biomaterials, 2002. 23(24): p. 4889-95.
125. Serrano, M.C., et al., *Vascular endothelial and smooth muscle cell culture on NaOH-treated poly(epsilon-caprolactone) films: a preliminary study for vascular graft development.* Macromol Biosci, 2005. 5(5): p. 415-23.
126. Ma, Z., et al., *Grafting of gelatin on electrospun poly(caprolactone) nanofibers to improve endothelial cell spreading and proliferation and to control cell Orientation.* Tissue Eng, 2005. 11(7-8): p. 1149-58.
127. Duling, R.R., et al., *Mechanical characterization of electrospun polycaprolactone (PCL): a potential scaffold for tissue engineering.* J Biomech Eng, 2008. 130(1): p. 011006.
128. Pektok, E., et al., *Degradation and healing characteristics of small-diameter poly(epsilon-caprolactone) vascular grafts in the rat systemic arterial circulation.* Circulation, 2008. 118(24): p. 2563-70.
129. Drilling, S., J. Gaumer, and J. Lannutti, *Fabrication of burst pressure competent vascular grafts via electrospinning: effects of microstructure.* J Biomed Mater Res A, 2009. 88(4): p. 923-34.
130. Lee, S.J., et al., *The use of thermal treatments to enhance the mechanical properties of electrospun poly(epsilon-caprolactone) scaffolds.* Biomaterials, 2008. 29(10): p. 1422-30.
131. Vaz, C.M., et al., *Design of scaffolds for blood vessel tissue engineering using a multi-layering electrospinning technique.* Acta Biomater, 2005. 1: p. 575-582.
132. Hanson, S.J., K. Jamshidi, and R.C. Eberhart, *Mechanical evaluation of resorbable copolymers for end use as vascular grafts.* ASAIO Trans, 1988. 34(3): p. 789-93.

133. **Watanabe, M., et al., *Tissue-engineered vascular autograft: inferior vena cava replacement in a dog model.* Tissue Eng, 2001. 7(4): p. 429-39.**
134. **Serrano, M.C., et al., *Endothelial cells derived from circulating progenitors as an effective source to functional endothelialization of NaOH-treated poly(epsilon-caprolactone) films.* J Biomed Mater Res A, 2008. 87(4): p. 964-71.**
135. **Bolgen, N., et al., *In vitro and in vivo degradation of non-woven materials made of poly(epsilon-caprolactone) nanofibers prepared by electrospinning under different conditions.* J Biomater Sci Polym Ed, 2005. 16(12): p. 1537-55.**
136. **Nottelet, B., et al., *Factorial design optimization and in vivo feasibility of poly(epsilon-caprolactone)-micro- and nanofiber-based small diameter vascular grafts.* J Biomed Mater Res A, 2008. 89(4): p. 865-75.**
137. **Vaz, C.M., et al., *Design of scaffolds for blood vessel tissue engineering using a multi-layering electrospinning technique.* Acta Biomater, 2005. 1(5): p. 575-82.**
138. **Williamson, M.R., R. Black, and C. Kielty, *PCL-PU composite vascular scaffold production for vascular tissue engineering: attachment, proliferation and bioactivity of human vascular endothelial cells.* Biomaterials, 2006. 27(19): p. 3608-16.**
139. **Hibino, N., et al., *The tissue-engineered vascular graft using bone marrow without culture.* J Thorac Cardiovasc Surg, 2005. 129(5): p. 1064-70.**
140. **Lim, S.H., et al., *Tissue-engineered blood vessels with endothelial nitric oxide synthase activity.* J Biomed Mater Res B Appl Biomater, 2008. 85(2): p. 537-46.**
141. **Kwon, I.K., S. Kidoaki, and T. Matsuda, *Electrospun nano- to microfiber fabrics made of biodegradable copolyesters: structural characteristics, mechanical properties and cell adhesion potential.* Biomaterials, 2005. 26(18): p. 3929-39.**
142. **Greisler, H.P., et al., *Prostacyclin production by blood-contacting surfaces of endothelialized vascular prostheses.* J Cardiovasc Surg (Torino), 1990. 31(5): p. 640-5.**
143. **Teebken, O.E., A.M. Pichlmaier, and A. Haverich, *Cell seeded decellularised allogeneic matrix grafts and biodegradable polydioxanone-prostheses compared with arterial autografts in a porcine model.* Eur J Vasc Endovasc Surg, 2001. 22(2): p. 139-45.**
144. **Boland, E.D., et al., *Electrospinning polydioxanone for biomedical applications.* Acta Biomaterialia, 2005. 1: p. 115-123.**
145. **Smith, M.J., et al., *Suture-reinforced electrospun polydioxanone-elastin small-diameter tubes for use in vascular tissue engineering: a feasibility study.* Acta Biomater, 2008. 4(1): p. 58-66.**
146. **McClure, M.J., et al., *Electrospun Polydioxanone, Elastin, and Collagen Vascular Scaffolds: Uniaxial Cyclic Distension.* Journal Of Engineered Fibers And Fabrics, 2009. 4(2): p. 18-25.**
147. **McClure, M.J., et al., *Cross-linking electrospun polydioxanone-soluble elastin blends: Material characterization.* Journal of Engineered Fibers and Fabrics, 2008. 3(1): p. 1-10.**

148. **Barnes, C.P., et al., *Preliminary investigation of electrospun collagen and polydioxanone for vascular tissue engineering applications.* International Journal of Electrospun Nanofibers and Applications, 2007. 1: p. 73-87.**
149. **McClure, M.J., et al., *Electrospinning-aligned and random polydioxanone-polycaprolactone-silk fibroin-blended scaffolds: geometry for a vascular matrix.* Biomed Mater, 2009. 4(5): p. 055010.**
150. **Garg, K., et al., *Angiogenic potential of human macrophages on electrospun bioresorbable vascular grafts.* Biomed Mater, 2009. 4(3): p. 031001.**
151. **Guan, J., et al., *Preparation and characterization of highly porous, biodegradable polyurethane scaffolds for soft tissue applications.* Biomaterials, 2005. 26(18): p. 3961-71.**
152. **Martz, H., et al., *Physicochemical characterization of a hydrophilic microporous polyurethane vascular graft.* J Biomed Mater Res, 1987. 21(3): p. 399-412.**
153. **Martz, H., et al., *Hydrophilic microporous polyurethane versus expanded PTFE grafts as substitutes in the carotid arteries of dogs. A limited study.* J Biomed Mater Res, 1988. 22(1): p. 63-9.**
154. **Stankus, J.J., et al., *Fabrication of cell microintegrated blood vessel constructs through electrohydrodynamic atomization.* Biomaterials, 2007. 28: p. 2738-2746.**
155. **El-Kurdi, M.S., et al., *Transient elastic support for vein grafts using a constricting microfibrillar polymer wrap.* Biomaterials, 2008. 29(22): p. 3213-20.**
156. **Nieponice, A., et al., *Development of a tissue-engineered vascular graft combining a biodegradable scaffold, muscle-derived stem cells and a rotational vacuum seeding technique.* Biomaterials, 2008. 29(7): p. 825-33.**
157. **Soletti, L., et al., *A bilayered elastomeric scaffold for tissue engineering of small diameter vascular grafts.* Acta Biomater. 6(1): p. 110-22.**
158. **Hong, Y., et al., *A small diameter, fibrous vascular conduit generated from a poly(ester urethane)urea and phospholipid polymer blend.* Biomaterials, 2009. 30(13): p. 2457-67.**
159. **Wolfe, P.S., et al., *Evaluation of thrombogenic potential of electrospun bioresorbable vascular graft materials: Acute monocyte tissue factor expression.* J Biomed Mater Res A, 2009. In Review.**
160. **Beckman, M.J., K.J. Shields, and R.F. Diegelmann, *Collagen*. Encyclopedia of Biomaterials and Biomedical Engineering. 2004, New York: Marcel Dekker.**
161. **Kolacna, L., et al., *Biochemical and biophysical aspects of collagen nanostructure in the extracellular matrix.* Physiol Res, 2007. 56 Suppl 1: p. S51-60.**
162. **Berglund, J.D., et al., *A biological hybrid model for collagen-based tissue engineered vascular constructs.* Biomaterials, 2003. 24(7): p. 1241-54.**
163. **Cummings, C.L., et al., *Properties of engineered vascular constructs made from collagen, fibrin, and collagen-fibrin mixtures.* Biomaterials, 2004. 25(17): p. 3699-706.**

164. **Matthews, J.A., et al., *Electrospinning of collagen nanofibers.* Biomacromolecules, 2002. 3(2): p. 232-238.**
165. **Venugopal, J.R., Y.Z. Zhang, and S. Ramakrishna, *In vitro culture of human dermal fibroblasts on electrospun polycaprolactone collagen nanofibrous membrane.* Artificial Organs, 2006. 30(6): p. 440-446.**
166. **Tillman, B.W., et al., *The in vivo stability of electrospun polycaprolactone-collagen scaffolds in vascular reconstruction.* Biomaterials, 2009. 30(4): p. 583-8.**
167. **Ju, Y.M., et al., *Bilayered scaffold for engineering cellularized blood vessels.* Biomaterials. 31(15): p. 4313-21.**
168. **He, W., et al., *Fabrication of collagen-coated biodegradable polymer nanofiber mesh and its potential for endothelial cells growth.* Biomaterials, 2005. 26(36): p. 7606-15.**
169. **Jeong, S.I., et al., *Tissue-engineered vascular grafts composed of marine collagen and PLGA fibers using pulsatile perfusion bioreactors.* Biomaterials, 2007. 28: p. 1115-1122.**
170. **Park, I.S., et al., *A collagen/smooth muscle cell-incorporated elastic scaffold for tissue-engineered vascular grafts.* J Biomater Sci Polym Ed, 2009. 20(11): p. 1645-60.**
171. **Rodgers, U.R. and A.S. Weiss, *Cellular interactions with elastin.* Pathol Biol (Paris), 2005. 53(7): p. 390-8.**
172. **Debelle, L. and A.M. Tamburro, *Elastin: molecular description and function.* Int J Biochem Cell Biol, 1999. 31(2): p. 261-72.**
173. **Vrhovski, B. and A.S. Weiss, *Biochemistry of tropoelastin.* Eur J Biochem, 1998. 258(1): p. 1-18.**
174. **Partridge, S.M. and H.F. Davis, *The chemistry of connective tissues. 3. composition of the soluble proteins derived from elastin.* Biochem. J., 1955. 61: p. 21-30.**
175. **Duca, L., et al., *Elastin as a matrikine.* Crit Rev Oncol Hematol, 2004. 49(3): p. 235-44.**
176. **Daamen, W.F., et al., *Elastin as a biomaterial for tissue engineering.* Biomaterials, 2007. 28(30): p. 4378-98.**
177. **Leach, J.B., et al., *Crosslinked alpha-elastin biomaterials: towards a processable elastin mimetic scaffold.* Acta Biomater, 2005. 1(2): p. 155-64.**
178. **Li, M., et al., *Electrospun protein fibers as matrices for tissue engineering.* Biomaterials, 2005. 26(30): p. 5999-6008.**
179. **Welsh, E.R. and D.A. Tirrell, *Engineering the extracellular matrix: a novel approach to polymeric biomaterials. I. Control of the physical properties of artificial protein matrices designed to support adhesion of vascular endothelial cells.* Biomacromolecules, 2000. 1(1): p. 23-30.**
180. **Nicol, A., D.C. Gowda, and D.W. Urry, *Cell adhesion and growth on synthetic elastomeric matrices containing Arg-Gly-Asp-Ser-3.* J Biomed Mater Res, 1992. 26(3): p. 393-413.**
181. **Wise, S.G., et al., *A multilayered synthetic human elastin/polycaprolactone hybrid vascular graft with tailored mechanical properties.* Acta Biomater.**

182. **Berglund, J.D., R.M. Nerem, and A. Sambanis, *Incorporation of Intact Elastin Scaffolds in Tissue-Engineered Collagen-Based Vascular Grafts.* Tissue Eng, 2004. 10: p. 1526-1535.**
183. **Buttafoco, L., et al., *Electrospinning of collagen and elastin for tissue engineering applications.* Biomaterials, 2006. 27(5): p. 724-734.**
184. **Stitzel, J., et al., *Controlled fabrication of a biological vascular substitute.* Biomaterials, 2006. 27(7): p. 1088-94.**
185. **Lee, S.J., et al., *In vitro evaluation of electrospun nanofiber scaffolds for vascular graft application.* J Biomed Mater Res A, 2007. 83(4): p. 999-1008.**
186. **McClure, M.J., et al., *A three-layered electrospun matrix to mimic native arterial architecture using polycaprolactone, elastin, and collagen: A preliminary study.* Acta Biomater, 2010. 6(7): p. 2422-2433.**
187. **Thomas, V., et al., *Functionally graded electrospun scaffolds with tunable mechanical properties for vascular tissue regeneration.* Biomed Mater, 2007. 2(4): p. 224-32.**
188. **Schaner, P.J., et al., *Decellularized vein as a potential scaffold for vascular tissue engineering.* J Vasc Surg, 2004. 40(1): p. 146-53.**
189. **Clarke, D.R., et al., *Transformation of nonvascular acellular tissue matrices into durable vascular conduits.* Ann Thorac Surg, 2001. 71(5 Suppl): p. S433-6.**
190. **Wilson, G.J., et al., *Acellular matrix: a biomaterials approach for coronary artery bypass and heart valve replacement.* Ann Thorac Surg, 1995. 60(2 Suppl): p. S353-8.**
191. **Nemcova, S., et al., *Evaluation of a xenogeneic acellular collagen matrix as a small-diameter vascular graft in dogs--preliminary observations.* J Invest Surg, 2001. 14(6): p. 321-30.**
192. **Lantz, G.C., et al., *Small intestinal submucosa as a small-diameter arterial graft in the dog.* J Invest Surg, 1990. 3(3): p. 217-27.**
193. **Gui, L., et al., *Development of decellularized human umbilical arteries as small-diameter vascular grafts.* Tissue Eng Part A, 2009. 15(9): p. 2665-76.**
194. **Rasmussen, B.L., E. Bruenger, and L.B. Sandberg, *A new method for purification of mature elastin.* Anal Biochem, 1975. 64(1): p. 255-9.**
195. **Lu, Q., et al., *Novel porous aortic elastin and collagen scaffolds for tissue engineering.* Biomaterials, 2004. 25(22): p. 5227-37.**
196. **Starcher, B.C. and M.J. Galione, *Purification and comparison of elastins from different animal species.* Anal Biochem, 1976. 74(2): p. 441-7.**
197. **L'Heureux, N., et al., *A completely biological tissue-engineered human blood vessel.* The FASEB Journal, 1998. 12(1): p. 47-56.**
198. **Konig, G., et al., *Mechanical properties of completely autologous human tissue engineered blood vessels compared to human saphenous vein and mammary artery.* Biomaterials, 2009. 30(8): p. 1542-50.**
199. **Stickler, P., et al., *Cyclically stretching developing tissue in vivo enhances mechanical strength and organization of vascular grafts.* Acta Biomater. 6(7): p. 2448-56.**

200. Lantz, G.C., et al., *Small intestinal submucosa as a vascular graft: a review.* J Invest Surg, 1993. 6(3): p. 297-310.
201. Quaglia, F., *Bioinspired tissue engineering: The great promise of protein delivery technologies.* International Journal of Pharmaceutics, 2008. 364: p. 281-297.
202. Chen, R.R. and D.J. Mooney, *Polymeric Growth Factor Delivery Strategies for Tissue Engineering.* Pharmaceutical Research, 2003. 20(8): p. 1103-1112.
203. Tayalia, P. and D.J. Mooney, *Controlled Growth Factor Delivery for Tissue Engineering.* Advanced Materials, 2009. 21: p. 3269-3285.
204. Zisch, A.H., M.P. Lutolf, and J.A. Hubbell, *Biopolymeric delivery matrices for angiogenic growth factors.* Cardiovascular Pathology, 2003. 12: p. 295-310.
205. Chen, R.R., et al., *Integrated approach to designing growth factor delivery systems.* FASEB J., 2007. 21: p. 3896-3903.
206. Visscher, G.D., et al., *The remodeling of cardiovascular bioprostheses under influence of stem cell homing signal pathways.* Biomaterials, 2010. 31: p. 20-28.
207. Pang, Y., et al., *Local delivery of a collagen-binding FGF-1 chimera to smooth muscle cells in collagen scaffolds for vascular tissue engineering.* Biomaterials. 31(5): p. 878-85.
208. Wissink, M.J.B., et al., *Improved endothelialization of vascular grafts by local release of growth factor from heparinized collagen matrices.* Journal of Controlled Release, 2000. 64: p. 103-114.
209. Thevenot, P.T., et al., *The effect of incorporation of SDF-1alpha into PLGA scaffolds on stem cell recruitment and the inflammatory response.* Biomaterials, 2010. 31(14): p. 3997-4008.
210. Richardson, T.P., et al., *Polymeric system for dual growth factor delivery.* Nature Biotechnology, 2001. 19: p. 1029-1034.
211. Saif, J., et al., *Combination of Injectable Multiple Growth Factor-Releasing Scaffolds and Cell Therapy as an Advanced Modality to Enhance Tissue Neovascularization.* Arteriosclerosis, Thrombosis, and Vascular Biology, 2010. 30: p. 1897-1904.
212. Zhang, G. and L.J. Suggs, *Matrices and scaffolds for drug delivery in vascular tissue engineering.* Advanced Drug Delivery Reviews, 2007. 59: p. 360-373.
213. Gu, F., B. Amsden, and R. Neufeld, *Sustained delivery of vascular endothelial growth factor with alginate beads.* Journal of Controlled Release, 2004. 96: p. 463-472.
214. Silva, E.A. and D.J. Mooney, *Spatiotemporal control of vascular endothelial growth factor delivery from injectable hydrogels enhances angiogenesis.* Journal of Thrombosis and Haemostasis, 2007. 5: p. 590-598.
215. Tilakaratne, H.K., et al., *Characterizing short-term release and neovascularization potential of multi-protein growth supplement delivered via alginate hollow fiber devices.* Biomaterials, 2007. 28: p. 89-98.
216. Kurane, A. and N. Vyavahare, *In vivo vascular tissue engineering: influence of cytokine and implant location on tissue specific cellular recruitment.* Journal of Tissue Engineering and Regenerative Medicine, 2009. 3: p. 280-289.

217. **Obara, K., et al.,** ***Photocrosslinkable chitosan hydrogel containing fibroblast growth factor-2 stimulates wound healing in healing-impared db/db mice.*** **Biomaterials, 2003. 24: p. 3437-3444.**
218. **Ishihara, M., et al.,** ***Controlled release of fibroblast growth factors and heparin from photocrosslinked chitosan hydrogels and subsequent effect on in vivo vascularization.*** **Journal of Biomedical Materials Research, 2003. 64A: p. 551-559.**
219. **Yamamoto, M., Y. Ikada, and Y. Tabata,** ***Controlled release of growth factors based on biodegradation of gelatin hydrogel.*** **Journal of Biomaterials Science, Polymer Edition, 2001. 12(1): p. 77-88.**
220. **Patel, Z.S., et al.,** ***In Vitro and In Vivo Release of Vascular Endothelial Growth Factor from Gelatin Microparticles and Biodegradable Composite Scaffolds.*** **Pharmaceutical Research, 2008. 25(10): p. 2370-2378.**
221. **Gosselin, C., et al.,** ***ePTFE Coating with Fibrin Glue, FGF-1, and Heparin: Effect on Retention of Seeded Endothelial Cells.*** **Journal of Surgical Research, 1996. 60(0052): p. 327-332.**
222. **Nillesen, S.T.M., et al.,** ***Increased angiogenesis and blood vessel maturation in acellular collagen-heparin scaffolds containing both FGF2 and VEGF.*** **Biomaterials, 2007. 28: p. 1123-1131.**
223. **Steffens, G.C.M., et al.,** ***Modulation of Angiogenic Potential of Collagen Matrices by Covalent Incorporation of Heparin and Loading with Vascular Endothelial Growth Factor.*** **Tissue Engineering, 2004. 10(9/10): p. 1502-1510.**
224. **Kanematsu, A., et al.,** ***Collagenous matrices as release carriers of exogenous growth factors.*** **Biomaterials, 2004. 25: p. 4513-4520.**
225. **Nagai, N., et al.,** ***Preparation and characterization of collagen microspheres for sustained release of VEGF.*** **Journal of Material Science: Material Medicine, 2010. 21: p. 1891-1898.**
226. **Chung, H.J. and T.G. Park,** ***Surface engineered and drug releasing pre-fabricated scaffolds for tissue engineering.*** **Advanced Drug Delivery Reviews, 2007. 59: p. 249-262.**
227. **Greisler, H., et al.,** ***Enhanced endothelialization of expanded polytetrafluoroethylene grafts by fibroblast growth factor type 1 pretreatment.*** **Surgery, 1992. 112(2): p. 244-254.**
228. **Deutsch, M., et al.,** ***In vitro endothelialization of expanded polytetrafluoroethylene grafts: A clinical case report after 41 months of implantation.*** **Journal of Vascular Surgery, 1997. 25: p. 757-763.**
229. **Lee, K.Y., et al.,** ***Controlled growth factor release from synthetic extracellular matrices.*** **Nature, 2000. 408: p. 998-1000.**
230. **Tabata, Y., et al.,** ***Controlled release of vascular endothelial growth factor by use of collagen hydrogels.*** **Journal of Biomaterials Science, Polymer Edition, 2000. 11(9): p. 915-930.**
231. **Pieper, J.S., et al.,** ***Loading of collagen-heparan sulfate matrices with bFGF promotes angiogenesis and tissue generation in rats.*** **Journal of Biomedical Materials Research, 2002. 62: p. 185-194.**

232. **Mann, B.K., R.H. Schmedlen, and J.L. West, *Tethered-TGF-β increases extracellular matrix production of vascular smooth muscle cells.* Biomaterials, 2001. 22: p. 439-444.**
233. **Lim, T.Y., C.K. Poh, and W. Wang, *Poly(lactic-co-glycolic acid) as a controlled release delivery device.* Journal of Material Science: Material Medicine, 2009. 20: p. 1669-1675.**
234. **Cleland, J.L., et al., *Development of poly-(D,L-lactice-coglycolide) microsphere formulations containing recombinant human vascular endothelial growth factor to promote local angiogenesis.* Journal of Controlled Release, 2001. 72: p. 13-24.**
235. **Sheridan, M.H., et al., *Bioabsorbable polymer scaffolds for tissue engineering capable of sustained growth factor delivery.* Journal of Controlled Release, 2000. 64: p. 91-102.**
236. **Kim, T. and D. Burgess, *Pharmacokinetic characterization of 14C-vascular endothelial growth factor controlled release microspheres using a rat model.* Journal of Pharmacy and Pharmacology, 2002. 54(7): p. 897-905.**
237. **Golub, J.S., et al., *Sustained VEGF delivery via PLGA nanoparticles promotes vascular growth.* American Journal of Physiological Heart and Circulation Physiology, 2010. 298: p. H1959-H1965.**
238. **d'Angelo, I., et al., *Nanoparticles Based on PLGA:Poloxamer Blends for the Delivery of Proangiogenic Growth Factors.* Molecular Pharmaceutics, 2010. 7(5): p. 1724-1733.**
239. **Lee, M., et al., *Modulation of protein delivery from modular polymer surfaces.* Biomaterials, 2007. 28: p. 1862-1870.**
240. **Baldwin, S.P. and W.M. Saltzman, *Materials for protein delivery in tissue engineering.* Advanced Drug Delivery Reviews, 1998. 33: p. 71-86.**
241. **Chen, R.R., et al., *Spatio-temporal VEGF and PDGF Delivery Patterns Blood Vessel Formation and Maturation.* Pharmaceutical Research, 2007. 24(2): p. 258-264.**
242. **Sell, S.A., et al., *Incorporating Platelet-Rich Plasma into Electrospun Scaffolds for Tissue Engineering Applications.* Tissue Eng Part A, 2011. 17(21 and 22): p. 1-15.**
243. **Shireman, P.K. and H.P. Greisler, *Mitogenicity and release of vascular endothelial growth factor with and without heparin from fibrin glue.* Journal of Vascular Surgery, 2000. 31: p. 936-943.**
244. **Ito, Y., G. Chen, and Y. Imanishi, *Artificial juxtacrine stimulation for tissue engineering.* Journal of Biomaterials Science, Polymer Edition, 1998. 9(8): p. 879-890.**
245. **Masters, K.S., et al., *Nitric oxide-generating hydrogels inhibit neointima formation.* Journal of Biomaterials Science, Polymer Edition, 2005. 16(5): p. 659-672.**
246. **Lipke, E.A. and J.L. West, *Localized delivery of nitric oxide from hydrogels inhibits neointima formation in a rat carotid balloon injury model.* Acta Biomaterialia, 2005. 1(6): p. 597-606.**

247. **Kanjickal, D., et al., *Sustained local drug delivery from a novel polymeric ring to inhibit intimal hyperplasia.* Journal of Biomedical Materials Research, 2010. 93A: p. 656-665.**
248. **Javerliat, I., et al., *Experimental Study of a New Vascular Graft Prebonded with Antibiotic: Healing, Toxicity, and Antibiotic Retention.* Annals of Vascular Surgery, 2007. 21(5): p. 603-610.**
249. **Cui, W., Y. Zhou, and J. Chang, *Electrospun nanofibrous materials for tissue engineering and drug delivery.* Science and Technology of Advanced Materials, 2010. 11(1).**
250. **Middleton, J.C. and A.J. Tipton, *Synthetic biodegradable polymers as orthopedic devices.* Biomaterials, 2000. 21: p. 2335-2346.**
251. **Kim, J.-S. and D.S. Lee, *Thermal Properties of Electrospun Polyesters.* Polymer Journal, 2000. 32(7): p. 616-618.**
252. **Zong, X., et al., *Structure and process relationship of electrospun bioabsorbable nanofiber membranes.* Polymer, 2002. 43: p. 4403-4412.**
253. **Ramdhanie, L., et al., *Thermal and Mechanical Characterization of Electrospun Blends of Poly(lactic acid) and Poly(glycolic acid).* Polymer Journal, 2006. 38(11): p. 1137-1145.**
254. **Doddi, N., C.C. Versfelt, and D. Wasserman, US Patent, 1977. No. 4,052,988.**
255. **Bezwada, R.S. and K. Cooper, US Patent, 1998. No. 5,714,551.**
256. **Bezwada, R.S., H.D. Newman, and S.W. Shalaby, US Patent, 1991. No. 5,007,923.**
257. **Bezwada, R.S., S.W. Shalaby, and D.F. Koelmel, US Patent, 1995. No. 5,470,340.**
258. **Raquez, J.-M., et al., *"Coordination-insertion" ring-opening polymerization of 1,4-dioxan-2-one and controlled synthesis of diblock copolymers with e-caprolactone.* Macromolecules Rapid Communications, 2000. 21(15): p. 1063-1071.**
259. **Hong, J.-T., et al., *Preparation and Characterization of Biodegradable Poly(Trimethylenecarbonate-e-Caprolactone)-Block-Poly(p-Dioxanone) Copolymers.* Journal of Polymer Science Part A: Polymer Chemistry, 2005. 43(13): p. 2790-2799.**
260. **Hong, J.-T., et al., *Biodegradable Studies of Poly(trimethylenecarbonate-e-caprolactone)-block-poly(p-dioxanone), Poly(dioxanone), and Poly(glycolide-e-caprolactone) (Monocryl) Monofilaments.* Journal of Applied Polymer Science, 2006. 102(1): p. 737-743.**
261. **Shin, T.J., et al., *Development of 3-D poly(trimethylenecarbonate-co-e-caprolactone)-block-poly(p-dioxanone) scaffold for bone regeneration with high porosity using a wet electrospinning method.* Biotechnology Letters, 2010. web publication date 8 March 2010(DOI 10.1007/s10529-010-0235-7).**
262. **Bhattarai, N., et al., *Nonisothermal crystallization and melting behavior of the copolymer derived from p-dioxanone and poly(ethylene glycol).* European Polymer Journal, 2003. 39(7): p. 1365-1375.**
263. **Bahadur, K.C.R., et al., *Amphiphilic Triblock Copolymer Based on Poly(p-dioxanone) and Poly(ethylene glycol): Synthesis, Characterization, and***

Aqueous Dispersion. **Journal of Applied Polymer Science, 2007. 103(4): p. 2695-2702.**

264. Yang, K.-K., et al., *ABA Triblock Copolymers from Poly(p-dioxanone) and Poly(ethylene glycol).* Journal of Applied Polymer Science, 2006. 102(2): p. 1092-1097.

265. Wang, H., et al., *Synthesis of PDON-b-PEG-b-PDON Block Copolymers and Drug Delivery System Thereof.* Journal of Applied Polymer Science, 1998. 68(13): p. 2121-2128.

266. Lochee, Y., et al., Submitted for publication, 2009.

267. McManus, M., et al., *Mechanical properties of electrospun fibrinogen structures.* Acta Biomaterialia, 2006. 2: p. 19-28.

268. Karacan, I., *Structure-property Relationships in High-strength High-modulus Polyethylene Fibres.* Fibres and Textiles in Eastern Europe, 2005. 13(4 (52)): p. 15-21.

269. Shenoy, S.L., et al., *Role of chain entanglements on fiber formation during electrospinning of polymer solutions: good solvent, non-specific polymer-polymer interaction limit.* Polymer, 2005. 46: p. 3372-3384.

270. Shenoy, S.L., W.D. Bates, and G.E. Wnek, *Correlations between electrospinnability and physical gelation.* Polymer, 2005. 46: p. 8990-9004.

271. Lin, A.S.P., et al., *Microarchitectural and mechanical characterization of oriented porous polymer scaffolds.* Biomaterials, 2003. 24(3): p. 481-489.

272. Baldwin, S.P. and M. Saltzman, *Materials for protein delivery in tissue engineering.* Advanced Drug Delivery Reviews., 1998. 33: p. 71-86.

273. Daubie, V., et al., *Tissue factor: a mini-review.* Journal of Tissue Engineering and Regenerative Medicine, 2007. 1: p. 161-169.

274. Versteeg, H.H., M.P. Peppelenbosch, and C.A. Spek, *Tissue factor signal transduction in angiogenesis.* Carcinogenesis, 2003. 24(6): p. 1009-1013.

275. He, Y., et al., *Soluble tissue factor has unique angiogenic activities that selectively promote migration and differentiation but not proliferation of endothelial cells.* Biochemical and Biophysical Research Communications, 2008. 370: p. 489-494.

276. Edwards, R.L., F.R. Rickles, and A.M. Bobrove, *Mononuclear cell tissue factor: cell of origin and requirements for activation.* Blood, 1979. 54: p. 359-370.

277. van Ginkel, C.J.W., et al., *Stimulation of Monocyte Procoagulant Activity by Adherence to Different Surfaces.* British Journal of Haematology, 1977. 37: p. 35-45.

278. Poulsen, L.K., et al., *Signal transduction via the mitogen activated protein kinase pathway induced by binding of coagulation factor VIIa to tissue factor.* Journal of Biological Chemicals, 1998. 273: p. 6228-6232.

279. Camerer, E., et al., *Coagulation factors VIIa and Xa induce cell signaling leading to the upregulation of the egr-1 gene.* Journal of Biological Chemicals, 1999. 274: p. 32225-32233.

280. Koch, A.E., et al., *Interleukin-8 as a Macrophage-Derived Mediator of Angiogenesis.* Science, 1992. 258: p. 1798-1801.

281. **Li, A., et al.,** ***IL-8 Directly Enhanced Endothelial Cell Survival, Proliferation, and Matrix Metalloproteinases Production and Regulated Angiogenesis.*** **The Journal of Immunology, 2003. 170: p. 3369-3376.**
282. **Ott, I., et al.,** ***Regulation of monocyte procoagulant activity in acute myocardial infarction: role of tissue factor and tissue factor pathway inhibitor-1.*** **Blood, 2001. 97: p. 3721-3726.**
283. **Falati, S., et al.,** ***Real-time in vivo imaging of platelets, tissue factor and fibrin during arterial thrombus formation in the mouse.*** **Nature Medicine, 2002. 8(10): p. 1175-1180.**
284. **Giesen, P.L.A., et al.,** ***Blood-borne tissue factor: Another view of thrombosis.*** **Proceedings of the National Academy of Sciences of the United States of America, 1999. 96(5): p. 2311-2315.**
285. **Egorina, E.M., M.A. Sovershaev, and B. Osterud,** ***In-Cell Western assay: a new approach to visualize tissue factor in human monocytes.*** **Journal of Thrombosis and Haemostasis, 2006. 4: p. 614-620.**
286. **Conte, M.S.,** ***The ideal small arterial substitute: a search for the Holy Grail?*** **The FASEB Journal, 1998. 12(1): p. 43-45.**
287. **Pawlowski, K.J., et al.,** ***Endothelial Cell Seeding of Polymeric Vascular Grafts.*** **Frontiers in Bioscience, 2004. 9: p. 1412-1421.**
288. **Clowes, A.W., T.R. Kirkman, and M.A. Reidy,** ***Mechanism of Arterial Graft Healing. Rapid Transmural Capillary Ingrowth Provides a Source of Intimal Endothelium and Smooth Muscle in Porous PTFE Prostheses.*** **American Journal of Pathology, 1986. 123: p. 220-230.**
289. **McManus, M.C., et al.,** ***Electrospun fibrinogen: Feasibility as a tissue engineering scaffold in a rat cell culture model.*** **J. Biomed. Mater. Res. A, 2007. 81(2): p. 299-309.**
290. **Jin, H.-J., et al.,** ***Human bone marrow stromal cell responses on electrospun silk fibroin mats.*** **Biomaterials, 2004. 25: p. 1039-1047.**
291. **Kumbar, S.G., et al.,** ***Electrospun nanofiber scaffolds: engineering soft tissues.*** **Biomed Mater, 2008. 3(3): p. 034002.**
292. **Sell, S.A., et al.,** ***The Use of Natural Polymers in Tissue Engineering: A Focus on Electrospun Extracellular Matrix Analogues.*** **Polymers, 2010. 2(4): p. 522-553.**
293. **Chew, S.Y., et al.,** ***The role of electrospinning in the emerging field of nanomedicine.*** **Curr Pharm Des, 2006. 12(36): p. 4751-70.**
294. **Lannutti, J., et al.,** ***Electrospinning for tissue engineering scaffolds.*** **Mater. Sci. Eng. C Biomimetic Supramol. Syst., 2007. 27(3): p. 504-509.**
295. **Sill, T.J. and H.A. von Recum,** ***Electrospinning: applications in drug delivery and tissue engineering.*** **Biomaterials, 2008. 29(13): p. 1989-2006.**
296. **Nisbet, D.R., et al.,** ***Review paper: a review of the cellular response on electrospun nanofibers for tissue engineering.*** **J Biomater Appl, 2009. 24(1): p. 7-29.**
297. **Baker, B.M., et al.,** ***The potential to improve cell infiltration in composite fiber-aligned electrospun scaffolds by the selective removal of sacrificial fibers.*** **Biomaterials, 2008. 29(15): p. 2348-58.**

298. **Baker, B.M., et al., *Fabrication and modeling of dynamic multipolymer nanofibrous scaffolds.* J Biomech Eng, 2009. 131(10): p. 101012.**
299. **Sell, S.A., et al., *Preliminary investigation of airgap electrospun silk fibroin-based structures for ligament analogue engineering.* J Biomater Sci Polym Ed, 2010. In Press.**
300. **Chen, F.M., M. Zhang, and Z.F. Wu, *Toward delivery of multiple growth factors in tissue engineering.* Biomaterials, 2010. 31(24): p. 6279-308.**
301. **Sahoo, S., et al., *Growth factor delivery through electrospun nanofibers in scaffolds for tissue engineering applications.* J Biomed Mater Res A, 2010. 93(4): p. 1539-50.**
302. **Foster, T.E., et al., *Platelet-rich plasma: from basic science to clinical applications.* Am J Sports Med, 2009. 37(11): p. 2259-72.**
303. **Anitua, E., et al., *Delivering growth factors for therapeutics.* Trends Pharmacol Sci, 2008. 29(1): p. 37-41.**
304. **Alsousou, J., et al., *The biology of platelet-rich plasma and its application in trauma and orthopaedic surgery: a review of the literature.* J Bone Joint Surg Br, 2009. 91(8): p. 987-96.**
305. **Creaney, L. and B. Hamilton, *Growth factor delivery methods in the management of sports injuries: the state of play.* Br. J. Sports Med, 2008. 42: p. 314-320.**
306. **Lyras, D.N., et al., *The effect of platelet-rich plasma gel in the early phase of patellar tendon healing.* Arch Orthop Trauma Surg, 2009: p. EPUB ahead of print.**
307. **Murray, M.M., et al., *Collagen-platelet rich plasma hydrogel enhances primary repair of the porcine anterior cruciate ligament.* J Orthop Res, 2007. 25: p. 81-91.**
308. **Mishra, A. and T. Pavelko, *Treatment of chronic elbow tendinosis with buffered platelet-rich plasma.* Am J Sports Med, 2006. 34(11): p. 1774-8.**
309. **Rozman, P. and Z. Bolta, *Use of platelet growth factors in treating wounds and soft-tissue injuries.* Acta Dermatovenerol Alp Panonica Adriat, 2007. 16(4): p. 156-65.**
310. **Anitua, E., et al., *Effectiveness of autologous preparation rich in growth factors for the treatment of chronic cutaneous ulcers.* J Biomed Mater Res B Appl Biomater, 2008. 84(2): p. 415-21.**
311. **Kocaoemer, A., et al., *Human AB serum and thrombin-activated platelet-rich plasma are suitable alternatives to fetal calf serum for the expansion of mesenchymal stem cells from adipose tissue.* Stem Cells, 2007. 25(5): p. 1270-8.**
312. **Sanchez, M., et al., *Platelet-rich therapies in the treatment of orthopaedic sport injuries.* Sports Med, 2009. 39(5): p. 345-54.**
313. **El-Sharkawy, H., et al., *Platelet-rich plasma: growth factors and pro- and anti-inflammatory properties.* J Periodontol, 2007. 78(4): p. 661-9.**
314. **Everts, P.A., et al., *Platelet-rich plasma and platelet gel: a review.* J Extra Corpor Technol, 2006. 38(2): p. 174-87.**

315. **Jacobson, M., et al., *Platelets, but not erythrocytes, significantly affect cytokine release and scaffold contraction in a provisional scaffold model.* Wound Repair Regen, 2008. 16(3): p. 370-8.**
316. **Jacobs, J.M., et al., *Utilizing human blood plasma for proteomic biomarker discovery.* J Proteome Res, 2005. 4(4): p. 1073-85.**
317. **Adkins, J.N., et al., *Toward a human blood serum proteome: analysis by multidimensional separation coupled with mass spectrometry.* Mol Cell Proteomics, 2002. 1(12): p. 947-55.**
318. **Anderson, L. and N.G. Anderson, *High resolution two-dimensional electrophoresis of human plasma proteins.* Proc Natl Acad Sci U S A, 1977. 74(12): p. 5421-5.**
319. **Sahoo, S., S.L. Toh, and J.C. Goh, *A bFGF-releasing silk/PLGA-based biohybrid scaffold for ligament/tendon tissue engineering using mesenchymal progenitor cells.* Biomaterials, 2010. 31(11): p. 2990-8.**
320. **McManus, M., et al., *Electrospun nanofibre fibrinogen for urinary tract tissue reconstruction.* Biomedical Materials, 2007. 2(4): p. 257-262.**
321. **McManus, M.C., et al., *Mechanical properties of electrospun fibrinogen structures.* Acta Biomater, 2006. 2: p. 19-28.**
322. **Bashur, C.A., L.A. Dahlgren, and A.S. Goldstein, *Effect of fiber diameter and orientation on fibroblast morphology and proliferation on electrospun poly(D,L-lactic-co-glycolic acid) meshes.* Biomaterials, 2006. 27: p. 5681-5688.**
323. **Francis, M.P., et al., *Isolating adipose-derived mesenchymal stem cells from lipoaspirate blood and saline fraction.* Organogenesis, 2010. 6(1): p. 1-4.**
324. **Kevy, S.V. and M.S. Jacobson, *Comparison of methods for point of care preparation of autologous platelet gel.* J Extra Corpor Technol, 2004. 36(1): p. 28-35.**
325. **Boland, E.D., et al., *Tailoring tissue engineering scaffolds using electrostatic processing techniques: A study of poly(glycolic acid) electrospinning.* J Macromol Sci, 2001. A38(12): p. 1231-1243.**
326. **Moroni, L., et al., *Fiber diameter and texture of electrospun PEOT/PBT scaffolds influence human mesenchymal stem cell proliferation and morphology, and the release of incorporated compounds.* Biomaterials, 2006. 27: p. 4911-4922.**
327. **Sun, X.-Y., et al., *Field-Driven Surface Segregation of Biofunctional Species on Electrospun PMMA/PEO Microfibers.* Macromolecular Rapid Communications, 2008. 29: p. 1455-1460.**
328. **Chiu, J.B., et al., *Functionalization of poly(L-lactide) nanofibrous scaffolds with bioactive collagen molecules.* Journal of Biomedical Materials Research, 2007. 83A: p. 1117-1127.**
329. **Sun, X.-Y., et al., *Field-Driven Biofunctionalization of Polymer Fiber Surfaces during Electrospinning.* Advanced Materials, 2007. 19: p. 87-91.**
330. **McDonagh, J., et al., *Molecular Weight Analysis of Fibrinogen and Fibrin Chains by an Improved Sodium Dodecyl Sulfate Gel Electrophoresis Method.* Biochimica et Biophysica Acta, 1972. 257: p. 135-142.**

331. **Hirayama, K., et al., *Rapid Confirmation and Revision of the Primary Structure of Bovine Serum Albumin by ESIMS and FRIT-FAB LC/MS.* Biochemical and Biophysical Research Communications, 1990. 173(2): p. 639-646.**

332. **Feng, R., Y. Konishi, and A.W. Bell, *High Accuracy Molecular Weight Determination and Variation Characterization of Proteins Up To 80 ku by Ionspray Mass Spectrometry.* Journal of American Society of Mass Spectrometry, 1991. 2: p. 387-401.**

333. **Aliberti, G., et al., *Association between fibrinogen plasma levels and platelet counts in an outpatient population and in patients with coronary heart disease.* Blood Coagulation and Fibrinolysis, 2010. 21: p. 216-220.**

334. **Man, D., H. Plosker, and J.E. Winland-Brown, *The Use of Autologous Platelet-Rich Plasma (Platelet Gel) and Autologous Platelet-Poor Plasma (Fibrin Glue) in Cosmetic Surgery.* Plastic and Reconstructive Surgery, 2001. 107: p. 229-237.**

335. **Barnes, C.P., et al., *Feasibility of electrospinning the globular protiens hemoglobin and myoglobin.* Journal of Engineered Fibers and Fabrics, 2006. 1(2): p. 16-29.**

336. **Lu, H.H., et al., *Controlled delivery of platelet-rich plasma-derived growth factors for bone formation.* J Biomed Mater Res A, 2008. 86(4): p. 1128-36.**

337. **Bir, S.C., et al., *Angiogenic properties of sustained release platelet-rich plasma: characterization in-vitro and in the ischemic hind limb of the mouse.* J Vasc Surg, 2009. 50(4): p. 870-879 e2.**

338. **Pietramaggiori, G., et al., *Freeze-dried platelet-rich plasma shows beneficial healing properties in chronic wounds.* Wound Repair Regen, 2006. 14(5): p. 573-80.**

339. **Pietramaggiori, G., et al., *Trehalose lyophilized platelets for wound healing.* Wound Repair Regen, 2007. 15(2): p. 213-20.**

340. **Pietramaggiori, G., et al., *Healing modulation induced by freeze-dried platelet-rich plasma and micronized allogenic dermis in a diabetic wound model.* Wound Repair Regen, 2008. 16(2): p. 218-25.**

341. **Sum, R., et al., *Wound-healing properties of trehalose-stabilized freeze-dried outdated platelets.* Transfusion, 2007. 47(4): p. 672-9.**

342. **Luong-Van, E., et al., *Controlled release of heparin from poly(ε-caprolactone) electrospun fibers.* Biomaterials, 2006. 27: p. 2042-2050.**

343. **Mohamed, M.S., M. Mukherjee, and V.V. Kakkar, *Thrombogenicity of heparin and non-heparin bound arterial prostheses: an in vitro evaluation.* Journal of the Royal College of Surgeons of Edinburgh, 1998. 43(3): p. 155-157.**

344. **Wolfe, P.S., et al., *The Creation of Electrospun Nanofibers from Platelet-Rich Plasma.* Biomed Mater, 2010. In Review.**

345. **McManus, M.C., et al., *Electrospun fibrinogen-polydioxanone composite matrix: Potential for in situ urologic tissue engineering.* Journal of Engineered Fibers and Fabrics, 2008. 3(2): p. 12-21.**

346. Fung, Y.C., *Blood Flow in Arteries*, in *Biodynamics: Circulation*. 1984, Springer-Verlag: New York.
347. Hiroshi, Y., *Strength of biological materials*. 1970, New York: Robert E. Krieger Publishing Company.
348. Catanese, J., 3rd, et al., *Mechanical properties of medical grade expanded polytetrafluoroethylene: the effects of internodal distance, density, and displacement rate.* J Biomed Mater Res, 1999. 48(2): p. 187-92.
349. *Guideline on Validation of the Limulus Amebocyte Lysate Test as an End-Product Endotoxin Test for Human and Animal Parenteral Drugs, Biological Products and Medical Devices*. 1987, U.S. Department of Health and Human Services, FDA.
350. Cheng, M., et al., *Platelets and plasma proteins are both required to stimulate collagen gene expression by anterior cruciate ligament cells in three-dimensional culture.* Tissue Eng Part A, 2010. 16(5): p. 1479-89.
351. Gassling, V.L., et al., *Platelet-rich plasma and platelet-rich fibrin in human cell culture.* Oral Surg Oral Med Oral Pathol Oral Radiol Endod, 2009. 108(1): p. 48-55.
352. Kakudo, N., et al., *Proliferation-promoting effect of platelet-rich plasma on human adipose-derived stem cells and human dermal fibroblasts.* Plast Reconstr Surg, 2008. 122(5): p. 1352-60.
353. Lei, H., et al., *Evaluation of the efficacy of platelet-rich plasma in delivering BMSCs into 3D porous scaffolds.* J Biomed Mater Res B Appl Biomater, 2009. 91(2): p. 679-91.
354. Lucarelli, E., et al., *Platelet-derived growth factors enhance proliferation of human stromal stem cells.* Biomaterials, 2003. 24(18): p. 3095-100.
355. Mishra, A., et al., *Buffered platelet-rich plasma enhances mesenchymal stem cell proliferation and chondrogenic differentiation.* Tissue Eng Part C Methods, 2009. 15(3): p. 431-5.
356. Vogel, J.P., et al., *Platelet-rich plasma improves expansion of human mesenchymal stem cells and retains differentiation capacity and in vivo bone formation in calcium phosphate ceramics.* Platelets, 2006. 17(7): p. 462-9.
357. Uebersax, L., H.P. Merkle, and L. Meinel, *Biopolymer-based growth factor delivery for tissue repair: from natural concepts to engineered systems.* Tissue Eng Part B Rev, 2009. 15(3): p. 263-89.
358. Chew, S.Y., et al., *Sustained release of proteins from electrospun biodegradable fibers.* Biomacromolecules, 2005. 6(4): p. 2017-2024.
359. Zhang, G. and L.J. Suggs, *Matrices and scaffolds for drug delivery in vascular tissue engineering.* Adv Drug Deliv Rev, 2007. 59(4-5): p. 360-73.
360. Chung, H.J. and T.G. Park, *Surface engineered and drug releasing pre-fabricated scaffolds for tissue engineering.* Adv Drug Deliv Rev, 2007. 59(4-5): p. 249-62.
361. Wolfe, P.S., et al., *The Creation of Electrospun Nanofibers from Platelet-Rich Plasma.* J Tissue Sci Eng, 2011. 2(2).
362. Johnson, P.J., et al., *Maintaining bioactivity of NGF for controlled release from PLGA using PEG.* J Biomed Mater Res A, 2008. 86(2): p. 420-7.

363. **Nimni, M.E., *Polypeptide growth factors: targeted delivery systems.* Biomaterials, 1997. 18(18): p. 1201-25.**
364. **Ratner, B.D. and S.J. Bryant, *Biomaterials: Where we have been and where we are going.* Annual Review of Biomedical Engineering, 2004. 6: p. 41-75.**
365. **Stout, R.D. and J. Suttles, *Functional plasticity of macrophages: reversible adaptation to changing microenvironments.* Journal of Leukocyte Biology, 2004. 76: p. 509-513.**
366. **Mosser, D.M., *The many faces of macrophage activation.* Journal of Leukocyte Biology, 2003. 73: p. 209-212.**
367. **Gordon, S. and P.R. Taylor, *Monocyte and Macrophage Heterogeneity.* Nature Reviews: Immunology, 2005. 5: p. 953-964.**
368. **Stout, R.D., et al., *Macrophages sequentially change their functional phenotype in response to changes in microenvironmental influences.* Journal of Immunology, 2005. 175(1): p. 342-349.**
369. **Mantovani, A., et al., *The chemokine system in diverse forms of macrophage activation and polarization.* TRENDS in Immunology, 2004. 25(12): p. 677-686.**
370. **Brown, B.N., et al., *Macrophage phenotype and remodeling outcomes in response to biologic scaffolds with and without a cellular component.* Biomaterials, 2009. 30(8): p. 1482-1491.**
371. **Badylak, S.F., et al., *Macrophage phenotype as a determinant of biologic scaffold remodeling.* Tissue Engineering Part A, 2008. 14(11): p. 1835-1842.**
372. **Stout, R.D. and J. Suttles, *T Cell Signaling of Macrophage Function in Inflammatory Disease.* Frontiers in Bioscience, 1997. 2: p. d197-206.**
373. **Classen, A., J. Lloberas, and A. Celada, *Chapter 3: Macrophage Activation: Classical vs. Alternative,* in *Macrophages and Dendritic Cells, Methods in Molecular Biology,* N.E. Reiner, Editor. 2009, Humana Press, a part of Springer Science + Business Media. p. 29-43.**
374. **Varin, A. and S. Gordon, *Alternative activation of macrophages: Immune function and cellular biology.* Immunobiology, 2009. 214: p. 630-641.**
375. **Chamberlain, L.M., et al., *Phenotypic non-equivalence of murine (monocyte-) macrophage cells in biomaterial and inflammatory models.* Journal of Biomedical Materials Research, 2009. 88A: p. 858-871.**
376. **Porcheray, F., et al., *Macrophage activation switching: an asset for the resolution of inflammation.* Clin Exp Immunol, 2005. 142(3): p. 481-9.**
377. **Vernon, R.B. and E.H. Sage, *A Novel, Quantitative Model for Study of Endothelial Cell Migration and Sprout Formation within Three-Dimensional Collagen Matrices.* Microvascular Research, 1999. 57: p. 118-133.**
378. **Polykandriotis, E., et al., *Autonomously vascularized cellular constructs in tissue engineering: opening a new perspective for biomedical science.* Journal Of Cellular And Molecular Medicine, 2007. 11(1): p. 6-20.**
379. **Crowther, M., et al., *Microenvironmental influence on macrophage regulation of angiogenesis in wounds and malignant tumors.* Journal of Leukocyte Biology, 2001. 70(4): p. 478-490.**

380. Chen, Z., et al., *In vitro angiogenesis by human umbilical vein endothelial cells (HUVEC) induced by three-dimensional co-culture with glioblastoma cells.* Journal of Neurooncology, 2009. 92: p. 121-128.
381. Pepper, M., *Transforming Growth Factor-beta: Vasculogenesis, Angiogenesis, and Vessel Wall Integrity.* Cytokine and Growth Factor Reviews, 1997. 8(1): p. 21-43.
382. Orlidge, A. and P.A. D'Amore, *Cell Specific Effects of Glycosaminoglycans on the Attachment and Proliferation of Vascular Wall Components.* Microvascular Research, 1986. 31: p. 41-53.
383. Greisler, H.P., et al., *Biointeractive polymers and tissue engineered blood vessels.* Biomaterials, 1996. 17: p. 329-336.
384. Thornton, S.C., S.N. Mueller, and E.M. Levine, *Human endothelial cells: use of heparin in cloning and long-term serial cultivation.* Science, 1983. 222(4624): p. 623-625.
385. Anitua, E., et al., *Fibroblastic response to treatment with different preparations rich in growth factors.* Cell Prolif, 2009. 42(2): p. 162-70.
386. Seimon, T. and I. Tabas, *Mechanisms and consequences of macrophage apoptosis in atherosclerosis.* J Lipid Res, 2009. 50 Suppl: p. S382-7.
387. Blanton, M.W., et al., *Adipose Stromal Cells and Platelet-Rich Plasma Therapies Synergistically Increase Revascularization during Wound Healing.* Plastic and Reconstructive Surgery, 2009. 123: p. 56S-64S.
388. Frechette, J.P., I. Martineau, and G. Gagnon, *Platelet-rich Plasmas: Growth Factor Content and Roles in Wound Healing.* Journal of Dental Research, 2005. 84(5): p. 434-439.
389. Lin, P.H., et al., *Evaluation of Platelet Deposition and Neointimal Hyperplasia of Heparin-Coated Small-Caliber ePTFE Grafts in a Canine Femoral Artery Bypass Model.* Journal of Surgical Research, 2004. 118: p. 45-52.
390. Cai, W.W., et al., *Heparin coating of small-caliber decellularized xenografts reduces macrophage infiltration and intimal hyperplasia.* Artificial Organs, 2009. 33(6): p. 448-455.
391. Visser, L.C., et al., *Growth Factor-Rich Plasma Increases Tendon Cell Proliferation and Matrix Synthesis on a Synthetic Scaffold: An In Vitro Study.* Tissue Eng Part A, 2009.
392. Maderna, P. and C. Godson, *Themed Section: Mediators and Receptors in the Revolution of Inflammation Review. Lipoxins: resolutionary road.* British Journal of Pharmacology, 2009. 158: p. 947-959.
393. Mehta, S. and J.T. Watson, *Platelet Rich Concentrate: Basic Science and Current Clinical Applications.* Journal of Orthopaedic Trauma, 2008. 22(6): p. 433-438.
394. Bernuzzi, G., et al., *Platelet gel in the treatment of cutaneous ulcers: the experience of the Immunohaematology and Transfusion Centre of Parma.* Blood Transfus, 2010. 8(4): p. 237-47.
395. Senet, P., et al., *Randomized trial and local biological effect of autologous platelets used as adjuvant therapy for chronic venous leg ulcers.* J Vasc Surg, 2003. 38(6): p. 1342-8.

396. **Chen, T.M., J.C. Tsai, and T. Burnouf,** ***A novel technique combining platelet gel, skin graft, and fibrin glue for healing recalcitrant lower extremity ulcers.*** **Dermatol Surg, 2010. 36(4): p. 453-60.**
397. **Altman, G.H., et al.,** ***Silk matrix for tissue engineered anterior cruciate ligaments.*** **Biomaterials, 2002. 23: p. 4131-4141.**
398. **Sell, S.A., et al.,** ***Electrospun polydioxanone-elastin blends: potential for bioresorbable vascular grafts.*** **Biomedical Materials, 2006. 1(2): p. 72-80.**
399. **Scevola, S., et al.,** ***Allogenic platelet gel in the treatment of pressure sores: a pilot study.*** **Int Wound J. 7(3): p. 184-90.**

Appendix A: Incorporating Platelet-Rich Plasma into Electrospun Scaffolds for Tissue Engineering Applications

Scott A. Sell[1, 2*], Patricia S. Wolfe[2*], Jeffery J. Ericksen[1, 3], David G. Simpson[4], and Gary L. Bowlin[2#]

[1]Physical Medicine & Rehabilitation Service, Hunter Holmes McGuire VA Medical Center, Richmond, VA 23249
[2]Department of Biomedical Engineering, Virginia Commonwealth University, Richmond, VA 23284
[3]Department of Physical Medicine and Rehabilitation, Virginia Commonwealth University, Richmond, VA 23298
[4]Department of Anatomy and Neurobiology, Virginia Commonwealth University, Richmond, VA 23298

[*]Authors contributed equally

[#]Address correspondence to:
Dr. Gary L. Bowlin
Department of Biomedical Engineering
Virginia Commonwealth University
P.O. Box 843067
Richmond, VA 23284
Email: glbowlin@vcu.edu

Abstract

Platelet-rich plasma (PRP) therapy has seen a recent spike in clinical interest due to the potential that the highly concentrated platelet solutions hold for stimulating tissue repair and regeneration. The purpose of this study was to incorporate PRP into a number of electrospun materials to determine how growth factors are eluted from the structures,

and what affect the presence of these factors have on enhancing electrospun scaffold bioactivity. PRP underwent a freeze-thaw-freeze process to lyse platelets, followed by lyophilization to create a powdered preparation rich in growth factors (PRGF), which was subsequently added to the electrospinning process. Release of protein from scaffolds over time was quantified, along with the quantification of human macrophage and adipose derived stem cell (ADSC) chemotaxis and proliferation. Protein assays demonstrated a sustained release of protein from PRGF containing scaffolds at up to 35 days in culture. Scaffold bioactivity was enhanced as ADSCs demonstrated increased proliferation in the presence of PRGF, while macrophages demonstrated increased chemotaxis to PRGF. The incorporation of PRGF into electrospun structures has a significant positive influence on the bioactivity of the scaffolds, and may prove beneficial in a number of tissue engineering applications.

Introduction

Platelet-rich plasma (PRP) therapy is a method of collecting and concentrating autologous platelets, through centrifugation and isolation, for the purpose of activating and releasing their growth factor-rich α- and dense granules. The discharge of these concentrated granules releases a number of growth factors and cytokines in physiologically relevant ratios, albeit in concentrations several times higher than that of normal blood, that are critical to tissue regeneration and cellular recruitment. Some of the more highly concentrated factors found within PRP include platelet derived growth factor (PDGF), transforming growth factor-β (TGF-β), vascular endothelial growth factor (VEGF), fibroblast growth factor (FGF), and epidermal growth factor (EGF) [302, 304, 305, 309, 312-314]. In addition, PRP has also been shown to contain a number of

macrophage and monocyte mediators such as RANTES (Regulated upon Activation, Normal T-cell Expressed, and Secreted), lipoxin, and an array of interleukins [313].

Clinically, PRP therapy has been used to stimulate tissue growth and regeneration in a number of different tissues; effectively accelerating the healing response in patients suffering from osteochondral defects [302-304], tendon/ligament injuries [302-308], and chronic skin wounds (diabetic and pressure ulcers) [303, 304, 309, 310]. Typically, these procedures involve a blood draw and centrifugation to concentrate the platelet portion, followed by a platelet activation step and the delivery of the activated PRP to the site of injury. There have been several methods reported in the literature on successfully activating and delivering PRP to an injury site, with most involving the creation of a platelet gel using thrombin [302-304, 311] or $CaCl_2$ [302-304, 312]. These PRP gels can be easily applied to wound sites through injection or topical application.

However, studies have shown that the use of thrombin as a clotting agent can result in a rapid activation of platelets and a bolus release of growth factors, with 70% of growth factors released within 10 minutes of clotting, and nearly 100% released within 1 hour [302]. This "dumping" method fails to maximize the cell stimulating potential of the PRP growth factors as most are cleared before they can take effect [336]. Growth factor release from PRP gels can be slowed when the gel is formed with $CaCl_2$ rather than thrombin. The addition of $CaCl_2$ to PRP results in the formation of autogenous thrombin from prothrombin and the eventual formation of a loose fibrin matrix that will secrete growth factors over 7 days [302].

Other techniques have been evaluated for further sustaining the release of growth factors from PRP and include the use of gelatin gel microspheres [337], lyophilized PRP

[338-341], and alginate beads [336]. The injection of PRP gelatin gel microspheres in a mouse ischemic hind limb model demonstrated sustained release of the PRP potent angiogenic components as illustrated by an increase in perfusion, capillary density, and mature blood vessel density [337]. Alginate beads were shown to be successful in delivering (based on cell proliferation) PRP-derived growth factors and cytokines over the course of 14 days [336]. The use of freeze-dried PRP in a dermal wound has been shown to significantly increase cellular proliferation (up to 21 days), tissue regeneration and angiogenesis in a mouse dermal wound [338-341]. Collectively, these studies demonstrate the importance of keeping PRP-derived growth factors and cytokines in the wound site and slowly releasing them as the wound site becomes infiltrated with reparative cells.

While a number of individual growth factors and/or cytokines have been used previously in an array of sustained release tissue engineering and regenerative medicine applications with positive results, the use of either single or multiple isolated growth factors/cytokines is often prohibitively expensive, and it can be difficult to replicate physiologically relevant quantities [302]. The purpose of this study was to attempt to harness the reparative potential found in PRP, namely the growth factor and cytokine milieu contained within, and apply it to tissue engineering through the creation of a PRP eluting electrospun scaffold. It was hypothesized that the inclusion of lysed and lyophilized PRP would create an effective preparation rich in growth factors (PRGF) capable of being introduced into the electrospinning process to create a scaffold with enhanced bioactivity capable of a sustained release of growth factors.

Materials and Methods

Creation of PRP and PRGF

Fresh human whole blood from 3 donors was purchased (Biological Specialty Corp.), pooled, and used in a SmartPREP® 2 (Harvest Technologies Corp.) centrifugation system to create PRP per manufacturers protocol. A small aliquot of both pooled whole blood and PRP were sent to the Harvard Immune Disease Institute's Blood Research laboratory to determine their respective platelet concentrations. PRP was then subjected to a freeze-thaw-freeze (FTF) cycle in a -70° C freezer for cell lysis and activation. Centrifuge tubes containing PRP were placed in a -70° C freezer for 24 hrs followed by a 37° C waterbath for 1 hr, and then returned to the -70° C freezer for 24 hrs. The degree of activation of the FTF lysed PRP, and thrombin (Recothrom, ZymoGenetics Inc.) and 10% $CaCl_2$ (American Regent) activated PRPs was quantified through an enzyme-linked immunosorbent assay (ELISA) analysis of VEGF and bFGF (Antigenix America Inc.). Frozen PRP was then lyophilized for 24 hrs to create a dry PRGF powder which was finely ground in a mortar and pestle prior to use.

Chemotactic Effect of PRGF on Macrophages

To determine the role that powdered PRGF had on human macrophage chemotaxis, and to demonstrate that lyophilized PRGF retained viable chemotactic proteins, PRGF was dissolved in macrophage serum-free media (MSFM, Invitrogen) in a range of concentrations (0, 0.01, 0.1, 1, 5, and 10 mg/ml). Using a 24-well Transwell plate with 8 µm diameter pores (Corning, Inc.), 600 µl of PRGF containing media was placed in the bottom wells, while the top insert was seeded with 100,000 human peripheral blood macrophages (ATCC, CRL9855) in 150 µl of control media for 18 hours (n=3). Following the 18 hour duration, the bottom wells were aspirated and the

average cell number was determined through the use an automated cell counter (Invitrogen Countess).

Creation of PRGF Eluting Electrospun Scaffolds

Scaffolds used in this study consisted of SF (extracted from *bombyx morii* silkworm cocoons[299, 397]), PGA (Alkermes), and PCL (Lakeshore Biomaterials, 125 kDa). Each of these materials was dissolved in HFIP (TCI America Inc.) at a concentration of 100 mg/ml to create the solutions used in the electrospinning process. These materials were chosen as they are three commonly used biomaterials that have been well characterized, and have well known degradation characteristics.

To each of these electrospinning solutions PRGF was added in concentrations of 10 or 100 mg of PRGF per ml of electrospinning solution (SF:PRGF(10), PGA:PRGF(10), and PCL:PRGF(10) and SF:PRGF(100), PGA:PRGF(100), and PCL:PRGF(100), respectively) and allowed to dissolve completely into solution. As PRGF can be successfully electrospun by itself from HFP at a concentration of 200 mg/ml[344], PRGF fibers were also integrated into PCL scaffolds using two additional electrospinning techniques: 1) a 2 input-1output nozzle that mixed separate PCL and PRGF solutions only at the outlet tip as electrospinning occurred (PCL:PRGF(2-1)) and 2) using two separate syringes of PCL and PRGF electrospinning solutions at 90° from each other targeting the same collection mandrel (PCL:PRGF). Both the PCL:PRGF(2-1) and PCL:PRGF scaffolds consisted of a 1:1 volume ratio of PCL:PRGF solution. Control scaffolds contained no PRGF.

Processing parameters varied with the polymer, while all solutions were electrospun onto a grounded rectangular stainless steel mandrel (1.9 cm wide x 7.5 cm

long x 0.5 cm thick) rotating at 400 RPM and translating at 6 cm/s over a distance of 12 cm, using a Becton Dickinson syringe fitted with a blunt tip 18 gauge needle and a KD Scientific syringe pump. SF solutions were electrospun using a charging voltage of +25 kV, an air gap distance of 15 cm, and a flowrate of 4 ml/hr. PGA and PCL solutions were electrospun using a charging voltage of +22 kV, an air gap distance of 15 cm, and a flowrate of 6 ml/hr. PCL:PRGF(2-1) used a charging voltage of +30 kV placed on the end of the output nozzle, an air gap distance of 15 cm, and a flowrate of 2.5 ml/hr. PCL:PRGF used charging voltages of +25 and +27 kV for the PCL and PRGF solutions, respectively, an air gap distance of 15 cm from each syringe to the collecting mandrel, and a flowrate of 2.5 ml/hr for each solution.

Characterization of Electrospun Structures

Dry, representative samples from each of the electrospun scaffolds was characterized through scanning electron microscopy (SEM, Zeiss EV050) to ensure the fibrous nature of the structures. Average fiber diameters and pore areas were calculated by taking 60 random fiber measurements/pore measurements from across the SEM image using ImageTool 3.0 software (Shareware provided by UTHSCSA).

Uniaxial tensile testing was performed on a set of representative dog-bone shaped samples (overall length of 20 mm, 2.67 mm at its narrowest point, gage length of 7.5 mm, n=5) punched from each of the materials electrospun. All specimens were soaked for 4 hours in DI water prior to testing, with all SF samples first being soaked in ethanol for 30 minutes to promote beta sheet formation. Samples were then uniaxially tested to failure at a rate of 10 mm/min (1.33 min^{-1} strain rate) using an MTS Bionix 200 testing system

with a 100 N load cell (MTS Systems Corp.). Peak stress, modulus, and strain at break were calculated using TestWorks version 4.

Evaluation of Cell Interaction

To determine the response of human cells on the PRGF containing scaffolds, 10 mm diameter disks from each electrospun scaffold were punched, disinfected (30 minute soak in ethanol followed by three 10 minute rinses in PBS), and placed in a 48-well plate. Each scaffold had a sterile Pyrex cloning ring (10 mm outer diameter, 8 mm inner diameter) placed on top to keep the scaffolds from floating, and to ensure that all cells stayed on the surface of the scaffold during culture. Each scaffold was then seeded with 50,000 human adipose derived stem cells (ADSC) in 500 µl of culture media (DMEM low glucose, 10% FBS, 1% penicillin/streptomycin, Invitrogen). Media was changed every third day, and samples were removed from culture and fixed in buffered formalin on days 7 and 21 for Hematoxylin and Eosin (H&E) staining.

Quantification of Protein Release Kinetics

From each electrospun material 10 mm diameter disks were punched (n=3), disinfected (30 minute soak in ethanol followed by three 10 minute rinses in PBS), and placed in a 48-well plate with 500 µl of PBS. The PBS was changed and retained for evaluation on days 1, 4, 7, 10, 14, 21, 28, and 35. Samples at each time point were subjected to a generic protein assay (BCA Protein Assay, Thermo Scientific Pierce) to quantify the concentration of total protein released. Based upon these results, specific ELISAs were run on the retained samples (days 1, 4, 7, 10, 14, and 21) to detect proteins found in high concentrations in PRP, RANTES, PDGF-BB (Antigenix America Inc.), and

TGF-β (Promega Corp.), to demonstrate that it was in fact PRGF being eluted from the scaffolds.

Released PRGF Effect on Cell Proliferation

To determine the mitogenic potential of the PRGF released from the electrospun scaffolds on both ADSCs and macrophages, 10 mm diameter disks of each electrospun material were punched, disinfected (30 minute soak in ethanol followed by three 10 minute rinses in PBS), and placed in a 48-well plate (n=3). Each well was then seeded with 300,000 human peripheral blood macrophages (ATCC, CRL9855) in 500 µl MSFM, as well as in a control tissue culture polystyrene (TCPS) well containing MSFM with 1 mg/ml PRGF added (TCPS:PRGF). The macrophage conditioned media was removed daily and used as a supplement to feed ADSCs (200 µl MSFM with 300 µl ADSC media) cultured on TCPS (25,000 cells/well) in a separate 48-well plate. On days 1, 4, and 7 media was removed from the wells containing macrophages and replaced with 300 µl trypsin to remove macrophages for counting. After 5 minutes trypsin was deactivated with 300 µl MSFM, pipetted up and down gently several times, and the suspended macrophages were counted using an automated cell counter (Invitrogen Countess). ADSC proliferation was analyzed using an MTS Assay (Promega) at days 1, 4, and 7.

This study was then replicated without the use of macrophage conditioned media to isolate the impact of the released PRGF on ADSC proliferation. That is, disinfected 10 mm diameter disks of each electrospun material were placed in a 48-well plate with 500 µl ADSC culture media. Media was removed daily and used as a supplement to feed ADSCs cultured at 25,000 cells/well in a separate 48-well plate. ADSC proliferation was determined with an MTS Assay (Promega) at days 1, 4, and 7.

Statistical Analysis

All statistical analysis was based on a Kruskal–Wallis one-way ANOVA on ranks and a Tukey–Kramer pairwise multiple comparison procedure ($\alpha = 0.05$) performed with the JMP®IN 8.0 statistical software package (SAS Institute, Inc.). Graphical depictions of mean data were constructed with Microsoft Excel 2007, with error bars representing standard deviations.

Results

Creation of PRP and PRGF

Based upon the platelet counts performed at the Harvard Immune Disease Institute's Blood Research laboratory, it was determined that the pooled whole blood used for this study contained 175 x 10^3 platelets/µl, while the PRP created with the SmarPReP^2 system yielded 955 x 10^3 platelets/µl. This 5.5 fold increase in platelets is consistent with published data[324], and should result in a similar fold increase in growth factor concentration based upon the linear relationship between platelet and growth factor concentration [315].

The results of the bFGF and VEGF ELISAs (Figure 1) reveal the FTF method of activation, essentially lysing platelets to release their α and dense granule contents, to be as effective, if not more so, than the traditional PRP activation techniques of thrombin and $CaCl_2$ for releasing growth factors. The FTF activation method resulted in average growth factor concentrations of 0.4 ng/ml for bFGF, and 1.6 ng/ml for VEGF. Using the traditional $CaCl_2$ and thrombin activation methods bFGF values were 0.8 and 0 ng/ml, respectively, while the VEGF values were 0.3 and 0.7 ng/ml, respectively. While there

were few statistical differences between the different methods in the bFGF ELISA, with only the $CaCl_2$ activated different from the thrombin activated, the VEGF ELISA results demonstrated clearly that the FTF method was significantly greater than the other activation methods. It should be noted that the thrombin activation method resulted in an instantaneous gel, making it difficult to obtain liquid samples for ELISA analysis. The $CaCl_2$ activated PRP contained visible floating thrombi, but was mostly liquidous, while the FTF activated PRP was completely liquid with no evidence of thrombus formation.

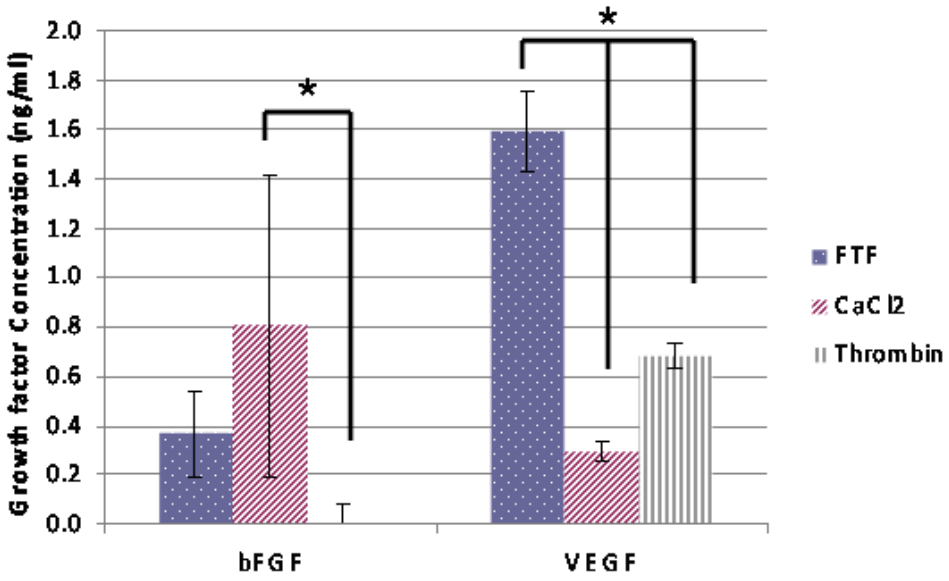

Figure 1. Results of PRP activation method on bFGF and VEGF concentration. * indicates significant differences between activation methods, $p < 0.05$. Minimum levels of detection for bFGF and VEGF were 0.11ng/ml and 0.059 ng/ml..

Chemotactic Effect of PRGF on Macrophages

The results of macrophage chemotaxis in response to a dose of PRGF dissolved in MSFM are shown in Figure 2. Macrophage chemotaxis increased with the amount of PRGF until the concentration of 1 mg/ml, above which it became significantly reduced. While a nice trend is apparent, the only value that was significantly different from the

group was the 1 mg/ml PRGF concentration, potentially indicating an ideal concentration for stimulating macrophage chemotaxis. It should be noted that the addition of powdered PRGF to MSFM resulted in a complete gel at 10 mg/ml, and a partial gel at 5 mg/ml. This resulting gelation may have had a negative impact on macrophage chemotaxis; however, it does indicate a reserve of active fibrinogen contained within the powdered PRGF capable of forming a clot in the presence of the Ca^{2+} found in the MSFM.

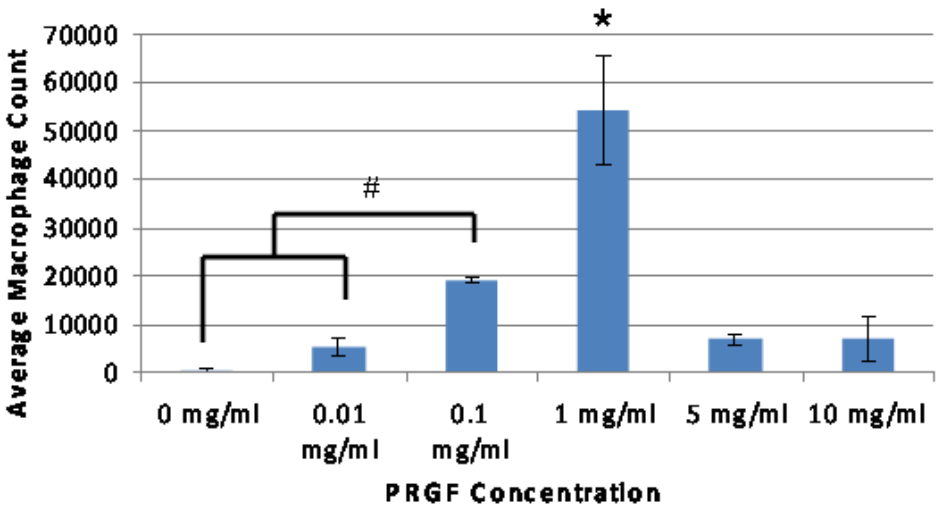

Figure 2. Results of macrophage chemotaxis in response to PRGF dose. * indicates statistically significant differences, $p < 0.05$, between the 1 mg/ml concentration and all other groups. # indicates statistically significant differences, $p < 0.05$, between 0.1 mg/ml and lower concentrations.

Characterization of Electrospun Structures

The results of the electrospun scaffold SEM characterization are shown in Figure 3. These SEMs demonstrate the fibrous nature of each of the electrospun scaffolds, both with and without PRGF. Mean fiber diameters for these scaffolds ranged from 0.5 µm for PGA:PRGF(10) to 5.8 µm for SF:PRGF(100). With the exception of the SF:PRGF(100), there were no significant differences in mean fiber diameter between the control scaffolds and the PRGF containing scaffolds. Somewhat surprisingly, the inclusion of PRGF had

no real impact on the average size of the electrospun fibers, although it does appear that with the inclusion of high concentrations of PRGF and in the PCL:PRGF(2-1) and PCL:PRGF scaffolds there are a number of extremely small diameter fibers. Disregarding the SF scaffolds, this potential divergent population of PRGF fibers and synthetic polymer fibers may be evident through the rather large standards of deviation determined for those structures. Additionally, those same scaffolds appeared to exhibit an increase in void space visible in the SEMs as PRGF content was increased. Average pore areas (Fig. 3) were found to correlate to average fiber diameters: as fiber diameter increased, pore area increased. This phenomenon has been well documented in previous electrospinning studies (25-27). The addition of 100 mg/ml PRGF to SF and PGA resulted in significantly increased pore areas over the control and 10 mg/ml PRGF-containing samples, whereas the only difference seen in the PCL structures was between the PCL:PRGF(2-1) and the PCL:PRGF(100), PCL:PRGF(10), and PCL control scaffolds.

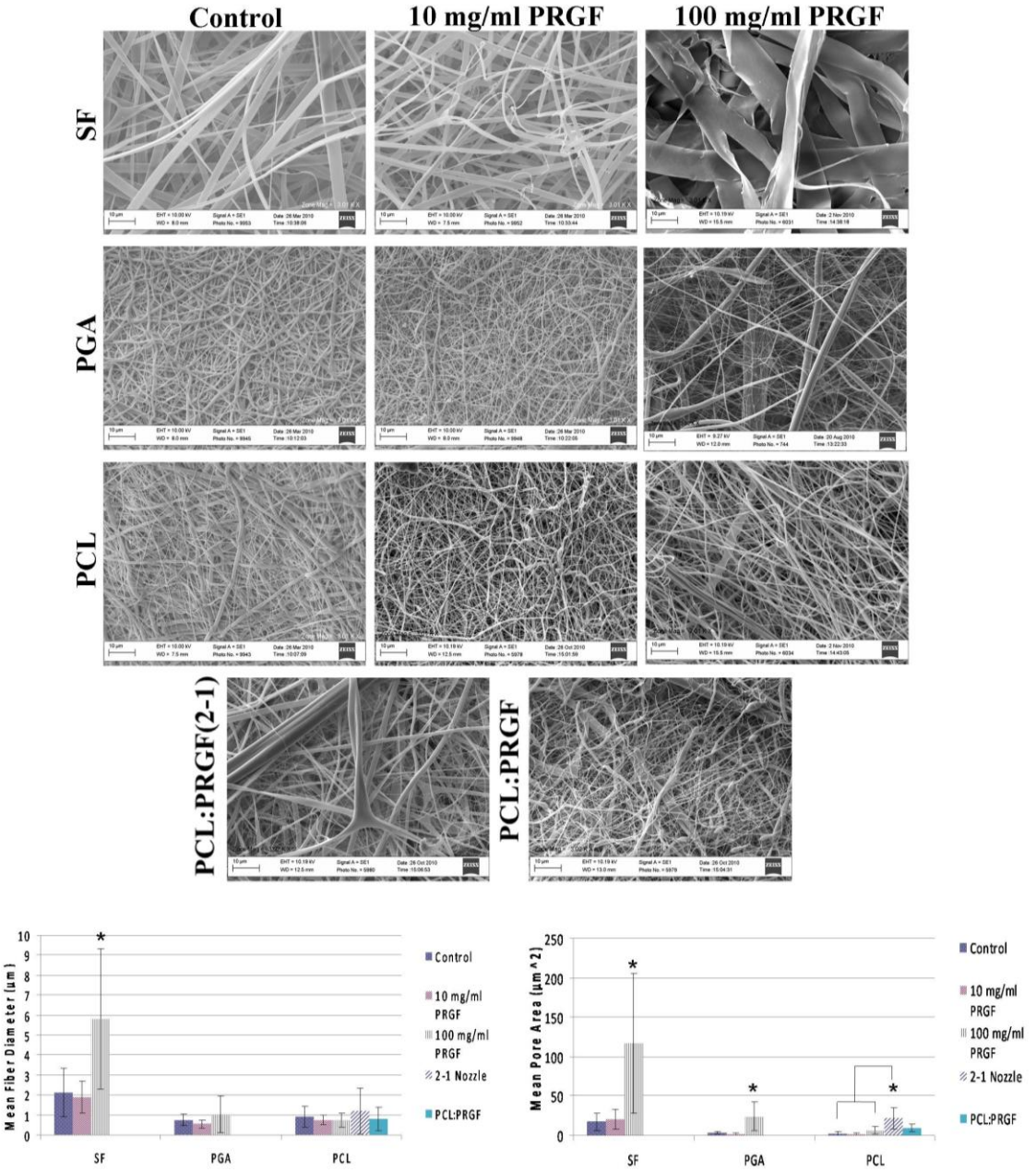

Figure 3. (Top) SEM micrographs of electrospun SF, PGA, and PCL scaffolds with and without PRGF. All images were taken at 3,000x, scale bar is 10 µm. (Bottom Left) Graph of mean fiber diameters for SF, PGA, and PCL scaffolds with and without PRGF. (Bottom Right) Graph of mean pore areas for SF, PGA, and PCL scaffolds with and without PRGF. * indicates significant differences within polymer group, $p < 0.05$.

The results of the scaffold uniaxial tensile testing are shown in Figure 4. Mean peak stresses ranged from 0.2 MPa for PGA+100 to 5.2 MPa for PGA control, moduli ranged from 0.9 MPa for SF+100 to 21.4 MPa for PGA control, while average strain at break values ranged from 25.4% for PGA+100 to 112.8% for PGA control. In general, mechanical properties were shown to decrease significantly as PRGF concentration increased compared to values achieved for the PRGF-free control scaffolds. With the exception of the PCL:PRGF(10), average peak stresses and moduli were significantly lower for SF, PGA, and PCL scaffolds containing PRGF. These results were not unexpected, as traditionally the combination of biologic proteins in large concentrations (collagen, elastin, fibrinogen, etc.) with electrospun polymers regarded for their tensile strength typically results in significantly reduced mechanical strength.[148, 345, 398]

The unique structures of PCL:PRGF(2-1) and PCL:PRGF, where both PRGF and PCL fibers were created, resulted in mechanical properties that fell between those of the PCL control and the PCL:PRGF(100) structures. This difference in mechanical properties would seem to indicate that these blended scaffolds resulted in materials that were structurally different from those where PRGF was added directly to the electrospinning solution. Additional work will be needed to fully differentiate the differences between the two methods of PRGF inclusion, and to understand what role individual PRGF fibers may play in providing/reducing mechanical strength of the scaffolds.

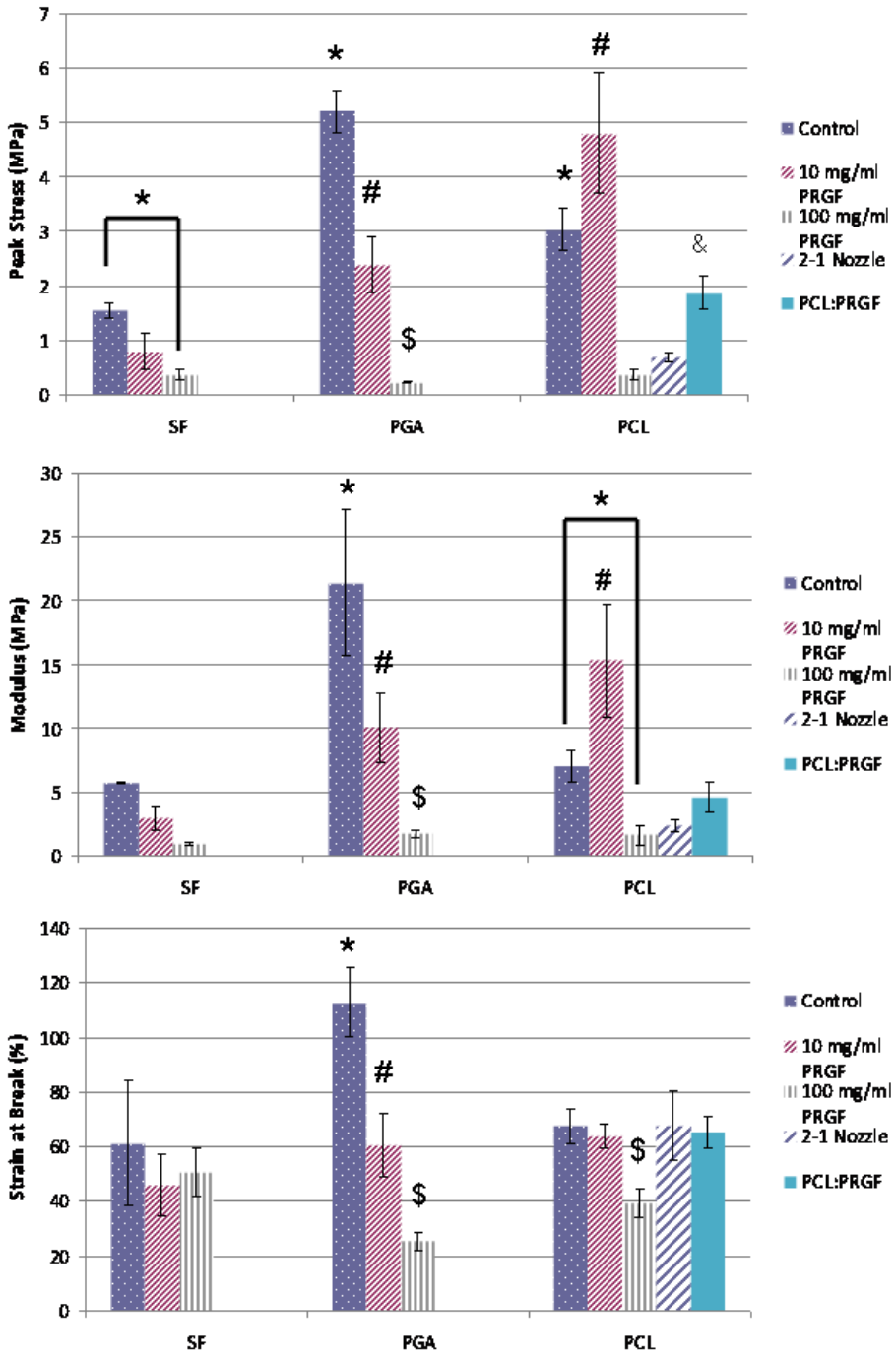

Figure 4. Results of uniaxial tensile testing of electrospun scaffolds. * indicates tatistically significant differences, $p < 0.05$, between control scaffolds and scaffolds containing PRGF. # indicates statistically significant differences, $p < 0.05$, between scaffolds containing 10 mg/ml PRGF and other scaffolds. $ indicates statistically significant differences, $p < 0.05$, between scaffolds containing 100 mg/ml PRGF other scaffolds. & indicates statistically significant differences, $p < 0.05$, between PCL:PRGF scaffolds and other scaffolds.

Evaluation of Cell Interaction

The results of the H&E staining are shown in Figures 5 and 6. H&E staining revealed confluent layers of ADSCs on the surfaces of the control scaffolds by day 7, while increased PRGF content resulted in increased cellular penetration into the scaffold. Surprisingly, after only 7 days ADSCs had migrated through half of the thickness of the PCL:PRGF(2-1) scaffold. By day 21 this trend was even more apparent, with clear cell migration through nearly the entire thickness of the PCL:PRGF(2-1) and PCL:PRGF scaffold (Figure 7). The SF:PRGF(100) scaffold also had nearly complete cellular penetration by day 21, compared to the SF scaffold containing no PRGF which exhibited only minimal migration into the depth of the structure. The PCL:PRGF(100) demonstrated a similar result, with the electrospun synthetic PCL material traditionally being difficult to cellularize *in vitro*[297-299], as it too exhibited increased cellular penetration when compared to the PCL scaffold containing no PRGF.

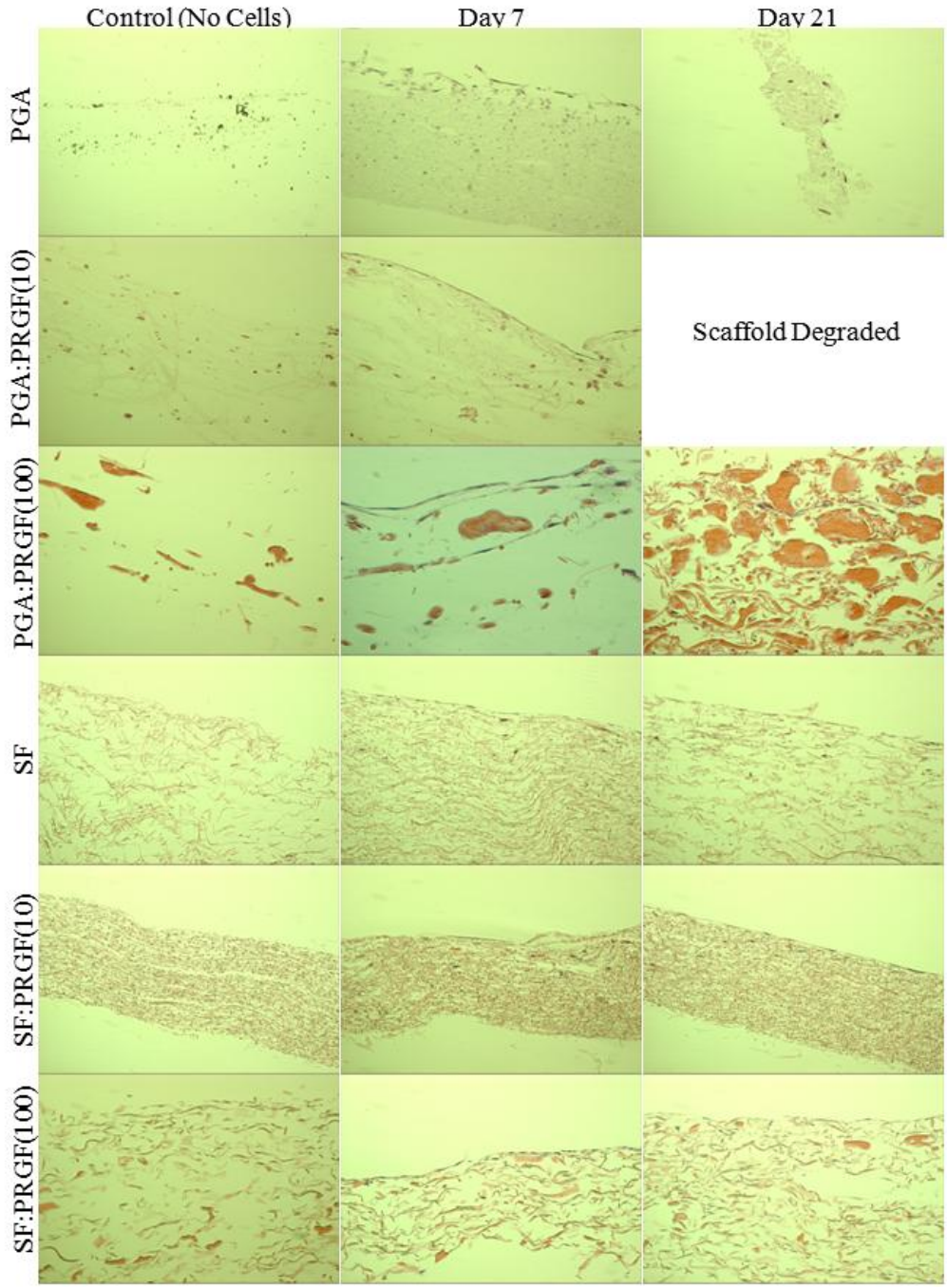

Figure 5. H&E staining of PGA and SF scaffolds at day 7 and 21. Images at 20x. Note, the PGA:PRGF(10) scaffold was completely degraded by day 21 and was unable to be processed for histological evaluation.

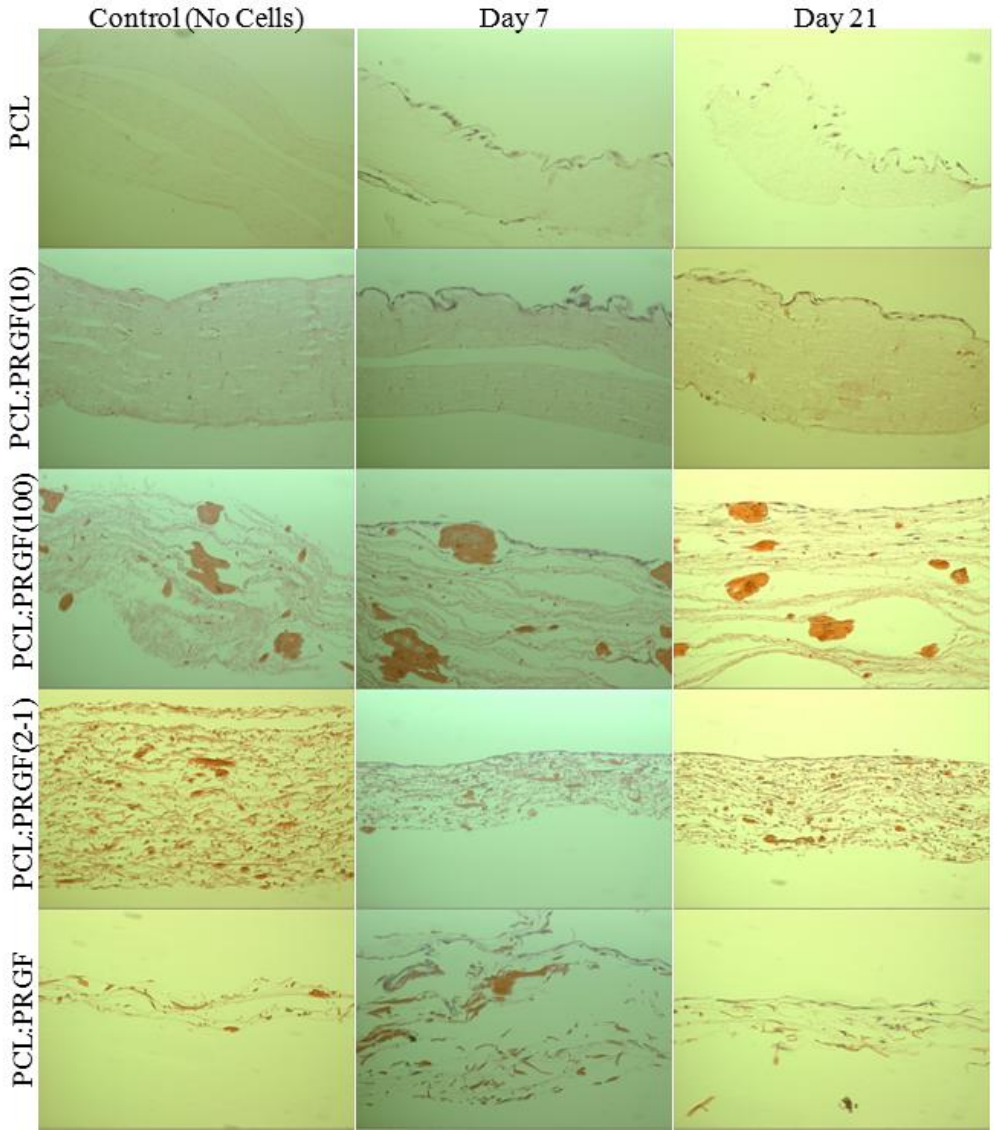

Figure 6. H&E staining of PCL scaffolds at day 7 and 21. Images at 20x.

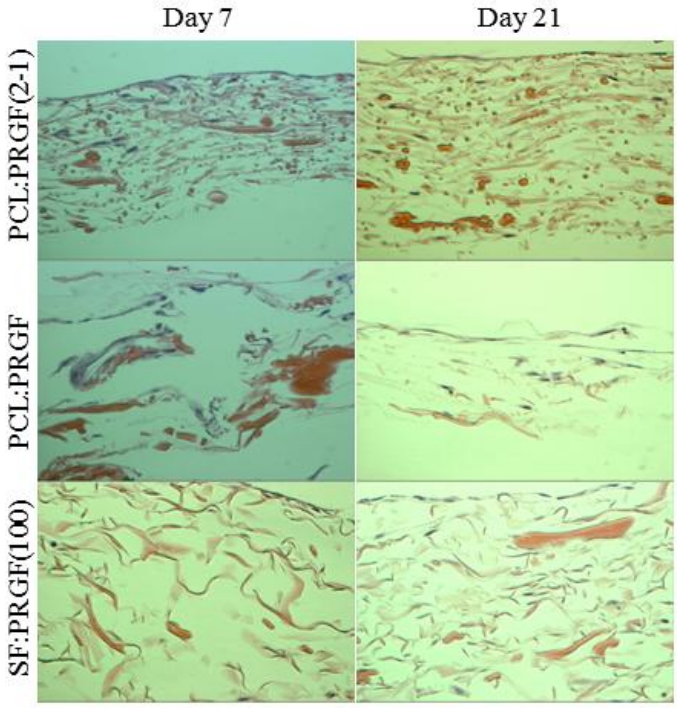

Figure 7. High magnification (40x) images of select scaffolds demonstrating significant cellular penetration.

Quantification of Protein Release Kinetics

The results of quantified protein release from PRGF containing scaffolds are shown in Figure 8. The results of this study demonstrated that scaffolds containing high concentrations of PRGF (SF:PRGF(100), PGA:PRGF(100), PCL:PRGF(100), and PCL:PRGF(2-1)) released detectable amounts of protein over 35 days in culture. The protein release from PRGF containing scaffolds peaked at day 1, decreased by about half on days 4 and 7, and reached a plateau that was sustained for the remainder of the duration. PCL:PRGF(2-1) scaffolds initially had the highest release of protein (300 µg/ml), but PCL:PRGF(100) had the highest release of protein at all time points after day 1 (125 µg/ml – 50 µg/ml). Surprisingly, PCL:PRGF scaffolds released the lowest amount of protein over the 35 days, even though the concentration of PRGF incorporated was the same as that of PCL:PRGF(2-1) scaffolds. PGA:PRGF(100) and SF:PRGF(100)

scaffolds had similar release kinetics as well, eliciting 240 µg/ml and 275 µg/ml of protein at day 1, respectively. Similar to the PCL:PRGF(100) and PCL:PRGF(2-1) structures, a plateau was acheived around 50 µg/ml and sustained until day 35. Minimal protein release was detected for PGA, SF, and PCL control scaffolds and scaffolds containing 10 mg/ml PRGF over the 35 days, indicating that the protein detected was in fact due to PRGF release and not simply an artifact of scaffold degradation.

Statistical analysis revealed protein release at day 1 from scaffolds of PGA:PRGF(100), SF:PRGF(100), PCL:PRGF(100) and PCL:PRGF(2-1) to be significantly greater than protein release from those respective scaffolds at all other time points (day 4-35). Additionally, scaffolds of PCL:PRGF(100) had significantly greater release at day 4 than day 35. The initial burst of release from the scaffolds at day 1 was expected as PRGF from the surface of the scaffolds was released. Remarkably, after the first day there was still a sustained release of protein from scaffolds of PGA:PRGF(100), SF:PRGF(100), PCL:PRGF(100) and PCL:PRGF(2-1) that continued throughout the 35 days, presumably due to the degradation of the polymer scaffolds and subsequent release of entrapped proteins.

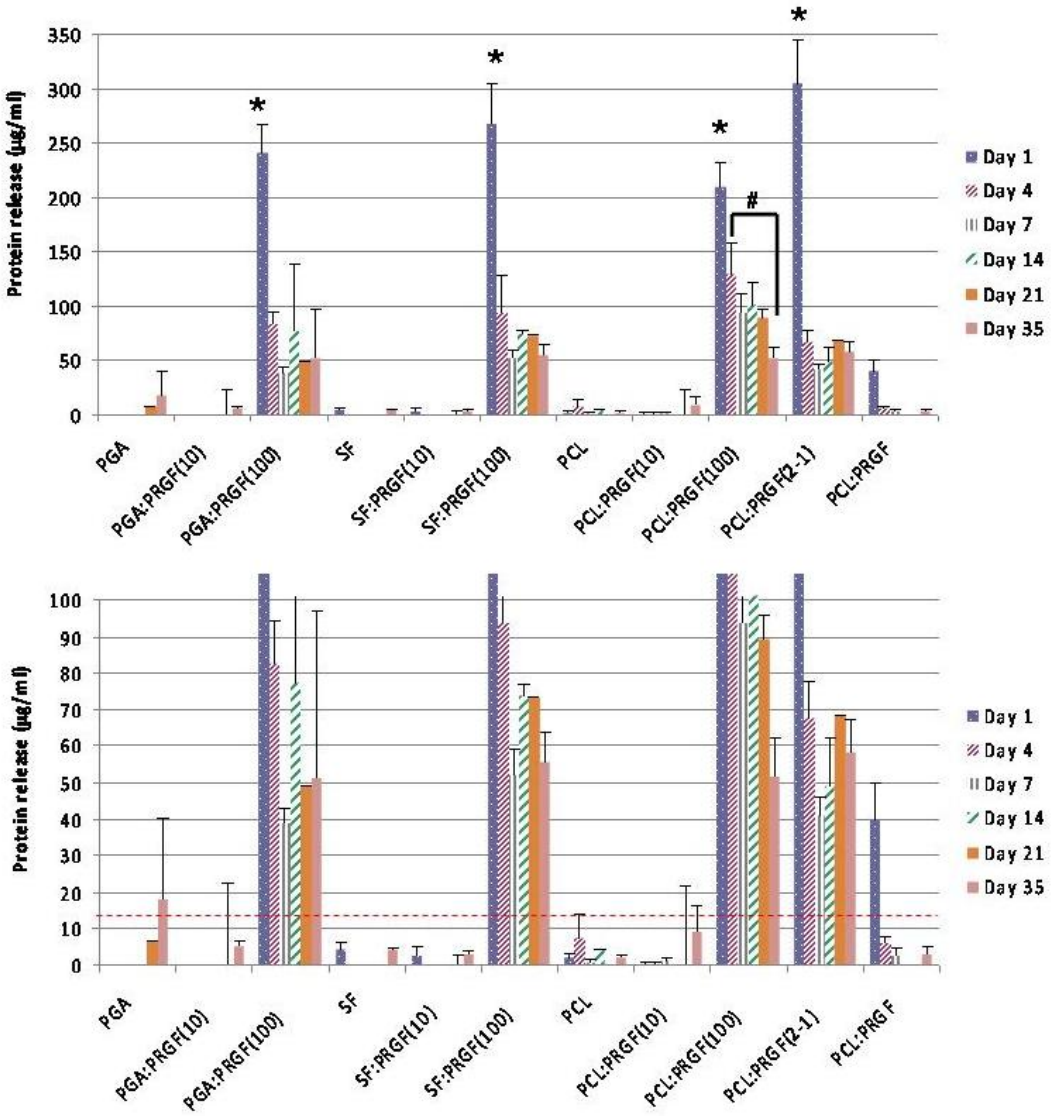

Figure 8. Quantification of generic protein released from PRGF containing scaffolds over 35 days (Top). * indicates a significant difference, $p < 0.05$, for day 1 when compared to all other time points for each material. # indicate statistically significant differences, $p < 0.05$, between day 4 and day 35 of PCL:PRGF(100). Y-axis scaled to emphasize decreased release from days 4-35 (Bottom). Minimum level of detection was 14.3 µg/ml (dashed line).

Quantification of RANTES and PDGF-BB, and TGF-β from the PRGF containing scaffolds revealed detectable release over 21 days (Figure 9) with kinetics similar to those of the protein assay results described previously. Scaffolds of PCL:PRGF(100) had the highest release of RANTES at day 1 (3 ng/ml), with a continual decrease in release

thereafter. PGA:PRGF(100), SF:PRGF(100), and PCL:PRGF(2-1) exhibited a similar trend, with peak values of RANTES at day 1 of 2.5 ng/ml, 1.1 ng/ml, and 1 ng/ml for each scaffold, respectively. RANTES release from PCL:PRGF scaffolds had a peak of 0.5 ng/ml at day 1, but values were not detectable after day 4. Statistical analysis revealed RANTES release at day 1 from scaffolds of PGA:PRGF(100), SF:PRGF(100), PCL:PRGF(100) and PCL:PRGF(2-1) was significantly higher than release from those same scaffolds at all other time points (days 4-21). For PCL:PRGF(100), RANTES release at day 4 was significantly higher than that of all other time points for that scaffold.

PDGF-BB release was highest from scaffolds of PCL:PRGF(2-1), peaking at day 1 (0.3 ng/ml), and decreasing thereafter, with values not detectable after day 7. PDGF-BB was also detectable from scaffolds of PGA:PRGF(100), SF:PRGF(100) and PCL:PRGF(100), with the highest release occurring at day 1 (0.1 ng/ml, 0.075 ng/ml, and 0.15 ng/ml, respectively). PCL:PRGF scaffolds elicited PDGF-BB release of 0.03 ng/ml at day 1, but was undetectable thereafter. PDGF-BB release at day 1 from scaffolds of PGA:PRGF(100), PCL:PRGF(100) and PCL:PRGF(2-1) was significantly higher than release from those same scaffolds at all other time points (days 4-21). PDGF-BB release from SF:PRGF(100) at day 1 was significantly greater than release from the same scaffold at days 7-21. For PCL:PRGF(100) and PCL:PRGF(2-1), PDGF-BB release at day 4 was significantly higher than that of days 10-21 and all other time points with detectable values, respectively, for those scaffolds.

Much like the release of PDGF-BB from the scaffolds, TGF-β release was highest from scaffolds of PCL:PRGF(2-1). Peak release was seen on day 4 (1.17 ng/ml), although

not significantly different from the release on day 1 (1.13 ng/ml), and decreased thereafter. Unlike RANTES and PDGF-BB, TGF-β release values were quantifiable for the PCL:PRGF(2-1), PCL:PRGF(100), and SF:PRGF(100) scaffolds throughout the 21 days evaluated. TGF-β release from scaffolds of PCL:PRGF(100) and PCL:PRGF(2-1) was significantly higher at days 1 and 4 than release from those same scaffolds at all other time points (days 7-21). In addition, release of TGF-β from scaffolds of PCL:PRGF(2-1) at days 7 and 10 was significantly higher than that at days 14 and 21. Surprisingly, PGA:PRGF(100) scaffolds did not exhibit a release above the minimum level of detection over the 21 days.

Similar to the protein assay results, RANTES, PDGF-BB, and TGF-β were undetectable from both the PGA, SF, and PCL control scaffolds and the scaffolds containing 10 mg/ml PRGF at all time points. The results of the statistical analysis illustrated that in general, after the initial release of growth factors from the surface of the scaffold at day 1, the release of RANTES and PDGF-BB that occurred at all time points thereafter is not significantly different, demonstrating a sustained release of growth factors from the scaffolds over the 21 day period as the polymer fibers begin to degrade. With regards to TGF-β, the PCL:PRGF(2-1) scaffolds exhibited a step-wise significant decrease in release until day 14, but still maintained a sustained quantifiable release.

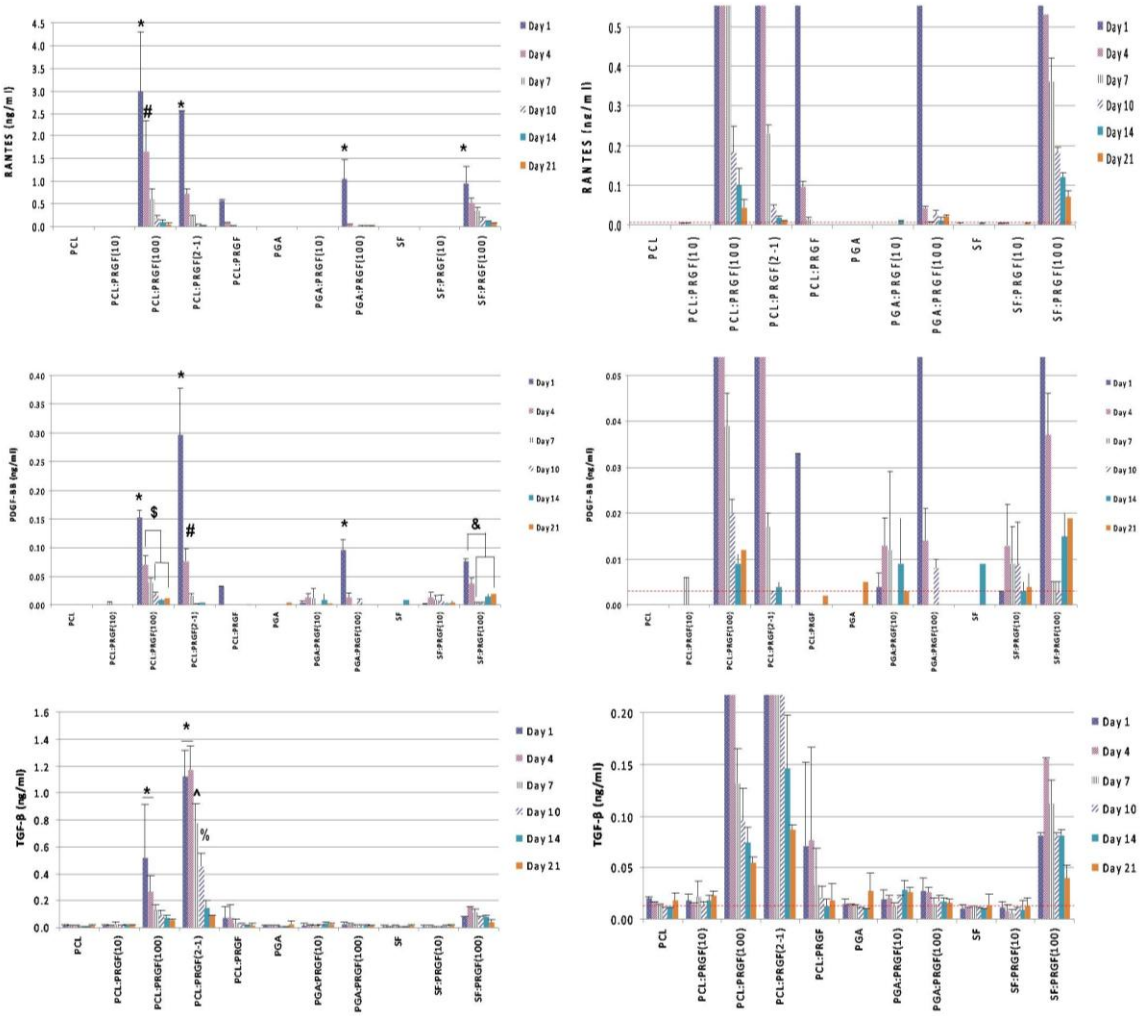

Figure 9. Results of RANTES, PDGF-BB, and TGF-β release from PRGF containing scaffolds over a duration of 21 days. * indicates statistically significant differences, $p < 0.05$, between day 1 and all other time points. # indicates statistically significant differences, $p < 0.05$, between day 4 and all other time points. $ indicates statistically significant differences, $p < 0.05$, between day 4 and days 10 and 21. & indicates statistically significant differences, $p < 0.05$, between day 1 and days 7 and 21. ^ indicates statistically significant differences, $p < 0.05$, between day 7 and all other time points. % represents statistical significance, $p < 0.05$, between day 10 and all other time points. Minimum levels of detection for RANTES, PDGF-BB, and TGF-β were 0.001ng/ml, 0.003ng/ml, and 0.011 ng/ml, respectively (dashed line).

Released PRGF Effect on Cell Proliferation

The effect of PRGF release on macrophage proliferation is shown in Figure 10. As expected, macrophages proliferated in the presence of all scaffolds from days 1 and 4, however, by day 7 proliferation slowed, and in some cases, cell number even decreased. This may be due to nutrient levels insufficient to support the large number of cells in each well, and hence, resultant cell apoptosis. At day 1, there was no significant difference in macrophage number between the different scaffolds and TCPS. At day 4, there were significantly less macrophages on scaffolds of PCL:PRGF(2-1) than on scaffolds of SF, SF:PRGF(10), TCPS, and TCPS:PRGF, and may indicate a loss of macrophages due to cellular penetration into the highly bioactive PCL:PRGF(2-1) scaffolds. By day 7, there were no significant differences in macrophage proliferation on any scaffold. While these results indicated that in general, PRGF did not have an affect on macrophage proliferation, taken with the results from the prior macrophage chemotaxis study, it could instead be anticipated that PRGF promotes macrophage chemotaxis rather than proliferation.

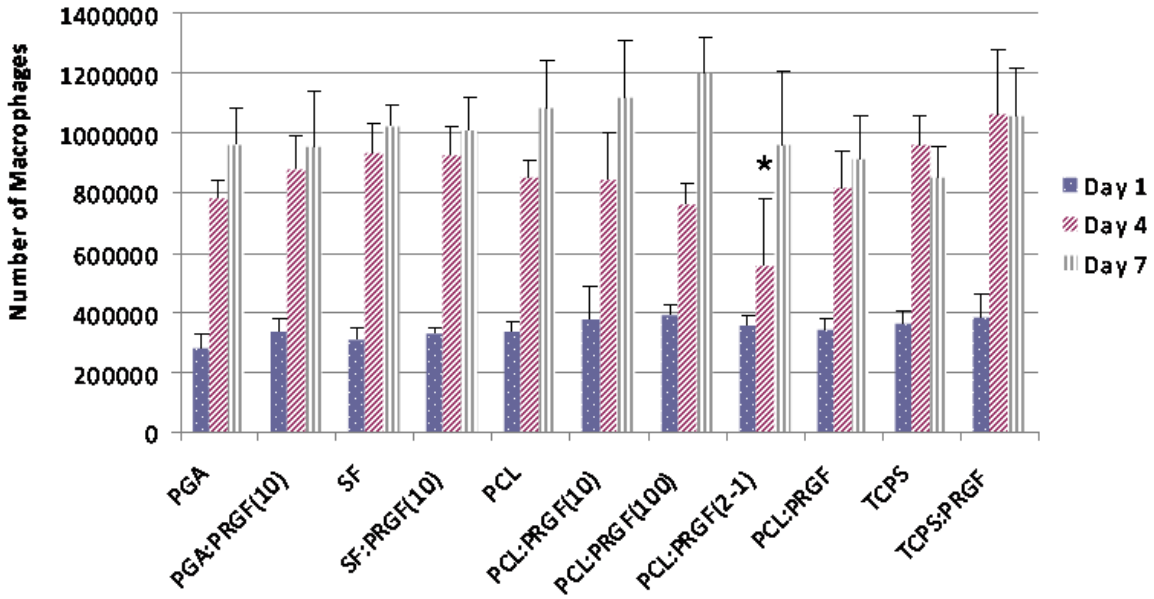

Figure 10. Results of macrophage proliferation when cultured on PRGF containing scaffolds. * indicates statistically significant differences between material groups of the same day, $p < 0.05$.

To determine the role that PRGF had in the secretion of macrophage growth factors, ADSCs were cultured in media conditioned by macrophages exposed to released PRGF. The results of ADSC proliferation, when cultured in macrophage conditioned media, demonstrated no significant differences in proliferation at day 1. However, by day 4 ADSCs cultured in macrophage conditioned media from scaffolds of PCL:PRGF(100) and PCL:PRGF(2-1) had significantly greater proliferation than ADSCs cultured in macrophage conditioned media from the PCL and TCPS control, as well as all other scaffolds (Figure 11). By day 7, there was significantly greater ADSC proliferation in macrophage conditioned media from scaffolds of PCL:PRGF(100), PCL:PRGF(2-1) and TCPS:PRGF than ADSCs cultured in conditioned media from PCL and TCPS control, as well as all other scaffolds. This was expected, as it had previously been demonstrated that PRGF, as well as growth factors secreted by macrophages, enhanced fibroblast,

mesenchymal and stromal stem cell proliferation [302, 352, 354-356, 385]. In general, ADSC proliferation in all preconditioned media increased from day 1 to day 4, however, by day 7 it appeared that proliferation slowed, and in some cases cell number even decreased, potentially due to induced contact inhibition as the cells became confluent in the wells, or died off following exhaustion of media nutrients. This may also have been due to the fact that the conditioned media used for the ADSCs was macrophage serum free media, which is unfavorable over the long-term for ADSC growth, or due to harmful factors expressed during macrophage apoptosis [386]. From the results in Figure 10, it was evident that the effect of macrophages on ADSC proliferation was due to macrophage interaction with PRGF containing scaffolds, and not the number of macrophages.

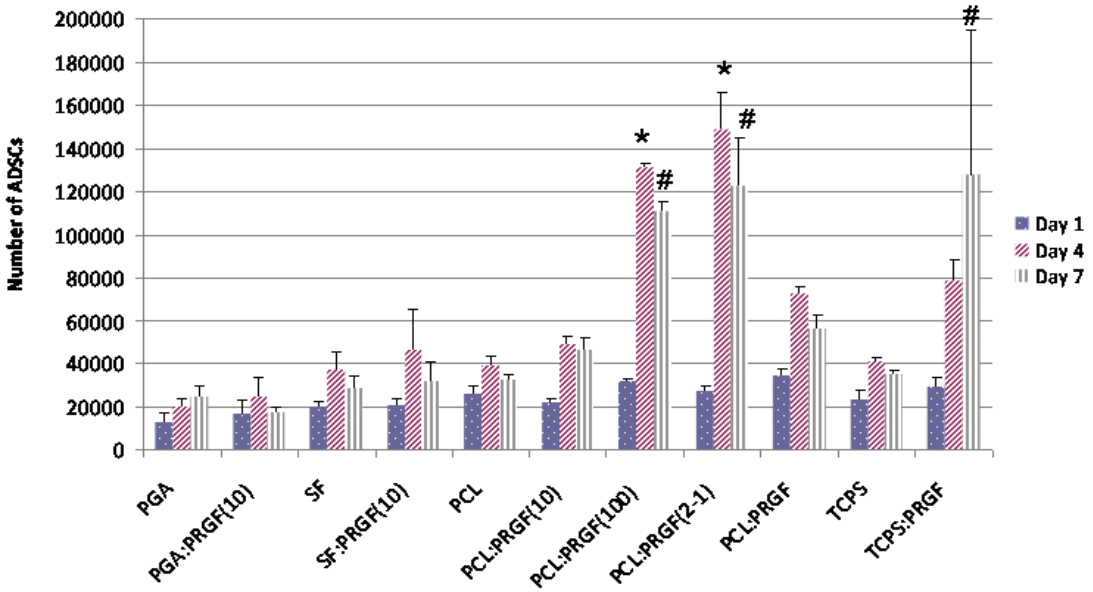

Figure 11. Results of ADSC MTS assay when cultured with macrophage conditioned media. * indicates statistically significant differences, $p < 0.05$, between material groups at day 4. # * indicates statistically significant differences, $p < 0.05$, between material groups at day 7.

ADSC proliferation when cultured in PRGF conditioned media without macrophages is displayed in Figure 12. Overall, ADSCs proliferated from day 1 to day 4 (with a few exceptions), and from day 4 to day 7, as expected. After 1 day, there were no significant differences in ADSC proliferation for any scaffold. By day 4, ADSCs cultured in media from scaffolds of SF:PRGF(100) had significantly greater proliferation than those cultured in media from SF control scaffolds. At day 7, ADSCs cultured in media from scaffolds of SF:PRGF(100) and PCL:PRGF(2-1) had significantly greater proliferation than cells cultured in media from SF and PCL control scaffolds, respectively. Compared to ADSCs cultured in media from the TCPS control, cells cultured in media from PCL:PRGF(2-1) and PCL:PRGF scaffolds had significantly greater proliferation at day 7. These results suggest that the presence of PRGF does impact ADSC proliferation, and corroborates previously published work [302, 352, 354-356]. It is clearly evident from these studies that the proliferation of ADSCs, cultured in conditioned media, is different depending on the presence or absence of macrophages and macrophage secreted factors over the 7 day study duration, and will be discussed further in the following section.

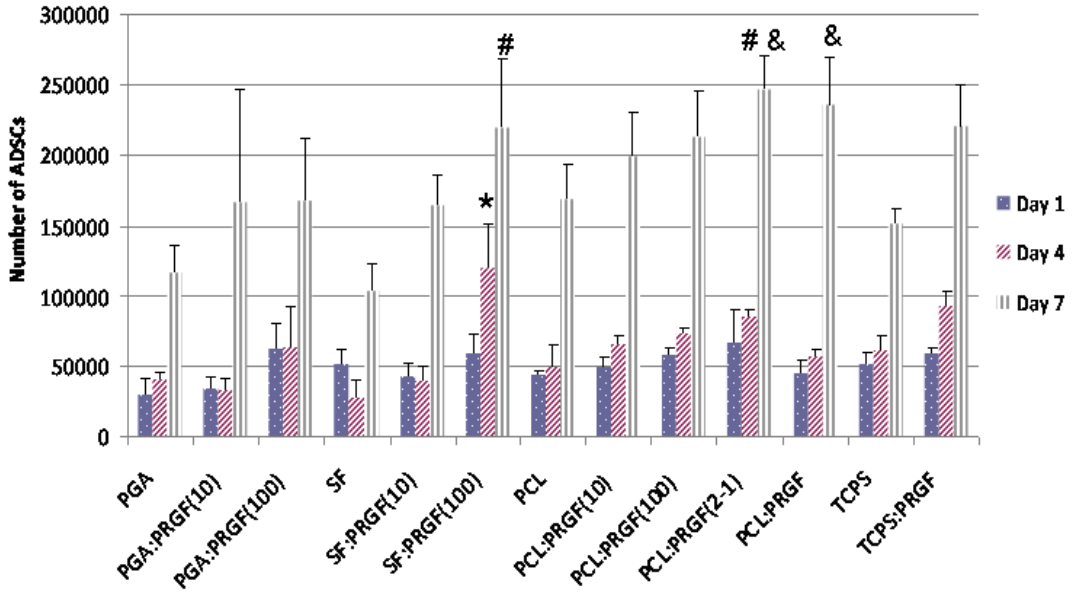

Figure 12. Results of ADSC MTS assay when cultured without macrophage conditioned media. * indicates statistically significant differences, $p < 0.05$, between PRGF containing scaffolds and their control scaffolds at day 4. # indicates statistically significant differences, $p < 0.05$, between PRGF containing scaffolds and their control scaffolds at day 7. & indicates statistically significant differences, $p < 0.05$, between PRGF containing scaffolds and the TCPS control at day 7.

Discussion

This present study provides a proof-of-principle for the incorporation of a powdered PRGF derived from human PRP into electrospun scaffolds of a number of materials. Through a number of evaluation methods, we were able to demonstrate that PRGF retained its physiologic activity after lyophilization and through the electrospinning process, subsequently enhancing the bioactivity of the electrospun scaffolds.

The use of PRP in clinical applications has been gaining in popularity as a means to stimulate tissue repair and regeneration with very minimal risk to the patient. However, the "black box" approach taken by many of the clinicians utilizing PRP leaves

much to be done in the realm of basic science to fully understand and standardize the practice. To date, the collection of whole blood and the concentration and isolation of platelets to make PRP has been proven effective *in vitro* for stimulating cellular activity in a number of formats, both in liquid[311, 350-356] and in lyophilized PRGF form [338-341].

To the best of the authors' knowledge, this manuscript serves as the first instance of a powdered PRGF being incorporated into an electrospun tissue engineering scaffold to serve as a controlled release vehicle for such a concentrated growth factor and cytokine milieu. While electrospun scaffolds have been used as growth factor delivery systems in the past[301, 319, 357-360], they have typically been limited to the incorporation of only a small number of growth factors due in part to the cost associated with purchasing the recombinant or isolated proteins [357]. The incorporation of a cost-effective PRGF protein array into an electrospun structure has the potential to deliver a multitude of growth factors, cytokines, and chemokines in physiologically relevant ratios. Such a platelet-based growth factor cocktail would essentially replicate the necessary factors found in a site of normal wound healing and promote the formation of healthy tissue through the stimulation of the healing cascade [300]. The results presented in this manuscript demonstrated the potential of such a sustained release vehicle through enhanced cellular activity consistent with other *in vitro* studies of PRP/PRGF.

Cellular migration and penetration into electrospun scaffolds was enhanced, regardless of polymer, with the addition of PRGF. While historically the ability for cells to migrate into an electrospun structure has been viewed as a challenge, especially with synthetic polymers such as PGA and PCL[297-299], the inclusion of PRGF yielded

structures that were readily infiltrated. The reason for this rapid infiltration is not yet fully understood in this preliminary investigation, and will need further investigation. However, the presence of an array of chemotactic proteins found in large quantities in PRP may be the most logical explanation. It may also be an affect of the change in scaffold mechanical properties; scaffolds with higher PRGF content exhibited decreased mechanical properties which may have allowed for cellular migration into the scaffold to occur more readily. The presence of PRGF fibers intermingled amongst the polymer fibers of the scaffolds, particularly in the case of the PCL:PRGF(2-1) and PCL:PRGF structures (Figure 3), may have also provided paths of easy entry into the thicknesses of the structures. These fibers of varying diameter had an apparent impact on the porosity of the scaffolds. As PRGF content increased, there was an increase in fiber diameter/pore area, which may have allowed for more rapid cellular infiltration while decreasing mechanical properties.

While the significant decrease in scaffold mechanical properties observed with the addition of large quantities of PRGF makes these scaffolds less than ideal for use in load-bearing tissue engineering applications, it was not completely surprising to the authors', nor was it seen as a negative result. As previously mentioned, this decrease in individual fiber mechanical properties may have contributed to the rapid cellular infiltration of the scaffolds. This enhanced cellular infiltration, regardless of its root cause, would allow for a tissue engineered product to be more rapidly remodeled with native collagen extracellular matrix; the production of which would readily supplement the strength of the scaffolds and encourage incorporation into surrounding tissues. Although not investigated in this study, the many factors found in PRGF have been proven to increase

collagen matrix production in a number of cell types [302, 309, 350, 391]. TGF-β, one such well-known matrix production related growth factor, was released by the electrospun scaffolds in detectable quantities, in some cases for up to 21 days. Should the presence of TGF-β and the other matrix production enhancing growth factors be actively taken up by the cells, it would be possible for accelerated matrix production to occur, and could therefore improve the mechanical strength of the weakened PRGF containing scaffolds.

With the creation of individual PRGF fibers within the electrospun scaffolds containing high concentrations of PRGF (SF:PRGF(100), PGA:PRGF(100), PCL:PRGF(100), PCL:PRGF(2-1), and PCL:PRGF), the loss of mechanical strength was not surprising. These PRGF fibers, consisting of a fibrinogen backbone mixed with any number of blood- and platelet-based proteins, lack inherent mechanical strength [344]. Similar in composition to electrospun fibrinogen[321, 345], which performs best mechanically when blended with synthetic polymers, and the presence of which can significantly decrease scaffold mechanical strength, the PRGF fibers are best utilized in a role of enhancing scaffold bioactivity rather than load bearing.

As demonstrated in the protein release assays conducted herein, detectable levels of proteins were released from the electrospun scaffolds for up to 35 days *in vitro*. While it can be assumed that a large percentage of the released proteins were in fact albumin and other blood proteins, not growth factors, the fact that RANTES, PDGF-BB, TGF-β were detectable in specific materials at up to 21 days attests to the sustained release nature of the structures. RANTES, PDGF-BB, and TGF-β release were analyzed as they are three of the more highly concentrated proteins contained within PRP/PRGF[313],

however from these results it can be interpolated that other factors such as PDGF-ab, FGF, and EGF will be released in the same fashion. The nature of the release demonstrated from the electrospun scaffolds may prove to be effective in proposed *in vivo* follow-up studies at enhancing migration of cells from surrounding tissues, with a large burst of protein creating a substantial chemotactic gradient, followed by a sustained release of protein to promote cell proliferation, and scaffold infiltration and remodeling. The incorporation and subsequent release of albumin, while seemingly inconsequential, may in fact serve as a protectant for the cytokines and chemokines included in the PRGF. The hydrophilic albumin molecules have been demonstrated in the literature to have the potential to encapsulate smaller proteins, and effectively shield them from potential denaturation [362, 363].

The retention of PRGF's biological activity following the electrospinning process, subjected to both high voltages and the organic solvent HFP, is displayed in the ADSC response to conditioned media from PRGF containing scaffolds cultured with and without macrophages. In both cases, ADSC proliferation was enhanced over 7 days when cultured in conditioned media from scaffolds containing PRGF versus those not containing PRGF. The presence of several growth factors within PRGF known to induce cell proliferation (VEGF, PDGF, IGF, FGF, and EGF, etc.) is most likely the reason for enhanced ADSC proliferation[302], however, future ELISA analysis will be needed to confirm this. Their proliferation profile over the 7 days was different depending on the presence or absence of macrophages, alluding to the fact that ADSC proliferation was affected by the interaction of macrophages with PRGF containing scaffolds. It is evident from this study that macrophage number is not the most critical factor in ADSC

proliferation; however, the specific mechanism by which macrophage interaction with the scaffolds affects ADSC proliferation was not specifically explored.

The authors hypothesize that the ADSC proliferation seen in this study might be due, in part, to the various growth factors and cytokines secreted by the macrophages. It has been shown previously that macrophages cultured on electrospun scaffolds have the ability to produce high levels of VEGF and FGF[150], and in the presence of PRGF, produce additional pro-angiogenic growth factors and cytokines, including those which enhance cell proliferation [313]. Although ADSC proliferation appeared to stop by day 7 when cultured in macrophage conditioned media, this was not perceived as a negative effect brought about by the presence of PRGF, rather most likely due to media mismatch and/or harmful factors produced during macrophage apoptosis induced by a lack of nutrient supply in the conditioned media [386].

In conclusion, this study demonstrated the potential for PRP to be subjected to a FTF process, lyophilized to create PRGF, and incorporated into electrospun scaffolds of various materials. This PRGF was released from the electrospun scaffolds in a controlled fashion over a period of 35 days in culture, and retained its potential to positively influence the proliferation of ADSCs and chemotaxis of macrophages at specific concentrations *in vitro*. Additionally, the presence of PRGF in high concentrations allowed for the rapid infiltration of ADSCs into electrospun structures of both natural and synthetic polymers when cultured *in vitro* for 21 days. Additional studies are needed to determine what effect the presence of PRGF will have *in vivo* on the recruitment of cells from the surrounding tissues, and the cellularization and remodeling of the electrospun structures. As one of the major advantages of PRP, when used clinically, is its ability to

deliver a milieu of growth factors and cytokines at the patients' bedside, the creation of an off-the-shelf electrospun scaffold incorporating PRGF from pooled allogenic blood may have the same benefits. While the use of pooled blood is typically frowned upon in the United States, the use of allogenic PRP has been gaining popularity in a number of European studies with no mention of adverse immune reactions [394-396, 399].

Acknowledgments

The authors would like to thank Drs. Sherwin Kevy and May Jacobsen from the Harvard Immune Disease Institute's Blood Research laboratory for conducting platelet counts on pooled whole blood and PRP. The authors would also like to thank Anatomic Pathology Research Services in the Department of Pathology at Virginia Commonwealth University for histological staining. SEM was performed at the Virginia Commonwealth University Department of Anatomy and Neurobiology Microscopy Facility, supported, in part with funding from NIH-NINDS Center core grant (5P30NS047463-02).

Vita

Patricia Sarah Wolfe was born in Charlottesville, VA on August 5, 1985. After attending elementary school in Canton, OH, and middle school in Carmel, IN, she moved to Rochester, MI where she graduated from Rochester Adams High School in 2003. She attended Virginia Polytechnic and State University, where she was awarded her Bachelors of Science degree in Mechanical Engineering in May 2007. Directly after that, she continued her education at Virginia Commonwealth University, where she pursued her doctorate degree in Biomedical Engineering. She currently resides in Richmond, VA, but will be moving shortly after obtaining her degree to Land O Lakes, FL.